

**EARLY-AGE BEHAVIOR OF CONTINUOUSLY
REINFORCED CONCRETE PAVEMENT AND
CALIBRATION OF THE FAILURE PREDICTION
MODEL IN THE CRCP-7 PROGRAM**

by

Young-Chan Suh
Ken Hankins
B. F. McCullough

Research Report Number 1244-3

Evaluation of Performance of Texas Pavements
Made with Different Coarse Aggregates

Research Project 2/3-8-90/2-1244

conducted for the

Texas Department of Transportation

in cooperation with the

**U.S. Department of Transportation
Federal Highway Administration**

by the

**CENTER FOR TRANSPORTATION RESEARCH
Bureau of Engineering Research
THE UNIVERSITY OF TEXAS AT AUSTIN**

March 1992

NOT INTENDED FOR CONSTRUCTION, BIDDING, OR PERMIT PURPOSES.

B.F. McCullough, P.E. (Texas No. 19914)
Study Supervisor

The contents of this report reflect the views of the authors, who are responsible for the facts and the accuracy of the data presented herein. The contents do not necessarily reflect the official views or policies of the Federal Highway Administration or the Texas Department of Transportation. This report does not constitute a standard, specification, or regulation.

PREFACE

The authors would like to thank all Texas Department of Transportation personnel who contributed to this research study and report. We would also like to thank the Center for Transportation Research staff, who assisted in various ways.

Young-Chan Suh
B. F. McCullough
Kenneth Hankins

LIST OF REPORTS

Report No. 422/1244-1, "Field Evaluation of Coarse Aggregate Types: Criteria for Test Sections," by Kenneth Hankins, Young-Chan Suh, and B. Frank McCullough, describes the design of the experimental test sections to be used for the verification of a design standard. The design standard is one of the first to incorporate those various physical design features that account for the variety in concrete mix properties. March 1992.

Report No. 422/1244-2, "Characterization of Concrete Properties with Age," by Terry Dossey and B. Frank McCullough, presents the laboratory measurements of concrete properties for eight aggregates commonly used in Texas for pavement construction. A series of models are developed for predicting concrete property behavior, either directly from aggregate type or indirectly from chemical composition of the aggregate. February 1992.

Report No. 422/1244-3, "Early-age Behavior of Continuously Reinforced Concrete Pavement and Calibration of the Failure Prediction Model in the CRCP-7 Program," by Young-Chan Suh, Kenneth Hankins, and B. Frank McCullough presents (1) the observations and findings from the short-term monitoring of the special test sections constructed in Houston, Texas, and (2) the calibration of the CRCP failure prediction model in the CRCP-7 computer program. March 1992.

ABSTRACT

This report focuses on (1) the observations and findings from the short-term monitoring of the special test sections constructed in Houston, Texas, and (2) the calibration of the CRCP failure prediction model in the CRCP-7 computer program.

To determine whether the performance of pavements in the field is in accordance with that predicted by the CRCP program, special test sections were constructed at four different locations in Houston. For approximately 1 month after construction, the behavior of the pavements was monitored for temperature (both air and concrete), slab movement, and cracking. Although additional long-term condition surveys should be scheduled to draw further conclusions from this test-section study, much valuable information about the early-age behavior of CRCP was obtained during the short-term monitoring. Major observations and findings from the test sections include (1) the importance of the heat of hydration on the early-age behavior of CRCP, (2) the effect of construction season and time of placement during the day on the early-age cracking, (3) detrimental characteristics of the early-age cracks in terms of their shapes and widths, (4) the effect of coarse aggregate type on cracking, (5) factors affecting crack width, (6) determination of setting temperature used as a reference temperature in the calculation of the temperature-induced stresses, and (7) correlation between the shrinkage of concrete pavement in the field and that of lab-cured cylinders. Based on these observations and findings, recommendations are provided as to how the early-age observations may be simulated in the CRCP program. Recommendations for the future design and construction are also presented.

Long-term distress curves having various reliabilities were developed for CRC pavements in terms of the number of failures per mile using the Rigid Pavement Database available at the Center for Transportation Research. Calibration of the failure prediction model in the computer program CRCP-7 was made based on these distress curves.

KEYWORDS: CRCP, coarse aggregates, siliceous river gravel aggregates, limestone aggregates, CRCP-7 computer program, pavement behavior, heat of hydration, crack spacing, crack width, pavement temperature.

SUMMARY

Based on a review of test sections constructed at four different project sites in Houston, Texas, this report documents the short-term performance of continuously reinforced concrete pavements (CRCP). Specifically, the test sections were designed to study (1) the importance of the heat of hydration on the early-age behavior of CRCP, (2) the effect of construction season and time of placement during the day on the early-age cracking, (3) detrimental characteristics of the early-age cracks in terms of their shapes and widths, (4) the effect of coarse aggregate type on cracking, (5) factors affecting crack width, (6) determination of setting temperature used as a reference temperature in the calculation of the temperature-induced stresses, and (7) the correlation between the shrinkage of concrete pavement in the field and that of lab-cured cylinders. Based on these observations and findings, recommendations are provided as to how the early-age observations may be simulated in the CRCP program. Recommendations for the future design and construction are also presented.

Long-term distress curves having various reliabilities were developed for CRCP in terms of the number of failures per mile using the Rigid Pavement Database available at the Center for Transportation Research. Using these distress curves, we next calibrated the failure prediction model in the CRCP-7 computer program.

IMPLEMENTATION STATEMENT

The evaluation of the test sections provided in this report yields a better understanding of the effect of different coarse aggregates on the performance of CRCP, which in turn can lead to improved pavement design. In addition, by comparing the pavement performance predicted by the CRCP-7 computer program with the measured values of four Houston test sections, the study team provides recommendations as to how the early-age observations may be simulated in the CRCP program (or revised to simulate the observations). Recommendations for future design and construction are also presented.

Long-term distress curves having various reliabilities were developed for CRCP in terms of the number of failures per mile using the Rigid Pavement Database available at the Center for Transportation Research. Calibration of the failure prediction model in the computer program CRCP-7 was made based on these distress curves.

Although additional long-term condition surveys should be scheduled to draw further conclusions from this test-section study, much valuable information about the early-age behavior of CRCP was obtained during the short-term monitoring documented in this report.

TABLE OF CONTENTS

PREFACE	iii
LIST OF REPORTS	iii
ABSTRACT	iv
SUMMARY	v
IMPLEMENTATION STATEMENT	v
CHAPTER 1. INTRODUCTION	
BACKGROUND	1
OBJECTIVES OF THE STUDY	1
SCOPE OF THE REPORT	1
CHAPTER 2. EXPERIMENT DESIGN AND CONSTRUCTION OF TEST SECTIONS	
THE NEW DESIGN STANDARD	3
EXPERIMENT DESIGN	3
CONSTRUCTION OF TEST SECTIONS	4
<i>SH 6 Summer</i>	7
<i>BW 8 Winter</i>	8
<i>SH 6 Winter</i>	8
<i>IH-45 Winter</i>	9
INSTRUMENTATION AND DATA COLLECTION	10
TESTING	11
CHAPTER 3. DATA PRESENTATION WITH DISCUSSIONS	
SLAB TEMPERATURE	15
CRACKING	16
SLAB MOVEMENT	17
PATTERN OF NEW CRACK IN A SLAB SEGMENT	19
EFFECT OF PRE-CONSTRUCTION CONDITIONS	20
<i>Reflection of Cracks</i>	20
<i>Effect of Steel Splices</i>	21
<i>Effect of Badly Deformed Surface of Bondbreaker</i>	21
<i>Cracks around Manhole</i>	22
<i>Transverse Cracks over Transverse Steel Bars</i>	22
SUMMARY	23
<i>Slab Temperature</i>	23
<i>Cracking</i>	24
<i>Slab Movement</i>	24
<i>Pattern of New Cracks in a Slab Segment</i>	24
<i>Effect of Pre-Construction Conditions</i>	24

CHAPTER 4. HEAT OF HYDRATION AND EARLY-AGE CRACKS IN CONCRETE PAVEMENT

HEAT OF HYDRATION AND EARLY-AGE CONCRETE (LITERATURE REVIEW)	26
<i>Nature of Hydration</i>	26
<i>Undesirable Effect of High Temperature on Concrete</i>	27
<i>Stresses in Concrete During the Hydration</i>	28
<i>Tensile Strain Capacity of Concrete at Early Ages</i>	28
<i>Summary of Literature Review</i>	29
INFLUENCE OF THE TIME OF PLACEMENT ON EARLY-AGE CRACKING	29
<i>Seasonal Effect</i>	30
<i>Effect of Placement Time During the Day</i>	32
<i>Time of Placement and Concrete Temperature</i>	34
CONTROL OF CONCRETE TEMPERATURE DURING HYDRATION	35
<i>Pre-Cooling</i>	35
<i>The Use of Pozzolanic Material</i>	35
<i>The Use of Retarder</i>	37
SUMMARY	37

CHAPTER 5. FACTORS AFFECTING CRACK WIDTH

EXPERIMENTS	39
FACTORS AFFECTING CRACK WIDTH	40
<i>Placement Season of the Year</i>	42
<i>Coarse Aggregate Type</i>	43
<i>Steel Reinforcement</i>	43
<i>Time of Crack Occurrence</i>	44
<i>Crack Spacing</i>	44
SUMMARY	44

CHAPTER 6. DETERMINATION OF CURING TEMPERATURE (SETTING TEMPERATURE) AND THE SHRINKAGE OF CONCRETE PAVEMENT

INTRODUCTION	46
CURING TEMPERATURE	46
DRYING SHRINKAGE	46
CONCEPTUAL DETERMINATION OF SETTING TEMPERATURE	46
INSTRUMENTATION	47
DATA COLLECTION	48
<i>Determination of Setting Temperature</i>	49
<i>Correlation between Slab Shrinkage and Cylinder Shrinkage</i>	50
SUMMARY	51

CHAPTER 7. CURRENT CONDITION OF THE TEST SECTIONS

CRACK SPACING AND CRACK WIDTH	52
<i>Winter Construction</i>	53
<i>Summer Construction</i>	54

**CHAPTER 8. COMPARISON OF PREDICTED WITH OBSERVED
CRACK PATTERNS**

INPUT DATA57
INTERPRETATION OF RESULTS57
SUMMARY59

**CHAPTER 9. DEVELOPMENT OF LONG-TERM FAILURE CURVES
AND CALIBRATION OF THE FAILURE PREDICTION
MODEL IN THE CRCP-7**

MAJOR FAILURE MODE IN CRCP60
DEVELOPMENT OF FAILURE CURVES CONSIDERING RELIABILITY61
 Application of the Reliability Concept.....62
BASIC ALGORITHM FOR THE PUNCHOUT PREDICTION63
CALIBRATION64

CHAPTER 10. DISCUSSION OF RESULTS AND SUMMARY

EFFECT OF COARSE AGGREGATE TYPE ON CRACKING66
EFFECT OF DIFFERENT STEEL DESIGNS (SIZE AND AMOUNT OF STEEL).....66
PATTERNS OF NEW CRACKS IN A SLAB SEGMENT66
FACTORS AFFECTING THE CRACK WIDTH67
EFFECT OF HYDRATION OF CEMENT AND TEMPERATURE CONDITIONS ON
EARLY-AGE CRACKING67
CURING TEMPERATURE (SETTING TEMPERATURE).....69
SLAB SHRINKAGE69
OTHER FINDINGS FROM THE TEST SECTIONS69
CALIBRATION OF THE FAILURE PREDICTION MODEL IN CRCP-769
SUMMARY70

CHAPTER 11. CONCLUSIONS AND RECOMMENDATIONS

INTRODUCTION72
GENERAL CONCLUSIONS.....72
 Recommendations for Future Construction73
 Recommendations for Ruture Research74

REFERENCES75

APPENDIX A79

APPENDIX B81

APPENDIX C86

APPENDIX D95

APPENDIX E105

APPENDIX F134

APPENDIX G143

APPENDIX H148

CHAPTER 1. INTRODUCTION

BACKGROUND

Condition surveys of continuously reinforced concrete pavements (CRCP) in Texas have revealed that significant performance differences exist among pavements constructed with different coarse aggregates (Ref 1). To reflect the difference in performance, a new design standard has been developed, one based on the material properties of concrete containing the two types of coarse aggregates most often used in Texas—siliceous river gravel (SRG) and limestone (LS). The new design standard was developed using the computer program CRCP-4, which is a mechanistic model developed at the Center for Transportation Research at The University of Texas at Austin. Using design parameters, material properties, environmental condition, and traffic loadings, the model predicts the performance of CRCP in terms of crack spacing, crack width, and steel stress.

To determine whether the performance of pavements in the field is in accordance with that predicted by the computer program, test sections were constructed and monitored for approximately 1 month after construction at four locations in Houston, Texas. The test sections were of CRCP and were constructed to permit observations of the effects of (1) the coarse aggregate type and (2) the quantity of reinforcing steel used. While it is expected that additional long-term condition surveys will yield further conclusions, much valuable information about the early-age behavior of CRCP was obtained during the short-term monitoring.

OBJECTIVES OF THE STUDY

Using the early-age observations of the test sections, the study team undertook the following objectives:

1. To provide recommendations as to how the early-age observations may be simulated in

the computer program (or revision steps made to simulate the observations), and provide recommendations for long-term observations for the study based on the early-age observations.

2. To use field data from the Rigid Pavement Database developed at the Center for Transportation Research to calibrate the fatigue relation used in CRCP-7 to predict punch-outs.

SCOPE OF THE REPORT

Specifically, this report documents and discusses (1) the findings of the short-term monitoring of the Houston test sections, and (2) the calibration of the fatigue equation in the CRCP-7 punchout prediction model. Chapter 2 describes the experiment design and the construction of the test sections, with the experiment design for the verification test sections, construction of the test sections, instrumentation, and testing for the concrete properties also presented. Chapter 3 gives the various data collected from the short-term monitoring of the test sections. Air and slab temperature, crack patterns, and slab movement are particularly discussed.

Chapter 4 investigates the effect of initial temperature condition on the hydration of cement and on the consequent early-age cracking of concrete pavement. The nature of hydration, the influence of time of placement on the early-age cracking, and the control of concrete temperature during hydration are all discussed.

Chapter 5 describes the factors affecting crack width based on the crack width data collected from the test sections; Chapter 6 introduces a method for determining the curing temperature (setting temperature) used as a reference temperature in the calculation of temperature-induced stresses. Also discussed in Chapter 6 is the correlation between the shrinkages of concrete pavement in the field- and lab-cured cylinders.

Chapter 7 summarizes the current condition of the test sections in terms of crack spacing and crack width, based on observations during the short-term monitoring. Chapter 8 presents a comparison of predicted crack patterns by CRCP computer program with observed crack patterns.

In Chapter 9, the fatigue equation used in the punchout prediction model in the computer program CRCP-7 is calibrated against the extensive

condition survey database available at the Center for Transportation Research at The University of Texas at Austin.

Chapter 10 summarizes the study's observations and findings. Recommendations as to how the early-age observations may be simulated in the CRCP program (or revised to simulate the observations) are also presented. Finally, conclusions and recommendations of this study are provided in Chapter 11.

CHAPTER 2. EXPERIMENT DESIGN AND CONSTRUCTION OF TEST SECTIONS

This chapter presents the experiment design, construction, instrumentation, data collection, and testing for the test sections.

THE NEW DESIGN STANDARD

The performance of CRCP constructed with siliceous river gravel (SRG) coarse aggregate differs significantly from that of CRCP constructed with limestone (LS) coarse aggregate. Specifically, for the same steel design, pavements containing siliceous river gravel experience substantially more distress (e.g., cracks, spalling, and punchouts) than those containing limestone. Because a large percentage of a pavement's concrete volume consists of coarse aggregates, researchers have tended to conclude that the various coarse aggregates affect differently the overall properties—and, hence, performance—of concrete. In Texas, such observations led to the development of the new CRCP design standard, CRCP(B)-89B.

In creating this new design standard, researchers at the Center for Transportation Research at The University of Texas at Austin first analyzed the properties of concrete samples constructed with both SRG and LS coarse aggregates and then entered the results in the CRCP-4 computer program as input values (Refs 2, 3, and 4) to predict the performance of pavements containing these materials. For various slab thicknesses and steel designs, the program predicted the performance of each pavement in terms of crack spacing, crack width, and steel stress. Using the CRCP design criteria (Ref 5), an optimum longitudinal steel design could be selected for each combination of slab thickness and coarse aggregate type.

Based on the results of this early analysis, the Texas State Department of Highways and Public Transportation (SDHPT, now the Texas Department of Transportation, or TxDOT) developed new design standards for both SRG and LS aggregates. (These standards are reproduced in Appendix A of this report, where it may be noted that

for different coarse aggregate types and for a given slab thickness, different bar spacings were used with same-sized bars.) The major feature of the new design standard was the use of different amounts of longitudinal steel for different coarse aggregate types in such a manner that similar crack spacings for the two aggregate types would be expected within the limiting design criteria. Since the major distresses of CRCP (i.e., punchouts and spalling) have a strong correlation with crack spacing, the new design standard sought to minimize the distress by controlling the crack spacing. And because SRG-constructed pavements showed narrower crack spacing than LS-constructed pavements, the new design for SRG concrete specified less longitudinal steel than specified for LS concrete.

EXPERIMENT DESIGN

The experiment included CRCP test sections placed at four locations in Houston. At each location, 1,840 feet of CRCP was placed, with one-half of the length (920 feet) constructed with SRG and the other half constructed with LS. Each of these lengths was then subdivided into four test sections. One of the four test sections for each coarse aggregate type used the same quantity of longitudinal steel as proposed in the new design standard (hereafter termed "medium" steel). Two other test sections used an amount of longitudinal steel about 0.1 percent higher (hereafter termed "high" steel) and 0.1 percent lower (hereafter termed "low" steel), respectively, than the medium steel; these three test sections also used a 3/4-inch-diameter bar size (No. 6 bar). The fourth test section used medium steel with a larger-sized bar (7/8-inch diameter, or No. 7 bar), an arrangement permitting an investigation of the interactive effect of bond area and concrete volume ratio. The experimental design for the test sections placed at each location is illustrated in Figure 2.1.

Amount of Steel (bar size)	Coarse Aggregate Type	
	SRG	LS
High (No. 6 bar)	X	X
Medium (No. 6 bar)	X	X
Low (No. 6 bar)	X	X
Medium (No. 7 bar)	X	X

Figure 2.1 Experimental design for the test sections

Each test section, 230 feet long, was separated by the different steel design. To eliminate the effect of steel splicing (required for transitioning between the contiguous sections), only the middle 200 feet were considered representative of the test section; 15 feet of both ends were excluded in the analysis as a transition area between the two contiguous sections. A typical steel lap technique arranged between sections having different steel designs is shown in Figure 2.2.

CONSTRUCTION OF TEST SECTIONS

The test sections were placed during summer and winter. Their general location, including the season in which they were constructed, is given in Figure 2.3. For convenience, the following abbreviations will be used throughout this report:

- SH 6 summer: test sections placed on State Highway 6 during the summer
- BW 8 winter: test sections placed on Beltway 8 during the winter
- SH 6 winter: test sections placed on State Highway 6 during the winter
- IH-45 winter: test sections placed on Interstate Highway 45 during the winter

The typical pavement structure associated with these projects is shown in Figure 2.4. The thickness of the concrete slab varied with the project, with the vertical location of the steel (a single layer of steel) in the slab most often at mid-depth; in the case of IH-45 winter, double layers of steel were used. Typical concrete mix designs used on the projects are given in Table 2.1. The following sections describe each project in detail.



Figure 2.2 Typical steel lap technique between sections with different steel design

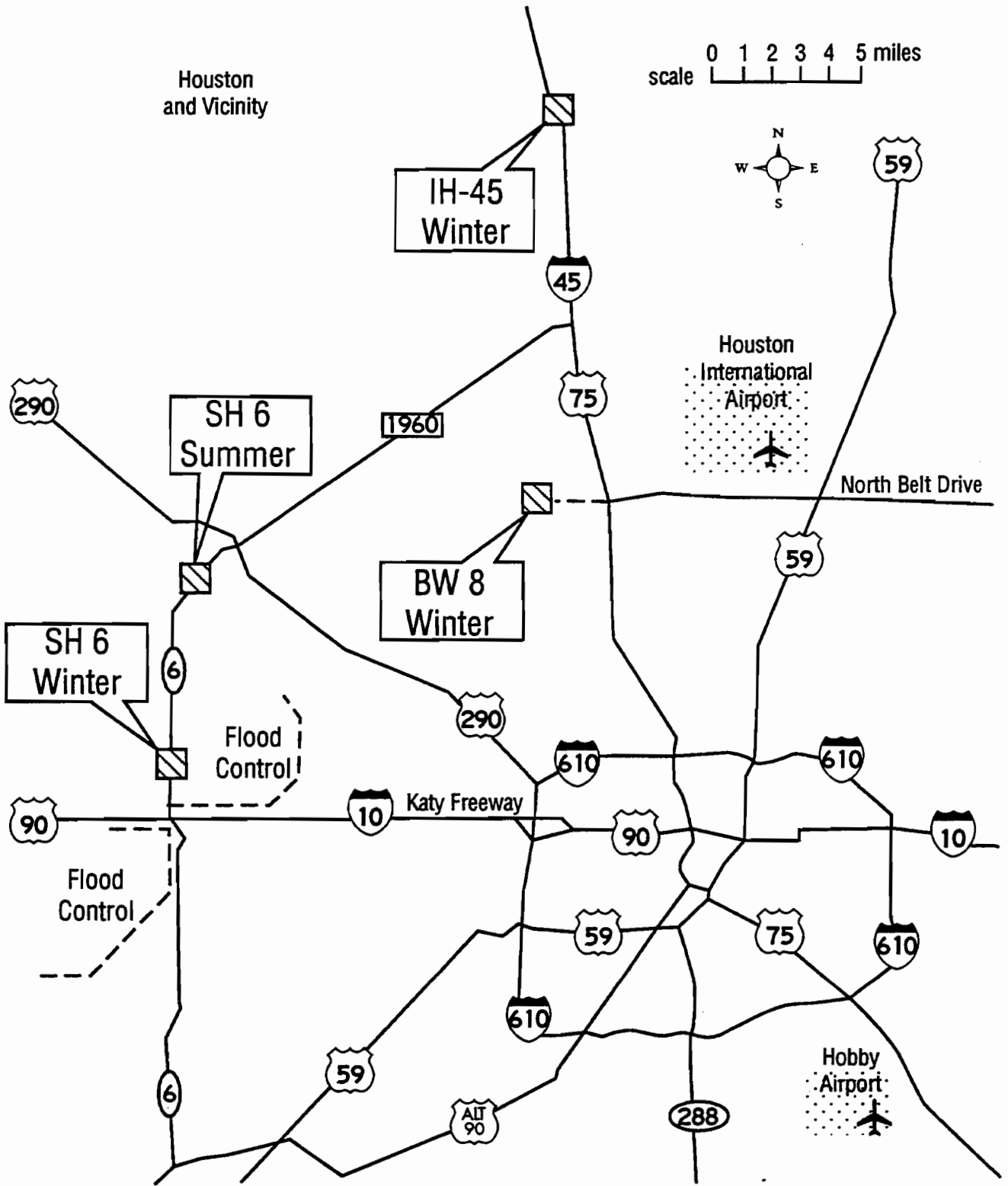


Figure 2.3 General locations and construction seasons of the projects

Table 2.1 Typical concrete mix design used on the projects

Project		SH 6 Summer		BW 8 Winter		SH 6 Winter		IH-45 Winter	
Aggregate Type		SRG	LS	SRG	LS	SRG	LS	SRG	LS
Unit									
Coarse aggregate	lbs/CY	2,030	1,900	2,056	1,887	2,083	1,900	1,990	1,990
Water	lbs/CY	234	225	224	220	210	224	220	220
Cement	lbs/CY	388	423	388	388	342	388	400	388
Fly ash (% replaced by vol.)	lbs/CY	106 (25%)	115 (25%)	105 (25%)	112 (25%)	160 (35%)	106 (25%)	136 (30%)	108 (25%)
Fine aggregate	lbs/CY	1,109	1,217	1,096	1,249	1,079	1,258	1,143	1,183
Entrained air	% vol.	5	5	5	5	5	5	5	5
W/C ratio		0.47	0.42	0.45	0.44	0.42	0.45	0.41	0.44
Cement factor	Sk./Cy	5.5	6	5.5	5.5	5.6	5.5	6	5.5
Coarse aggregate factor		0.78	0.76	0.76	0.72	0.78	0.76	0.74	0.74
Max. coarse aggregate size	inch	1.5	1.5	1.5	1.5	1.5	1.5	1.5	1.5

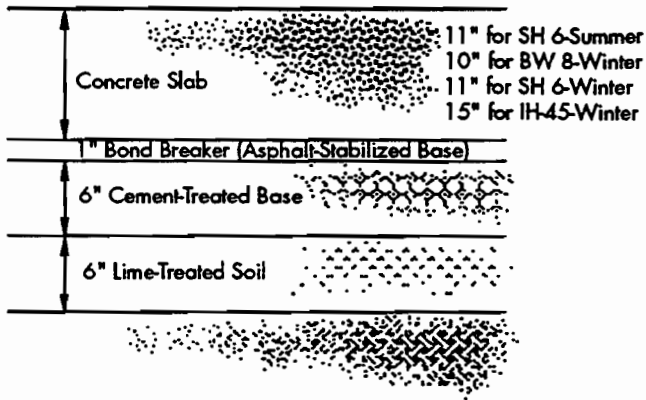


Figure 2.4 Typical pavement structure of the test sections

SH 6 Summer

This project, located on the two outside north-bound lanes of SH 6 approximately one-half mile south of US 290 in Houston, Texas, was the first to be constructed. The SRG sections are south of Huffmeister Road, while the LS sections are north of Huffmeister Road. The location and layout of the test sections are shown in Figure 2.5.

The concrete slab, 11 inches thick, used a single layer of steel (H. B. Zachry was the contractor). Placed on June 16, 1989, starting about 7:30 a.m., the SRG sections were completed about 3:30 p.m. that same day. Figure 2.6 shows the concrete

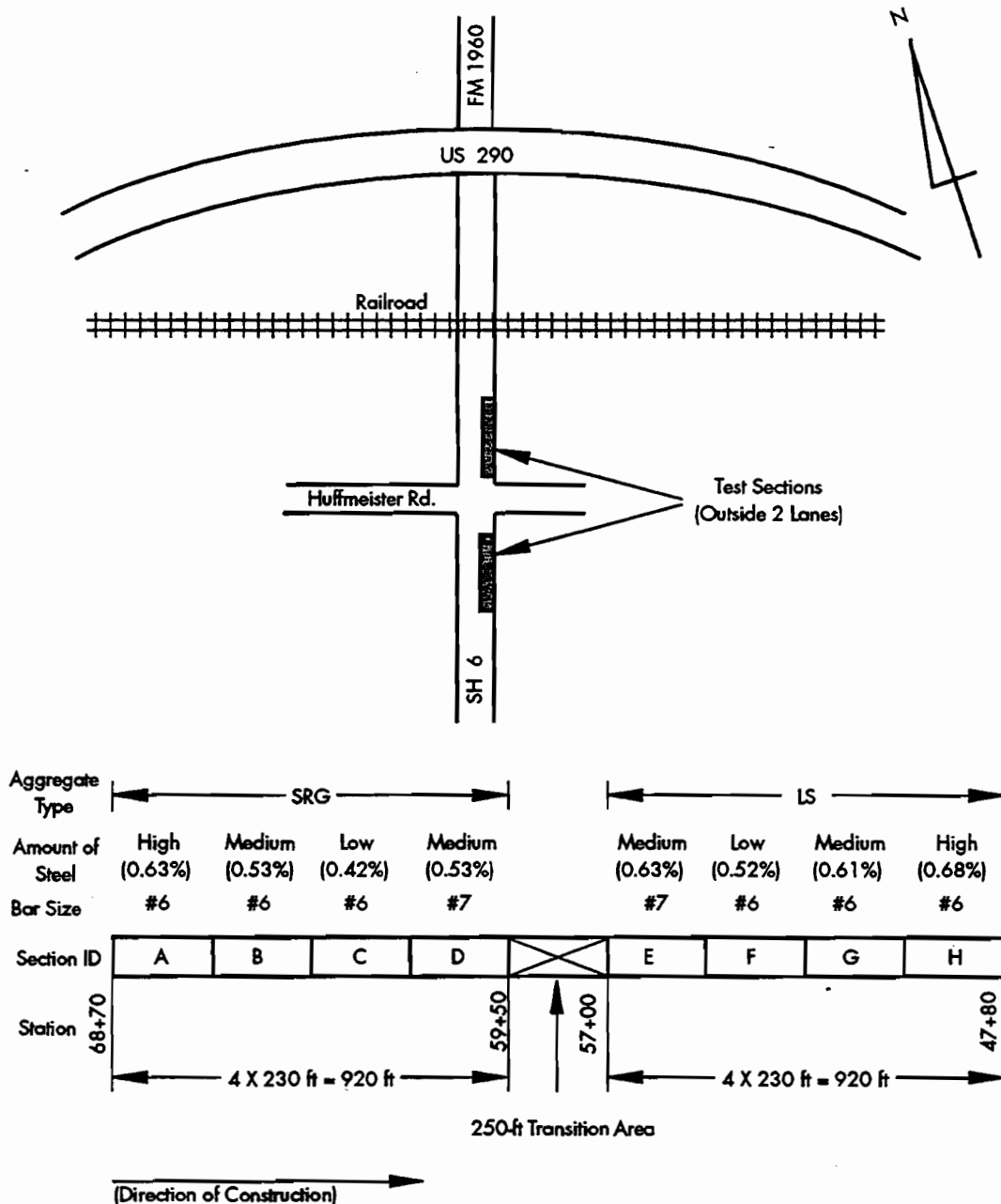


Figure 2.5 Location and layout of the first set of test sections (SH 6 summer)

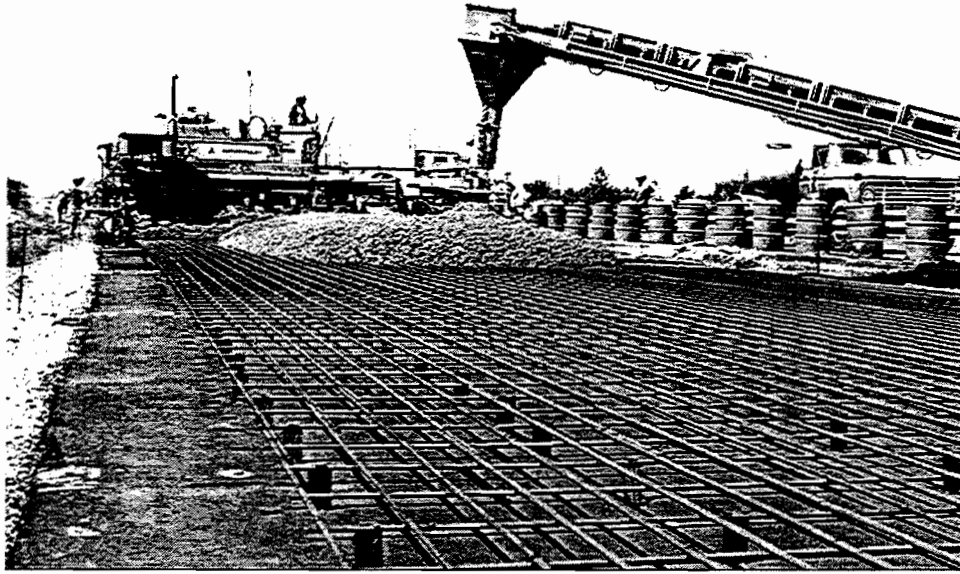


Figure 2.6 Concrete placement of test sections (SH 6 summer)

placement on the project. (As a parenthetical note, the equipment containing the tube float got stuck in a manhole about 500 to 600 feet from the beginning of placement, a mishap that delayed the concrete trucks for a short period until the equipment could be freed.)

The LS sections were placed on June 19, 1989. Again, the placement began about 7:30 a.m. and was completed about 3:30 p.m., with construction for the most part proceeding according to plans. (In another parenthetical note, we should mention that on the day before placement the steel had fallen onto the "bond breaker," leaving it relatively scarred and rough. The steel had to be repositioned onto the chairs before placement.)

BW 8 Winter

The second set of test sections was placed on Beltway 8 (north) on the eastbound frontage road on the inside two of the three lanes. Section A begins 315 feet east of the centerline of Antoine Road, with the sections continuing east. The location and layout of the test sections are shown in Figure 2.7.

The concrete slab, 10 inches thick, used a single layer of steel (the contractor was Brown and Root). The SRG sections were placed on November 24, 1989, while the LS sections were placed on November 25, 1989. It should be noted that, because of a breakdown at the mixing plant,

fly ash was not included in the construction of section H, and only partly included in the construction of section G.

SH 6 Winter

The third set of test sections was placed on State Highway 6 just south of Patterson Road, which is about 2-3 miles north of Interstate Highway 10. Test sections are on the two outside southbound lanes in a fill area marked by reinforced earth retaining walls. A concrete shoulder lies between the sections and the coping of the retaining wall. The location and layout of the test sections are shown in Figure 2.8.

The concrete slab was 11 inches thick and used a single layer of steel. The contractor of this project was, again, H. B. Zachry, who began construction of the test sections on January 10, 1990. Sections A and B were placed on January 10; sections C, D, and E were placed on January 11; sections F, G, and H were placed on January 12. The shoulder was placed a few days after the test sections. The contractor had a mixing plant set up near the job at Groeschke Road, with the concrete arriving at the project in flatbed trucks. Because the contractor did not have a sufficient supply of crushed limestone, SRG aggregates were used in the last 50 feet of section H (the last section). Overall, the placement of the test sections went well, though most of section C had problems with air dosage (only 3.5 percent air was noted).

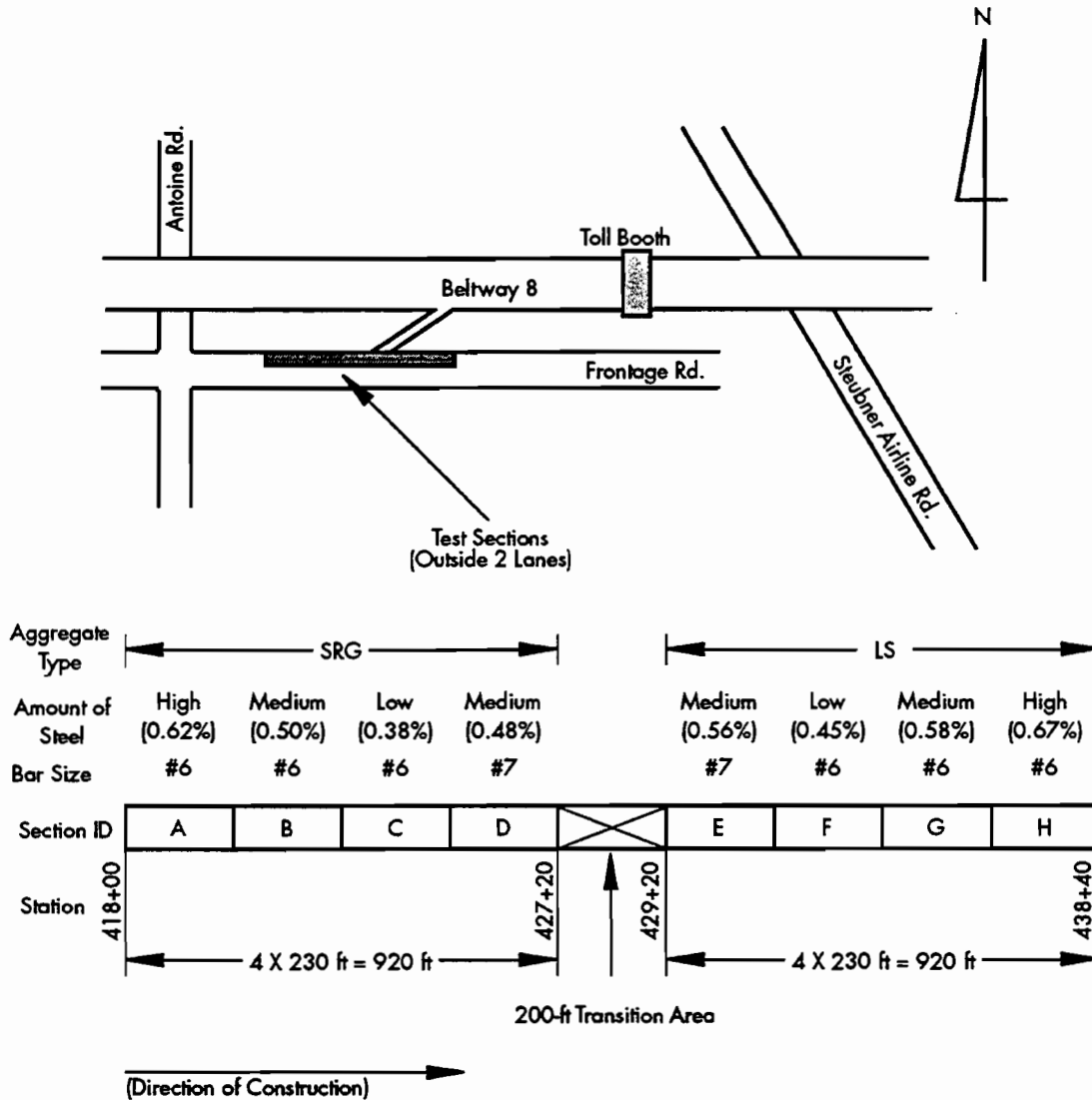


Figure 2.7 Location and layout of the second set of test sections (BW 8 winter)

IH-45 Winter

The last set of test sections was placed on Interstate Highway 45 on the north side of Houston at the Hardy Toll Road Interchange near Spring Creek. The cross section includes four lanes with a full-depth CRCP shoulder and an inside median. The test sections are on the two inside northbound lanes, with the median located next to the inside lane. (This location was chosen because it would allow for future observations using the inside median without having to control traffic.) The location and layout of the test sections are shown in Figure 2.9, where it may be noted that the order of placement of the

test sections was opposite that of other projects; that is, section D was placed first in SRG sections, and section H was placed first in LS sections. The end of section E is about 300 feet north of the north end of the Spring Creek Bridge.

The concrete slab for these sections was 15 inches thick and used double layers of steel (the contractor was McCarth Brothers). While the SRG sections were placed on January 14, 1990, the placement of the LS sections was delayed due to bad weather until January 21, 1990. The overall placement of the test sections was performed in good order, with no unusual construction problems occurring.

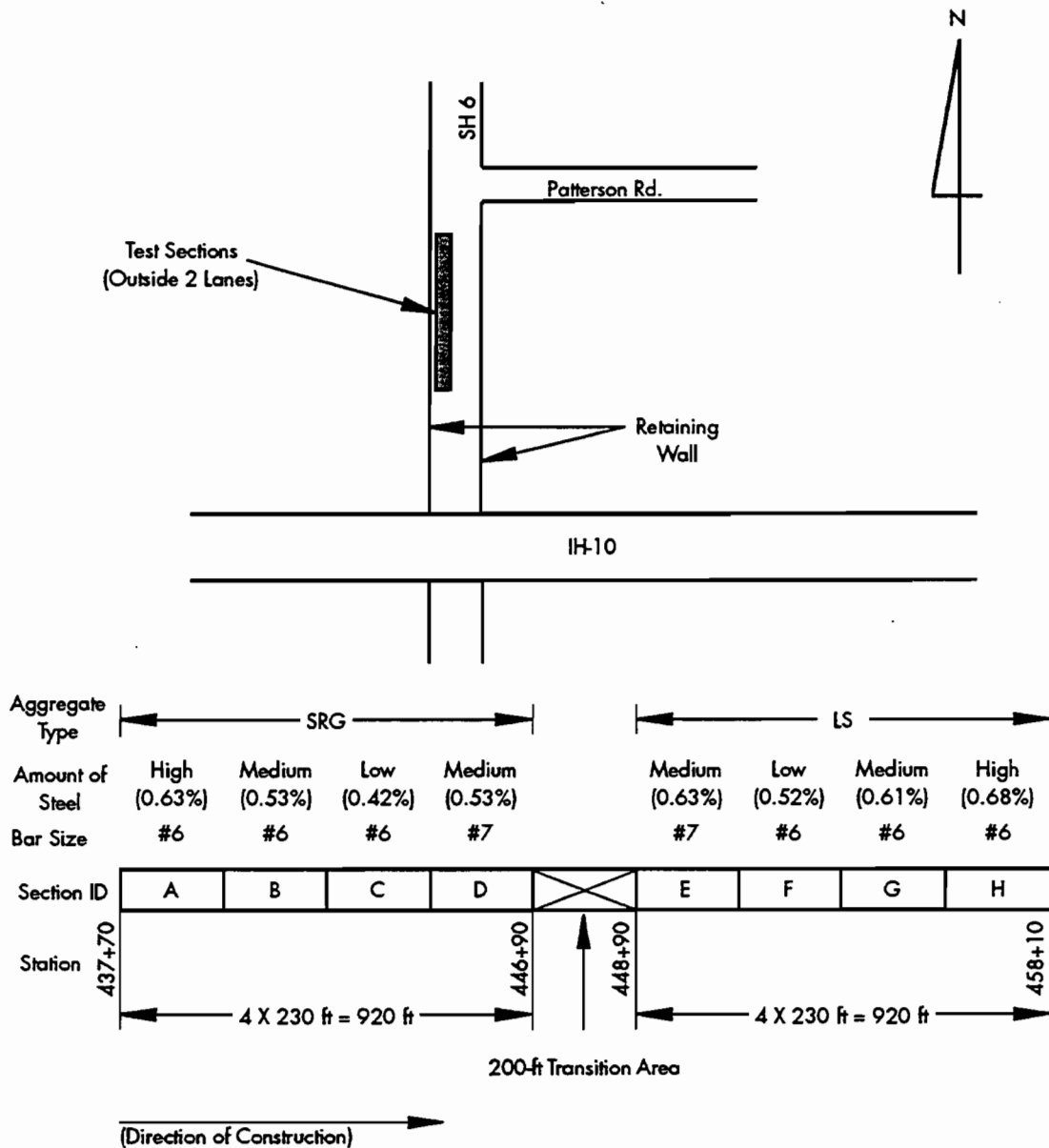


Figure 2.8 Location and layout of the third set of test sections (SH 6 winter)

INSTRUMENTATION AND DATA COLLECTION

The primary instrumentation installed in the test sections included thermocouples and Demac points for monitoring the concrete temperature and slab movement, respectively. Layout of the Demac points was designed to measure the slab movement longitudinally along a pavement from crack to crack. All instrumentation was placed about 3 feet from the pavement edge for ease of measuring. (Provisions for measuring the shrinkage of the concrete slab in the field are presented in Chapter 6.)

To provide a vertical temperature distribution throughout the slab, thermocouples were positioned 1 inch from the surface, at mid-depth, and 1 inch from the bottom of the slab. Four to seven

sets of thermocouples were imbedded at various locations in each project. Table 2.2 gives the locations of the thermocouples in each project, along with the time of concrete placement and the fresh concrete temperature at each thermocouple location.

To measure slab movement, 20 to 30 Demac points were placed at 10-inch intervals (SH 6 summer used 8-inch intervals) on the surface of the concrete. For each project, two sets of brass Demac points (one for SRG sections and the other for LS sections), covering a length of about 15 to 20 feet, were installed in sections with medium steel (sections B and G). Table 2.3 gives the locations of the Demac points in each project.

Data collected during the short-term monitoring (about 1 month after construction) included

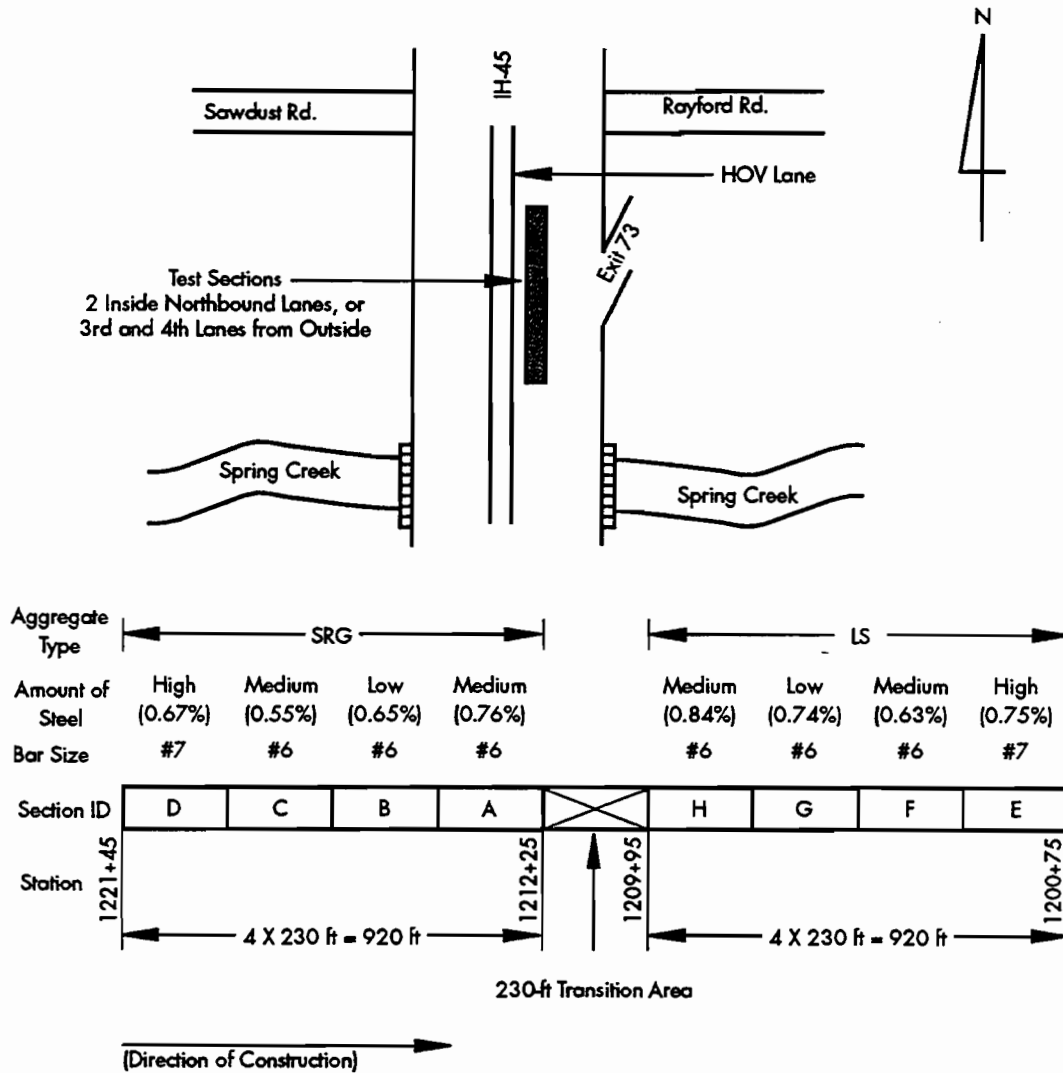


Figure 2.9 Location and layout of the fourth set of test sections (IH-45 winter)

(1) air and concrete temperature, (2) atmospheric conditions, (3) slab movement, and (4) transverse and longitudinal crack locations. Data were collected periodically over 24 hours for several days after construction. Although new cracks were monitored at various times throughout the day, most often they were surveyed in the morning, when the concrete temperature was low and when crack visibility was enhanced by the wider crack width associated with morning. Instruments used for measuring temperature, solar radiation, and slab movement are shown in Figures 2.10 to 2.12, respectively. In addition, crack width and concrete movement of experimental slabs were measured (see Chapters 5 and 6).

TESTING

To determine the concrete properties of the test sections, about 74 to 94 cylinders from each project were cast at the job sites using the same

concrete used in the test sections (Fig 2.13). The material was obtained from four different trucks for each project: two from the SRG sections and two from the LS sections.

On the day following casting, about one-half of the cylinders in each project were transported to the lab at the Center for Transportation Research in Austin for storage (until they could be tested in a chamber having a temperature of 75°F and a relative humidity of 45 percent). The remaining cylinders were cured in the field in the same manner as the pavement and transported to the lab 1 day before testing. The results of these tests were then used to compare the properties of the concretes cured under the two different conditions.

The lab-cured cylinders were tested at 3, 7, and 28 days, while the field-cured cylinders were tested at 7 and 28 days. Properties tested included split tensile strength, compressive modulus of elasticity, compressive strength, drying shrinkage, and thermal coefficient.

Table 2.2 Summary of instrumentation of thermocouples

Project	CAT¹	Section	Station	Time of Placement²	Fresh Conc. Temp. (°F)³
SH 6 summer	SRG	A	68+41	8:30 am (6/16/89)	86.4
		C	63+70	12:20 pm (6/16/89)	86.8
	LS	E	55+68	9:40 am (6/19/89)	84.4
		G	51+09	1:00 pm (6/19/89)	85.8
BW 8 winter	SRG	A	419+11	10:05 am (11/24/89)	65.4
		C	423+72	12:55 pm (11/24/89)	69.0
		D	425+91	2:15 pm (11/24/89)	71.0
	LS	E	430+20	8:25 am (11/25/89)	69.6
		F	432+85	10:10 am (11/25/89)	69.4
		G	435+35	11:35 am (11/25/89)	69.4
		H	437+10	1:15 pm (11/25/89)	69.4
	SH 6 winter	SRG	A	438+02	1:00 pm (1/10/90)
B			441+21	3:00 pm (1/10/90)	68.6
C			444+43	10:00 am (1/11/90)	67.0
LS		E	451+00	4:00 pm (1/11/90)	69.0
		F	452+70	10:00 am (1/12/90)	57.0
		G	455+24	11:20 am (1/12/90)	58.0
IH-45 winter	SRG	C/D ⁴	1219+15	8:00 am (1/14/90)	62.2
		A	1213+28	12:00 noon (1/14/90)	64.4
	LS	H	1208+10	10:15 am (1/21/90)	64.6
		E	1201+12	2:40 pm (1/21/90)	67.6

¹Coarse aggregate type

²Time of concrete placement at the location of thermocouple

³Measured in place when the mixed concrete was dumped from delivery truck

⁴Boundary of sections C and D

Table 2.3 Locations of Demac points

Project	CAT	Section	Beginning Station	End Station
SH 6 summer	SRG	B	64+70	64+50
	LS	G	50+96	50+76
BW 8 winter	SRG	B	421+23	421+47
	LS	G	435+09	435+34
SH 6 winter	SRG	B	441+19	441+47
	LS	G	455+25	455+51
IH-45 winter	SRG	B	1215+89	1215+64
	LS	G	1206+62	1206+38

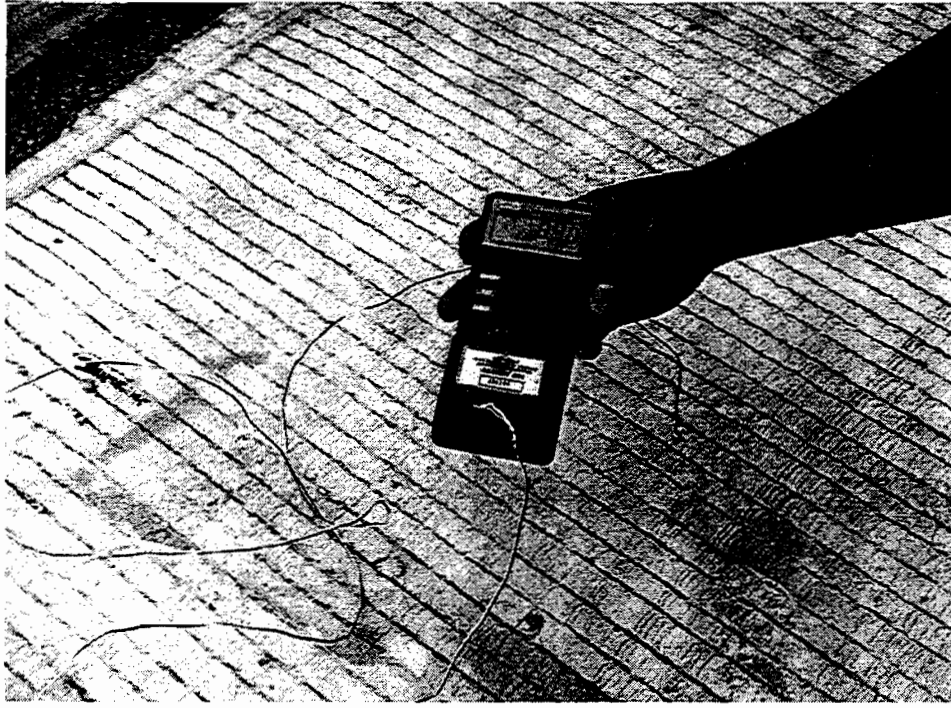


Figure 2.10 Thermometer for measuring air and concrete temperature

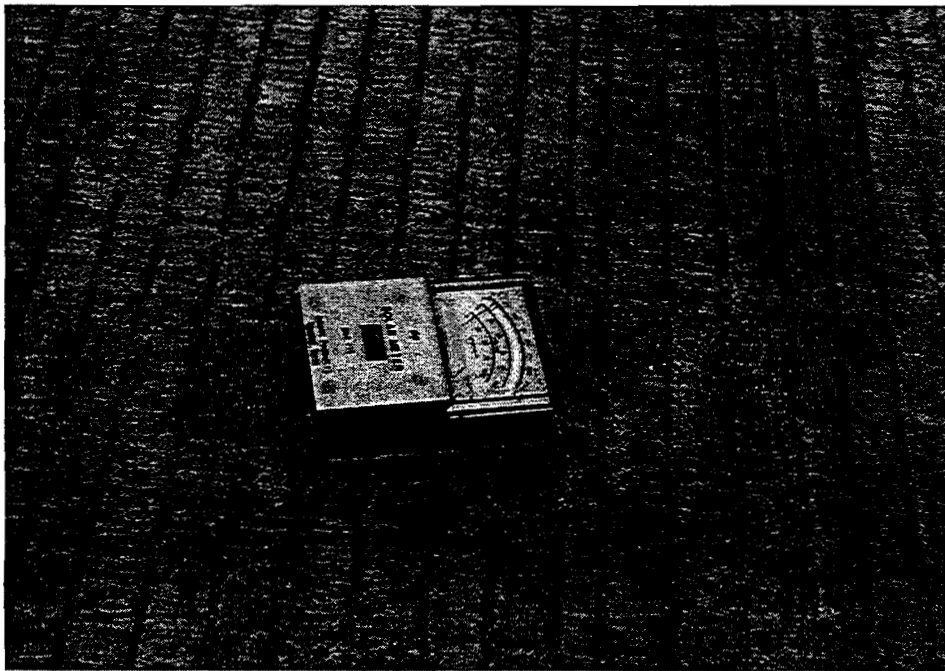


Figure 2.11 Solar-meter for measuring solar radiation

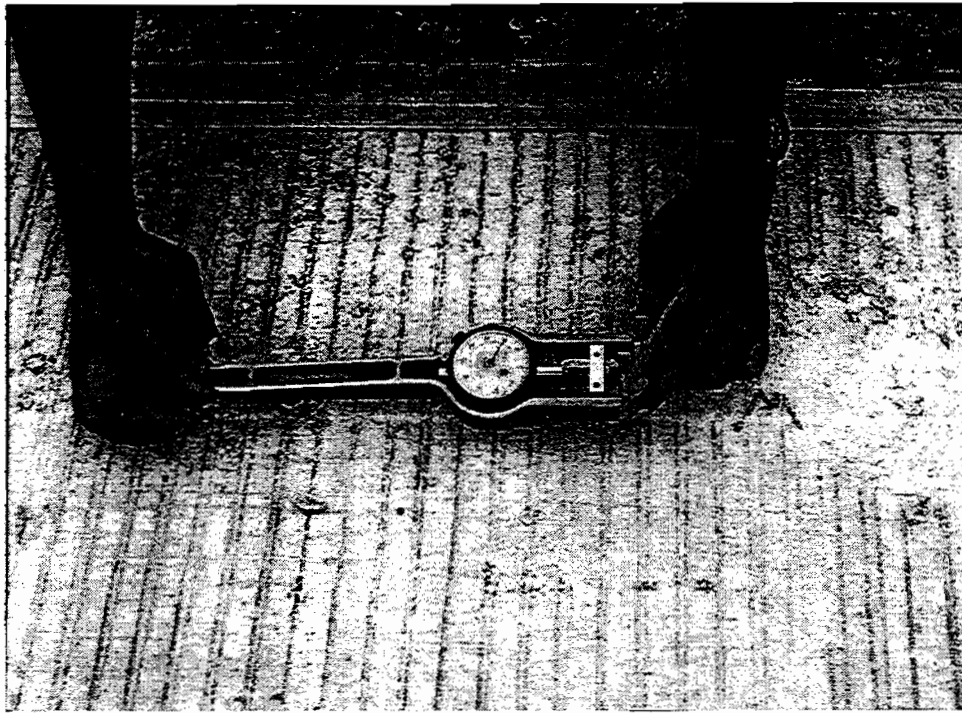


Figure 2.12 *Multi-position strain gauge for measuring slab movement*



Figure 2.13 *Cylinders being cast in the field*

CHAPTER 3. DATA PRESENTATION WITH DISCUSSIONS

This chapter discusses, first, the collected test section data relating to temperature, cracking, and slab movement. Second, this chapter reports on the location of new cracks between the two existing cracks, and the effect of pre-construction conditions on the early-age behavior of the CRCP. Topics that require detailed discussions are presented in Chapters 4 through 6, with cylinder test results summarized in Appendix B. The data for crack width and shrinkage correlation will be presented in Chapters 5 and 6, respectively.

SLAB TEMPERATURE

On pavements not yet opened to traffic, most cracks occur as a result of the volume changes brought about by concrete drying shrinkage and temperature variation. Unlike drying shrinkage, slab temperatures are very sensitive to the surrounding temperature condition. Accordingly, it is important to understand the nature of slab temperature when attempting to predict the behavior of concrete pavements, especially in their early ages. In this section, the nature of slab temperature for various conditions is discussed based on the temperature data collected from the test sections.

One of the most important characteristics associated with concrete temperature during the early age of the pavement is the heat of hydration (discussed in Chapter 4). Since the concrete mix releases heat during the cement hydration, the pattern of concrete temperature during the construction day is somewhat different from that occurring during the later ages of the pavement. The pattern of slab temperature occurring during the hydration depends on the surrounding temperature conditions (i.e., fresh concrete temperature, air temperature, and solar radiation).

Figure 3.1 shows the air and concrete temperature 3 days after construction for a typical summer placement. (Similar plots for other test sections are given in Appendix C; weather information during the short-term monitoring is given in Appendix D.) It was interesting that the temperature rise from initial conditions at the surface of the slab (measured at 1 inch below the

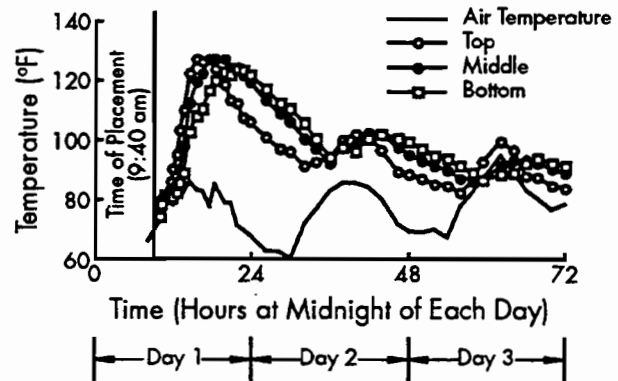


Figure 3.1 Typical temperature curves for concrete pavement placed in the summer (section E, SH 6 summer)

surface) for about 6 hours after construction was as high as 60°F. The peak concrete slab temperature during the hydration occurred about 6 to 12 hours after placement, depending on the depth of the slab. The peak magnitudes were about 140°F. The high peak and subsequent cooling of the slab temperature during the night resulted in a large variation of slab temperature during the first 24 hours after construction. This large temperature variation exerted a detrimental effect on the volumetric stability of the concrete.

Figure 3.2 shows typical temperature curves for concrete pavement placed in the winter. The

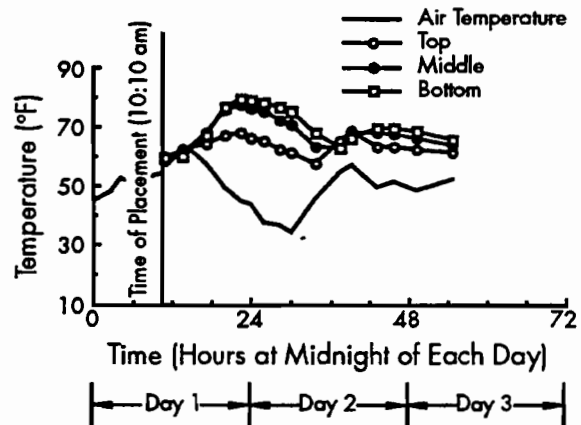


Figure 3.2 Typical temperature curves for concrete pavement placed during winter (section F, SH 6 winter)

maximum concrete temperature occurred during the night following the construction day, with a lower temperature rise (maximum temperature rise of 20°F at the middle of the slab) than that of summer construction. The peak concrete slab temperature was only about 80°F. Since the hydration heat was liberated during the night, the variation of slab temperature during the first 24 hours after construction was relatively small, providing a relatively good volumetric stability of the concrete.

The time of peak slab temperature for the summer construction depended on the depth of the slab. The slab temperature at the top reached its peak first and dropped quickly, whereas the slab temperature at the bottom peaked last and dropped relatively slowly, perhaps because the rate of hydration is affected by such variables as high solar radiation, high air temperature, and heat loss through the subbase. However, this order was not significant in the winter construction when the general temperature condition was low. As seen in Figure 3.2, the times at which peak temperatures were reached for different depths were almost the same.

It can be seen from Figures 3.1 and 3.2 that, at a given time, there were large differences between the concrete temperatures in the vertical direction of the concrete. The vertical temperature gradient may cause significant warping stresses.

The influence of atmospheric conditions on the slab temperature is shown in Figure 3.3. As may be noted, little variation in slab temperature was observed during the rainy/cloudy period. This might be a result of (1) the fairly constant air

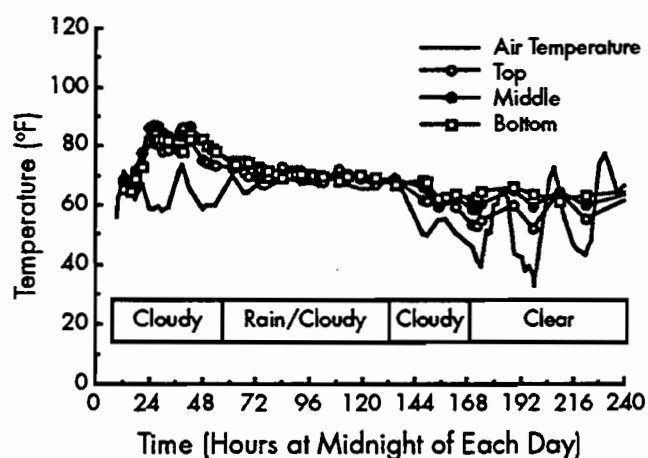


Figure 3.3 The influence of atmospheric conditions on the slab temperature (section A, IH-45 winter)

temperature, and (2) the near absence of solar radiation during this period. The high humidity and small variations in slab temperature during this period provided good curing conditions for the pavement. Until this period ended, no cracks were observed in this section. Because it reduces temperature variations and drying shrinkage, the occurrence of this type of weather during curing is beneficial to the concrete.

CRACKING

Figures 3.4 through 3.7 present plots of transverse crack patterns at several ages during the first month for the medium steel sections placed on SH 6 in the two different seasons. (In Appendix E, similar plots are given for the other sections.) On the plots for each age, the cracks that occurred since the previous age are shown progressively as one moves from top to bottom of the graph. Plots of mean crack spacing versus time will be presented in Chapter 8.

Cracking of the concrete pavement exhibited a strong correlation with the slab temperature variations. Almost without exception, cracks occurred when the slab temperature dropped significantly. As may be noted in Figures 3.4 to 3.7, the summer construction showed many more cracks, especially during the first several days, than the winter construction. Several longitudinal cracks were also observed during this period. This greater tendency toward cracking might be the result of the large temperature differential of the summer placement during the first 24 hours after construction (Fig 3.1). This subject is discussed further in Chapter 4.

The LS sections, without exception, showed fewer cracks, even though a little more steel was used in these sections than in the SRG sections (see Chapter 2 for the steel design for each aggregate type). It is believed that the steel did not have as much influence on cracking during the early ages because the bond between concrete and steel may not have been fully developed.

The LS sections sustained fewer cracks, perhaps because of the lower thermal coefficient, larger strain capacity, and lower elastic modulus of the concrete (Refs 4 and 6). Since the cracking that occurs in a pavement prior to traffic opening is mainly caused by the concrete's volume change, the lower thermal coefficient values of some

concretes serve to stabilize concrete volume. Lower elastic modulus and larger strain capacity decrease the potential for cracking for the same volume change.

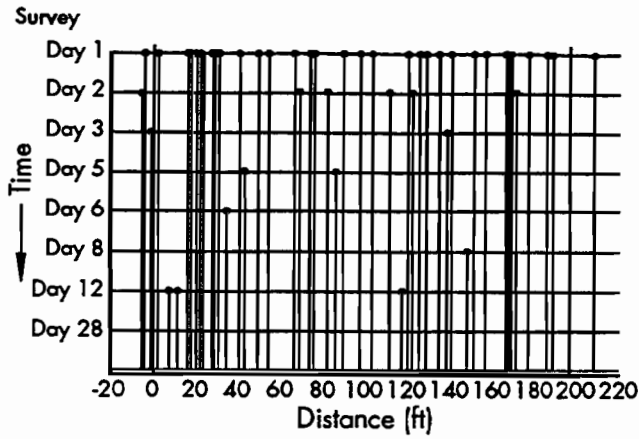


Figure 3.4 Time after placement until transverse cracks were observed (SRG, medium steel, SH 6 summer)

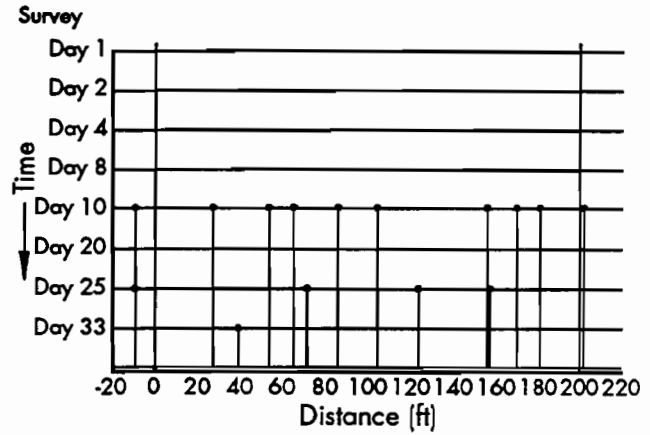


Figure 3.7 Time after placement until transverse cracks were observed (LS, medium steel, SH 6 winter)

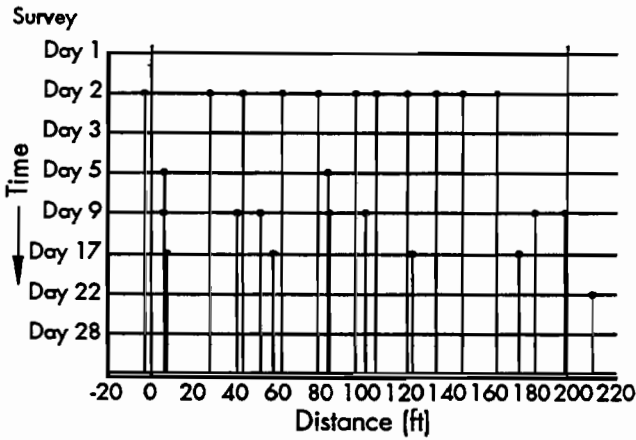


Figure 3.5 Time after placement until transverse cracks were observed (LS, medium steel, SH 6 summer)

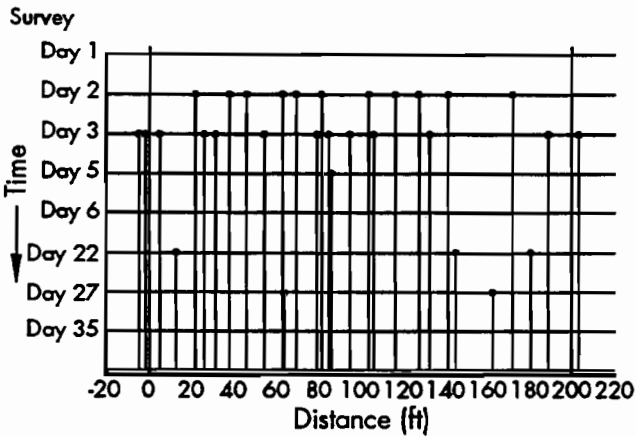


Figure 3.6 Time after placement until transverse cracks were observed (SRG, medium steel, SH 6 winter)

SLAB MOVEMENT

Slab movement data were collected by periodically measuring the distances between Demac points imbedded in the concrete. As an example use of these data, slab movements at different ages of the concrete slab are plotted (Fig 3.8). These were measured at about the same temperature conditions. It is shown that the slab movements at the cracks create large expansions caused by the crack opening, and that these large movements are absorbed by the cumulative contractions between the cracks. It is also shown that the crack width increases with time, possibly because of the progressive drying shrinkage of the concrete.

It was possible to determine the approximate time of transverse crack occurrence and the crack-mechanism by plotting the slab movement

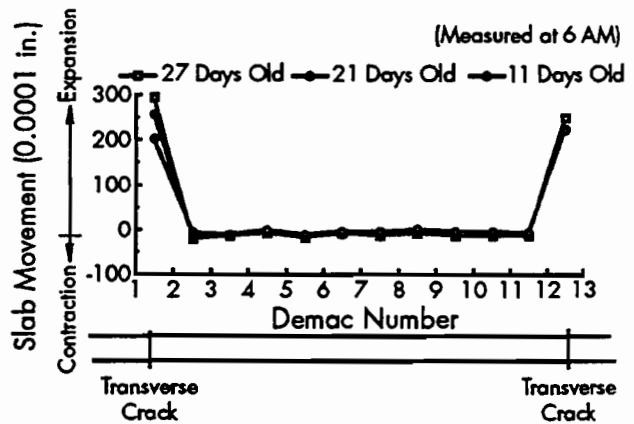


Figure 3.8 Slab movement at different ages of the concrete slab

data. Figure 3.9 shows the time of crack opening and the slab temperature at that time for typical summer construction. This crack was the first one detected from the area where the Demac points had been imbedded. This test section was placed on a hot summer day.

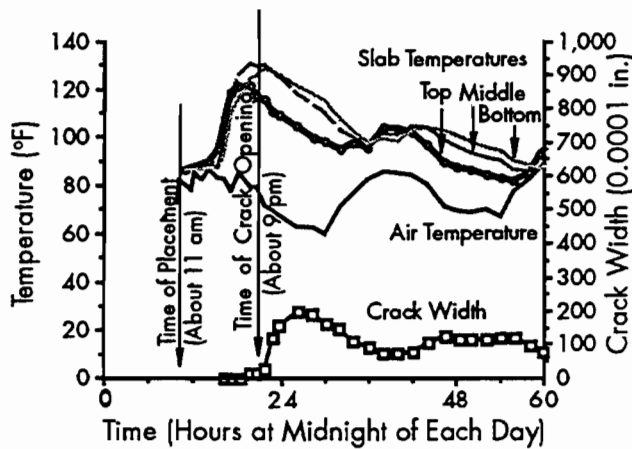


Figure 3.9 Time of crack opening and the condition of the slab temperature at that time (SRG, SH 6 summer)

As seen in Figure 3.9, the crack began to open when the slab temperature at the top surface dropped slightly after the peak; the difference between the top and bottom temperatures was fairly large, indicating that the crack occurred as a result of the warping stress created by the upward warping movement that results from the temperature gradient. It should be noted that the slab temperatures at the middle and bottom had not dropped.

As the slab temperature (at all positions through the thickness) dropped further, several more cracks were detected before the slab temperature reached the minimum for the day. These cracks may have occurred as a result of the tensile stress induced by the restraint of contraction movement (by subbase friction) caused by temperature drop and warping stresses.

Figure 3.10 shows a similar plot for winter construction. As can be seen, the first crack of the winter construction occurred much later than occurred in the summer construction, a result of the lower temperature change. Although stress conditions at the time of the first crack were fairly similar to those of the summer construction, we believe that tensile stress especially contributed to the cracking, insofar as the warping stress of the winter case was less than that of the summer case.

It should be noted that the transverse cracks for the summer construction began to occur during the night following the construction day, or about

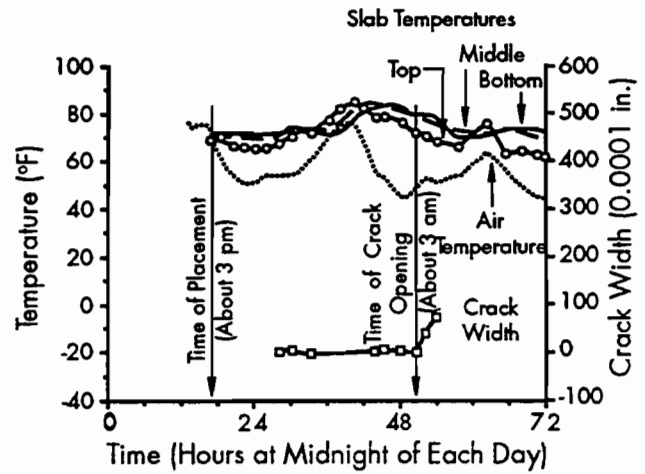


Figure 3.10 Time of crack opening and the condition of the slab temperature at that time (SRG, SH 6 winter)

10 hours after placement. Coincidentally, we found that the time of longitudinal crack occurrence appeared to be coextensive with that of transverse crack occurrence. The next day after construction (24 hours after placement), following the sawing of the longitudinal joints, several longitudinal cracks were observed. It is believed that these longitudinal cracks had occurred prior to the sawing of the joints. Thus, based on our observations, we recommend—as a way of avoiding unwanted longitudinal cracks—that the longitudinal joint of the concrete pavement placed in hot weather be sawed during the evening of the construction day, or as soon as the concrete gains sufficient strength for the sawing operation, and before the concrete temperature drops too low. However, pavements placed later in the afternoon might be too soft to withstand sawing, and should thus be sawed the next day, since, in any event, such pavement has a much lower risk of sustaining longitudinal cracks during the first night after construction (see Figs 4.13 and 4.14 in Chapter 4). Figure 3.11 shows the proposed sawing schedule for the summer construction.

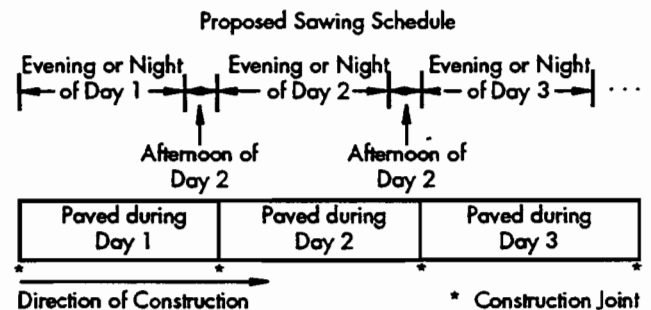


Figure 3.11 Proposed sawing schedule for the longitudinal joint for the summer construction

Figure 3.9 also shows the changes of crack width at various times of the day. Once the crack occurred, the crack width varied with the recorded slab temperature changes. Specifically, crack width increased when the slab temperature went down, and it decreased when the slab temperature rose. Since the slab movements were measured from the top surface, slab temperature at the top showed better correlation with the crack width change than slab temperature at the middle or bottom. It was interesting to note, however, that the maximum crack width occurred when the temperature gradient began to decrease (not when the slab temperature at the top was at its minimum reading). This effect might be the result of the relief of the upward warping movement caused by reduced temperature gradient after the time of maximum crack width.

PATTERN OF NEW CRACKS IN A SLAB SEGMENT

It has long been theorized that, for any homogeneous concrete pavement slab on a subbase, transverse cracks would occur near the center of the slab segment, given that the tensile stress by temperature change or drying shrinkage is greatest at the center. And as new slabs are formed by the cracking, they in turn would crack near the center. The process would continue until the maximum concrete stress was checked by the concrete strength. Since, however, there are many other factors affecting crack location (e.g., variability of the concrete strength and subbase friction), cracks may not necessarily occur near the center.

To investigate the pattern of new cracks occurring in the slab segments in the field, the location of the new cracks were plotted from the crack survey data of the test sections. This plot is presented in Figure 3.12, where each data point represents the distance of the new crack from the center line in proportion to the existing crack spacing (relative location in terms of the longitudinal length of the slab segment). For example, if the slab segment was 8 feet long and the new crack formed 2 feet from the middle of the slab segment, the proportionate distance would be 25 percent of the original length (2 ft/8 ft = 0.25). In some case, however, two or more cracks occurred within one slab segment between crack surveys. These data were not considered in this plot, since the sequential occurrences of the new cracks could not be ascertained.

Figure 3.12 shows that the location of the new cracks depends on the length of the existing crack spacing. There was a relatively consistent trend in

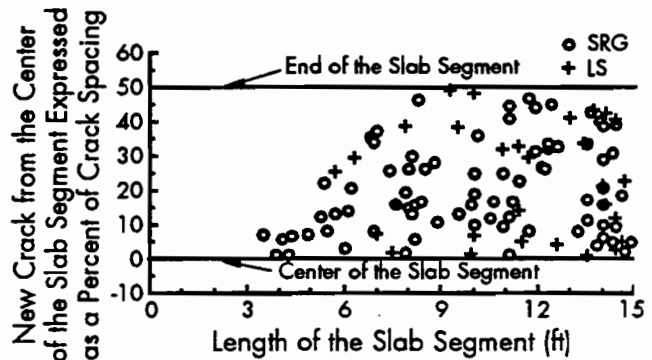


Figure 3.12 Distribution of the locations of the new cracks in various lengths of slab segments

the location of the next crack when the slab length was less than about 8 feet: (1) when the existing crack spacing was about 3 feet, the next crack within the slab segment, if any, occurred almost without exception near the middle of the slab segment; and (2) as the length of the slab segment increased, the maximum distance of the new cracks occurring in the middle of the slab segment increased. When the crack spacings were larger than about 8 feet, the locations of the new cracks were randomly distributed. Figure 3.12 also shows that, for less than 5 feet, the LS slab segments did not crack.

From these distributions, it may be postulated that when the crack spacing is small, the concrete stresses induced by temperature change, drying shrinkage, and warping movement increase from zero at the crack to a maximum at the middle of the slab segment, as conceptually shown in Figure 3.13(a). For that reason, cracks should occur at the center of the slab if the concrete strengths and restraint by the steel bars and subbase friction are homogeneous. In the field, however, the new cracks would not necessarily occur exactly at the middle of the slab segment, a result of the

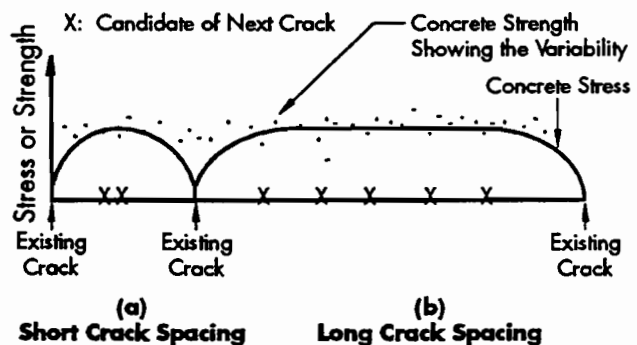


Figure 3.13 Distribution of concrete stress for different crack spacings (conceptual)

variability of concrete strength (represented by the data points in Figure 3.13). Thus, for the short slab segment (i.e., 3 feet), the maximum stress occurs only over a small area near the center, a circumstance that minimizes the effect of variability. If the slab segments are long enough, the entire middle area of the slab segment has approximately the same stresses (Fig 3.13), which then allows variability of strength to come into effect. Therefore, the locations of the next cracks will be randomly scattered over the high stress area. This phenomenon can best be modeled by tensile strength variation, assuming a normal distribution.

EFFECT OF PRE-CONSTRUCTION CONDITIONS

To evaluate the effects of various pre-construction conditions, steel layouts and the surface condition of the bondbreaker/subbase were surveyed. For future monitoring, locations of interest were recorded or marked on the subbase outside the slab with paint before the concrete placement. These locations included areas showing bondbreaker/subbase cracks, steel splices, badly deformed bondbreaker surfaces, and manholes. During the period of the short-term monitoring, pavement conditions at these marked spots were surveyed in terms of the existence of cracks and their shapes.

Reflection of Cracks

Surveys were performed on two projects, SH 6 summer and BW 8 winter, to identify the effect of subbase cracks on the slab cracking. Figure 3.14 shows an example of the cracks in the bondbreaker. From our observations, it appears that most of these cracks were reflected from the subbase (6-inch cement-treated base).

Figure 3.15, a graph of percent reflected cracks by coarse aggregate type and seasonal placement, summarizes the survey results. In that survey, we found that many of the transverse cracks in the CRCP occurred directly over transverse cracks in the bondbreaker/subbase. During the short-term monitoring (approximately 1 month after construction), about one-half of the cracks in the bondbreaker/subbase were reflected through the concrete slab. In general, more subbase cracks were reflected in the summer construction than in the winter construction. And, as shown in Figure 3.15, a greater percentage of subbase crack reflections occurred in the SRG sections than in the LS sections.

Most of the reflected cracks of the summer construction, occurring within a few days, had meandering shapes of the kind shown in Figure 3.16, an example of the meandering transverse cracks associated with early-age reflection. The entire length of this kind of crack may not have

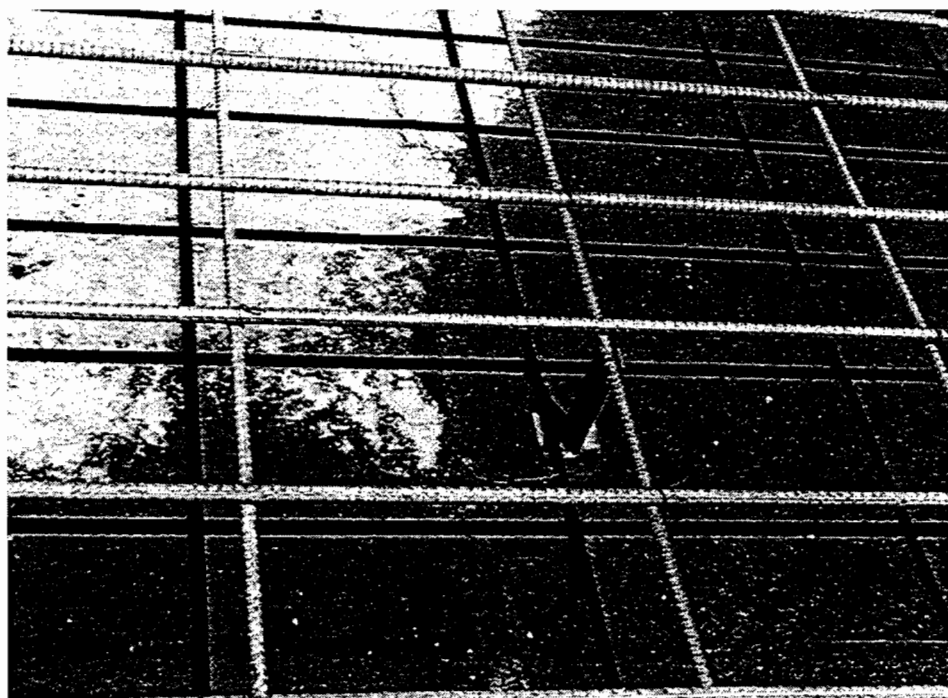


Figure 3.14 An example of cracks in the bondbreaker

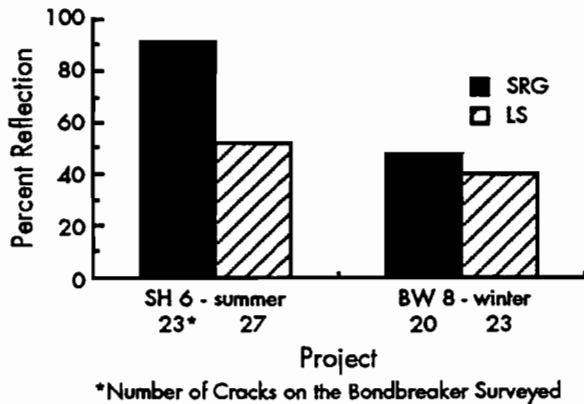


Figure 3.15 Reflection of cracks in the bondbreaker

occurred directly over the crack in the bondbreaker, but the randomness may have occurred as a result of the interaction of reflection and the spatial variability of concrete strengths.

Compared with the summer construction, the winter construction showed a lower rate of reflection of cracks, and the shapes of the reflected cracks were less meandering. It should be noted that the summer and winter projects were at different locations and had slabs of different thicknesses; however, the materials and mix designs of the concrete were similar.

Interestingly, the bondbreaker, whose purpose is to circumvent reflection cracks, allowed about half the cracks to reflect through. In such cases, water will directly infiltrate through the reflected cracks into the roadbed soil or lime-treated base, making these layers soft. And because the same thermal and shrinkage volume changes that occur in concrete are applicable to cement-stabilized base, it is recommended that additional studies be made to improve the bondbreaker/subbase system.

Effect of Steel Splices

Cracks in the concrete slab were surveyed in the areas of the normal longitudinal steel splices (two bars are tied). Surveys were performed in the LS sections of SH 6 summer and in both the SRG and LS sections of BW 8 winter.

For the summer construction (LS sections of SH 6 summer), 94 percent (16 out of 17) of the spliced areas experienced cracks within 10 days. Most of these cracks occurred near one end of the spliced area (rather than in the middle), a result perhaps of the sudden change in the amount of steel apportioned at the ends of the staggered splices. However, the general shapes of the cracks were not meandering.

For the winter construction (BW 8 winter), only 18 percent (3 out of 17) of the spliced areas

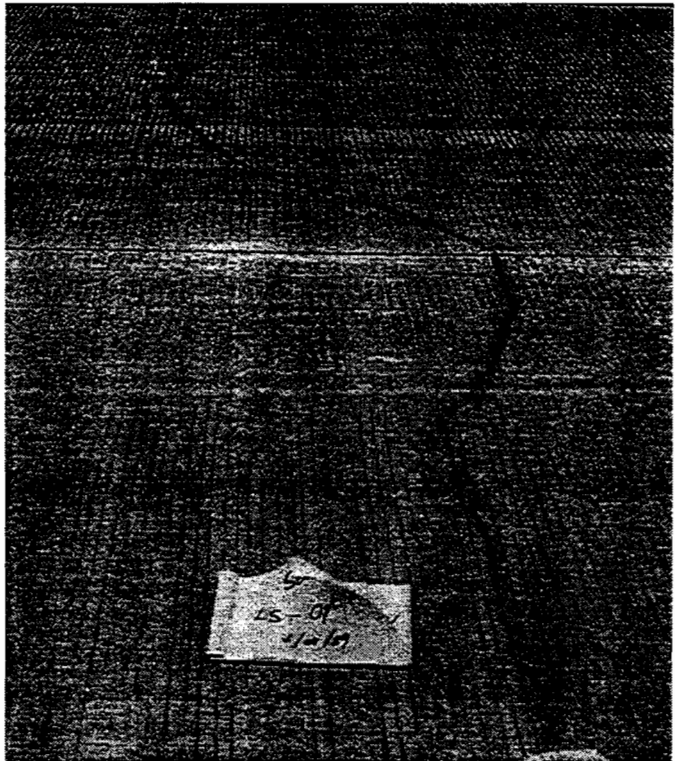


Figure 3.16 Examples of meandering transverse cracks associated with early-age reflection

on the LS sections showed cracks near one end of the splices. For the SRG sections, 73 percent (11 out of 15) of spliced areas showed the same kind of cracks.

Effect of Badly Deformed Surface of Bondbreaker

LS sections of SH 6 summer showed "construction scars" and other bad surface conditions. A typical example of a badly deformed surface is shown in Figure 3.17.

A total of nine deformed surfaces, three of which were very closely spaced together, were marked and monitored after construction. Figure 3.18 shows cracks in this area at the age of 10 days. For the longitudinal cracks appearing on the badly deformed surfaces, we decided on one possible explanation: The rough surface of the bondbreaker increased the friction between the concrete and the bondbreaker, restraining the movement of the concrete in the transverse direction. Two other deformed surface areas also showed longitudinal or meandering cracking. The remaining four showed cracks of no special shape.

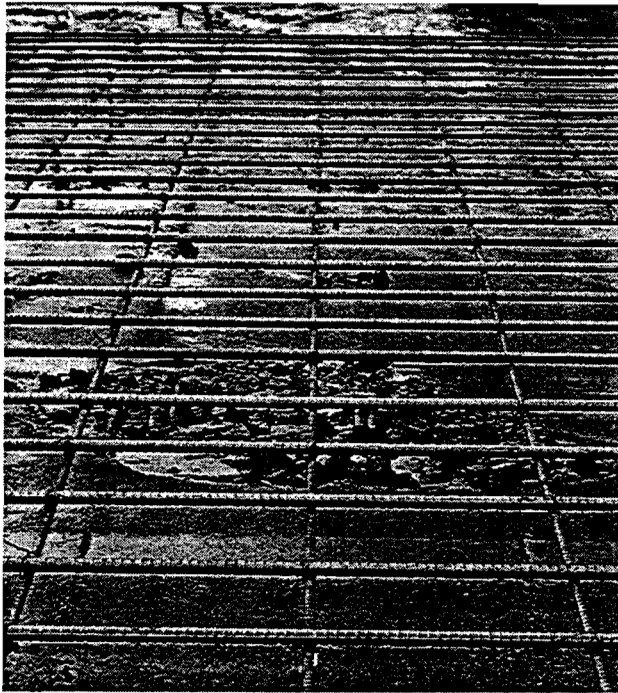


Figure 3.17 Typical example of the badly deformed surface of the bondbreaker

Cracks around Manhole

Of the several manholes in the paved area of the SH 6 summer project, all showed two to five meandering cracks in the surrounding area. Within 1 year after construction, these areas were showing severe distress and spalling along the cracks. Figure 3.19 gives an example of this type of crack. To mitigate such cracking, we recommend either that the manholes be relocated at the design stage (based on the long-term benefit-cost study), or that the steel design be adjusted for the condition.

Transverse Cracks over Transverse Steel Bars

One surprising observation made during the crack surveys was that many of the transverse cracks occurred over the transverse steel bars, a phenomenon even more evident in the sections constructed with double-layered steel.

On two of the projects (SH 6 winter and IH-45 winter), measurements were obtained on new construction by observing the longitudinal pavement edge. In each case where multiple transverse tie bars were used, the location of the transverse steel could be seen easily from the edge. On another project (BW 8 winter), the placement of the adjacent lane obscured the longitudinal placement edge, making difficult a determination of the relationship of the transverse crack to the transverse bar; a Pachometer had to be used

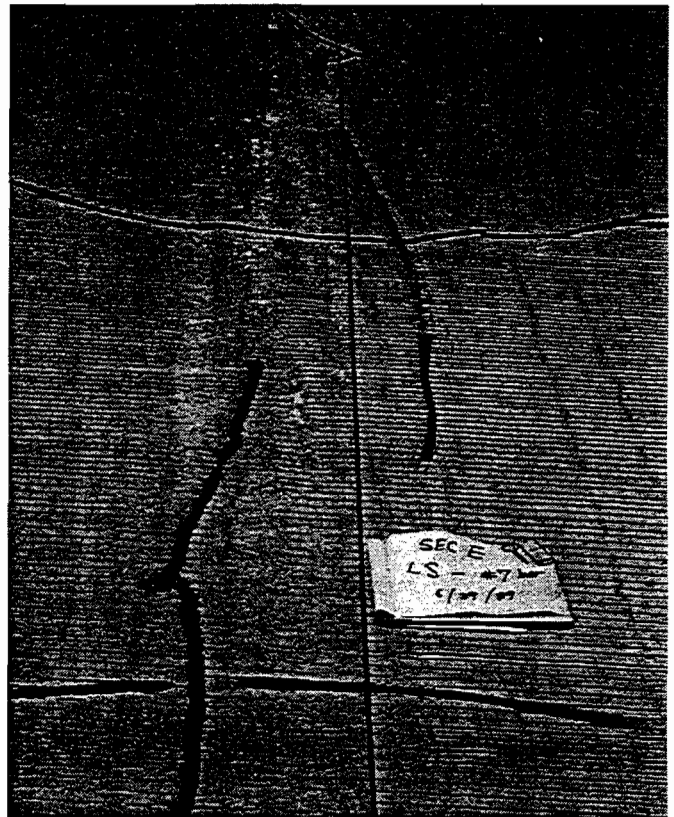


Figure 3.18 Longitudinal cracks occurred in the pavement (under which three badly deformed bondbreaker surfaces are closely spaced)

to find the transverse bar. As this device was positioned along the pavement and the bar was located, the pavement was marked. Records were then made of the location of the crack with respect to the bar.

Figure 3.20 shows the percent of transverse cracks that occurred over transverse steel by placement season, number of steel layers, and coarse aggregate type. In general, sections with double-layered steel showed a higher probability for sustaining these types of cracks.

The higher probability of this type of crack occurring in the pavement with double-layered steel is perhaps owing to the placement of two transverse steel bars at different depths in the same vertical plane, as shown in Figure 3.21(a). The cross-sectional area of the concrete of the plane including the two layers of transverse steel is smaller than other planes by the cross-sectional area of the steel (10 percent reduction in the cross-sectional area when two layers of No. 6 bars are used in a 15-inch slab). The result is a weakened plane, one that increases the probability of cracking along the plane. Such cracking, in turn, increases the possibility of water contacting the steel, a situation that can result in steel corrosion.

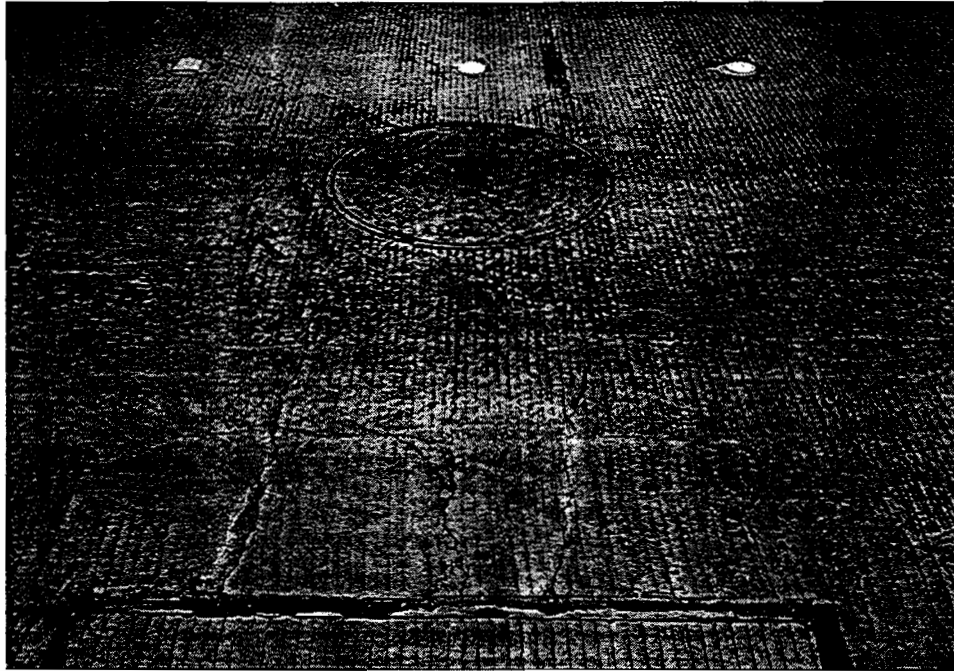


Figure 3.19 Typical cracks around the manhole (SH 6, summer, 1 year after construction)

As shown in Figure 3.21(b), a staggered layout of the transverse steel (top to bottom) is recommended as a way of avoiding this problem.

SUMMARY

In this chapter, data collected from the test sections were presented with brief discussions. These data included slab temperature, cracking, slab movement, pattern of new cracks, and the

effect of pre-construction conditions. Detailed discussions are presented in the following chapters.

Slab Temperature

The pattern of slab temperature during the hydration depends on the surrounding temperature conditions (i.e., fresh concrete temperature, air temperature, and solar radiation). For the summer construction, the temperature rise owing to the hydration was as high as 60°F (Fig 3.1). The peak concrete slab temperature during the hydration occurred during the daylight hours, about 6 to 12 hours after placement (depending on the depth of the slab). The peak magnitudes were about 140°F.

For the winter construction, on the other hand, the maximum concrete temperature occurred during the night following placement, with such temperatures lower than those recorded during summer construction (Fig 3.2). The peak concrete slab temperature was only about 80°F (maximum

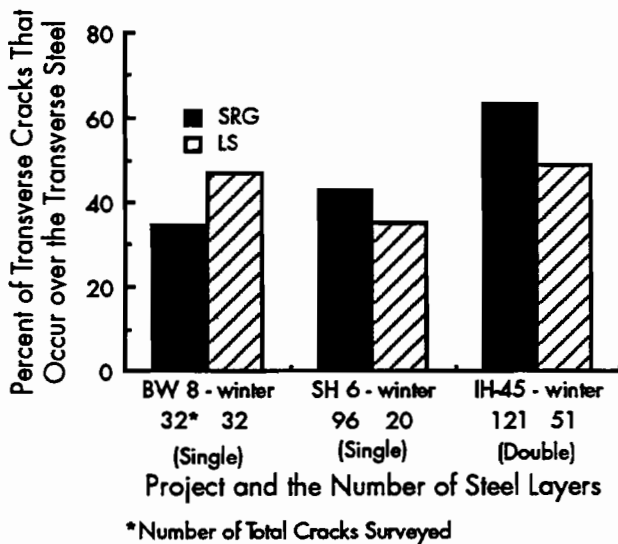


Figure 3.20 Percent transverse cracks occurred over the transverse steel for each steel arrangement type and coarse aggregate type

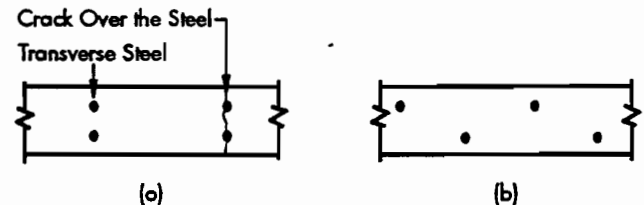


Figure 3.21 (a) Current steel layouts of the double-layered steel, and (b) recommended steel layouts

temperature rise of 20°F at the middle of the slab).

The time of peak slab temperature for the summer construction depended on the depth of the slab (Fig 3.1). The slab temperature at the top reached its peak first and dropped quickly, whereas the slab temperature at the bottom peaked last and dropped relatively slowly. This effect might be the result of the rate of hydration, which is affected by such variables as high solar radiation, high air temperature, and heat loss through the subbase. However, this order was not significant for the winter construction, when temperatures were generally low (Fig 3.2).

There were large differences between the concrete temperatures in the vertical direction of the concrete. The vertical temperature gradient may cause significant warping stresses (Figs 3.1 and 3.2).

Cracking

Cracking of the concrete pavement had a strong correlation with the slab temperature variations. Almost without exception, cracks occurred when the slab temperature dropped significantly. The summer construction showed many more cracks, especially during the first several days, than the winter construction. Several longitudinal cracks were also observed in the summer construction during this period. No longitudinal cracks were observed in the winter construction.

The LS sections showed fewer cracks, even though slightly more steel was used in these sections than in the SRG sections (Figs 3.4 to 3.7). It is believed that the steel did not have as much influence on cracking during the early ages (i.e., before the bond between concrete and steel had fully developed). Possible reasons for less cracking in the LS sections include the lower thermal coefficient, larger strain capacity, and lower elastic modulus of the concrete.

Slab Movement

It was possible to determine the approximate time of first transverse crack occurrence and the cracking mechanism by plotting the slab movement data. For the summer construction, transverse cracks began to open when the slab temperature at the top surface dropped slightly after the peak, and when the difference between the top and bottom temperatures was fairly large, indicating that the crack occurred as a result of the warping stress created by the temperature-gradient-induced upward warping movement (Fig 3.9). For the winter construction, the temperature

gradient was smaller than that of the summer construction (Fig 3.10).

For the summer construction, the transverse cracks began to occur during the night following the construction day, or about 10 hours after placement. The time of longitudinal crack occurrence may be coextensive with that of the transverse cracks. Longitudinal joints were sawed during the next day after construction, or 24 hours after placement. Several longitudinal cracks were observed during the cracking survey conducted the morning after construction. It is believed that these longitudinal cracks had occurred prior to sawing the joints. To avoid unwanted longitudinal cracks, we recommend that the longitudinal joint of the concrete pavement placed in hot weather be sawed during the evening of the construction day, or as soon as the concrete gains sufficient strength for the sawing operation (Fig 3.11).

Pattern of New Cracks in a Slab Segment

The location of the new cracks depended on the length of the existing crack spacing (Fig 3.12). There was a relatively consistent trend in the location of the next crack when the slab length was less than about 8 feet: (1) when the existing crack spacing was about 3 feet, the next crack within the slab segment, if any, occurred almost without exception near the middle of the slab segment; and (2) as the length of the slab segment increased, the maximum distance of the new cracks extending from the middle of the slab segment increased. When the crack spacings were larger than about 8 feet, the locations of the new cracks were randomly distributed.

Effect of Pre-Construction Conditions

Many of the transverse cracks in the CRCP occurred directly over transverse cracks in the bondbreaker/subbase (Figs 3.14 and 3.15). During the short-term monitoring (about 1 month after construction), about one-half of the cracks in the bondbreaker/subbase were reflected through the concrete slab. In general, more subbase cracks were reflected in the summer construction than in the winter construction. It was also shown that greater reflection of the subbase cracks occurred in the SRG sections than in the LS sections.

Most of the reflected cracks of the summer construction occurred within a few days, and these cracks had meandering shapes (Fig 3.16). The entire length of this kind of crack may not be directly over the crack in the bondbreaker, but

the randomness might occur as a result of the interaction of reflection and the spatial variability of concrete strengths. Compared with the summer construction, the winter construction showed a lower rate of reflection of cracks; additionally, the shapes of the reflected cracks were less meandering.

For the summer construction, 94 percent of the spliced areas experienced cracks within 10 days. Most of these cracks occurred near one end of the spliced area, rather than in the middle. This might be a result of the sudden change in the amount of steel used at the ends of the splice, even though the splices were staggered. However, the general shapes of the cracks were not meandering. For the winter construction, only 18 percent of spliced areas on LS sections showed cracks near one end of the splice. For the SRG sections, 73 percent of spliced areas showed the same kind of cracks.

LS sections of SH 6 summer showed "construction scars" and other bad surface conditions (Fig 3.17). Meandering longitudinal cracks were

observed where three of the construction scars were very closely spaced together (Fig 3.18).

There were several manholes in the paved area of the SH 6 summer project, all of which showed two to five meandering cracks in the surrounding area. Within 1 year after construction, these areas were showing severe stress and spalling along the cracks (Fig 3.19). Either the manholes should be relocated at the design stage (based on the long term benefit-cost study), or the steel design should be adjusted for the condition.

One interesting observation made during the crack surveys was that many of the transverse cracks occurred over the transverse steel bars, a phenomenon that was more significant in the sections having double layers of steel. Cracking over the steel bars increases the possibility of water contacting the steel, resulting in a higher probability of steel corrosion. As shown in Figure 3.21(b), a method for mitigating these types of cracks is to provide a staggered (top to bottom) layout of the transverse steel.

CHAPTER 4. HEAT OF HYDRATION AND EARLY-AGE CRACKS IN CONCRETE PAVEMENT

In our monitoring of the test sections constructed in the summer (SH 6 summer), we found that the concrete temperature rose from 89°F to 141°F within the first 6 hours after concrete placement, primarily as a result of the interaction of the heat of hydration and the hot-weather condition. During the first night the concrete temperature dropped to 100°F, creating a significant temperature differential (41°F) that contributed to the formation of numerous early-age cracks (including longitudinal cracks).

This report defines early-age cracks as those cracks occurring within a few days (1 or 2 days) after construction and which are attributed to a large shrinkage and temperature differential between the peak temperature from the heat of hydration and subsequent cooling. The early-age crack patterns have a tendency to be meandering, with relatively wide crack widths (see Ref 7 and Chapter 6 of this report). Because it increases the probability of Y-cracking, punchouts, spalling, and steel rupture, both the meandering tendency and the wide widths of cracks may have an adverse effect on the long-term performance of the concrete pavement.

It is believed that the dominant factor influencing the occurrence of early-age cracks is the placement season. Most of the early-age cracks observed were in the test sections placed during the hot season; fewer early-age cracks were observed for the cool-weather placement. For the hot-weather placement, the frequency of early-age cracking varied even with the time of placement during the day.

In documenting the effect of heat of hydration and temperature condition on the early-age behavior of concrete pavement, the following issues are discussed in this chapter:

- (1) heat of hydration and early-age concrete,
- (2) influence of the time of concrete placement, and
- (3) control of concrete temperature during hydration.

HEAT OF HYDRATION AND EARLY-AGE CONCRETE (LITERATURE REVIEW)

Nature of Hydration

First of all, we must report that a survey of the literature revealed that no research has been conducted on the specific effect of the heat of concrete hydration on the early-age behavior of concrete pavement. Consequently, the following remarks are based on our own experiences and on the general observations of other researchers.

Hydration of the fresh concrete is accompanied by the release of energy in the form of heat, with the actual rate of heat release varying with time. Figure 4.1 (Ref 8) shows a typical pattern of heat generation during the hydration of tricalcium silicate, the major compound of cement. The hydration reactions of other compounds have a similar pattern.

Mixing portland cement compounds with water results initially in a rapid release of heat, which then ceases within about 15 minutes. (This reaction probably represents the heat of the solution of aluminates and sulfates in the mixture; see Ref 9). The primary heat-generation cycle begins hours after the cement compounds are mixed with water. Before this primary cycle, concrete is in a plastic state and is relatively inactive chemically. The peak of the primary cycle is reached several hours after concrete is mixed with water. At this stage, the major hydration products crystallize from the solution of the mixture. This stage includes the time of initial and/or final set of the concrete. As hydration products grow, they form a barrier to the infiltration of additional water; the reaction slows and may eventually stop when there is no room for further growth of crystals, or when hydration is theoretically completed (Ref 8).

It should be noted that, because the reaction is chemically controlled, the rate of hydration is very sensitive to temperature, especially during the primary cycle (Ref 8). Therefore, the

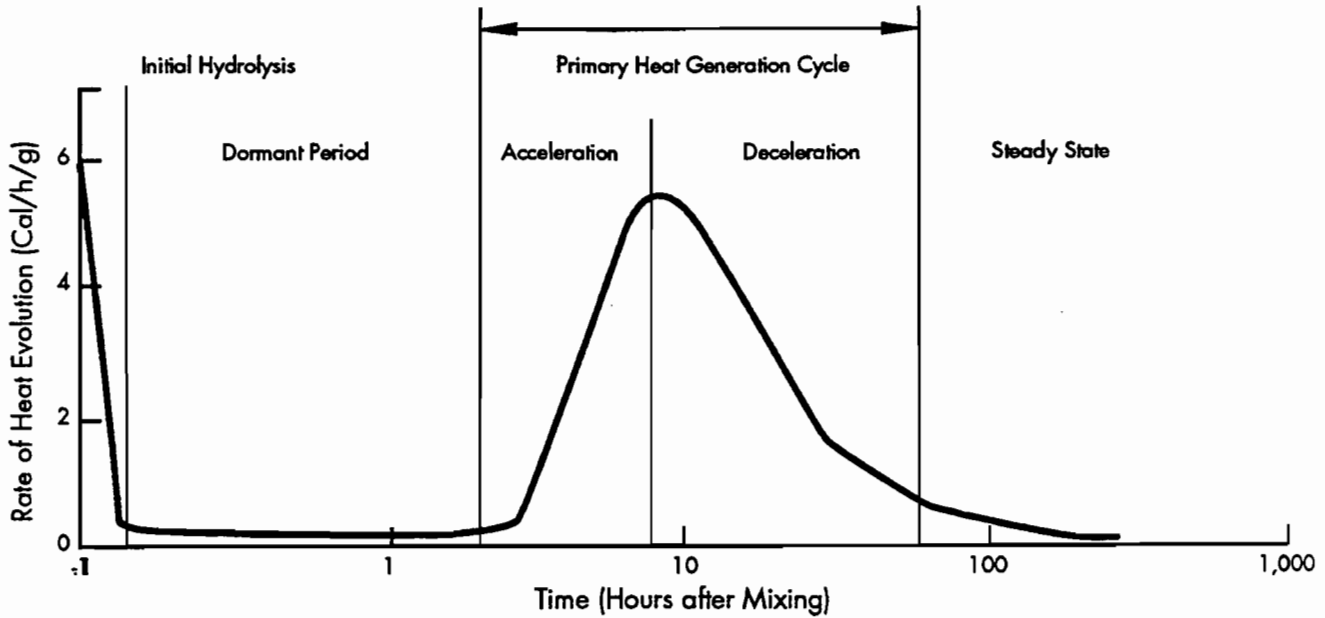


Figure 4.1 Typical pattern of heat generation during the hydration of tricalcium silicate (Ref 8)

temperature condition during construction is an important factor affecting the rate of hydration. Figure 4.2 (Ref 10) shows the effect of curing temperature on the hydration of tricalcium silicate. It can be seen that the higher the curing temperature, the faster the heat release and the higher the peak.

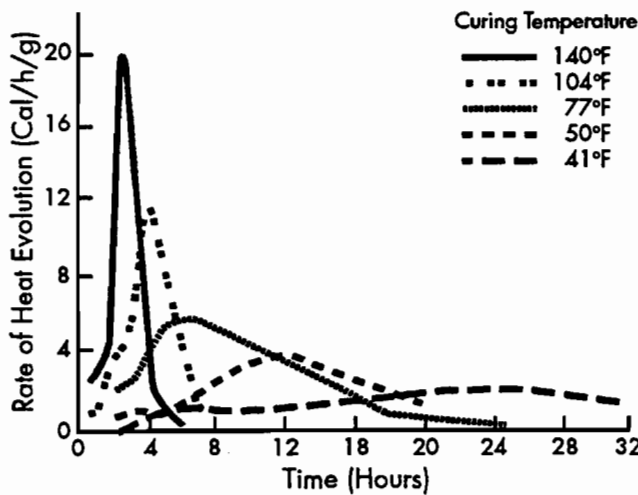


Figure 4.2 Effect of curing temperature on the hydration of tricalcium silicate (Ref 10)

Heat generation and buildup depend on many factors, including the chemical composition of the cement, water-cement ratio, fineness of the cement, amount of cement, admixture, dimension of the concrete, ambient temperature, and fresh

concrete temperature. Tricalcium silicate ($3\text{CaO} \cdot \text{SiO}_2$) and tricalcium aluminate ($3\text{CaO} \cdot \text{Al}_2\text{O}_3$) are the compounds of cement primarily responsible for the high heat generation. An increase in the water-cement ratio, fineness of cement, and/or curing temperature increases the heat of hydration (Ref 11).

Heat of hydration can be useful in cold weather placement: It often generates enough heat to provide a satisfactory curing temperature, obviating the need for other temporary heat sources (Ref 11). In hot weather, however, heat of hydration can be detrimental to the concrete.

Undesirable Effect of High Temperature on Concrete

High temperature may induce in fresh concrete such undesirable effects as increased water demand, increased rate of slump loss, increased rate of setting, increased tendency for plastic shrinkage cracking, difficulties in controlling entrained air, and critical need for prompt curing. On hardened concrete, high temperature may result in decreased strength, increased shrinkage, increased creep, decreased durability, and non-uniformity of surface (Refs 11 and 12). Detailed information about these effects is given in many sources (Refs 11, 12, and 13). In this section, only the effects associated with the heat of hydration will be discussed.

Because hydration of cement, as mentioned earlier, is a chemical process, the higher the

temperature of concrete mix, the greater the rate of hydration. A large temperature rise by hydration may cause excessive internal stresses when differences exist in thermal expansion factors of various concrete constituents (Refs 14 and 15). In addition, because the curing temperature affects the rate of hydration, and because the strength of concrete depends on its time-temperature history, the strength of the concrete is also influenced by curing temperature (Ref 16). While it is generally known that the higher the curing temperature, the higher the early strength, this advantage is subsequently offset by lower long-term strength potential (Refs 12, 15, and 17). Higher early-age strength is a result of the faster hydration of cement with high temperature. Decrease of long-term strength is caused by the poor physical properties of the micro-structure of the concrete (a large portion of the pores) resulting from a rapid initial hydration (Ref 18). Klieger (Ref 19) stated that there is a temperature during the early life of the concrete that may be considered optimum with regard to strength at later ages. For Types I and II cement, this temperature is 55°F (Ref 19).

Stresses in Concrete During the Hydration

Most of the heat of hydration is generated during the early age of the concrete. When a concrete is volumetrically restrained, the expansion force by the hydration heat will cause compressive stress. This compressive stress is relatively low, owing to the stress relief provided by creep and to the relatively low elastic modulus characteristic of early-age concrete (Ref 17).

The compressive stress will be relieved soon after the concrete begins to cool after the peak of hydration (Refs 20 and 21). A further decrease in temperature and subsequent contraction of the concrete will cause tensile stress to develop. This contraction occurs at a later age when the elastic modulus is greater and stress relief provided by creep is less. The tensile stress will cause cracking if the stress exceeds the tensile strength of the concrete (Ref 15). The higher the temperature drop, the greater the possibility of cracking.

Tensile Strain Capacity of Concrete at Early Ages

For a given shrinkage and/or temperature drop, whether the concrete cracks depends on the strain capacity of the concrete. Tensile strain capacity is the tensile strain at the failure or extensibility of concrete. Many investigators (Refs 22, 23, and 24) have pointed out that the tensile strain capacity

varies with time, and that there is a period at which tensile strain capacity becomes minimum. Variations in the strain capacity result from the difference in the development patterns of elastic modulus and strength during the early age of concrete; when elastic modulus develops fast and strength develops slowly, the strain capacity becomes small (brittle), and vice versa. Development patterns of elastic modulus and flexural strength with time for mortar beams (Ref 24) are shown respectively in Figures 4.3 and 4.4, where we see that the elastic modulus begins to develop at a higher rate than strength during the first several hours; the result is a small strain capacity during this period.

Kasai (Ref 22) determined the relationship between the age and the tensile strain corresponding to 95 percent of the tensile strength for concrete with ordinary portland cement (Fig 4.5). The time of minimum tensile strain varies with temperature (Ref 23), water-cement ratio, and use of admixture (Ref 22). In this example, the minimum tensile strain capacity occurred approximately 7 hours after mixing.

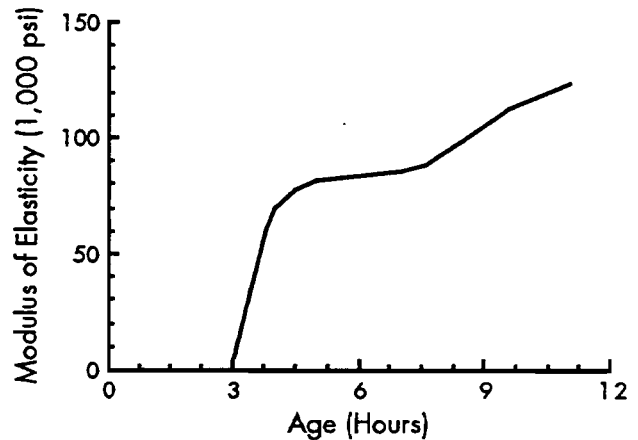


Figure 4.3 Development pattern of elastic modulus with time for mortar beams (Ref 24)



Figure 4.4 Development pattern of flexural strength with time for mortar beams (Ref 24)

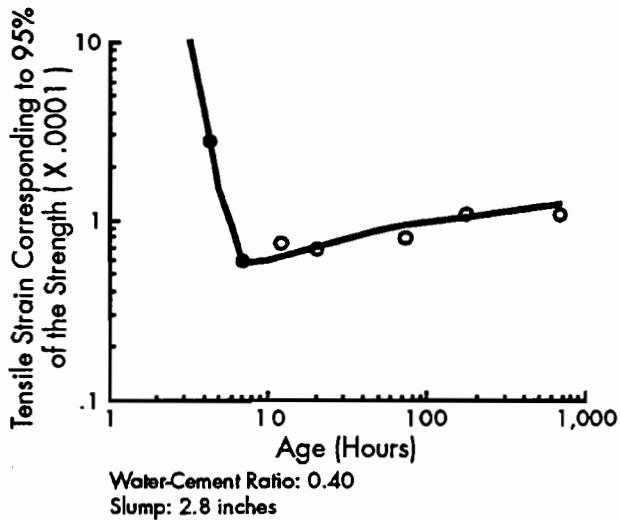


Figure 4.5 Variations of tensile strain corresponding to 95 percent of the tensile strength (Ref 22)

During the period of minimum strain capacity, concrete will be very brittle and sensitive to volume changes, with even minimal drying shrinkage or slight temperature drop both capable of causing cracks. For this reason, proper curing at this time is very important.

Summary of Literature Review

Hydration of the fresh concrete is accompanied by the release of energy in the form of heat, with the rate of heat generation varying with time. The primary heat generation cycle begins several hours after the cement compounds are mixed with water; before this primary cycle, concrete is in a plastic state and is relatively inactive chemically (Fig 4.1).

Since the reaction is chemically controlled, the rate of heat generation is very sensitive to ambient temperature conditions, especially during the primary cycle. The higher the ambient temperature conditions, the higher the peak concrete temperature and the shorter the time needed to reach that peak temperature (Fig 4.2).

High temperature rise by rapid hydration may cause excessive internal stresses when the thermal expansion factors of various concrete constituents differ. Temperature conditions during the construction day also affect the strength of concrete. The higher the curing temperature, the higher the early strength, but this advantage is subsequently offset by lower long-term strength.

Many investigators have pointed out that the tensile strain capacity varies with time, especially during the first 24 hours, and that there is a

period at which tensile strain capacity becomes minimum (Fig 4.5). During the period of minimum strain capacity, concrete will be very brittle and sensitive to volume changes. Again, for this reason, proper curing at this time is very important.

INFLUENCE OF THE TIME OF PLACEMENT ON EARLY-AGE CRACKING

Our monitoring revealed that the test sections constructed during various seasons of the year displayed differences in crack patterns. As explained in Chapter 2, one project was constructed in the summer, three were constructed in the winter. In the summer project, many more early-age cracks were observed than in the winter projects. These early-age cracks tended to be wider and have more meandering shapes.

The existence of this seasonal effect on the behavior of concrete pavement was confirmed in the mid-1950s in experiments using test sections placed in Pennsylvania (Refs 25 and 26). There, a seasonal difference in the crack pattern was observed in two experimental CRCP test sections constructed during opposing seasons of the year. One project was constructed under hot-weather conditions (average high temperature was 85°F and average low was 67°F), whereas the other project was constructed under cool-weather conditions (the average high was 66°F and the average low was 44°F). The hot-weather-placed section displayed approximately 85 percent more cracks than were found in the same length of cool-weather-placed section. And in spite of the closer crack spacing exhibited for the hot-weather construction, crack widths were greater than those for the cool-weather construction.

In a 16-year study on an experimental CRCP placed on IH-45 in Walker County, Texas, substantially more failures were found with higher curing temperatures (Ref 27). The effect of the curing temperature (or seasonal effect) on the crack spacing during the early age of the pavement was also significant (the pavement having the higher curing temperature had smaller crack spacings), although the crack spacing leveled out with time.

Another interesting phenomenon associated with the hot-weather construction was that the crack pattern also varied with the time of day of the placement. In all the test sections placed in Houston in 1989, in those placed in Walker County in 1960, and in those placed in Pennsylvania in 1957, it was observed that there were more early-age cracks in the pavement placed earlier in the day, as compared with that placed

later in the day. For the cool-weather construction, however, this effect of the time of placement was not observed.

In the following section, these phenomena are investigated vis-à-vis the effect of the ambient temperature condition on the hydration of cement. Temperature and crack data were obtained from the two projects placed in the summer and winter on State Highway 6 in Houston (SH 6 summer and SH 6 winter). Both projects had the same thickness (11 inches), had the same materials in the concrete, and were constructed by the same contractor. Using the temperature curves obtained from these projects, the following sections discuss the effect of the time of concrete placement on the early-age behavior of the concrete pavement.

Seasonal Effect

Demonstrating that the effect of slab temperature (measured 1 inch from the surface) is related to the season during which construction takes place, Figure 4.6 shows that, for the summer construction, the peak concrete temperature was high (in excess of 140°F)—an effect attributed to the high air temperature and to the high initial temperature of the fresh concrete.

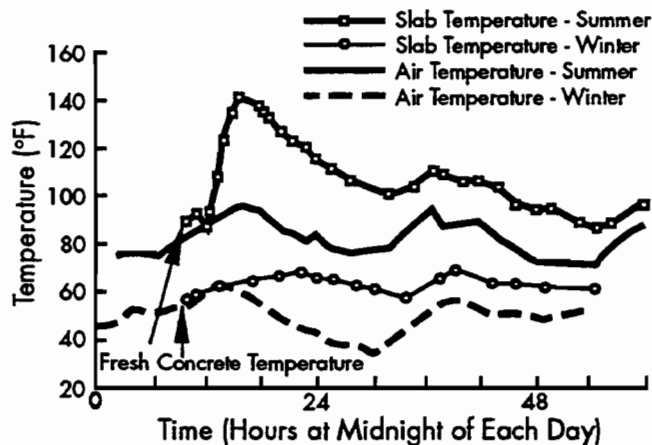


Figure 4.6 Seasonal effect on the slab temperature during the first 3 days after construction

Since the hydration of cement is a chemical process, a high ambient temperature will increase the rate at which the concrete hydrates. High solar radiation during construction also plays an important role in increasing the concrete temperature and the rate of hydration. This faster rate of hydration produces a higher and earlier peak concrete temperature during the construction day (see Fig 4.2).

During the first night following placement, the concrete temperature dropped drastically as the air cooled. The next morning we observed numerous transverse cracks, a result of the first night's large temperature differential. Numerous longitudinal cracks were also observed prior to the sawing of the longitudinal joint. Finally, additional cracks were observed as the concrete slab continued to cool.

For winter construction, on the other hand, both air temperature and fresh concrete temperature were much lower than they were during summer construction. Hydration, therefore, proceeded at a much slower rate, producing a very small temperature rise. To a certain degree, the hydration heat essentially compensated for the heat lost during the night. This resulted in the small temperature changes observed during the first 24 hours after placement. Owing to the low temperature differential, the section sustained no cracking (until a cold front passed through the area).

The higher probability of early-age cracking in pavements placed under higher temperature conditions was also reported in the experiments on the test sections in Pennsylvania (Ref 26). Figure 4.7 shows the relationship between crack spacing (at 7 days after construction) and the maximum air temperature on the construction day, with each data point representing the average crack spacing of each day's run. The data show that the higher the curing temperature, the greater the cracking.

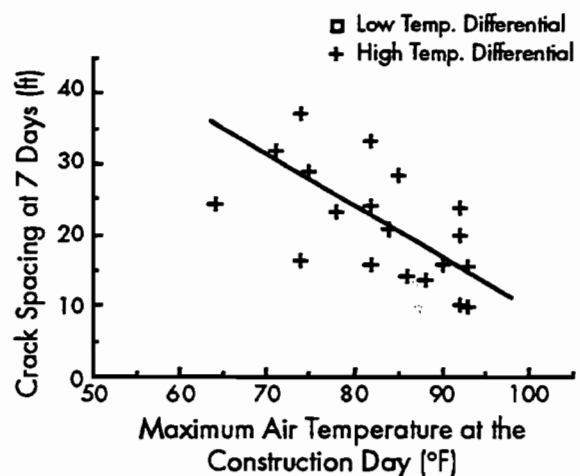


Figure 4.7 Relationship between crack spacing at 7 days after construction and the maximum air temperature at the construction day (daily air temperature differential greater than 10°F; plot drawn using the data in Ref 26)

While cracking itself is not a problem in CRCP, we did note that the shapes of cracks observed during summer construction were significantly more meandering than those observed during winter construction (Ref 7). It should also be noted that the summer construction resulted in many more early-age cracks than resulted from winter construction. Among cracks observed during summer construction, cracks occurring during the first night following construction showed more meandering shapes (Ref 7) and were wider than those observed later. Typical early-age cracks occurring during summer placement are shown in Figure 4.8 (early-age crack widths will be discussed in detail in Chapter 5). It is believed that the tendency of crack meandering at early ages is caused by the relatively heterogeneous state of the freshly hardened concrete (Ref 27). The aggregate in the concrete, much stronger than the mortar at early ages, can cause cracks to extend in different directions.

Longitudinal cracking was another problem associated with summer construction (Fig 4.9). Both the wide, meandering cracks and the longitudinal cracks increase the possibility of distress at later ages.

Figure 4.10 shows the percentage of the roadway experiencing failure after 14 years of service for a range of maximum air temperatures during concrete placement. As may be noted, substantially more failures occurred when the concrete

placement temperature was in the range of 90°F to 99°F.



Figure 4.9 Typical longitudinal crack occurring with summer placements (SH 6 summer)

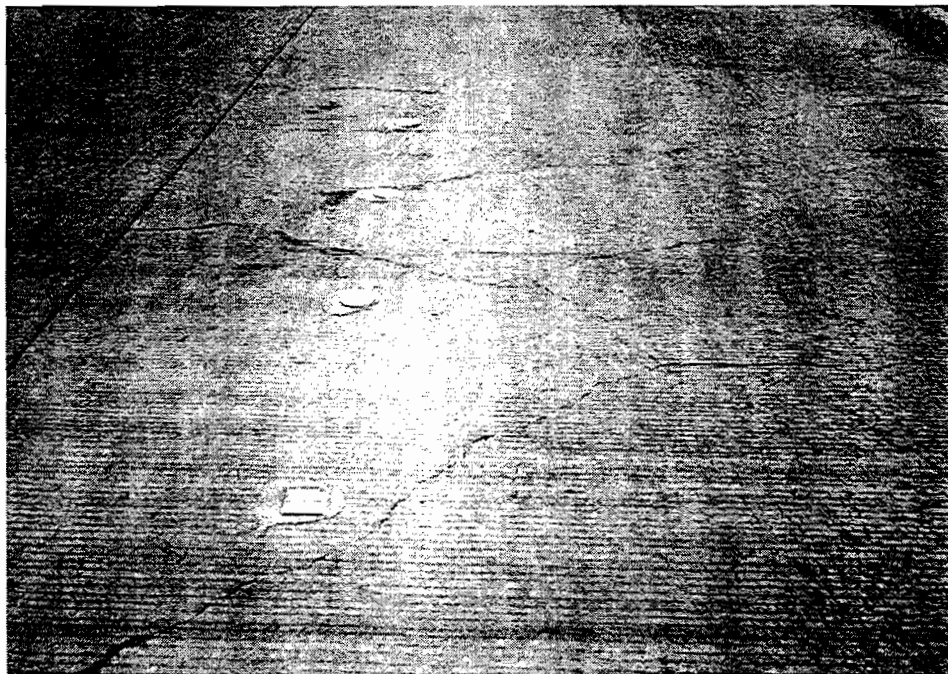


Figure 4.8 Typical early-age cracks occurring with summer placements (SH 6 summer)

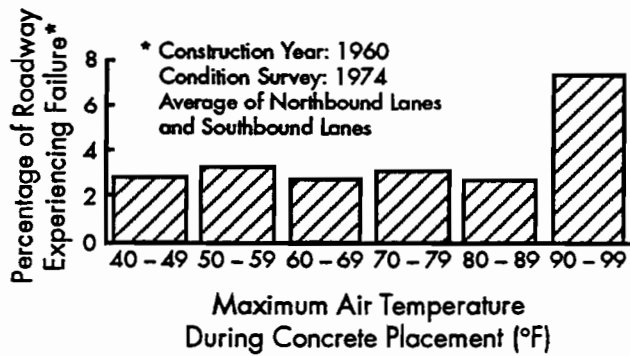


Figure 4.10 Relationship between percentage of roadway experiencing failure and temperature conditions during concrete placement (plot drawn using the data in Ref 28)

Effect of Placement Time During the Day

It is generally understood that the higher the amount of longitudinal steel in CRCP, the larger the number of cracks, a result of the bond between concrete and steel reinforcement restricting concrete movement. However, it was noted from the test sections constructed in the summer (SH 6 summer) that neither the amount of steel reinforcement nor the size of the reinforcing bar had a significant influence on the early-age cracking. Instead, time of placement was the important variable for the occurrence of early-age cracks.

Figure 4.11 shows the influence of the amount of steel reinforcement on early-age cracking. The SRG sections, in general, were found to have fewer cracks where lower amounts of steel reinforcement were used; for the LS sections, a contrary trend was found.

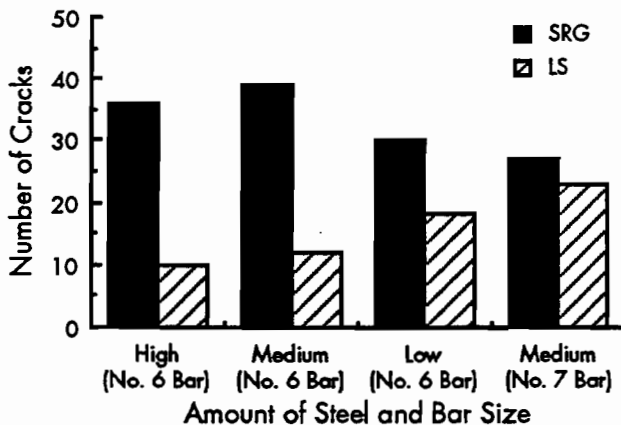


Figure 4.11 Number of cracks occurring 5 days after construction for different steel designs (SH 6 summer)

On the other hand, the time of placement showed a high correlation with the number of early-age cracks (Fig 4.12). The placement sequence of the SRG sections begins with the section having the largest percent steel early in the morning, and proceeds to the medium percentage, the low percentage, and then to the section having the larger bars (No. 7 bars). The sequence of placement for the LS sections reversed that used for SRG sections: The section with the large-sized bar was placed first, while the section with high steel was placed last (see Chapter 2 for the direction of placement of each project).

The general linear model (GLM) procedure in SAS was used to check the significance of each variable (coarse aggregate type, amount of steel, and time of placement) on the early-age cracking. The dependent variable was the number of cracks in a 100-foot section at the age of 5 days. Owing to the small number of observations, interactions between variables were ignored.

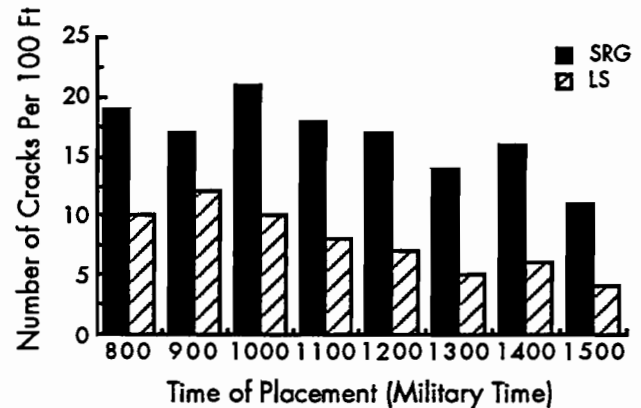


Figure 4.12 Time of placement and the number of cracks in a 100-foot section occurring 5 days after construction (SH 6 summer)

Table 4.1, which summarizes the results of the analysis of variance for the summer construction, shows that time of placement, as well as coarse aggregate type, is a significant variable for the early-age cracking at the 0.05 level. The effect of the percentage of steel was not statistically significant. However, this does not mean that the reinforcing steel is not important in cracking; rather, other factors, such as time of placement and coarse aggregate type, may be more important in early-age cracking. Table 4.2 shows the results of the same analysis for the winter construction. It is shown that the time of placement and coarse aggregate type are not significant for the winter construction.

Table 4.1 Analysis of variance (SH 6 summer)*

Variable	F-value	Pr >F	Significance
Coarse agg. type	108.0	.0001	Yes
Amount of steel	0.4	.7803	—
Time of placement	29.8	.0003	Yes

* Dependent variable is the number of cracks per 100 feet occurring during 5 days after construction

Table 4.2 Analysis of variance (BW 8 winter)*

Variable	F-value	Pr >F	Significance
Coarse agg. type	0.0	.9481	—
Amount of steel	4.0	.0419	Yes
Time of placement	0.9	.3544	—

* Dependent variable is the number of cracks per 100 feet occurring during 5 days after construction

Because the bond between steel and concrete is not fully developed during the concrete's early life, it is difficult to control the meandering early-age cracks through a reinforcing steel design. It would be better to construct on a cool day or to control the slab temperature by other techniques to reduce development of early-age cracks.

To isolate the effect of time of placement from the effect of different steel designs on the early-age cracking, cracks in a normal CRCP section placed during one day (June 20, 1989) were surveyed the following day. The transverse crack distribution of this pavement, shown in Figure 4.13, reveals the effect of time of placement on the

early-age cracking: Most of the cracks occurred in the area placed earlier in the morning.

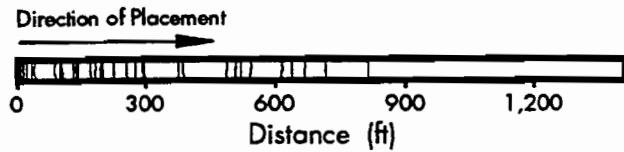
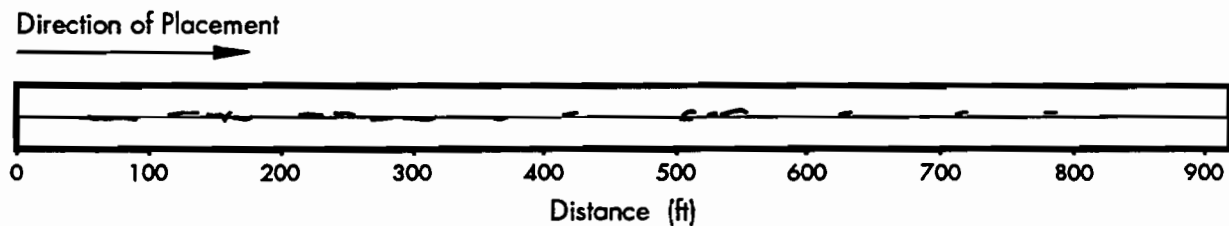


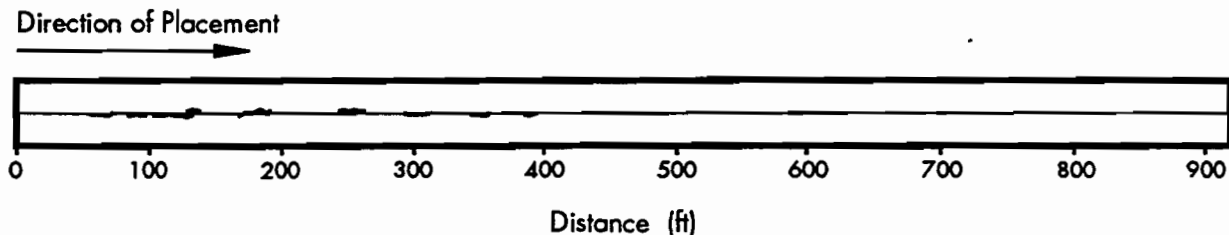
Figure 4.13 Distribution of transverse cracks in a normal CRCP placed in a day, showing the significance of the effect of time of placement on the early-age cracking (pavement age at the time of crack survey was 1 day)

The distribution of longitudinal cracks also shows the significance of the time of construction. Figure 4.14 shows that the earlier the time of placement, the greater the occurrence of longitudinal cracks. The figure also shows that the SRG sections had more longitudinal cracks than the LS sections.

A similar trend regarding early-age transverse cracking was reported in the test sections constructed both in Walker County, Texas, in 1960 (Ref 27) and in Pennsylvania in 1957 (Refs 26 and 29). The frequency of cracking was always greater in the area comprising the beginning of the day's placement. A typical cracking pattern for one day's placement is shown in Figure 4.15, which also shows that the effect of placement time on cracking leveled out with time, indicating that the annual temperature drop is also an important factor in cracking.



(a) Siliceous River Gravel (SRG) Sections



(b) Limestone (LS) Sections

Figure 4.14 Distribution of longitudinal cracks showing the significance of the time of placement during the day

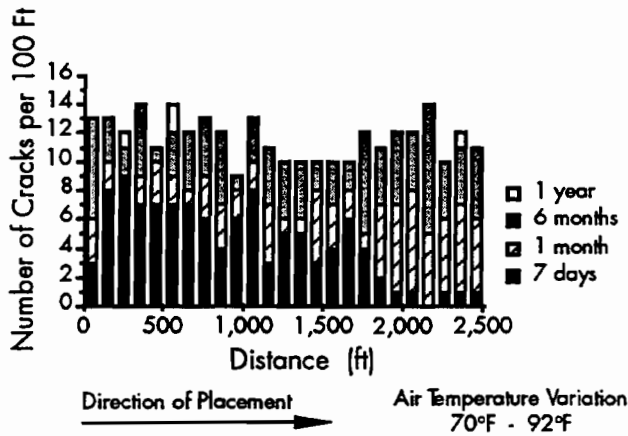


Figure 4.15 Cracking trend of a test section placed in Pennsylvania showing the effect of time of placement during the day on the early-age cracking (Ref 29)

Time of Placement and Concrete Temperature

The magnitude of the peak slab temperature by hydration depends on the ambient temperature condition prevailing at the time the primary heat generation cycle of the hydration occurs. Since the primary heat generation cycle begins several hours after concrete is mixed with water (see Fig 4.1), the primary cycle for the concrete placed early in the morning will occur coincidentally with the occurrence of the day's peak ambient temperature condition (from 1:00 to 4:00 p.m.). For concrete placed during the afternoon, the primary cycle will occur within the relatively lower ambient temperature conditions of the evening or night following the construction day. Finally, if the primary cycle occurs during the evening or night, the peak will be much smaller than if it had occurred in the high ambient temperature conditions that characterize the daylight hours.

Figure 4.16 shows the slab temperature variations for the pavements placed at two different times (morning and afternoon) on a summer day. Slab temperature of the morning placement shows a much higher peak than that of the afternoon placement, a possible explanation being that the time of the primary heat generation cycle of the hydration coincided with the high air temperature and high solar radiation (approximately 3:00 p.m.). For the afternoon placement, however, since the primary heat generation cycle occurred at a relatively low temperature during the evening, the rate of hydration was also low, resulting in a low peak slab temperature. It should be noted that the fresh concrete temperatures were the same for the both pavements.

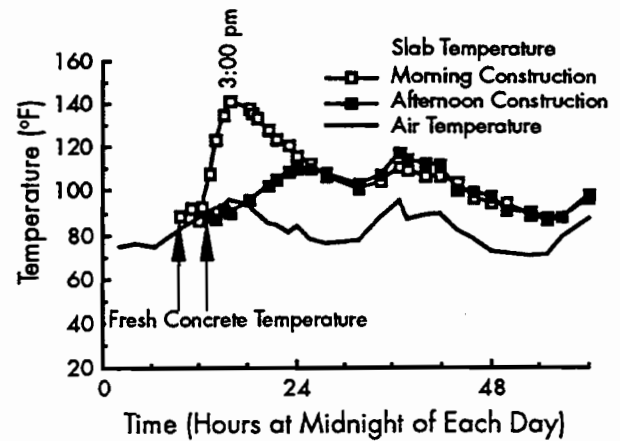


Figure 4.16 Temperature variations for different time of placement (SH 6 summer)

The temperature differential defined by the peak temperature of 3:00 p.m. (141°F) and the minimum temperature the following morning (101°F) was approximately 40°F. As a result, numerous cracks occurred during the first night for the pavement placed in the morning. Many of the cracks were meandering and longitudinal cracks. On the other hand, no cracks occurred during the night for the pavement placed during the afternoon, a result of the relatively small temperature differential (less than 10°F). In addition, the first cracks for the afternoon placement, observed two days later, had shapes that were less meandering.

For winter construction, the effect of placement time was negligible. Because of the lower temperatures throughout the day (Fig 4.17), the primary heat generation cycles, regardless of placement time, occurred during the nighttime. Consequently, the peak slab temperatures were not as high, with no cracks observed until several days after construction.

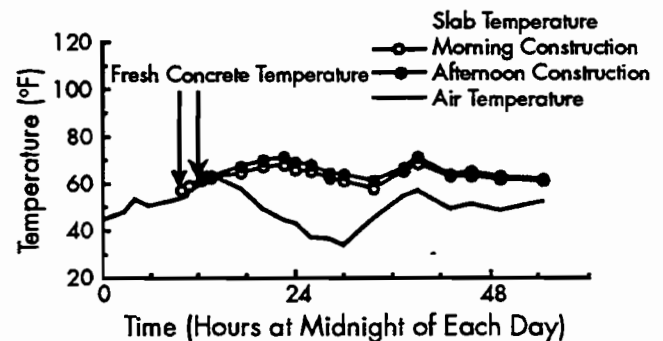


Figure 4.17 Temperature variations for different time of placement (SH 6 winter)

Once cement hydration is completed, daily temperature drops determine subsequent

cracking. Figure 4.18, showing the relationship between daily temperature drop and the number of new cracks for the test sections placed in Illinois in 1988 (Ref 28), indicates that the larger the temperature drop, the larger the number of new cracks. Accordingly, long-term crack spacing may be affected by the temperature differential of the setting temperature and the minimum concrete temperature throughout the pavement life.

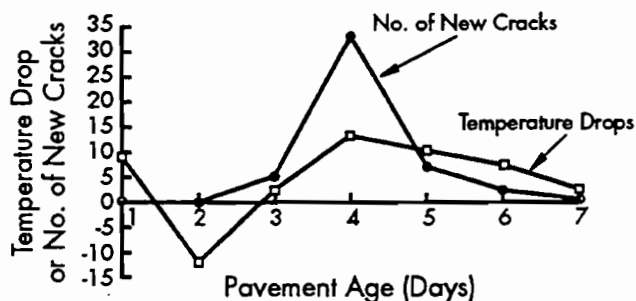


Figure 4.18 Relationship between new cracks and daily temperature drop (Ref 28)

CONTROL OF CONCRETE TEMPERATURE DURING HYDRATION

In previous sections of this chapter, we described how the heat of hydration (and its accompanying temperature rise) can lead to early-age cracking in concrete. Thus, to minimize the number of early-age cracks, concrete should be placed during cool weather. If work schedules require that placement occur in hot weather, it is recommended that placement begin in the afternoon rather than in the morning.

Reducing the temperature rise associated with hydration can also help stem the development of unwanted early-age cracks. Among the methods or combinations of methods that have been used for reducing the temperature rise in mass concrete (Refs 14 and 15), the following have particular practical application to pavement concrete:

- (1) pre-cooling concrete ingredients to reduce the fresh concrete temperature,
- (2) the use of pozzolanic material, and
- (3) the use of retarder.

Further research into the use of any of these methods is highly recommended to determine their performance and practical feasibility.

Pre-cooling

Chilled aggregate or cooled water can be used in mixing the concrete. Since aggregate occupies the major portion of the concrete volume, chilling the aggregate is a very efficient way of pre-cooling. Using ice shavings instead of mixing water is another efficient way of pre-cooling. All of the ice chips should be completely melted during the mixing procedure.

Pre-cooling of concrete permits the use of smaller water and cement contents; and, if these are held constant, it will produce concrete of greater strength and durability at later ages (Ref 15).

The Use of Pozzolanic Material

The use of fly ash or slag reduces the temperature rise in the early-age concrete by reducing the heat of hydration. Mailvaganam (Ref 30) demonstrated this effect by analyzing the temperature-time curves for two different mixes—one which used 100 percent portland cement mortar, and another which used fly ash and slag at 30 percent replacement of portland cement by weight (Fig 4.19). Temperature was measured periodically from 152x305-mm (6x12-inch) cylinders cured at 22°C (71.6°F). Considerably less heat was generated from the mixture of fly ash or slag than from the 100-percent portland cement mixes.

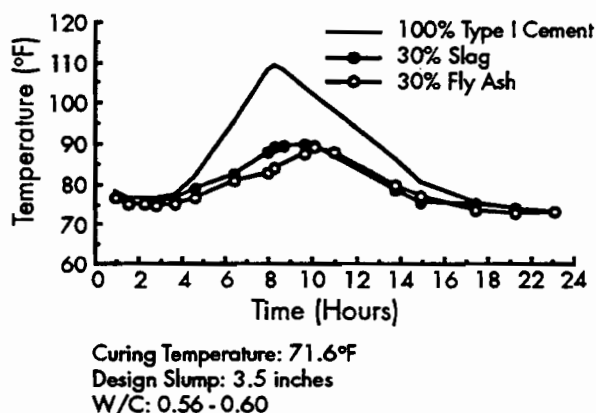
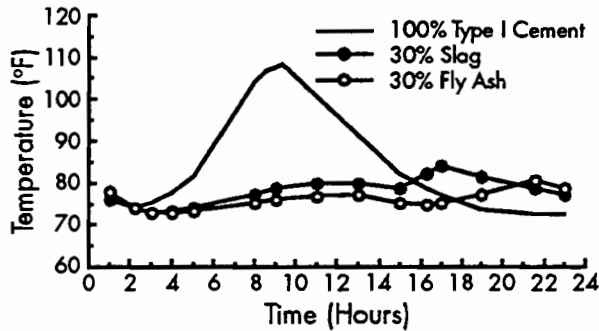


Figure 4.19 Temperature-time curves for the 100-percent portland cement mortar and fly ash and slag at 30 percent replacement by weight (Ref 30)

Mailvaganam also noted that the use of non-chloride accelerator (23 percent solid solution of sodium tetraformate) was effective in offsetting

the early-age strength reduction resulting from cement replacement. Further decreases in heat generation were observed from the use of non-chloride accelerator with fly ash or slag (Fig 4.20).



Curing Temperature: 71.6°F
Design Slump: 3.5 inches
W/C: 0.56 - 0.60

Figure 4.20 Temperature-time curves of Figure 4.19 when non-chloride accelerator was used (Ref 30)

The results of a study conducted at the Center for Transportation Research (Ref 31) showed that the replacement of cement with Type A fly ash resulted in a significant reduction in the temperature rise in concrete under adiabatic conditions (Fig 4.21), whereas replacement of cement with Type B fly ash had no significant effect on the temperature rise in concrete. On the other hand, Type B fly ash required a longer time to reach peak temperature than did Type A cement (Fig 4.22).

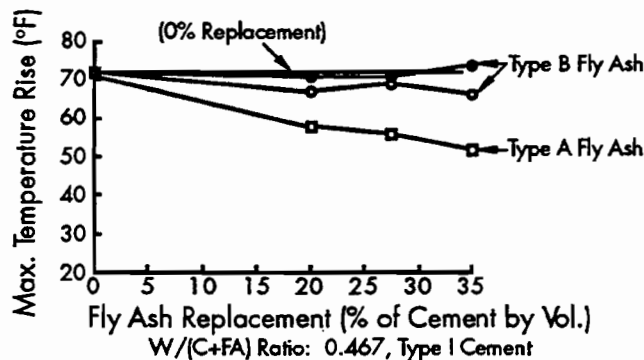


Figure 4.21 Effect of fly ash on maximum temperature rise in mortar (Ref 31)

The longer time required for Type B fly ash mixes to peak may indicate that, though the peak temperature was not significantly decreased under nearly adiabatic conditions, the longer time to peak may, under conditions where the rate of heat loss is significant, result in a lower temperature

rise in concrete in service. The reason: As the time to the peak temperature increases, there is more time for heat to dissipate (Ref 31).

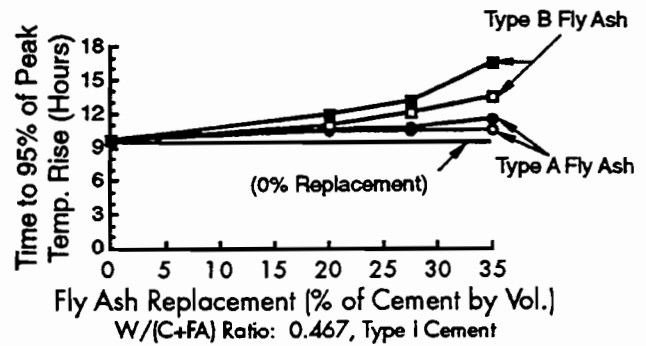


Figure 4.22 Effect of fly ash on the time to 95 percent of the peak temperature rise in mortar (Ref 31)

One problem associated with the use of fly ash or slag was the strength reduction at early ages (Fig 4.23). We found, however, from research conducted by Carette and Malhotra (Ref 32), that the problem of low early-age strength using fly ash replacement could be overcome to a certain degree by the incorporation of small amounts of condensed silica fume.

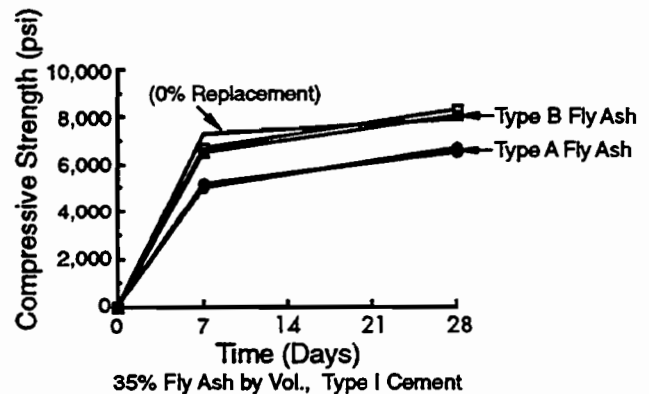


Figure 4.23 Strength reductions associated with the use of fly ash (Ref 31)

Other investigators (Ref 33) developed a blended cement with low heat of hydration. This cement is composed of 50 percent Type II cement, 35 percent slowly reactive slag, and 15 percent condensed silica fume. They found that the peak temperature of an insulated mass of concrete was reduced from 44.4°C (112°F) to 34.4°C (94°F) by replacing the Type II cement with this blended cement. The curing temperature was 20°C (68°F).

The Use of Retarder

The use of a retarder might be considered an alternative method for preventing the simultaneous occurrence of the peak air temperature and the primary heat generation period. Retarders have in fact been used to offset the accelerating effect of hot weather on the setting of concrete (Ref 11). If peak air temperature and primary heat generation period could be separated by using a retarder or other techniques, the hydration rate—and, consequently, the peak temperature of the hydration—could be lowered. One problem associated with retarder use is the possibility of higher fluidity. When used with the slip-form paver, a retarder could cause slump at the pavement edge. (For the effect of retarder on temperature rise and setting time, see Refs 34, 35, and 36.)

SUMMARY

It was found during our monitoring of the test sections constructed at various times of the year that there was a difference in crack patterns between pavements placed during two different seasons (summer and winter). For the summer project, many more early-age cracks, including longitudinal cracks (Figs 4.8 and 4.9), were observed than for the winter projects. These early-age cracks had the tendency to be wider and to have meandering shapes. The greater width and the meandering shape of cracks may cause an adverse effect on the long-term performance of the concrete pavement, contributing as they do to such distresses as Y-cracking, punchouts, spalling, and steel rupture.

For the summer project, the frequency of early-age cracking varied even with the time of placement during a day; the frequency of cracking was always greater in the area placed earlier in the morning than in areas placed later (Figs 4.11, 4.12, and 4.13).

The existence of the seasonal effect and the effect of time of placement during a day on the early-age behavior of concrete pavement had been recognized in the experimental test sections placed in Pennsylvania in 1957 (Figs 4.7 and 4.14) and in Walker County, Texas, in 1960. An attempt to explain these phenomena was made by investigating the effect of temperature condition on the hydration of cement. As we know, hydration of the fresh concrete is accompanied by the release of energy in the form of heat, with the primary heat generation cycle of the hydration beginning several hours after the water is added (Fig 4.1). Since the reaction is chemically controlled, the rate of hydration is very sensitive to temperature, especially during this

primary cycle. The faster the rate of hydration, the higher and the earlier the peak of the concrete temperature (Fig 4.2).

For the summer project, the rapid occurrence of hydration, a result of the high temperature conditions (high air temperature, high fresh concrete temperature, and high solar radiation), led to a very high concrete temperature peak (Fig 4.6). During the first night after placement, the concrete temperature dropped drastically as air cooled. Because of the large temperature differential of the first night, numerous transverse cracks were observed the next morning. Numerous longitudinal cracks were also observed before the sawing of the longitudinal joint.

For the winter project, on the other hand, the lower temperature resulted in a much slower rate of hydration, with the primary heat generation occurring much later than for the summer project, producing a very small temperature rise. Part of the hydration heat essentially compensated for the heat loss during the night. This resulted in the small temperature changes during the first 24 hours after placement. As a result of the low temperature differential, the concrete sustained no cracks until a cold front passed through the area.

The different crack patterns appearing within a day's run (effect of time of placement during the day) for the summer project might be caused by the difference in the time at which the primary hydration cycle occurs (Fig 4.16). Since the primary heat generation cycle begins several hours after concrete is mixed with water, the primary cycle for the concrete placed early in the morning will occur with high ambient temperature conditions during the daylight hours. The primary cycle for the concrete placed in the afternoon, on the other hand, will occur with the relatively lower ambient temperature conditions in the evening or the night following the construction day. If the primary cycle occurs during the evening or night, the peak concrete temperature will be, because of the cool air and lack of solar radiation, much lower than when the cycle occurs with the high temperature conditions during the daytime. As a result, many cracks occurred during the first night in the pavement placed in the morning, whereas no cracks occurred during the first night in the pavement placed during the afternoon. The first cracks of the afternoon placement were observed 2 days later, but the shapes of the cracks were less meandering.

For winter construction, however, the effect of placement time was negligible. Because of the low temperature conditions throughout the day, the primary heat generation cycles occurred during

the nighttime regardless of placement time during the day (Fig 4.17). Consequently, the peak slab temperatures were lower and no cracks were observed for several days after construction.

Early-age cracking and longitudinal cracking are more prevalent with summer construction (especially in the area placed earlier in the day). These cracks are caused by the large temperature changes during the first 24 hours after construction resulting from the high concrete temperature rise (by the interactions between high ambient temperature and cement hydration) and subsequent cooling. Once the cement hydration is completed, subsequent cracking occurs primarily as a result of the daily temperature drop. Annual temperature drop is also important, since it determines the long-term crack spacing.

It is not easy to control the early-age cracks associated with hot-weather placement using reinforcing design, because the bond between steel and concrete is not fully developed during the concrete's early age. It would be more advisable to construct concrete pavements in cool weather. To reduce early-age cracks formed in hot weather, it is recommended that placement begin in the afternoon rather than in the morning; night placement may be even better if it is feasible. Since the high temperature rise during the hydration causes the problems, reduction of temperature rise by some technique will also decrease the tendency toward unwanted early-age cracks. These techniques may include pre-cooling of materials, the use of pozzolanic material, and the use of retarder.

CHAPTER 5. FACTORS AFFECTING CRACK WIDTH

Crack width significantly influences CRCP behavior and performance. Excessive crack width can lead to (1) the loss of load transfer, causing extreme flexing of the concrete slab under traffic that, in turn, leads to concrete spalling, possible punchouts, and steel rupture; (2) the infiltration of incompressible material, causing spalling and blowups; and (3) water infiltration, which can reduce roadbed support and cause rusting of the steel (Ref 37). Thus, to ensure effective pavement performance, engineers seek narrow crack widths that provide sufficient aggregate interlocking and which inhibit infiltration of an appreciable amount of water. A maximum allowable crack width of 0.04 inch was suggested by AASHTO (Ref 38), based on the considerations of spalling and water penetration.

Crack width varies with temperature; that is, cracks are wider in cold weather, when the concrete slab has contracted, and narrower in hot weather, when the concrete slab has expanded. Crack width also changes with age. Both drying shrinkage after the initial crack formation and incompressible foreign material entering the crack contribute to the increase of crack width over time (Refs 39 and 40), though the actual *rate* of increase decreases with time (Ref 37). Additionally, many researchers (Refs 6, 37, and 41) have indicated that crack width varies with the depth of the crack, being greatest at the surface and progressively smaller at increasing depths.

With respect to steel reinforcement in the concrete, it is generally accepted that crack width is a function of the amount of longitudinal steel, where the greater the amount of longitudinal steel, the smaller the crack width (Refs 37 and 42). In other words, crack width is a function of steel stress and the effectiveness of the bond between the concrete and steel near the crack.

Crack width also varies with certain construction variables, including coarse aggregate type and placement time of the year. To investigate the effect these design and construction factors have on crack width, an experimental crack width study was performed on the Houston test sections.

EXPERIMENTS

For the crack width measurements, the study team selected six transverse cracks from each test section, with eight transverse cracks especially selected from State Highway 6 constructed in the summer (SH 6 summer). This selection resulted in a total of 208 transverse cracks, of which 64 cracks (8 cracks from each of 8 sections) were selected from SH 6 summer, and 48 cracks (6 cracks from each of 8 sections) were selected from the BW 8, SH 6 winter, and IH-45 projects. The cracks were randomly selected within a section using a random number table (Ref 43).

The crack widths were measured at various times and at various slab temperatures using a graduated-eyepiece microscope containing a vernier scale and capable of measuring to the closest 0.001 inch (Fig 5.1). Measurements were performed by one operator, a precaution taken to



Figure 5.1 Crack width measurement with a measuring microscope

reduce measurement error by eliminating operator variance. Slab temperatures were measured at three thickness depths: top (1 inch from the surface), middle (center of the slab), and bottom (1 inch from the bottom).

To determine the position at which the temperatures most nearly identified with the crack width, temperatures at the three positions (depths) were correlated with the crack width, which was measured under various time-and-temperature conditions. The typical plots of correlations, given in Figure 5.2, indicated that the top slab temperatures provided the best correlation with the crack widths. Accordingly, the slab temperatures at the top were used to represent the slab temperature in this crack width study. Table 5.1 summarizes the time of crack width measurements and the corresponding slab temperature.

It should be noted that the crack widths were measured near the center of the traffic lane. At first, three locations along the crack—near both ends and at the center of the traffic lane—were measured and averaged to represent the width of

the crack. But there was no significant difference between the average of the crack widths measured at the three locations and the crack widths measured at the center. For this reason, the crack width at the center location was used.

Averages and standard deviations of the crack widths collected from the test sections are shown for the four different steel reinforcement designs in Figures 5.3 to 5.6. The 'T' marks on the columns in the figures represent the standard deviations of the crack widths; the numbers at the bottom of the columns represent the average pavement ages at the time of measurement. It is apparent that a difference in average crack width exists among the pavements constructed with different types of coarse aggregate; that is, sections with siliceous river gravel showed wider cracks than those with limestone. This was true for all sections except for those placed on State Highway 6 (high steel) in the summer (Fig 5.3); in that case, the crack width patterns were reversed, though the difference was not significant.

FACTORS AFFECTING CRACK WIDTH

Since the measurements of the crack widths were conducted under different conditions in terms of slab temperature and pavement age, it was difficult to extract additional information from Figures 5.3 to 5.6. To identify and evaluate the factors affecting the crack width, the crack width data were statistically analyzed using the general linear model (GLM) procedure in SAS.

Variables considered in this analysis included project (with two different seasons), coarse aggregate type, amount of longitudinal steel, time of crack occurrence, crack spacing, pavement age, and slab temperature. Some of the two-factor interactions investigated in this analysis include crack spacing/coarse aggregate type, amount of steel/coarse aggregate type, and slab temperature/coarse aggregate type.

In theory, there is a nonlinear relationship between pavement age and crack width, a result of the nonlinearities of drying shrinkage and creep. Since, however, the range of pavement ages at the time the crack width measurements were made represented a relatively short time period (9 to 35 days after construction), a linear relationship was assumed. The nonlinearity of the effect of pavement age on crack width can be considered once long-term crack width data are collected.

It was found from GLM analysis that the significant factors at the 0.05 level included project, coarse aggregate type, amount of longitudinal steel, time of crack occurrence, pavement age, slab temperature, and the interaction between

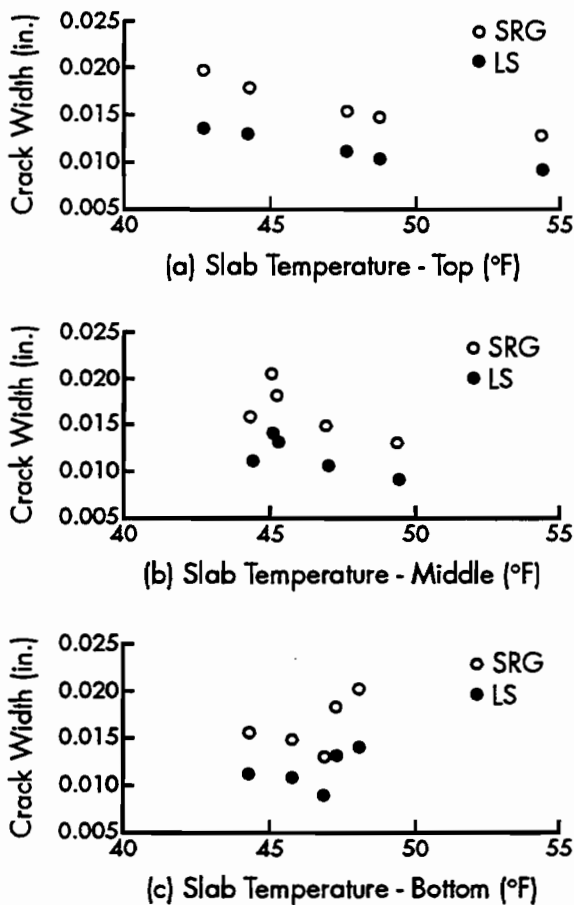
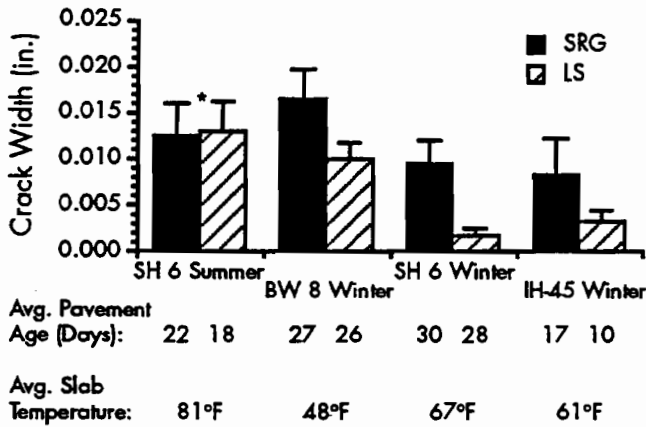


Figure 5.2 Correlation of the slab temperature at various positions with the corresponding crack width

Table 5.1 Time of crack width measurements and corresponding slab temperature

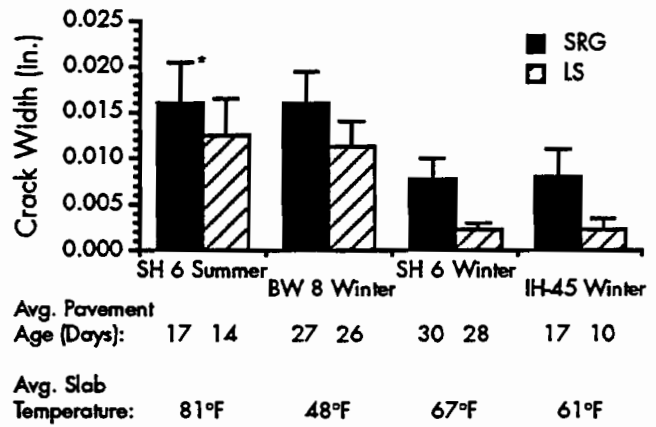
		TEST SECTION			
		SH 6 Summer	BW 8 Winter	SH 6 Winter	IH-45 Winter
1st Measurements	Date	6/28/89	12/20/89	2/1/90	1/31/90
	Time	6:12 AM	1:14 PM	10:42 AM	9:00 AM
	Slab temperature*	73.3	54.4	65.8	58.2
2nd Measurements	Date	6/28/89	12/21/89	2/1/90	1/31/90
	Time	1:54 PM	6:50 AM	3:50 PM	11:30 AM
	Slab temperature	79.4	42.7	64.2	61.3
3rd Measurements	Date	6/29/89	12/21/89	2/13/90	1/31/90
	Time	1:28 PM	9:50 AM	12:00	3:05 PM
	Slab temperature	76.5	44.2	69.9	62.2
4th Measurements	Date	7/6/89	12/21/89	2/13/90	2/14/90
	Time	6:30 AM	12:50 PM	2:00 PM	4:30 PM
	Slab temperature	76.1	47.6	73.4	70.2
5th Measurements	Date	7/19/89	12/21/89	2/14/90	2/15/90
	Time	3:05 PM	2:00 PM	7:55 AM	8:57 AM
	Slab temperature	96.3	48.8	63.5	65.7
Construction date	SRG sections	6/16/89	11/24/89	1/10-11/90	1/14/90
	LS sections	6/19/89	11/25/89	1/11-12/90	1/21/90

* Slab temperature 1 inch below the concrete surface (°F)



* 'T' marks on the columns represent the standard deviations.

Figure 5.3 Average crack width of each test section (high steel)



* 'T' marks on the columns represent the standard deviations.

Figure 5.4 Average crack width of each test section (medium steel)

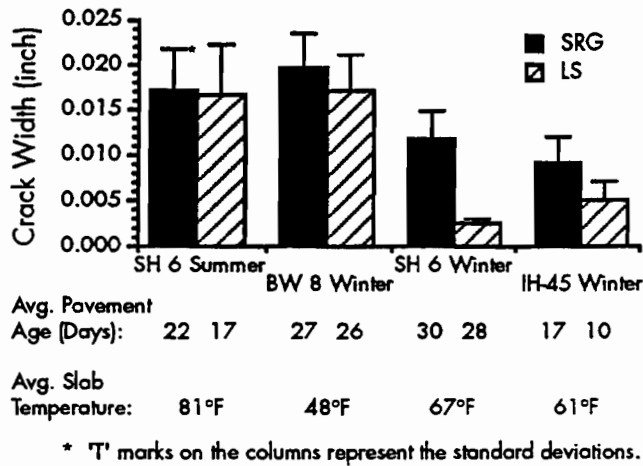


Figure 5.5 Average crack width of each test section (low steel)

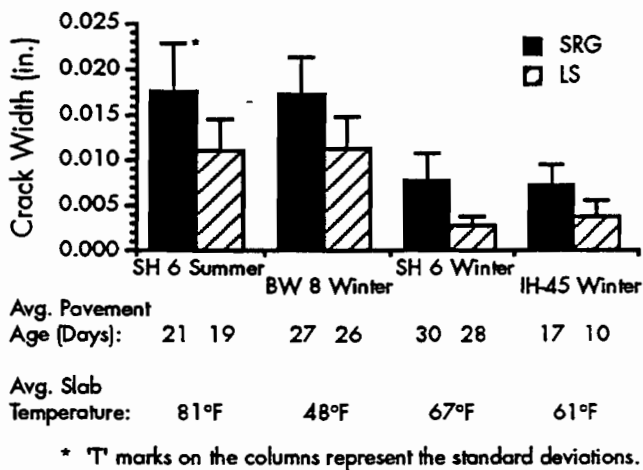


Figure 5.6 Average crack width of each test section (medium steel with larger No. 7 bar)

slab temperature and coarse aggregate type. These factors were significant even at the significance level of 0.0001. On the other hand, the factor of crack spacing and the interactions of crack spacing/coarse aggregate type and amount of steel/coarse aggregate type were not significant at the 0.05 level. The R-square value of the model was 0.82, indicating a good fit. The model is as follows:

$$CW = 34.1 + PROJ + CAT + STL + TCR + 0.15 * AGE - 0.50 * TEMP + TEMP * CAT$$

where:

CW = crack width in 0.001 inch;
 PROJ = project and the season of placement:
 14.9 for SH 6 summer,

1.5 for BW 8 winter,
 0.0 for SH 6 winter, and
 0.7 for IH-45 winter;

CAT = coarse aggregate type:
 - 0.0 for siliceous river gravel, and
 - 10.0 for limestone;

STL = amount of longitudinal steel:
 - 0.3 for high steel with No. 6 bar,
 0.0 for medium steel with No. 6 bar,
 2.9 for low steel with No. 6 bar, and
 0.4 for medium steel with No 7 bar;

TCR = time of crack occurrence in terms of pavement age:
 4.0 for 1 day,
 3.3 for 2 day,
 3.4 for 3 day, and
 from -1.4 to 1.4 for 4 days or later (see Fig 5.10);

AGE = age of the pavement at the time of crack width measurement (days) (note: inference space of the pavement age is 9 to 35 days);

TEMP = slab temperature (°F); and
 TEMP * CAT = interaction between slab temperature and coarse aggregate type:
 0.0 for siliceous river gravel, and
 0.097 times slab temperature for limestone.

It can be seen from this model that the placement season, the coarse aggregate type, and (to a lesser extent) the time of crack occurrence were all significant factors affecting the crack width for a given age and temperature. Each of these three factors proved more dominant than the amount of longitudinal steel. Therefore, in the effort to control the crack width, more attention should be given to these three factors than to steel design. Finally, we might add that controlling these factors can be less expensive than controlling the amount of steel.

The following sections discuss each factor considered in this analysis. It should be noted that, for a fair comparison of the levels in each factor, the levels of other factors (except the factor in discussion) were fixed.

Placement Season of the Year

Test sections were placed during two opposing seasons, summer and winter. Figure 5.7 shows the effect of placement season on the crack width

when all other conditions are the same. As can be seen, crack widths associated with the summer placement (SH 6 summer) were much wider than those associated with winter placement. This might be mainly a consequence of the high curing temperature of the summer placement. Again, crack width is a function of temperature differential, which is the difference between the curing temperature and the temperature at the time of crack width measurement; the higher the temperature differential, the wider the crack. Consequently, the higher the curing temperature, the greater the crack width at a given temperature.

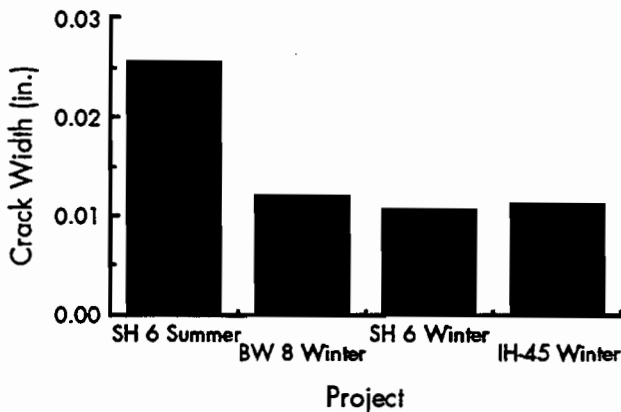


Figure 5.7 Effect of placement season on crack width

Coarse Aggregate Type

Since there exists an interaction between the factors of coarse aggregate type and slab temperature, the effect of coarse aggregate type should be interpreted along with the effect of slab temperature.

The effect of coarse aggregate type on the crack width is shown in Figure 5.8. There we see that

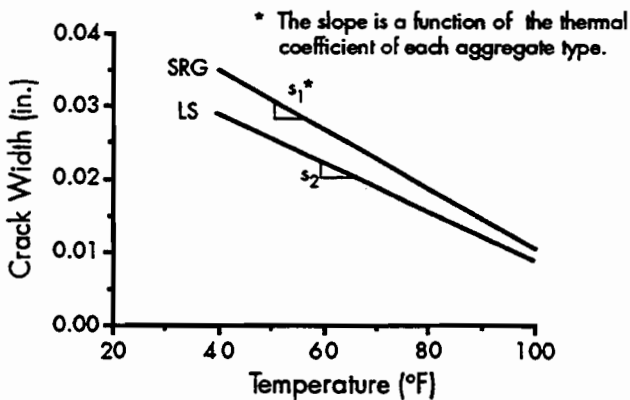


Figure 5.8 Effect of coarse aggregate type and slab temperature on crack width

the use of siliceous river gravel (SRG) resulted in wider cracks than did the use of limestone (LS), and the difference was larger at lower temperatures (note the difference in the slopes in Fig 5.8). This difference may be the result of the higher SRG thermal coefficient.

Steel Reinforcement

The effect of the amount of longitudinal steel on the crack width was statistically significant. In general, the greater the amount of longitudinal steel, the narrower the crack width (Fig 5.9). This effect occurs because the heavier steel holds the cracks more tightly by creating a larger bond area between steel and concrete.

It should be noted from Figure 5.9 that the difference in crack width between the high steel and the medium steel was much less than that between the low steel and the medium steel, even though the differences in the amounts of steel were about the same. In this sense, the medium steel, which is the standard steel percentage specified in the new design standard, can be said to be a cost-efficient design.

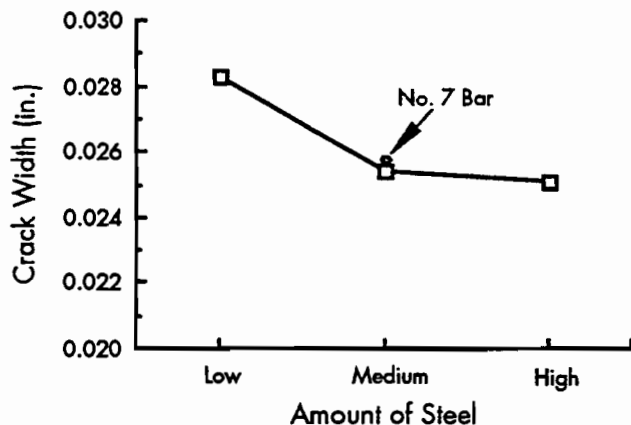


Figure 5.9 Effect of longitudinal steel design on crack width

The effect of the size of steel bar on crack width is also shown in Figure 5.9. The use of a larger bar, for the same total amount of steel, resulted in slightly greater crack width; the use of No. 7 bars (7/8 in. diameter) instead of No. 6 bars (3/4 in. diameter) showed a little wider crack. This might be a result of the smaller total bond area existing between steel and concrete of the larger bar (the crack width is minimized by the bond between the steel and concrete). It should be noted, however, that the increase in crack width by use of No. 7 bars instead of No. 6 bars was very small.

Time of Crack Occurrence

One of the unique findings of this study was the effect of the time of crack occurrence on the crack width. The cracks occurring during the first 3 days after construction were significantly wider than those that occurred later (Fig 5.10).

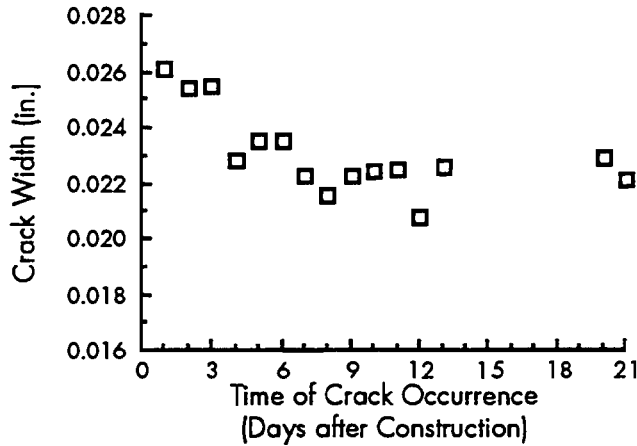


Figure 5.10 Effect of time of crack occurrence on crack width

One explanation for the greater width of early-age cracks suggests that, once a crack occurs, its width increases as a consequence of the drying shrinkage of the concrete (Ref 39). It is believed that the increase in crack width is a function of the residual shrinkage (drying shrinkage after formation of the crack); an early-age crack will have higher residual shrinkage than a later crack (Fig 5.11), a fact that results in the greater width. But, it should be recognized that these are early-age observations and the results should be checked after 1 year.

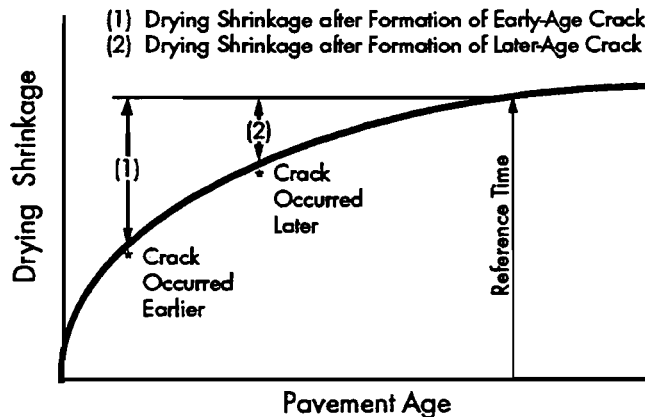


Figure 5.11 Conceptual explanation of wider crack width of the early-age cracks by the difference in the residual shrinkage

Crack Spacing

It is generally believed that the greater the crack spacing, the wider the crack width. But the effect of crack spacing (slab length between two cracks) on crack width was not statistically significant at the significance level of 0.05. The crack spacing used in this analysis was half the distance between the two nearest cracks (one upstream and the other downstream) from the crack of interest. Figure 5.12 shows the plot of the crack width versus the crack spacing, indicating no significant correlation between crack spacing and crack width.

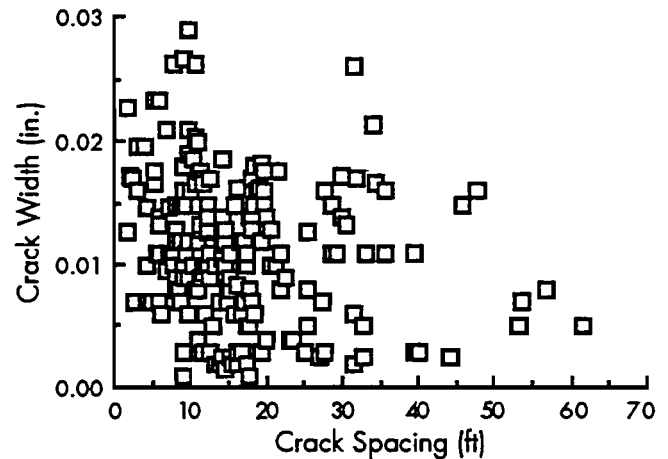


Figure 5.12 Relationship between crack spacing and crack width (showing no significant correlation)

SUMMARY

In this chapter, the statistical analysis conducted on the crack width data collected from the test sections served as the basis for a discussion of the various factors affecting crack width. Findings from the statistical analysis can be summarized as follows:

- (1) Hot-weather placement resulted in much wider cracks than cool-weather placement (Fig 5.7).
- (2) The use of siliceous river gravel (SRG) resulted in greater crack widths than the use of limestone (LS), and the difference was larger at a lower temperature (Fig 5.8). This difference might be a consequence of the different thermal coefficients of the two coarse aggregate types used in the concretes.
- (3) The larger the amount of longitudinal steel, the narrower the crack width (Fig 5.9). But

the difference in crack width between the high steel and the medium steel was less than that between the low steel and the medium steel, while the differences in the amount of longitudinal steel were about the same.

- (4) Cracks that occurred during the first 3 days of construction were significantly wider than those occurring later (Fig 5.10). It has been

noted in the previous chapters that early-age cracks are more prevalent with summer placement than with winter placement. Therefore, special care should be taken during hot weather placement to reduce early-age cracks.

- (5) The effect of crack spacing on crack width was not significant (Fig 5.12).

CHAPTER 6. DETERMINATION OF CURING TEMPERATURE (SETTING TEMPERATURE) AND THE SHRINKAGE OF CONCRETE PAVEMENT

INTRODUCTION

Although curing temperature and drying shrinkage of concrete are very important considerations in the mechanistic analysis and design of concrete pavement, researchers have not accorded to these variables the attention they deserve. This chapter will review salient issues and points relating to curing temperature and drying shrinkage.

CURING TEMPERATURE

The curing temperature used in mechanistic analysis or the design of concrete pavements is a reference temperature from which temperature-induced stresses may be calculated. Many design procedures now use as the curing temperature the fresh-concrete temperature recorded at the time of placement. Theoretically, however, the curing temperature should be the temperature at which the concrete begins to display stresses induced by shrinkage or temperature change. This temperature is not necessarily the fresh concrete temperature, since stress does not occur while the concrete is in a plastic state. Thus to clarify meanings, the term "setting temperature," rather than "curing temperature," is used in this chapter to represent the reference temperature for the stress calculation.

DRYING SHRINKAGE

Drying shrinkage tests for concrete pavement, in many cases, involve nothing more than measuring the shrinkage of concrete specimens cured in the lab (a test whose simplicity appeals to many researchers). However, some engineers have questioned whether the shrinkage of a laboratory specimen can sufficiently represent the shrinkage of a concrete pavement in the field. Weather conditions, the shape of the specimen, and the surface area exposed to the air, among other factors, are often cited as significant variables specifically affecting field specimens.

A common source of errors associated with most shrinkage tests is the use of a different volume-to-surface ratio (Refs 44, 45, and 46). With laboratory cylinder shrinkage, moisture can evaporate at the top surface or at the side of the cylinder if the mold of the cylinder is removed. In the field, however, evaporation occurs at the surface of the slab, with possibly a minute amount evaporating through the cracks or lost into the base.

Another source of error has to do with the curing conditions. Drying shrinkage is very sensitive to the curing conditions. Specimens for shrinkage tests are normally cured in a chamber under specific temperature and moisture conditions, or in a water bath with a controlled temperature. Thus, unlike field specimens, lab specimens are not subjected to rain, wind, sunlight, and temperature change.

With the basic issues and concepts relating to curing temperature and drying shrinkage now introduced, the balance of this chapter discusses an experimental study performed (1) to identify a method for determining the setting temperature for the mechanistic analysis, and (2) to obtain a correlation between the shrinkage of concrete slabs and lab-cured concrete cylinders.

CONCEPTUAL DETERMINATION OF SETTING TEMPERATURE

The setting temperature, as mentioned earlier, is the temperature at which the concrete begins to resist loads induced by drying shrinkage or temperature change. A method for determining the setting temperature for the mechanistic analysis is illustrated in Figure 6.1.

It is assumed that the concrete was placed at A and the setting temperature occurred at P in Figure 6.1. As the concrete temperature increases from the setting temperature, P, to the peak temperature, B, the concrete will have a compressive stress, as the expansion of the concrete caused by the temperature rise is restrained. After the peak

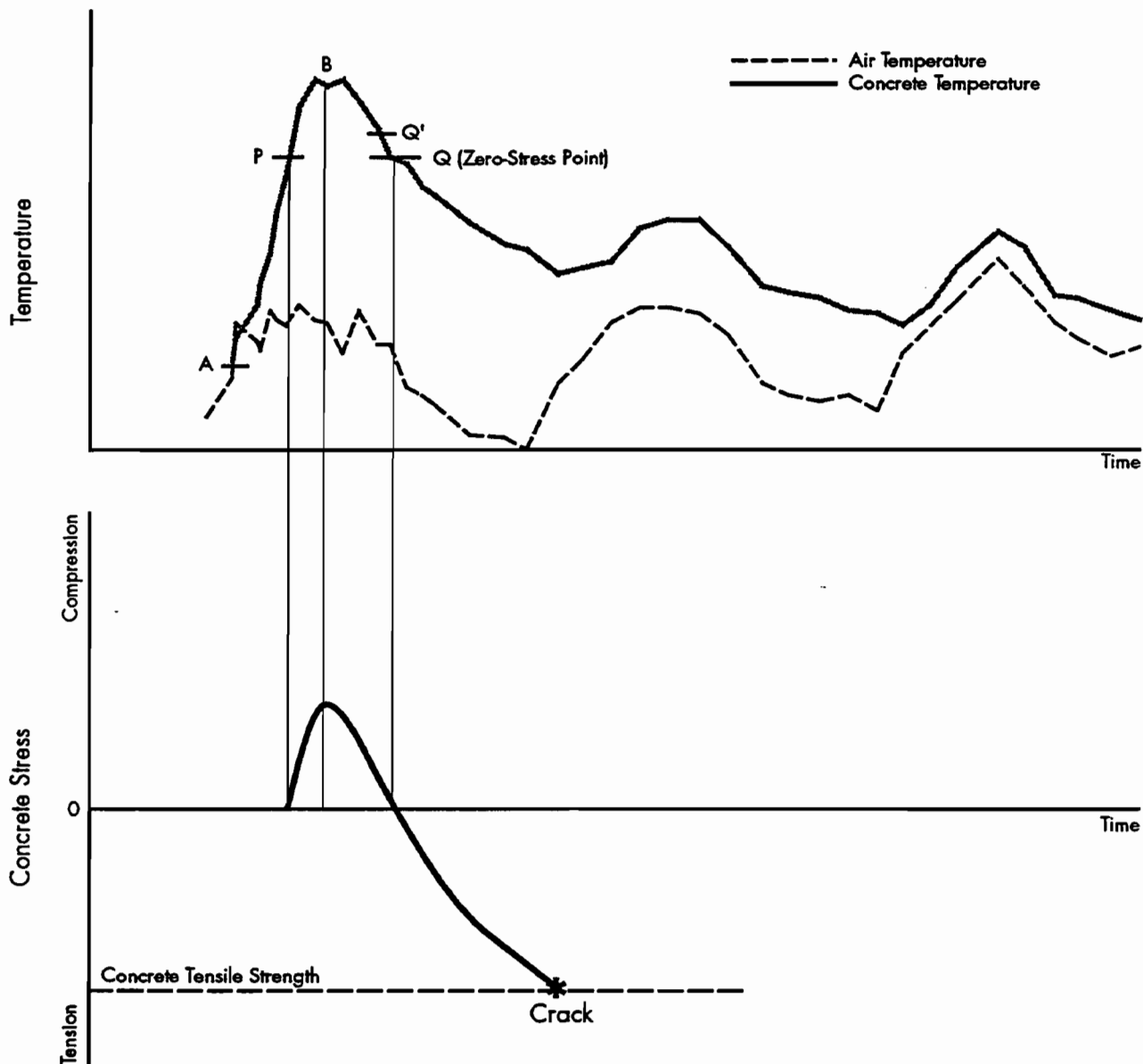


Figure 6.1 A conceptual determination of setting temperature

temperature, as the concrete cools, the compressive stress will be relieved until the concrete temperature drops to a certain point (zero stress point, Q), where the stress condition changes from compression to tension. If the tensile stress caused by a further temperature drop exceeds the strength of the concrete, a crack will occur.

Assuming that there is no drying shrinkage or creep (or plastic flow) of concrete during this period, the temperature at the zero stress point, Q, will be the same as the setting temperature, P. But, if the effect of drying shrinkage and creep are considered, the zero stress point will occur at a slightly higher temperature, possibly at Q'; this is because part of the compressive stress gained during the temperature change from P to B will be

relieved by shrinkage and creep. The temperature at the zero stress point is the reference temperature needed in the stress calculation.

INSTRUMENTATION

To find the zero stress point and to measure the slab shrinkage, an instrument was imbedded in the test section. The instrument was a 6x12-inch cardboard cylinder mold that was cut longitudinally along each side of the mold. A two-ply plastic sheet made of two layers of plastic film was fitted inside the mold to minimize the friction between the inside of the mold and the concrete (Fig 6.2). Similar two-ply plastic sheets were also used at both ends of the mold as membranes

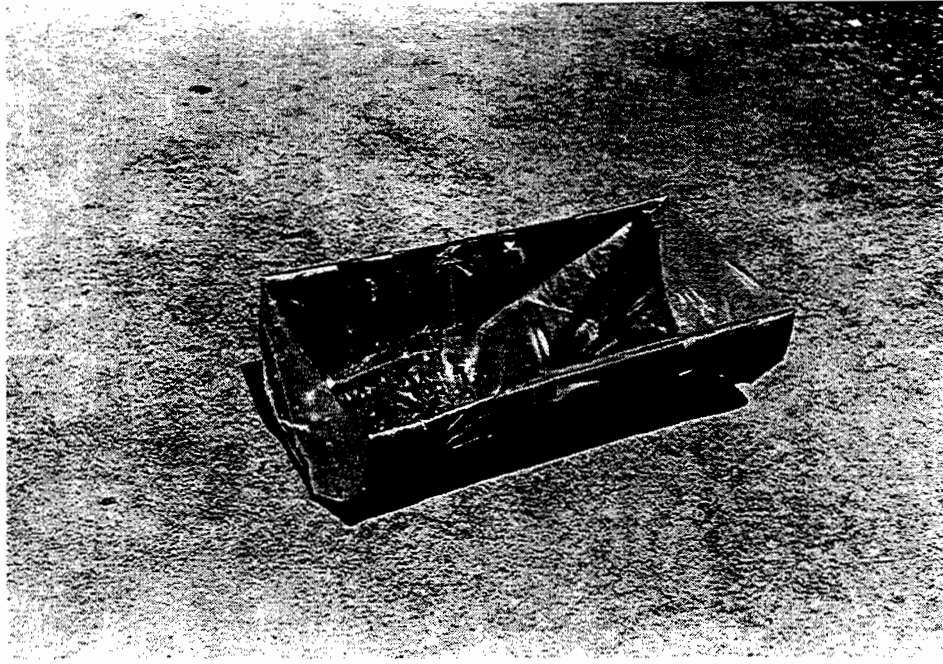


Figure 6.2 A mold devised for the experimental study

to ensure that the separation of the concrete inside and outside the mold occurred at this location when the concrete began to have tensile stress. Eight brass plugs were inserted in the concrete as measuring points after the cylinder mold was imbedded in the concrete. Figure 6.3 shows the shape and dimension of the instrument, while Figure 6.4 shows the imbedded instrument and the field-cured cylinder (for shrinkage correlation). A thermocouple was imbedded in the center of the mold to monitor the concrete temperature.

If no adhesion is assumed between the concrete in the instrumented mold and the plastic sheets, then theoretically the concrete inside the mold will shrink as soon as the concrete has tensile stress, and the concrete in the mold will part or separate from the surrounding concrete in the slab. The zero stress occurs at the moment the concrete separates. The objective is to obtain the concrete temperature at this moment.

The shrinkage of concrete pavement in the field can be obtained by monitoring the shrinkage of the concrete within the instrumented mold. To get a correlation between shrinkages of the concrete pavement and the cylinder, shrinkage specimens were cast from the batch of concrete placed in the pavement and in the instrumented mold. One cylinder was transported to the lab after initial reading and cured in a chamber having a temperature of 75°F and a relative humidity of 40 percent. The other cylinder was

cured in the field alongside the experimental slab. The molds of the cylinders were not removed during the curing period.

DATA COLLECTION

To monitor the shrinkage and the separating movement of the experimental slab, distances L (left), C (center), and R (right) in Figure 6.3 were periodically measured. A change in the distance at C gave shrinkage information, while a change in the distances L and R gave information about separating movement between the concrete inside and outside of the mold.

Each distance (L, C, or R) in Figure 6.3 was the average of two distances; that is, distance C was the average of distances C1 and C2. The distance at each location was measured every 2 hours with a 10-inch multiposition strain gauge for the first few days until the concrete separated. Thereafter, measurements were performed less frequently. Believing that the separation would occur in the cooler temperatures, we took our measurements during the evening and at nighttime only. At the same time, distance measurements were collected from the instrumented mold; the concrete temperature and the shrinkage of the field-cured cylinder were also measured.

After 28 days of curing, the field-cured cylinder was also transported to the laboratory and the shrinkage was measured for both field- and lab-cured cylinders at the same time.

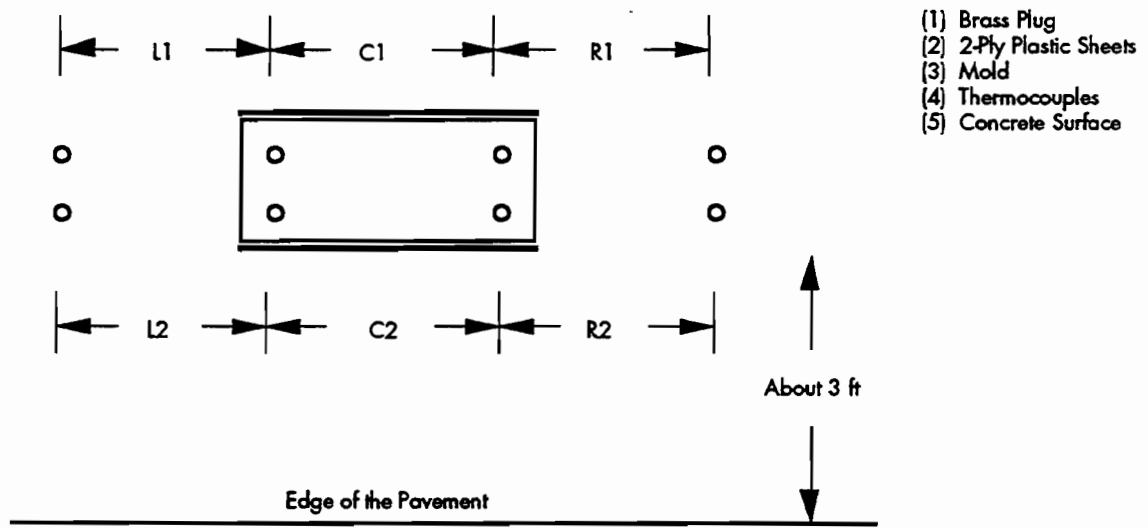
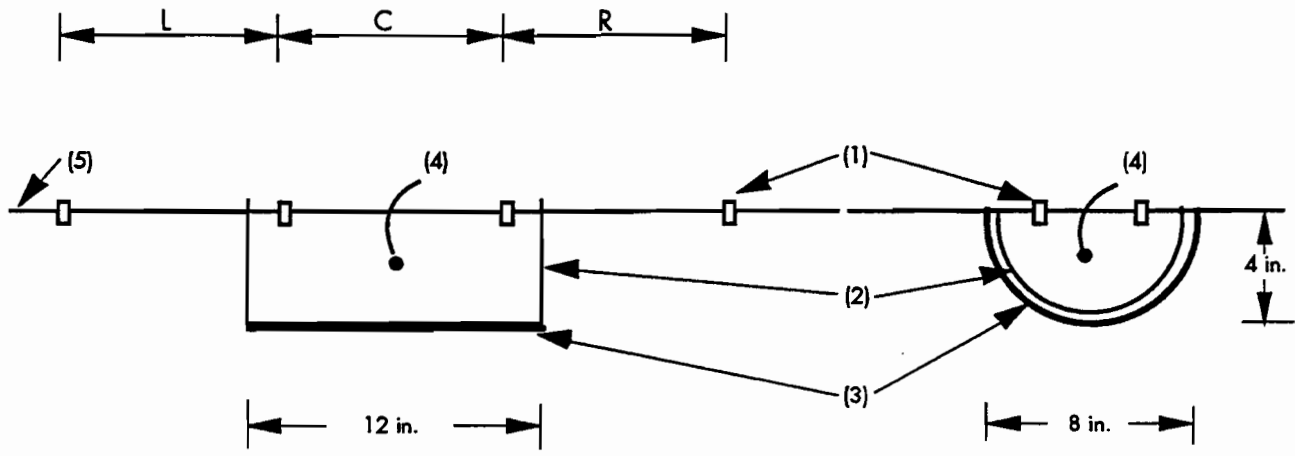


Figure 6.3 Dimensions and layout of the experimental slab

DETERMINATION OF SETTING TEMPERATURE

Figure 6.5 presents a plot for selecting the setting temperature. The vertical axis on the left side represents the slab temperature, and the vertical axis on the right side represents the separating movement of the experimental slab at one of the ends (L or R in Fig 6.3). The fresh concrete temperature, as the concrete was delivered at the site, was 70°F.

Theoretically, before the concrete inside the instrumented mold separates from the pavement, there is no movement except nominal movement by plastic flow, since the expansion of the concrete within the mold is restricted by the surrounding concrete. Once there is a separation,

however, a substantial movement begins to occur. After separation, the crack width between the inside and the outside of the mold changes inversely to the slab temperature: if the slab temperature drops, the crack width become wider; if the slab temperature increases, the crack width become narrower.

Time of separation (or zero stress point) can be determined by selecting the time at which the separating movement begins to be substantially larger while the slab temperature drops. Before this time, separation does not occur, even though the concrete temperature is lower than the setting temperature (because the concrete is still in a plastic state). The small fluctuation in the movement before separation might be owing either to the plastic flow of the concrete or to measurement error.

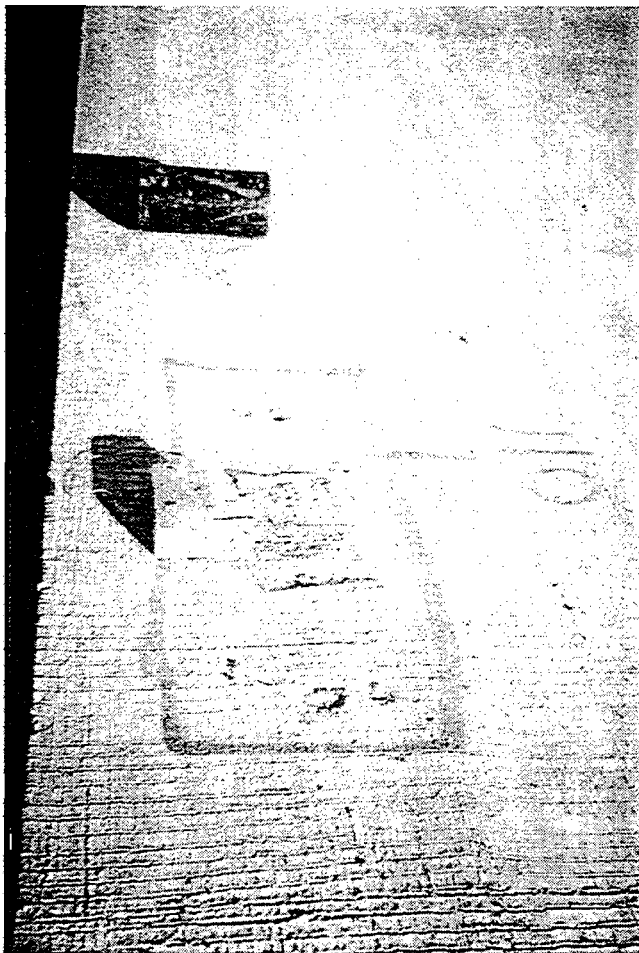


Figure 6.4 Experimental slab and field-cured cylinder

Figure 6.5 shows that the separation of the experimental slab occurred at about 8:00 p.m. on the second day of construction. The slab temperature at this time, 78°F, is the setting temperature of this concrete. The first crack in the pavement

was observed several hours after the separation of the experimental slab, when the slab temperature dropped further during the night.

Because this method of selecting the setting temperature is somewhat impractical, a correlation of the setting temperature obtained by this method with other variables that are easy to determine (such as fresh concrete temperature and air temperature) is recommended for future research.

CORRELATION BETWEEN SLAB SHRINKAGE AND CYLINDER SHRINKAGE

First, the shrinkage of the field-cured cylinder was correlated with the shrinkage of the concrete slab (shrinkage of the concrete inside the instrumented mold). Then the shrinkage of the lab-cured cylinder was correlated with that of the field-cured cylinder. The shrinkage of the lab-cured cylinder was not directly correlated with the slab shrinkage because they were not measured at the same time and temperature.

Figure 6.6 shows the correlation between the slab shrinkage and the shrinkage of the field-cured cylinder. Again, it should be noted that the measurements of the slab and the field-cured cylinder were performed at the same time. Figure 6.7 shows the correlation between the field-cured and the lab-cured cylinder shrinkages. As seen in the two figures, the regression line lies very close to the line of equality in both plots, indicating that the lab shrinkage can be used without any correction to predict slab shrinkage. And, again, it should be noted that the cylinder mold was not removed from the shrinkage cylinder during the curing period.

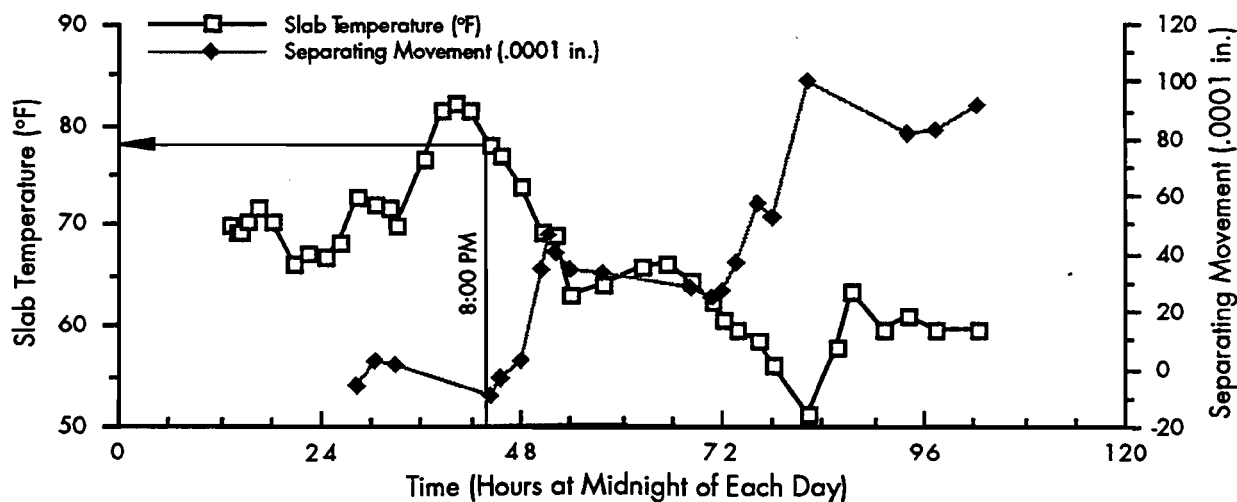


Figure 6.5 Determination of setting temperature

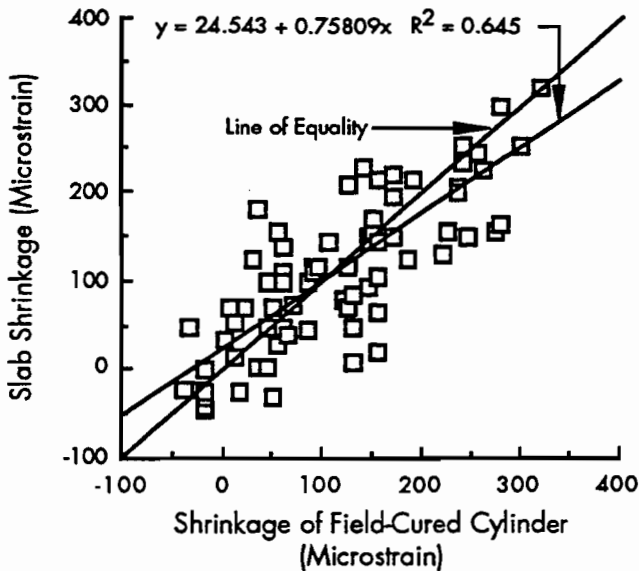


Figure 6.6 Correlation of shrinkages between pavement slab and field-cured cylinder - (all projects)

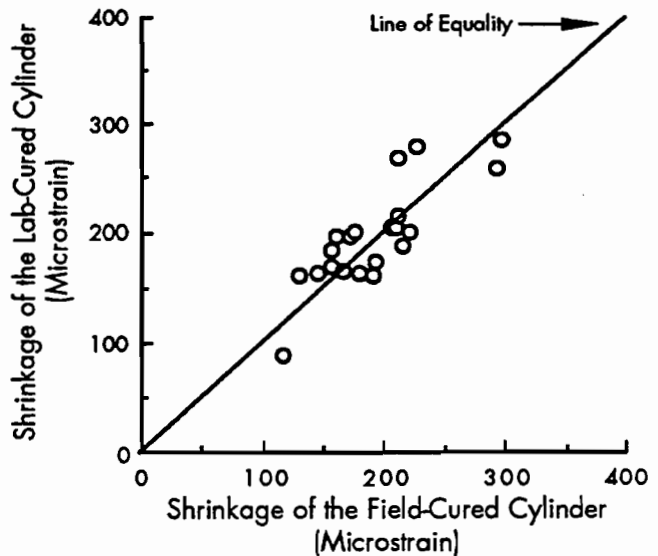


Figure 6.7 Correlation of shrinkages of the cylinders cured in the lab and in the field (all projects)

SUMMARY

To introduce a method for determining the setting temperature for the stress calculations in concrete pavements, and to determine correlation of shrinkages between the concrete slab and the concrete cylinder, a modified cylinder mold was imbedded in the test section.

The mold was designed so that the interior concrete could shrink freely by drying shrinkage (or by any temperature-induced contraction), with the expansion of the concrete inside the mold restrained by the surrounding concrete. In this way we monitored the separating movement of the concrete inside and outside of the mold, the drying shrinkage of the concrete inside the mold, the drying shrinkage of the cylinder, and the slab temperature.

As soon as the concrete began to show tensile stress, the concrete inside the mold separated from the pavement, a response to the lack of restriction to the contraction movement. Setting temperature (needed for the stress calculation in the mechanistic analysis) was determined by reading the slab temperature at the beginning of the separation. This is the zero stress point, where the stress condition changed from compression to tension.

From the correlations between slab shrinkage and cylinder shrinkage, we found that the drying shrinkage of a cylinder cured in the laboratory at 75°F and at 40 percent relative humidity sufficiently represents the drying shrinkage of concrete slab. It should be noted that the concrete cylinder was cured without removing the cylinder mold.

CHAPTER 7. CURRENT CONDITION OF THE TEST SECTIONS

Having described the short-term monitoring of the test sections during the first month following construction, we turn now to a discussion of the condition of the test sections at the end of the short-term monitoring.

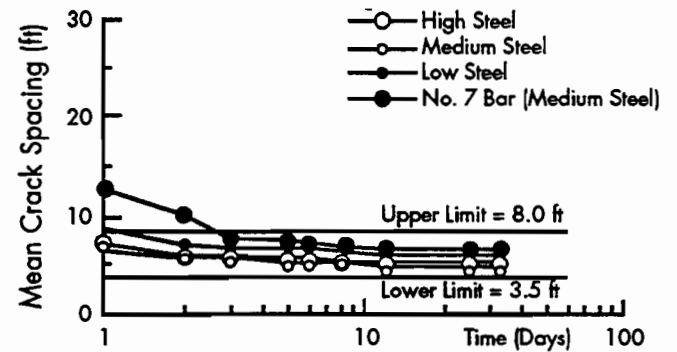
CRACK SPACING AND CRACK WIDTH

While the three parameters considered in the steel design of CRCP include crack spacing, crack width, and steel stress, this section discusses only the data associated with crack spacing and crack width; the issue of steel stress, because it was not measured in the test sections, will not be addressed. (We might add, however, that neither excessive elongation nor rupture of steel has been observed in the test sections.)

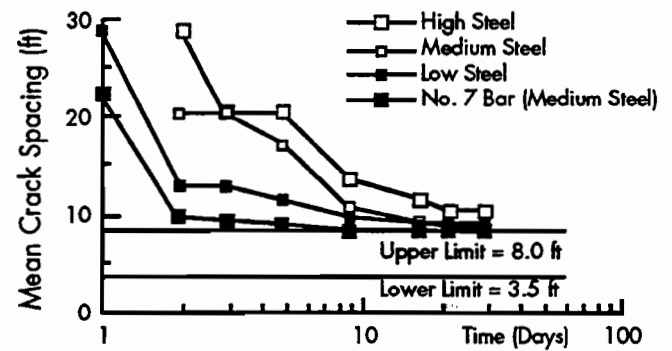
Figures 7.1 to 7.4 show the mean crack spacing versus time during the short-term monitoring period for the different steel designs for different projects and coarse aggregate types. Since the pavement age at the time of the last survey was only about 1 month, mean crack spacings were still fairly large. Except for the SRG sections in the SH 6 summer project, most sections showed the mean crack spacing to be larger than or near the upper limit (8 feet as proposed by AASHTO Guide; Ref 38) of the design crack spacing, which has been set to avoid excessive spalling (Ref 5). However, to ascertain whether the performance of pavements in the field is in accordance with that predicted by the CRCP program, at least 1 year of monitoring is necessary (since more cracking is expected after the short-term monitoring period).

Figures 7.1 to 7.4 are based on the mean values of the crack spacings (not individual crack spacing) in each section. Since variability exists in the crack spacings in the field, a wide range of crack spacings may actually exist. Figures 7.5 and 7.6 present the distribution of crack spacings at the end of the short-term monitoring (pavement ages were approximately 1 month old) for the medium steel sections of SRG and LS, respectively.

Similar plots for the sections with other steel quantities are given in Appendix F. As may be noted, certain portions of the crack spacings are smaller than the lower limit (3.5 feet as suggested by AASHTO Guide; Ref 38) of the crack spacing design criteria, which has been set to reduce the possibility of punchouts (Ref 5).



(a) SRG



(b) LS

Figure 7.1 Mean crack spacing versus time (SH 6 summer)

Plots of crack width data measured from the test sections are shown in Figures 6.3 through 6.6 of Chapter 6. As may be noted, all crack widths were less than the crack width limiting criterion (0.04 inch as suggested by AASHTO Guide; Ref

38). Since, however, the ages of the pavements at the time of measurements were less than 1 month, long-term measurements of the crack widths in a cold period are highly recommended to obtain the final decision on this test section study.

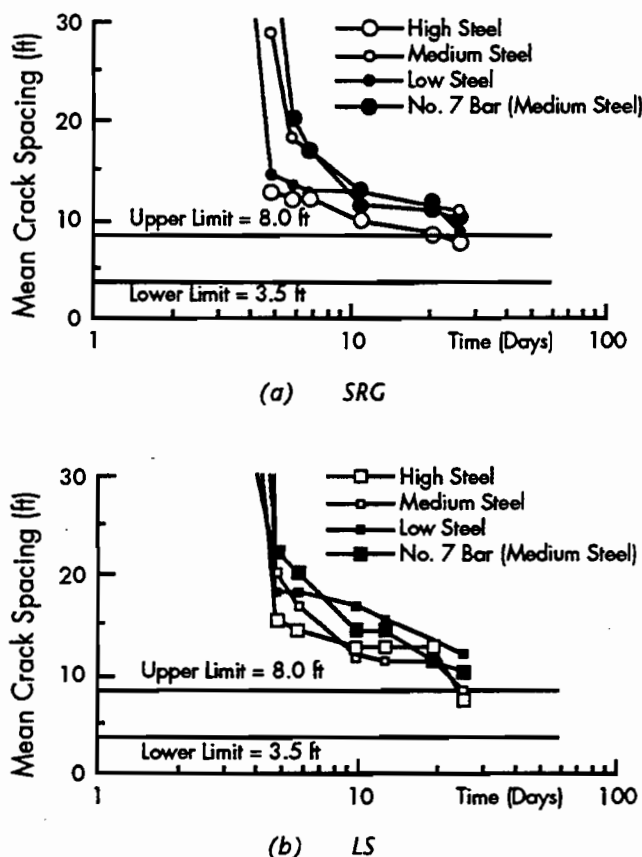


Figure 7.2 Mean crack spacing versus time (BW 8 winter)

It is commonly believed that the greater the crack spacing in CRCP, the greater the crack width. In the experimental test sections, however, the LS sections showed much smaller crack widths than the SRG sections, even though the crack spacings were larger. When the effect of aggregate type on both crack spacing and crack width is considered, all the test sections show significant differences between SRG and LS. This might be attributed to the lower thermal coefficient and greater tensile strain capacity of the concrete with LS.

Since there was a substantial seasonal difference in the early-age behavior of the test sections, test sections constructed in different seasons are discussed separately.

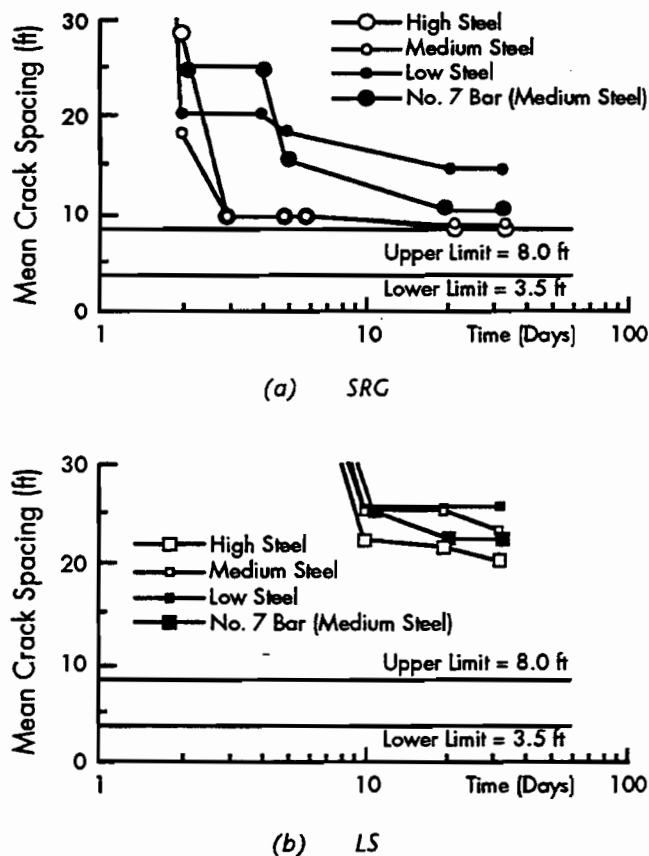
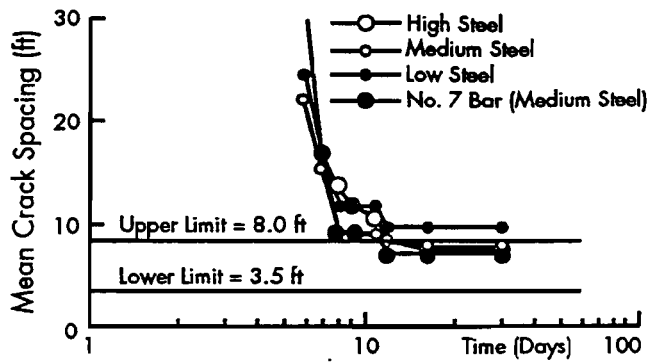


Figure 7.3 Mean crack spacing versus time (SH 6 winter)

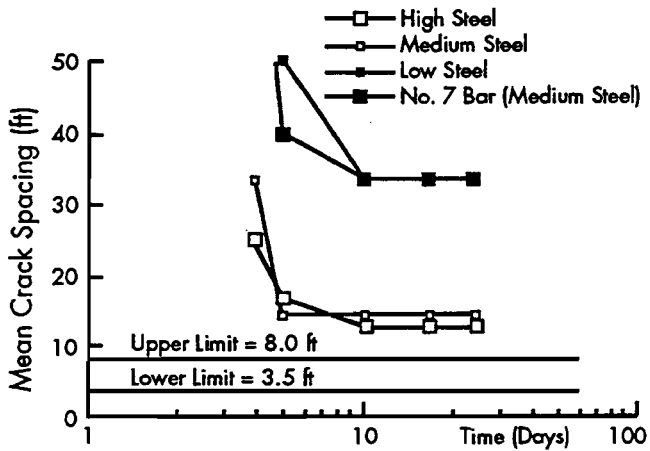
Winter Construction

All the test sections constructed in the winter were in good condition. The shapes of the cracks were fairly straight (see Chapter 5) and no longitudinal cracks were observed in the winter construction.

The LS sections especially appear to be in excellent condition. The cracks were very tight, even though the crack spacings were relatively large (mean crack spacings of LS sections after 1 month of construction were approximately 7 to 35 feet). The SRG sections seem to be in good condition as well, but the cracks were slightly wider, spaced closer, and a little more meandering in shape than those of the LS sections (mean crack spacings of SRG sections after 1 month of construction were 7 to 15 feet). As expected, the greater the amount of longitudinal steel, the narrower the crack width and the greater the number of cracks. Neither the differential bond area nor the use of different bar sizes (No. 7 bars) has shown significant difference in crack width or spacing thus far.



(a) SRG



(b) LS

Figure 7.4 Mean crack spacing versus time (IH-45 winter)

Summer Construction

Unlike those of winter construction, the sections constructed in the summer seem to be in much worse condition, probably because of the large variation of concrete temperature resulting from the rapid cement hydration (see Chapter 4). The first crack was noted about 10 hours after placement (see Chapter 3), and numerous cracks occurred within the first several days after construction. These early-age cracks were relatively wide and very random in shape.

For the SRG sections, mean crack spacings were already within the acceptable level (3.5 to 8 feet) even before the pavement experienced the complete temperature cycle of the year (Fig 7.1a).

Many of the individual cracks were spaced closer than 3.5 feet (Fig 7.5a). More cracking is expected during the cold season.

Crack widths of the summer project, presented in the Figures 6.3 to 6.6, are within an acceptable region (0.04 inch). Since, however, these measurements were performed at the time of high slab temperatures (average slab temperature of 81°F) in the summer, maximum crack width in the cold period would be much greater than that shown in the plots. This might be a result of the high setting temperatures of summer construction.

The shapes of cracks were quite meandering. Many longitudinal cracks were also observed in the summer construction. Cracks occurring within 24 hours after construction had shapes that meandered significantly (see Chapter 5). This type of meandering increases the possibility of Y-cracks or punchouts in the future.

In general, the SRG sections seemed to be in worse condition than the LS sections, since the cracks were wider and more meandering. Minor spalls (1/8 to 1/4 inch wide) were also observed on the SRG sections within 6 months after construction.

It was apparent also in the summer project that tighter crack widths are associated with larger steel quantities, but the crack spacing was not significantly affected by the steel design. High peak temperature resulting from the rapid hydration and subsequent temperature drop in the concrete during the first night after construction resulted in many early-age cracks, and it is believed that many of these cracks occurred before sufficient bond between the steel and concrete was developed. Instead, time and temperature of the construction day were the more influential factors than the steel reinforcement for hot weather construction (see Chapter 4).

Therefore, it may be difficult to control the cracking of summer construction by controlling the amount of longitudinal steel. If the amount of longitudinal steel is decreased to reduce the number of cracks, crack width may be excessive. On the other hand, if the steel amount is increased to reduce the crack width, more cracks will develop. Since the shapes of the cracks occurring with summer construction are quite meandering, these cracks will increase the chances of future punchouts.

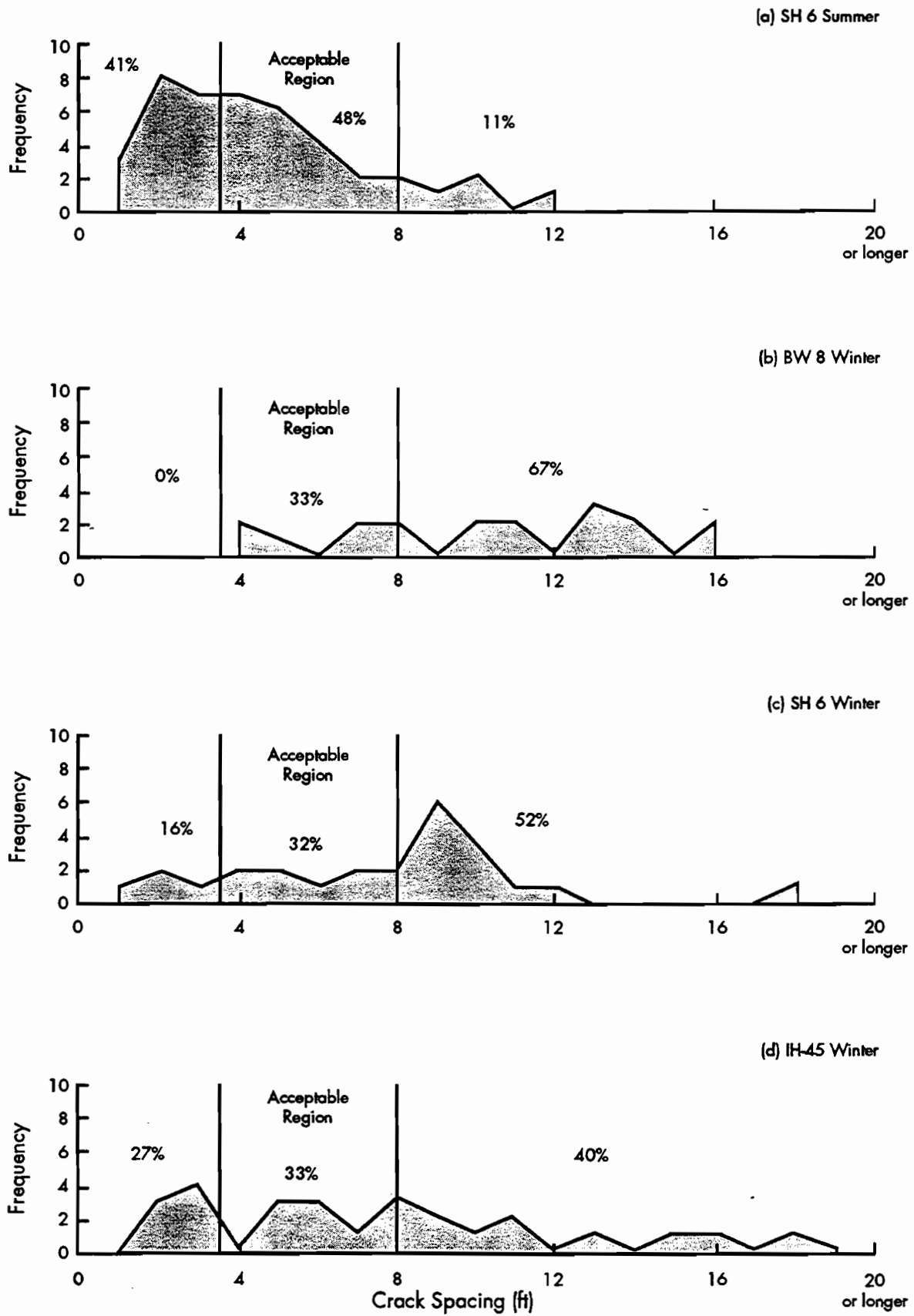


Figure 7.5 Distribution of crack spacings for the medium steel sections (SRG)

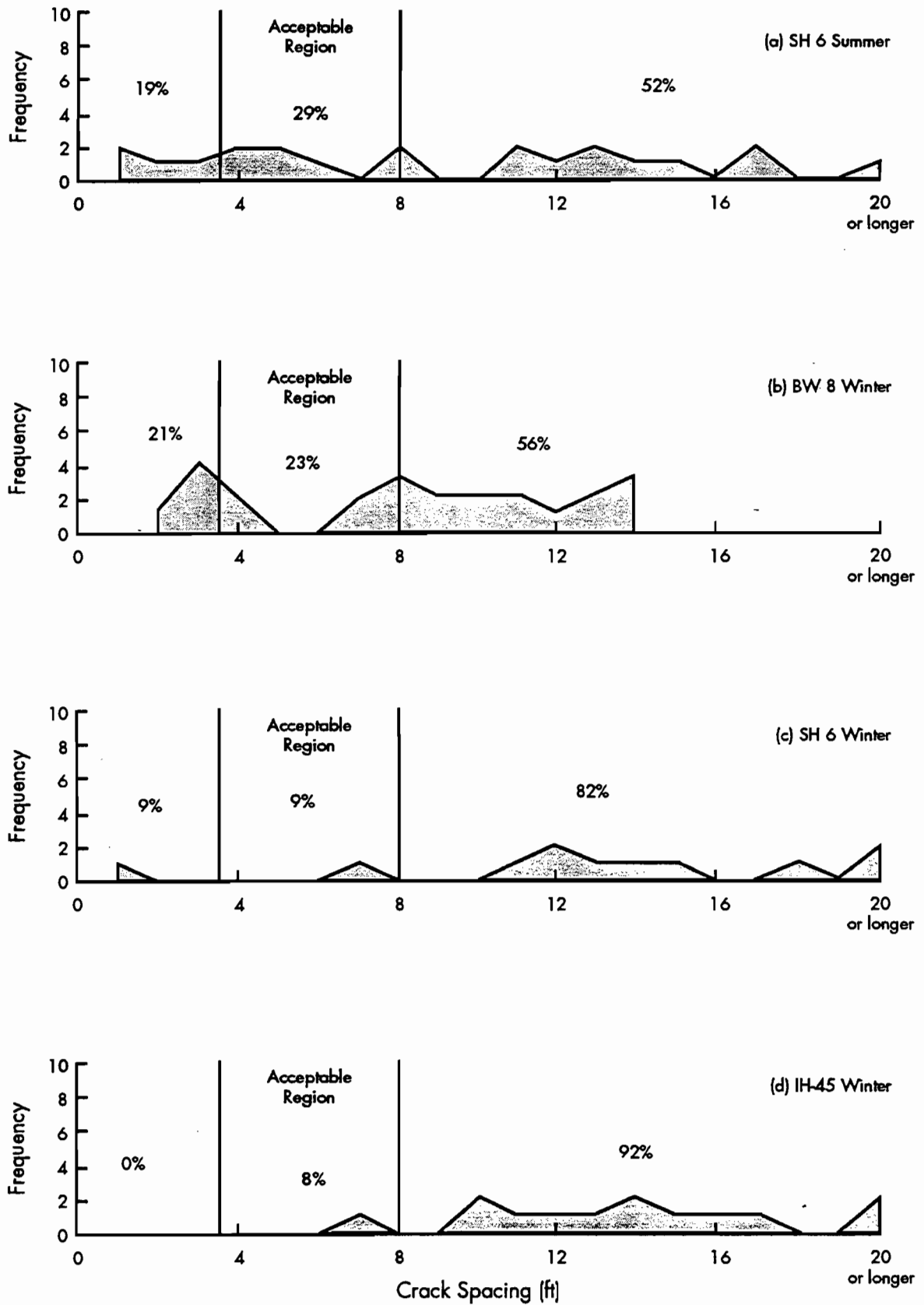


Figure 7.6 Distribution of crack spacings for the medium steel sections (LS)

CHAPTER 8. COMPARISON OF PREDICTED WITH OBSERVED CRACK PATTERNS

In this chapter we examine the cracking (both the crack spacings and crack widths) exhibited by the test sections during the first month after construction, comparing them with the cracking patterns predicted by the latest version of CRCP computer program (CRCP-7). Input data used in running the program and discussions of the results are presented in the following sections.

INPUT DATA

Concrete material properties (strength, shrinkage, thermal coefficient, and elastic modulus) were obtained from the cylinder tests (Appendix B). Design variables, including slab thickness, percent steel, and steel bar size, were obtained from the design of the test sections mentioned in Chapter 2. For the inputs of daily minimum temperatures, slab temperatures, rather than air temperatures, were used for a more realistic prediction.

Curing temperature used in the input data was the average value of the fresh concrete temperature and the maximum concrete temperature during hydration ($[\text{maximum slab temperature} + \text{fresh concrete temperature}]/2$). A material variability of 20 percent (coefficient of variation of concrete strengths) was used. These values were selected based on their good fit with the computer program. A reasonable method for selecting curing temperature considering actual concrete setting was proposed in Chapter 6. But this method was not applied in this chapter. This method can be used in the future when a correlation of the setting temperature obtained by this method with other easily measurable variables such as fresh concrete temperature and air temperature.

INTERPRETATION OF RESULTS

Figures 8.1 to 8.4 show the comparison of predicted with observed crack spacings for the medium steel sections of each test location. Plots for the other sections are presented in Appendix G.

Solid lines in the figures represent observed crack spacings during the short-term monitoring of the test sections. Dotted lines show predicted crack spacings during the first 6 months by CRCP program. Figure 8.5 presents a comparison of predicted and observed crack spacing distributions at the end of the short-term monitoring. As may be seen in the figures, the program reliably predicted crack spacing history during the early life. The comparisons should be checked after the minimum temperatures have been experienced.

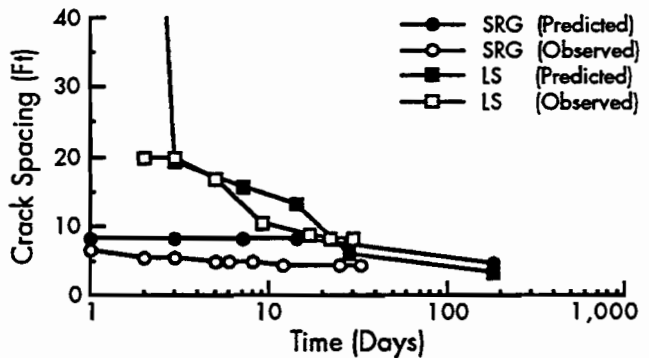


Figure 8.1 Comparison of predicted crack spacings with observed crack spacings (SH6-summer, medium steel)

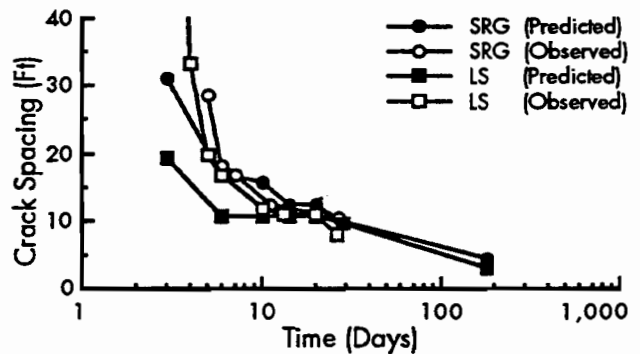


Figure 8.2 Comparison of predicted crack spacings with observed crack spacings (BW8-winter, medium steel)

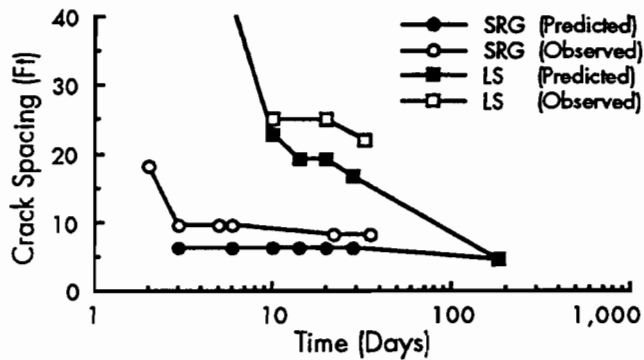


Figure 8.3 Comparison of predicted crack spacings with observed crack spacings (SH6-winter, medium steel)

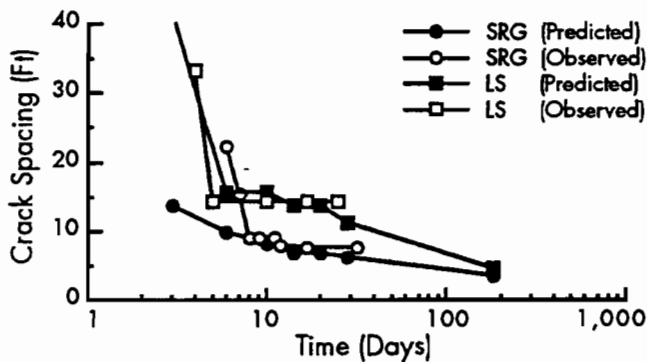


Figure 8.4 Comparison of predicted crack spacings with observed crack spacings (IH45-winter, medium steel)

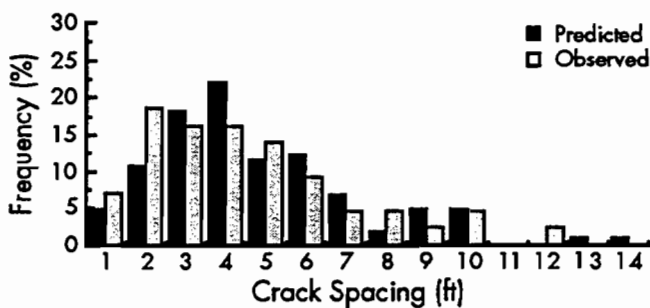


Figure 8.5 Comparison of predicted crack spacing distribution with observed crack spacing distribution (SH6-summer, medium steel)

Figures 8.6 to 8.9 present plots showing the comparison of predicted crack widths with observed crack widths for medium steel sections of the test sections placed on State Highway 6 (both summer and winter projects). Plots for the other sections are presented in Appendix H. In general, the CRCP program overpredicted crack widths.

There are several explanations for such a finding. The overprediction of the crack widths may be attributed to the prediction model which calculates crack width as a direct function of the

crack spacing. Thus, larger crack spacings result in greater crack widths. Since crack spacings were relatively large during the first month after construction, the program predicted large crack widths. And because the LS sections had larger crack spacings than the SRG sections, overprediction was more significant in the LS sections. The current crack width prediction model might be overly sensitive to the crack spacing during the early pavement life. Actually, the relationship between crack spacing and crack width is still not clear. During the short-term monitoring of the test sections, it was noted that there was not a relationship between crack spacings and crack widths within a specific test section (Fig. 5.12).

Another reason for the overprediction may be that the program does not consider the effect of crack occurrence age on crack width (Figs 5.10 and 5.11). Observations of the test sections show wider cracks occurring when the crack was formed at an early age. However, the crack used in the crack width prediction is one that occurred at the beginning of the construction.

Overprediction of crack widths in steel design of CRC pavement will result in a conservative design. For better prediction of crack width, however, modification of the crack width prediction model in CRCP program may be considered. It is suggested that the relationship between crack spacing and crack width be redefined, and that the effect of crack occurrence time be considered in the modification.

Although the CRCP program overpredicted crack widths, it predicted the effect of the steel quantity and steel bar size reasonably. As can be seen in Figure 8.10, greater crack widths were predicted with lower steel quantities (or larger bar sizes). This trend is the same as that for the observed crack widths on the test sections (Fig 5.9).

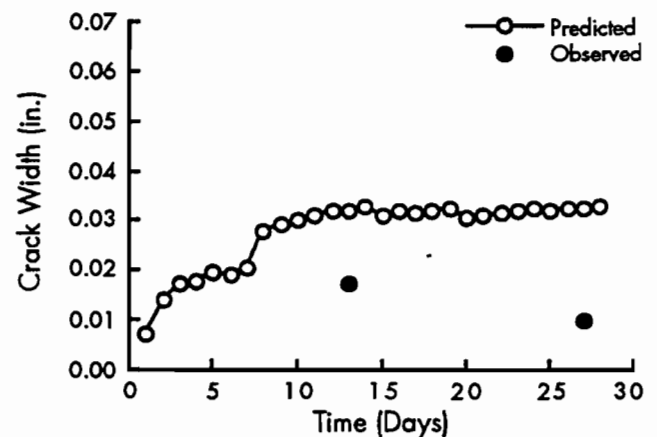


Figure 8.6 Comparison of predicted crack spacing distribution with observed crack spacing distribution (SH6-summer, medium steel)

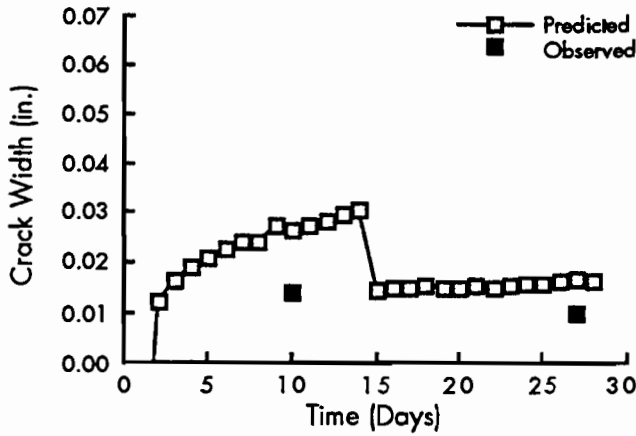


Figure 8.7 Comparison of predicted crack widths with observed crack widths (SH6-summer, LS, medium steel)

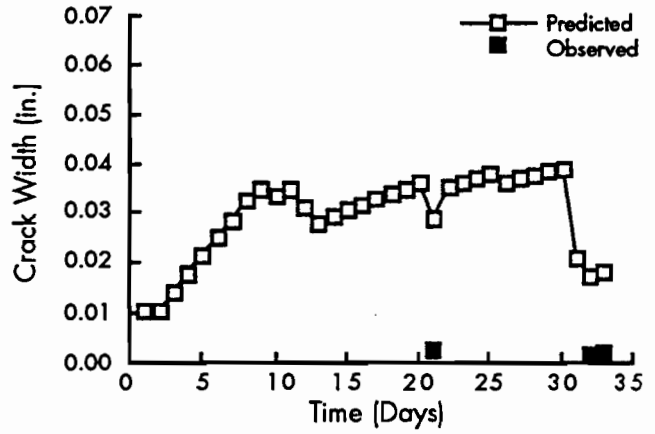


Figure 8.9 Comparison of predicted crack widths with observed crack widths (SH6-winter, LS, medium steel)

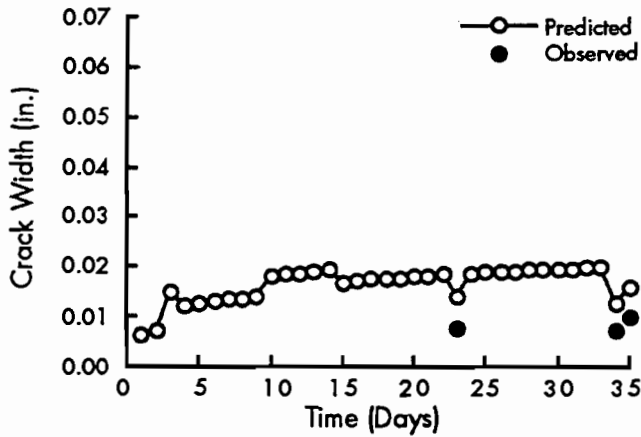


Figure 8.8 Comparison of predicted crack widths with observed crack widths (SH6-winter, SRG, medium steel)

SUMMARY

In this chapter, cracking histories (both crack spacings and crack widths) obtained from the test sections during the first month after construction were compared with the cracking patterns predicted by CRCP-7 computer program. Our finding was that the program reliably predicted crack spacing history during the early life. In general, however, the CRCP program overpredicted crack widths, possible explanations being that (1) the current crack width prediction model might be overly sensitive to the crack spacing during the early pavement life, and (2) the program does not consider the effect of crack occurrence age on crack width. Modification of the crack width model may be considered after long-term condition survey of the test sections.

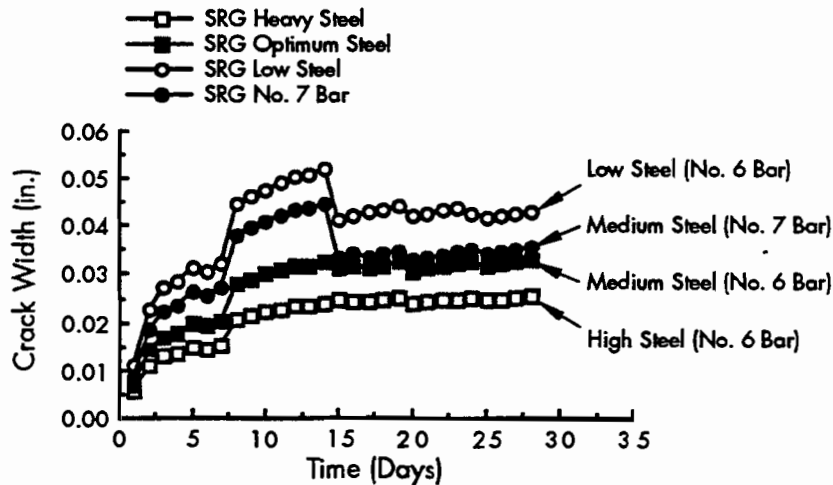


Figure 8.10 Effect of steel quantity and steel bar size on crack width (SH6-summer, SRG)

CHAPTER 9. DEVELOPMENT OF LONG-TERM FAILURE CURVES AND CALIBRATION OF THE FAILURE PREDICTION MODEL IN THE CRCP-7

This chapter discusses the major failure of CRCP under long-term traffic applications. Using the Rigid Pavement Database available at the Center for Transportation Research, we developed failure curves showing the relationship between the number of failures per mile and the number of traffic applications. These failure curves, in turn, allowed us to calibrate the failure prediction model in the CRCP-7 computer program.

CRCP-7 is the most recent version of a series of CRCP computer programs used to predict the performance of CRCP for a given design, material, traffic, and environmental condition. The calibrated model can now be used to estimate CRCP service life (in terms of the frequency of failures) of pavements functioning under various environmental and design conditions.

MAJOR FAILURE MODE IN CRCP

There are two types of failures in CRCP, structural and functional. Structural failure includes a collapse of the pavement structure or a breakdown of one or more of the pavement components. Functional failure may or may not be accompanied by structural failure, but it represents a condition in which the pavement can no longer carry out its intended function because of its roughness (Ref 47).

The functional condition of the pavement can be explained by the performance of the pavement—that is, by the history of its serviceability. Currently, the present serviceability index (psi) is used as the tool for representing this functional condition.

Yet, as many researchers have pointed out, the serviceability of a pavement with heavy maintenance does not change with time or traffic, though the distress increases significantly (Ref 48). Rather, serviceability changes mainly with roughness, and in CRCP there are few distress types that affect roughness significantly.

Therefore, the psi, which is an index of the functional condition of pavement, is not the best

tool for the design and scheduling of maintenance and rehabilitation of CRCP. In its place, Gutierrez and McCullough (Ref 48) have proposed that the condition of CRCP be represented in terms of the distress index, an index of the structural condition of pavement.

The major variable in the distress index is the number of punchouts. Representing the most severe distress manifestation associated with CRCP, the punchout is a structural failure in which a small segment of pavement is separated from the main body and displaced downward under traffic. The punchout is usually bounded by two closely spaced transverse cracks, a longitudinal crack, and the pavement edge, or sometimes by the branches of a Y-crack and the pavement edge (Ref 49).

A punchout is an area that has sustained a localized loss of support. This loss of support, which leads to relatively high slab deflections under heavy traffic (Ref 49), can occur through moisture accumulation (which softens the base or underlying material) or through the ejection of base material by pumping.

Under heavy traffic, higher slab deflections at the point of support loss result in excessive spalling and a loss of aggregate interlock at the crack. The wider the crack width, the sooner the aggregate interlock will break down under repeated loadings, an action that further increases both the deflection and transverse tensile stress of the slab (Fig 9.1).

Increasing transverse tensile stress and cumulative load fatigue damage eventually causes a longitudinal crack to form between the two transverse cracks. This longitudinal crack, along with the pavement edge, becomes the initial boundary of the potential punchout. The transverse tensile stress for a given thickness of the pavement depends on the spacing between the two transverse cracks; the closer the spacing of the cracks, the higher the transverse tensile stress (Fig 9.1). It is for this reason that punchouts are often associated with short transverse crack spacings.

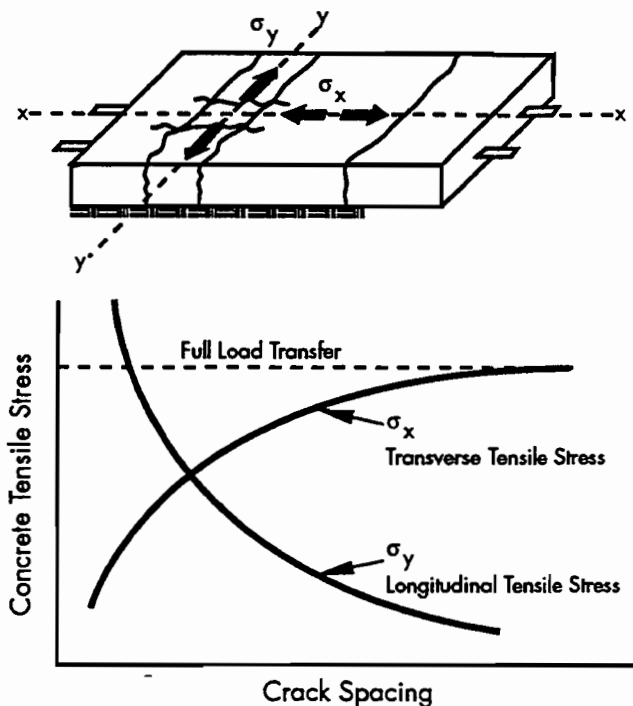


Figure 9.1 Relationship between crack spacing and concrete tensile stresses (Ref 5)

DEVELOPMENT OF FAILURE CURVES CONSIDERING RELIABILITY

Since 1974, the Center for Transportation Research has periodically conducted extensive condition surveys on CRCP in Texas. This database has now become a very valuable source of information for studies of the long-term performance of CRCP.

Customarily, a condition survey seeks to collect information on structural capacity, riding quality, skid resistance, and distress manifestations. Information on the environmental condition and traffic is also obtained. Condition survey procedures (Refs 1, 50, 51, 52, 53, and 54) have, since their initiation, been continuously modified for better efficiency.

Using the database, we developed failure curves showing the relationship between the number of failures per mile and traffic applications. A special data set was established from the database for the development of these failure curves. Variables in the data set include coarse aggregate type, swelling condition, number of failures per mile, and cumulative traffic in 18-kip equivalent single axle loads (ESAL).

Because a major portion of the database consists of 8-inch-thick CRCP, pavement sections with different thicknesses were excluded from the data set to reduce the variability. To eliminate the effect of overlay on the failure curves, survey data collected

after overlay were also excluded. For each section, the number of failures was calculated by summing the number of punchouts and patches.

Since condition surveys were conducted only on the outside lane, and since traffic data available in the database were of two-way traffic in 18-kip ESAL, a modification was necessary to obtain traffic information specific to the outside lane. For this modification, a directional distribution of 50 percent was used in conjunction with the lane distribution factors recommended in the AASHTO design guide (Ref 38).

Figure 9.2 shows the plot of the number of failures per mile with the number of traffic applications. Each data point represents the number of failures for a pavement section (about 1 mile of outside lane) for a certain survey year. Data were plotted using different symbols for the two different coarse aggregate types (SRG and LS) and the two different swelling conditions (high swelling and low swelling). If the roadbed soil was a high swelling soil and the annual rain was greater than or equal to 30 inches, the pavement was classified as a high swelling condition. If the roadbed soil was a low swelling soil, or if the annual rain was less than 30 inches (even though the soil is a high swelling soil), the pavement was classified as a low swelling condition.

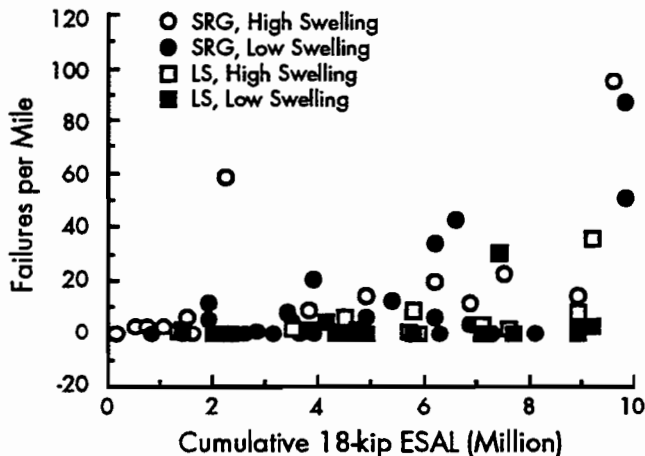


Figure 9.2 Number of failures with traffic application

In seeking a mean failure curve for each combination of coarse aggregate types and swelling conditions, we applied a logarithmic transformation to the number of failures to obtain a fairly uniform variation throughout the various traffic applications. A GLM (general linear model) procedure in SAS was run on the transformed data. Figure 9.3 shows the mean failure curves based on the results of GLM procedure.

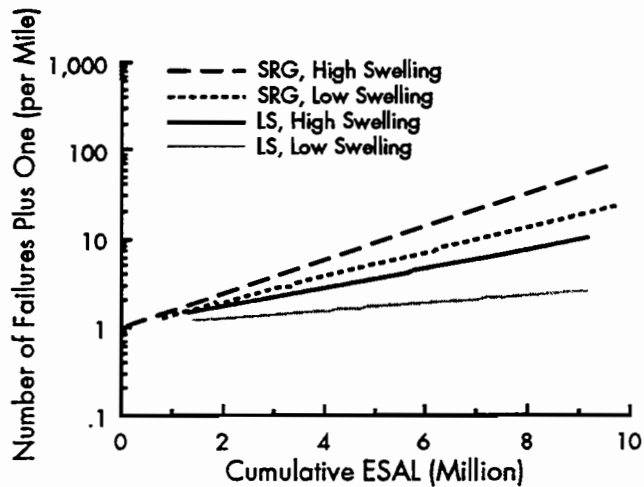


Figure 9.3 Mean failure curves for different coarse aggregate types and swelling conditions

To make the logarithmic transformation possible, the operation was conducted on the number of failures plus one, rather than on just the number of failures (since there were quite a few observations with zero failure). Also, to satisfy the boundary condition that there will be no failure at the beginning of load application, intercepts of the models were assumed to be zero. This was accomplished by using "NOINT" (no intercept) option in GLM procedure.

Residuals of the models were scattered randomly with fairly uniform variation throughout the many traffic applications, indicating that the models fit the data fairly well. The low R-square values of the models recorded (less than 60 percent) were probably caused by the variabilities in design and construction parameters that were not included in the models.

It should be noted that the inference space for the model is 8-inch CRCP in Texas. Accordingly, caution should be exercised when applying this model outside this inference space. Also, the condition surveys were performed in the outside lane (design lane) only.

Figure 9.3 indicates that concrete with LS showed better long-term performance than that with SRG, and that the swelling soil condition had an adverse effect on the performance of the pavements. The high possibility of failure associated with high swelling condition may be caused by the voids beneath the pavement (a result of the local swelling). Filling the voids may allow

application of the low swelling performance curves in Figure 9.3 to high swelling pavements.

Application of the Reliability Concept

The failure curves developed in the previous section show the average number of failures at certain traffic applications. The term "average" indicates that the models represent the number of failures with 50 percent reliability. (Failure curves of higher reliabilities are required in the design process.)

The failure curves for the higher reliability were obtained using the CLI option in GLM. The ALPHA (probability for out of the prediction interval) of the CLI option was doubled, because the CLI option gives interval estimates (upper limit and lower limit), whereas reliability requires upper limit only. Figure 9.4 shows a graphical illustration of the failure curves with various reliabilities (plotted in a log-scale). Figures 9.5 to 9.8 show the failure curves plotted in a normal scale (not log-scale) for each combination of coarse aggregate type and swelling condition. Data points in these figures represent the observed data.

It is shown that the concretes with siliceous river gravel (SRG) deteriorated at a much faster rate than those with limestone (LS). It is also shown that the high swelling condition accelerated deterioration of the pavements.

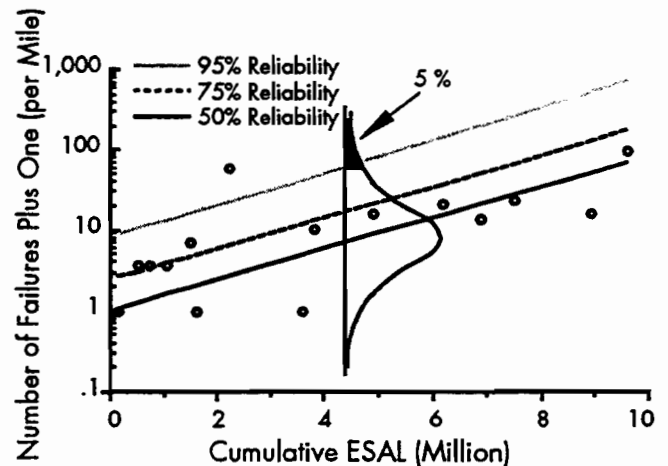


Figure 9.4 Failure curves with various reliabilities plotted in a log-scale (SRG, high swelling)

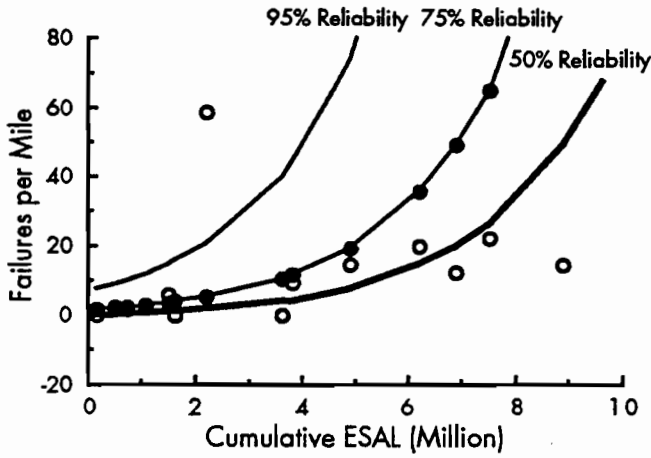


Figure 9.5 Failure curves with various reliabilities (SRG, high swelling)

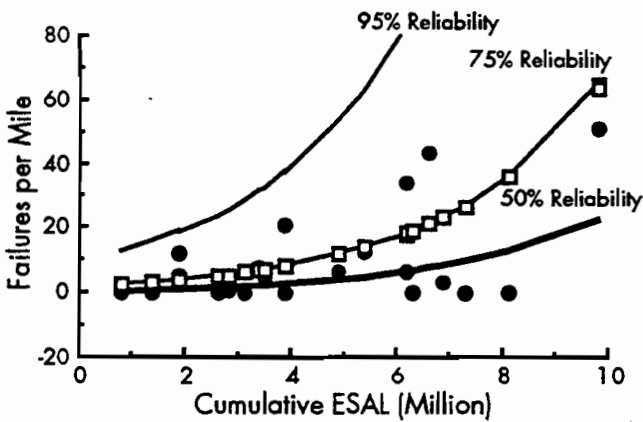


Figure 9.6 Failure curves with various reliabilities (SRG, low swelling)

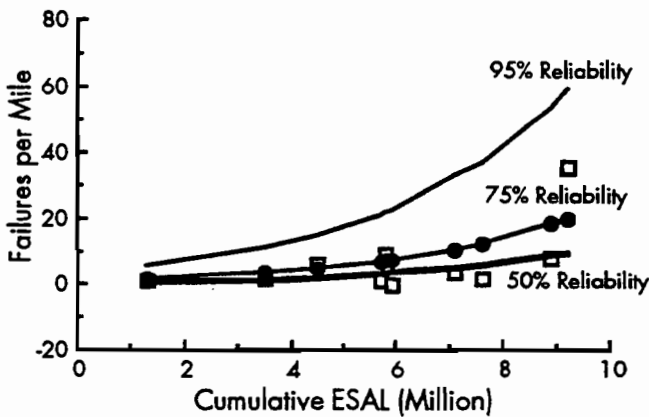


Figure 9.7 Failure curves with various reliabilities (LS, high swelling)

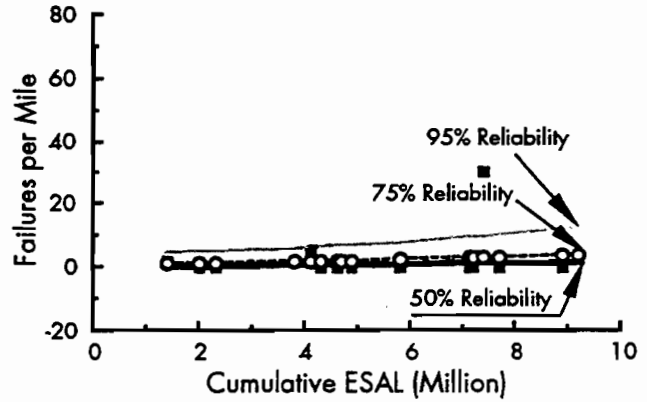


Figure 9.8 Failure curves with various reliabilities (LS, low swelling)

BASIC ALGORITHM FOR THE PUNCHOUT PREDICTION

Using the fatigue failure model, along with the relationship between the crack spacing and transverse tensile stress (Fig 9.1), Won (Ref 27) developed an algorithm for mechanistic failure prediction model.

The transverse tensile stresses developed by a wheel load (9,000 lbs) for various crack spacings and slab thicknesses were estimated by the computer program ILLISLAB developed at the University of Illinois. Because of the limitations inherent in ILLISLAB, the effects of aggregate interlock and longitudinal reinforcement on the transverse tensile stress were ignored. Using the results, we derived the following regression equation for the transverse tensile stress as a function of crack spacing and slab thickness (Ref 27):

$$s = e^{9.8474} D^{-1.8143} X^{-0.4477} \quad (9.1)$$

where:

- s = wheel load stress in transverse direction (psi),
- e = base of natural log,
- D = slab thickness (in.), and
- X = crack spacing (ft).

The generally accepted form of the fatigue failure model is

$$N = A \left(\frac{f}{s} \right)^B \quad (9.2)$$

where:

- N = number of load applications,
- f = flexural strength,
- s = flexural stress,
- A = coefficient (to be calibrated), and
- B = coefficient (widely used value is 4.0).

The variability of the fatigue life of the concrete was also considered. A graphical presentation of Equation 9.2 expressing the variability of the concrete strength is shown in Figure 9.9. For a given slab thickness, transverse tensile stress varies with the crack spacing (Fig 9.1). In Figure 9.9, fatigue lives for two different transverse tensile stresses (obtained from Equation 9.1 for two different crack spacings) are illustrated. For each stress level, there is variability in the fatigue life because there is variability in the concrete strength. The fatigue life variability is represented by the coefficient of variation (CV), which is a dimensionless index of variability obtained by expressing the standard deviation of the fatigue life as a percentage of the mean fatigue life.

The shaded areas in Figure 9.9 represent the possibility of a fatigue failure (or the possibility of longitudinal cracking between the transverse crack spacing, resulting in a punchout) at the given load replication, N. If the load replication increases, the possibility also increases. Using this methodology, the number of punchouts for various load replications can be predicted if the crack spacing distribution and the slab thickness are given. A detailed procedure of the prediction is presented in Ref 27.

CALIBRATION

The unknown coefficient A in Equation 9.2 and the CV value shown in Figure 9.9 are determined by correlating the failure curves predicted by the failure prediction model with the actual failure curves developed from the database of the long-term condition survey (shown in Figs 9.5 to 9.8).

For this purpose, the subroutine of the failure prediction in CRCP-7 was separated and modified to form an individual program so as to minimize the computer running time. Distributions of the transverse crack spacings for each coarse aggregate type and swelling condition were obtained from the database of the long-term condition survey. Flexural strengths were obtained from the results of the lab tests conducted at the Center for Transportation Research (647 psi for LS and 628 psi for SRG).

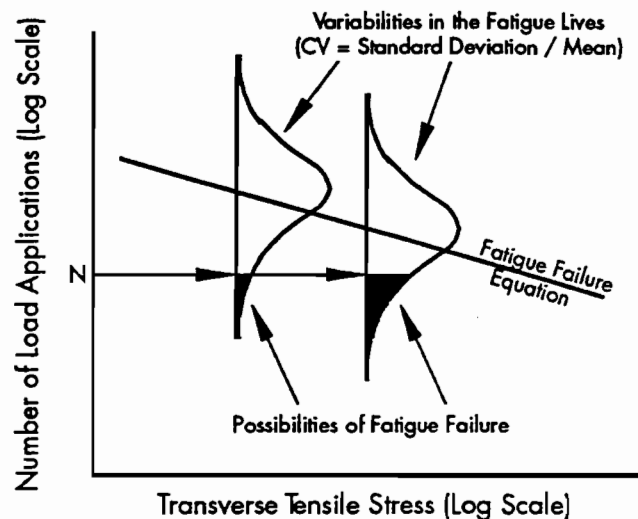


Figure 9.9 Fatigue failure of concrete considering the variability of the concrete strength

For each of the twelve actual failure curves (2 different coarse aggregate types \times 2 different swelling conditions \times 3 different levels of reliabilities), predicted failure curves, using various combinations of CV values and coefficient A values, were generated by running the modified subroutine of the failure prediction program. Predicted failure curves were compared with each of the actual failure curves, with the best fit curve selected by the least square method.

From the results of the above procedures, we found that the predicted failure curves with a CV value of around 30 percent showed a fairly close fit to the actual failure curves in most cases. Therefore, we decided to recommend the fixed CV value of 30 percent for future use of the failure prediction model. Figure 9.10 shows the coefficient A values for various conditions when the CV value is 30 percent.

Reliability	Swelling Condition	Coarse Aggr. Type			
		SRG		LS	
		Yes	No	Yes	No
95%		1.4	2.0	1.8	2.6
75%		2.4	3.1	2.5	3.7
50%		3.1	4.2	3.1	4.8

Figure 9.10 Coefficient A values that result in best fit to the actual failure curves (Unit: Million, CV: 30 percent)

As may be noted, the values obtained are very large as compared with the corresponding coefficients of other fatigue failure models of concrete. This discrepancy might be owing to the overestimation of the transverse tensile stresses that result from the neglect of the effect of the load transfer by aggregate interlock and longitudinal reinforcement in Equation 9.1. Figure 9.11 shows an example of how well the predicted failure curves (solid lines) fit the actual failure curves (dotted lines).

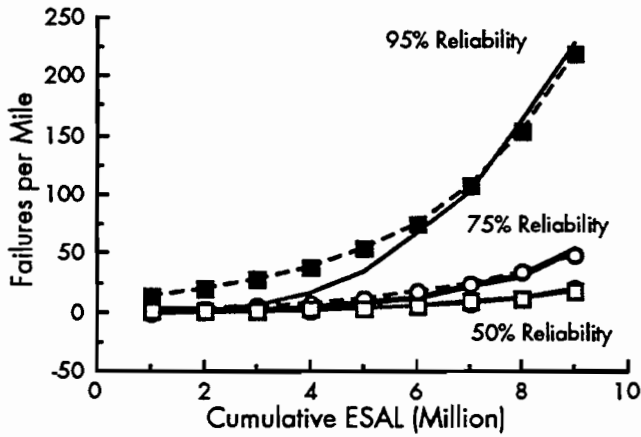


Figure 9.11 Fitness of the predicted failure curves to the actual failure curves (SRG, high swelling)

The higher the coefficient A , the higher the resistance of the concrete to cracking; the result is fewer failures and, consequently, a longer life. Figure 9.10 shows that the higher the reliability,

the lower the coefficient A , indicating higher conservatism for the higher reliability. In general, concrete with LS has a higher coefficient A than that with SRG, and the low swelling condition has a higher coefficient A than the high swelling condition.

The calibration has been conducted based on 8-inch CRCP, as mentioned earlier. To verify the calibration, a different data set consisting of 9-inch CRCP was obtained from the database. Figure 9.12 shows the failure curves of 9-inch CRCP predicted by the calibrated model. Actual failure data are also plotted. Although few actual data points are shown, the calibrated model predicted the number of failures fairly well. Further verification using more survey data is recommended.

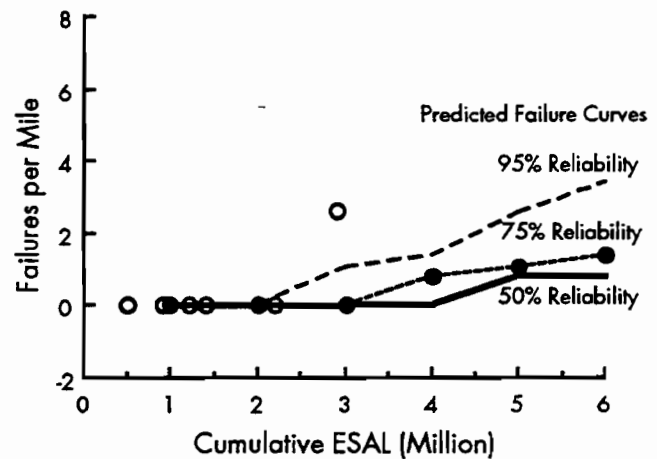


Figure 9.12 Verification of the calibration using CRCP with different thickness (9-inch CRCP, SRG, low swelling)

CHAPTER 10. DISCUSSION OF RESULTS AND SUMMARY

This chapter summarizes the early-age behavior of CRCP as observed during our short-term monitoring of the test sections. How these observations figure into the CRCP computer program is also discussed.

Since its introduction in 1975, the CRCP-1 program, the first version of the computer program used for predicting the performance of CRCP, has gone through several modifications (Ref 55). The most recent version, CRCP-7, is capable of predicting various structural responses to environmental and traffic loadings, responses that include mean crack spacing, distribution of individual crack spacings, crack width, concrete and steel stresses, and number of failures (punchouts) that can be expected after a certain number of load applications. And while most factors affecting the behavior and performance of CRCP are considered in this version of the program, there are some important factors that are necessarily omitted, a consequence of the program model's need to simplify the complex nature of a pavement system. These excluded factors will be discussed in this chapter.

EFFECT OF COARSE AGGREGATE TYPE ON CRACKING

Our observations revealed that significant crack spacing and crack width differences exist between the siliceous river gravel (SRG) sections and the limestone (LS) sections. The LS sections, without exception, showed fewer cracks (larger crack spacings) than the SRG sections during the short-term monitoring of the test sections (Figs 7.1 to 7.4). In addition, the LS sections showed smaller crack widths than the SRG sections, even though the crack spacings were larger (Figs 5.3 to 5.6). The factors that might account for the fewer cracks and smaller crack widths observed in the LS sections include that pavement's lower thermal coefficient, higher strain capacity, and lower elastic modulus.

We found that the difference in the cracking patterns (both crack spacing and crack width) for

concretes with various coarse aggregate types can be predicted satisfactorily using the CRCP program; one need only enter the different material properties relating to thermal coefficient, drying shrinkage, concrete strength, and elastic modulus, as part of the input data.

EFFECT OF DIFFERENT STEEL DESIGNS (SIZE AND AMOUNT OF STEEL)

It was observed in the winter projects (the summer project will be discussed later in this chapter) that the test sections having greater longitudinal steel quantities generally had more cracks and narrower crack widths. The reason: The greater quantity of longitudinal steel more effectively restrained slab movement, resulting in more and tighter cracks. At the end of the short-term monitoring, the use of different bar sizes (No. 6 and No. 7 bars) had not shown a significant difference in cracking. Theoretically, for the same percent of longitudinal steel, the larger bar provides a smaller steel/concrete bond area, which in turn should decrease the restraint of the slab movement and result in fewer cracks. Again, the CRCP program can, through the use of inputs, predict the effect of steel quantity and bar size.

PATTERNS OF NEW CRACKS IN A SLAB SEGMENT

The location of the new cracks in a slab segment seemed to depend on the length of the slab segment (crack spacing). There was a relatively consistent trend in the location of new cracks in slab segments less than about 8 feet long. For slab segments 3 feet long, the new cracks within the slab segment occurred, almost without exception, near the middle of the slab segment. Slab segments of greater length sustained a higher scattering of new cracks near the middle of the slab segment. When the crack spacings were longer than about 8 feet, the locations of the new cracks were randomly distributed (Fig 3.12). One possible

explanation for this phenomenon is that, if the crack spacing is greater than a certain length, the entire middle area of the slab segment from a certain distance from the two existing cracks is experiencing the same (or nearly the same) high stress (Fig 3.13). Accordingly, the location of the new cracks will be scattered somewhere between the two existing cracks.

While early models of the CRCP program placed the new crack at the middle of the slab segment, recent versions of the CRCP program (CRCP-5 and CRCP-7) consider the effect of the random location of the crack occurrences by using the variability of concrete strength (Ref 27). The distribution of individual crack spacings, which is used in the failure prediction of CRCP, can be predicted using one of these versions of the program. The randomness of the crack spacing distribution, as shown in Figure 3.12, supports the assumption (made in CRCP-5 and CRCP-7) that the variability of crack spacing is primarily owing to tensile strength variation and the application of a normal distribution of strength.

FACTORS AFFECTING THE CRACK WIDTH

Factors that significantly affect crack width include construction season, coarse aggregate type, amount of steel, and time of crack occurrence.

Regarding construction season, hot-weather placement yielded a much wider crack width at a given slab surface temperature condition than cool-weather placement (Fig 5.7), a result perhaps of the high curing temperatures (setting temperature) brought about by the high concrete temperatures associated with summer construction.

Regarding coarse aggregate type, the use of SRG aggregates resulted in crack widths wider than those of LS aggregates, with the differences more pronounced in the case of cold-weather placement (note the different temperature sensitivity of the crack width for the two different coarse aggregate types in Figure 5.8). This effect is the result of the different thermal coefficients of the concrete with the two coarse aggregate types.

The greater the amount of longitudinal steel, the narrower was the crack width; in other words, the greater the amount of steel, the more tightly the steel held the cracks. But the difference in crack width between the high steel and the medium steel was less than that between the low steel and the medium steel. These differences occurred even though the differences in the amount of longitudinal steel between high to medium and medium to low were about the same (Fig 5.9). In

this sense, the medium steel, which is the design standard, is a cost-effective design.

Cracks that occurred during the first 3 days of construction were significantly wider than those occurring later (Fig 5.10), a result of the larger residual crack shrinkage that occurred at the early age of the pavement (Fig 5.11). Since the early-age cracks are more prevalent in the summer placement than in the winter placement, special care should be taken during summer placement to avoid the wide early-age cracks.

The effects of placement season, coarse aggregate type, and steel design on the crack width can be considered in the CRCP program by utilizing (1) different curing temperatures for the different placement seasons, (2) different thermal coefficients for the different coarse aggregate types, and (3) different amounts of steel and bar sizes, respectively, in the input. However, the effect of the time of crack occurrence on the crack width is not considered in the CRCP program, since the program uses total drying shrinkage (the drying shrinkage that occurs from the time of initial placement to a later specified time) rather than residual drying shrinkage (the drying shrinkage that occurs from the time of cracking to a later specified time).

Contrary to the general belief that greater crack spacing leads to wider cracks, no significant correlation was observed between the crack spacing and the crack width (Fig 5.12). The computer program also predicts the crack width as a function of crack spacing; that is, the greater the crack spacing, the greater the crack width, since a longer slab segment would shrink more at the same temperature differential. More research in this area could improve the CRCP program.

EFFECT OF HYDRATION OF CEMENT AND TEMPERATURE CONDITIONS ON EARLY-AGE CRACKING

The heat caused by the hydration of cement significantly affects concrete temperature patterns in the pavement slab during the first 24 hours after construction. (Fresh concrete temperature, ambient temperature, and solar radiation prevalent during hydration primarily determine the pattern of concrete temperature.) Since the reaction of hydration is chemically controlled, the rate of hydration is very sensitive to the ambient temperature condition, such that a higher ambient temperature condition results in a higher rate of hydration. The higher the rate of hydration, the higher and the earlier the maximum peak of the concrete temperature (Fig 4.2). There were significant differences in the temperature patterns

between summer construction and winter construction, mainly a result of the different rate of hydration (Fig 4.6).

For the summer construction, the high ambient temperature conditions caused hydration to proceed very quickly, resulting in a very high peak in the concrete temperature during the construction day. As the air cooled and the temperature dropped during the first night after placement, numerous early-age cracks (Fig 4.6) and several longitudinal cracks (Fig 4.9) developed. Early-age cracks observed within the first several days after construction in the summer project tended to have large crack widths and meandering crack shapes—a tendency that increases the probability of Y-cracking, punchouts, spalling, and steel rupture in the future.

For the winter project, on the other hand, the low temperature conditions of the season caused hydration to proceed at a much slower rate. Because the primary heat generation of hydration occurred during the night (when the ambient air temperature dropped), there was only a very small temperature rise (Fig 4.6); in this case, part of the hydration heat essentially compensated for the heat lost during the night, resulting in small temperature changes during the first 24 hours after placement. The winter construction displayed fewer early-age cracks than the summer construction, with such cracks as observed being relatively straight (not meandering) and tight.

The frequency of early-age cracking in the summer project varied even with the time of placement in a day. The frequency of cracking was always greater in the area placed earlier in the morning than in the areas placed later during the day (Figs 4.12 to 4.16). For winter construction, however, the effect of placement time was negligible. The different crack patterns appearing in a day's run for the summer project might be the result of the difference in the time at which the primary hydration cycle occurs (Fig 4.16). Since the primary heat generation cycle begins several hours after the cement is mixed with water (Fig 4.1), the primary hydration cycle for the concrete placed early in the morning will occur during the high ambient temperature conditions of the daylight hours. The primary hydration cycle for the concrete placed in the afternoon, on the other hand, will occur under the relatively lower ambient temperature conditions of the evening or night following the construction day. If the primary hydration cycle occurs during the evening or night, the peak concrete temperature will be much lower, as compared with the high temperature conditions prevalent during the daytime. For the winter construction, however, the low temperature conditions prevailing throughout

the day cause the main heat generation cycle to occur during the night, regardless of placement time during the day (Fig 4.17). Consequently, the peak slab temperatures are lower.

For the summer construction, the transverse cracks that occurred during the first several days were not significantly affected by the amount or size of the reinforcing steel (Fig 4.11). This is probably because the placement time and temperature condition of the construction day were more influential than reinforcing steel (Fig 4.12).

Lowering the temperature variations by reducing the peak temperature of concrete (e.g., by pre-cooling or retarding the rate of hydration) can help minimize the problems associated with early-age cracks. In this method, setting temperature could be also lowered, resulting in less concrete tensile stress and smaller crack widths. (Although several temperature control techniques are introduced in Chapter 4, more research on this subject is suggested.)

Because of the high temperature variations, the use of an aggregate having a low thermal coefficient, like LS, is recommended for hot-weather placement. A small difference in the thermal coefficient can cause a large difference in the total strain when the temperature differential is large. Lowering the peak temperature by the techniques mentioned earlier will ensure a greater reliability of the pavement with LS. The use of aggregates with a high thermal coefficient, like SRG, in the hot-weather construction should be minimized (unless steps are taken to lower the peak temperature).

Cracking of the concrete pavement bears a strong relationship to the concrete temperature variations. Cracks occurred, almost without exception, when the concrete temperature dropped significantly. The effect of temperature differential on cracking is considered in the CRCP program by utilizing curing temperature, daily minimum temperatures, and annual minimum temperature. However, the effect of hydration heat has not previously been considered in the computer program. This effect can be incorporated by using the proper curing temperature along with the daily minimum temperatures in the input. Another way to consider the effect of the hydration heat is to modify the computer program in such a manner that the program can predict the concrete temperature pattern affected by the hydration heat. The modification should consider the various factors affecting the rate of hydration, including ambient temperature, solar radiation, atmospheric condition, and placement time.

It was found from the monitoring of the slab movement and slab temperature at various

positions through the depth (Fig 3.9) that the first cracks of the summer construction occurred as a result of the warping stress caused by the temperature gradient. Currently, the CRCP program does not consider the warping stress in the stress calculation.

CURING TEMPERATURE (SETTING TEMPERATURE)

Curing temperature, because it is a reference temperature in the calculation of the temperature differential at the time of interest, is very important in running the CRCP program. Therefore, the proper selection of the setting temperature is required for the correct prediction of the structural response of the pavement. Many design procedures now use the fresh concrete temperature recorded at the time of placement as the curing temperature. Theoretically, however, the curing temperature should be the concrete pavement temperature at which the concrete begins to assume stresses induced by shrinkage or temperature change. This temperature is not necessarily the fresh concrete temperature, since stress does not occur while the concrete is in a plastic state.

For determining the curing temperature in concrete pavements, we developed a method that accounts for the effect of hydration heat by monitoring the concrete temperature and the movement of concrete within a modified cylinder mold (Chapter 7). Since this method is somewhat cumbersome for practical use, a correlation of the setting temperature obtained by this method with other easily determined variables, such as fresh concrete temperature and air temperature, is recommended.

SLAB SHRINKAGE

The study team also determined the correlation of shrinkages between the concrete slab (actual pavement) and the concrete cylinder. It was found that the shrinkage of a cylinder cured in the laboratory at 75°F and 40 percent relative humidity sufficiently represented the shrinkage of the concrete slab (Figs 6.6 and 6.7). Therefore, shrinkage data collected from lab-cured concrete cylinders can be used as the shrinkage values for running the CRCP program (or other research) without high risk. (It should be noted that the concrete cylinder was cured without removing the cylinder mold.)

OTHER FINDINGS FROM THE TEST SECTIONS

About half of the cracks in the bondbreaker/subbase reflected through the concrete slab

during the short-term monitoring of the test sections (Figs 3.14 and 3.15). In general, more bondbreaker/subbase cracks were reflected in the summer construction than in the winter construction, probably as a result of the greater slab movement (concrete stress) at early ages caused by the large temperature change. More reflection occurred in the SRG sections than in the LS sections (Fig 3.15), probably as a consequence of the greater slab movement that results from the larger thermal coefficient for the same temperature change. Most of the reflected cracks of the summer construction occurred within a few days, with such cracks characterized by very meandering shapes (Fig 3.16).

Many of the transverse cracks occurred over the transverse steel bars, a phenomenon that was more significant in the sections having double-layered steel. Since the cross-sectional area of the concrete of a vertical plane that includes the two layers of transverse steel is smaller than other planes by the diameter of the steel, this plane becomes a weak plane. This reduced cross-sectional area of the concrete increases the possibility of cracking along the plane. Cracking over the steel bars increases the probability that water will contact the steel, resulting in a higher possibility of steel corrosion. A staggered (top to bottom) layout of the transverse steel, as shown in Figure 3.21(b), is recommended as a way of avoiding this problem.

Many of the longitudinal steel-spliced areas showed transverse cracks in the concrete, usually at one of the splice ends. Such cracks could be the result of the sudden change in the amount of steel at the ends of the splice. However, the general shapes of the cracks were not meandering.

All of the manhole areas showed two to five meandering cracks around the manhole, probably a result of the reduction of the cross-sectional area and the discontinuity of the longitudinal steel in this area. Within 1 year after construction, these areas showed punchouts or severe spalling along the cracks (Fig 3.19).

The CRCP program does not consider reflection cracking, the location of transverse steel, the effect of splices, or manholes. But because these items can be considered using other design techniques, changes to the CRCP program are not recommended.

CALIBRATION OF THE FAILURE PREDICTION MODEL IN CRCP-7

Using the long-term condition survey data available at the Center for Transportation

Research, we developed failure curves showing the number of failures at various load applications and reliabilities (Figs 9.5 to 9.8). Next, using the failure curves, we calibrated the failure prediction model in the computer program CRCP-7 (Fig 9.10). The calibrated model can be used to estimate CRCP life in terms of the frequency of failures for pavements functioning under various environmental and design conditions.

SUMMARY

This chapter has summarized this study's observations and findings; how these observations and findings are considered in the CRCP program was also discussed. Observations considered in the CRCP program, those which require modifications of the program, and those which require further research are summarized with brief discussions in Tables 10.1 to 10.3, respectively.

Table 10.1 Observations considered in the CRCP program

Observation	Method of Considering in Design
Effect of coarse aggregate type on crack spacing and width	Coarse aggregate type affects the following concrete properties considered in the program: <ol style="list-style-type: none"> a. Thermal coefficient b. Shrinkage c. Elastic modulus d. Strength
Effect of steel quantity and size on crack spacing and width	Steel design is considered in the program by the following input variables: <ol style="list-style-type: none"> a. Type of steel bar b. Percent c. Size of steel bar
Seasonal effect on crack spacing and width	Can be simulated by entering proper values of the following input variables: <ol style="list-style-type: none"> a. Curing temperatures b. Daily minimum temperatures c. Annual minimum temperature
Patterns of new cracks in a slab segment	Random crack patterns can be considered in the program by using the coefficient of variation of the concrete strength as an input variable.

Table 10.2 Observations which require modification of the CRCP program

Observation	Recommendation
Effect of hydration on crack spacing and width	Develop a temperature prediction model for early-age concrete using factors affecting the rate of the hydration, such as fresh concrete temperature, air temperature, solar radiation, and placement time. Then, add the model in the program.
Effect of crack occurrence time on crack width	During the long-term monitoring, determine if the effect is still significant. If so, modify the program to account for the residual shrinkage.
Insignificant effect of crack spacing on crack width	Check this effect during the long-term monitoring. If the effect is still not significant, modify the crack width prediction model in the program.
Effect of warping stress on cracking	Identify warping stress mechanism in CRCP by studying temperature gradient. If the effect of the warping stress is significant, modify the stress prediction model in the program.

Table 10.3 Observations which require further research

Observation	Recommendation
Randomness of crack	Use the Randomness Index (Ref 7) to evaluate crack shapes quantitatively for various placement seasons, times of crack occurrence, and coarse aggregate types. Then correlate the results with the probability of punchout. Reflect the results in the punchout prediction model in the program.
Pavement life prediction	Use the calibrated punchout prediction model to predict lives of CRCP with various designs, materials, environmental conditions, and traffic conditions.
Determination of the curing temperature	Correlate the curing temperature obtained by the method given in Chapter 7 with easily determined variables, such as fresh concrete temperature, air temperature, and solar radiation. Then, curing temperature can be predicted using this correlation.

CHAPTER 11. CONCLUSIONS AND RECOMMENDATIONS

In this final chapter, conclusions and recommendations are outlined based on the observations and findings from the study. Discussion in detail is presented in Chapter 10.

BASIC CONCLUSIONS

Short-term monitoring of the test sections during the first one month after construction has been completed. In this report, observations and findings from the short-term monitoring of the test sections are presented. A discussion is also presented as to how these observations and findings are considered in the CRCP computer program.

Based on the long-term condition survey data available at the Center for Transportation Research, failure curves showing the number of failures at various numbers of load applications (considering various reliabilities) have been developed. Using the failure curves, the failure prediction model in the computer program CRCP-7 has been calibrated. The calibrated model can be used to estimate CRC pavement life in terms of the frequency of failures for the pavements with various environmental and design conditions.

GENERAL CONCLUSIONS

In this section, general conclusions from the short-term monitoring of the test sections are presented. The conclusions will discuss both those items which have been considered in the CRCP program and those items which require further research or modification of the CRCP program.

Conclusions from the short-term monitoring of the test sections which are considered in the CRCP program are outlined below.

- (1) For all the paired test sections, there were significant differences in both crack spacing and crack width between the siliceous river gravel (SRG) sections and the limestone (LS) sections. The LS sections, without exception, experienced fewer cracks and larger crack spacings than the SRG sections. The LS sections also experienced smaller crack widths than the SRG sections, even though the crack spacings were larger.
- (2) Generally, with the winter projects, the crack spacing and crack width decreased as the percent steel increased. At the age of one month, a change in bond area achieved by the use of different bar sizes (No. 6 and No. 7 bars) had not shown a significant difference in cracking.
- (3) The location of the new crack between the two adjacent old cracks in CRC pavement seemed to depend on the distance between the two old cracks (longitudinal length of the slab segment). There was a relatively consistent trend in the location of the new crack in a slab segment when the slab segment was less than about 8 feet long. When the slab segment was about 3 feet long, the new crack within the slab segment occurred, almost without exception, near the middle of the slab segment. Longer slab segments showed greater scattering of the new cracks near the middle of the slab segment. When the slab segments were longer than about 8 feet, the locations of the new cracks were randomly distributed. This supports the assumptions made in CRCP-5 or CRCP-7, that the variability of crack spacing is primarily due to tensile strength variation and the application of a normal distribution of strength.
- (4) Factors which significantly affect crack width were construction season, coarse aggregate type, amount of steel, and time of crack occurrence. Hot weather placement showed much wider cracks at a given slab surface temperature condition than cool weather placement. The use of SRG aggregates resulted in wider cracks than use of LS aggregates, and the difference was larger at lower temperatures. The greater the amount of longitudinal steel, the narrower the crack width. Cracks occurring during the first three days of construction were significantly wider than those which occurred later.

- (5) Shrinkage of a concrete cylinder cured in the laboratory at 75°F and 40 percent relative humidity, without removing the cylinder mold, sufficiently represented the field shrinkage of the concrete slab.
- (6) The CRCP program reliably predicted crack spacing history (both mean crack spacings and crack spacing distribution) during the early life.

Observations and findings from the short-term monitoring which require further research or modification of the CRCP program are outlined below.

- (1) The heat caused by the hydration of the cement significantly affects the pattern of the concrete temperature in the pavement slab during the first 24 hours after construction, and consideration should be given to controlling the temperature especially in summer placements. Fresh concrete temperature, ambient temperature conditions, and solar radiation influence the pattern of concrete temperature during the hydration. Since the reaction of the hydration is chemically controlled, the rate of hydration is very sensitive to the ambient temperature conditions. A higher ambient temperature condition results in a higher rate of hydration. The higher the rate of hydration, the higher and the earlier is the maximum peak of the concrete temperature.
- (2) There were significant differences in the crack patterns between summer construction and winter construction. For the summer construction, numerous early-age cracks and several longitudinal cracks were observed, whereas a much smaller number of early-age cracks and no longitudinal cracking were observed in the winter construction. This may be related to the higher temperature change associated with the summer construction, resulting from the higher rate of hydration.
- (3) Early-age cracks observed within the first several days after construction in the summer project tended to be wide and meander badly. This tendency will increase the probability of Y-cracking, punchouts, spalling, and steel rupture in the future.
- (4) The frequency of early-age cracking in the summer project varied even with the time of placement during a day. The frequency of cracking was always greater in the area placed earlier in the morning than in the areas placed later during the day. For winter

construction, however, the effect of placement time was negligible.

- (5) For the summer construction, the transverse cracks which occurred during the first several days did not differ significantly with the amount or size of the reinforcing steel. This may be because placement time and temperature are more important than reinforcing steel.
- (6) Contrary to the general belief that the greater the crack spacing the wider the cracks, no significant correlation was observed between the crack spacing and crack width during the short-term monitoring. It is recommended that the correlation be checked again during long-term monitoring of the test sections.
- (7) In general, the CRCP program overpredicted crack widths. The overprediction of the crack widths may be because (1) the current crack width prediction model might be overly sensitive to the crack spacing during the early pavement life, and (2) the program does not consider the effect of crack occurrence age on crack width. Modification of the crack width model may be considered after long-term condition survey of the test sections.
- (8) A method for determining the curing temperature used in calculating the temperature-induced stress in concrete pavements has been developed by monitoring the concrete temperature and the movement of concrete within a modified cylinder mold.

RECOMMENDATIONS FOR THE FUTURE CONSTRUCTION

- (1) In this study, problems associated with early-age cracks in summer construction, meandering shapes and wide cracks, have been discussed. In order to avoid these unwanted early-age cracks, it is better to place concrete in cool weather, because the early-age cracks are a product of hot-weather concreting. It may be difficult to control the early-age cracks by controlling the amount of longitudinal steel, because the bond between steel and concrete is not fully developed during the first several days after construction.
- (2) If it is necessary to place concrete during hot weather, it is recommended that placement begin in the afternoon rather than in the morning to reduce early-age cracks, because afternoon construction produces less temperature rise. Nighttime construction should be also considered.

- (3) Since the temperature rise by hydration during the construction day and subsequent cooling during the night cause the problems, a reduction of the temperature rise during construction by some technique will also decrease the tendency toward unwanted early-age cracks. These techniques could include pre-cooling, the use of pozzolanic material, and the use of retarder. A much lower variation in concrete temperature can be expected if the concrete temperature can be controlled by these techniques in such a manner that the main heat generation period of hydration occurs during the nighttime when the ambient temperature is lower. Reducing the temperature rise by these methods will delay the time of crack occurrence, and a substantial amount of the tensile stresses induced by the drying shrinkage and temperature drop can be relieved by creep. The pavement benefits most from the creep effect when the time of cracking is delayed as long as possible. The curing temperature (setting temperature) of the concrete could also be lowered by reducing the temperature rise, resulting in a lower concrete tensile stress and smaller crack width.
- (4) Due to the high temperature variations, the use of aggregate with a low thermal coefficient, like limestone, is recommended for hot-weather placement. The use of aggregates with a high thermal coefficient, like siliceous river gravel, in hot-weather construction should be minimized unless steps are taken for lowering the peak temperature.
- (5) It should be noted that longitudinal cracks began to occur during the first night after the construction day. In order to avoid unwanted longitudinal cracks, it is recommended that the longitudinal joint of the concrete pavement placed in hot weather be sawed during the evening of the day of construction as soon as the concrete gains enough strength for the sawing operation. A proposed sawing schedule is given in Figure 3.11.
- (6) Many of the transverse cracks occurred over the transverse steel bars, and this phenomenon was more significant in the sections with double-layered steel. Cracking over the steel bars increases the possibility of water contact to the steel, resulting in a higher possibility of steel corrosion. A staggered steel layout is recommended to reduce this problem (Fig 3.21).
- (7) All of the manhole areas showed two to five meandering cracks around the manhole. Within one year after construction, these areas showed punchouts or severe spalling along the cracks. Relocation of the manholes is recommended at the design stage based on the long-term benefit-cost analysis, or the design around the manhole should be improved.

RECOMMENDATIONS FOR THE FUTURE RESEARCH

- (1) In order to observe the long-term performance of the test sections, condition surveys should be conducted annually for the first two or three years after construction, and thereafter less frequently. It is recommended that the condition surveys be performed during the winter so that cracks can be easily observed and the maximum crack widths can be measured.
- (2) Comparison of the predicted crack patterns by the CRCP program with measured crack patterns from the test sections, in terms of crack spacing and crack width, is recommended.
- (3) Checking design details, considering future punchouts using the calibrated distress prediction model in CRCP-7, is recommended.
- (4) Further research efforts on the use of the slab temperature controlling techniques during the first 24 hours after placement (i.e., pre-cooling, use of flyash, and use of retarder) are highly recommended to determine the performance and practical feasibility of each technique.

REFERENCES

1. Velasco, M. G., and B. F. McCullough, "Summary Report for 1978 CRCP Condition Survey in Texas," Research Report 177-20, Center for Transportation Research, The University of Texas at Austin, January 1981.
2. Green, W. J., R. L. Carrasquillo, and B. F. McCullough, "Coarse Aggregate for PCC—Pilot Study Evaluation," Research Report 422-1, Center for Transportation Research, The University of Texas at Austin, September 1987.
3. Aslam, M. F., C. L. Saraf, R. L. Carrasquillo, and B. F. McCullough, "Design Recommendations for Steel Reinforcement of CRCP," Research Report 422-2, Center for Transportation Research, The University of Texas at Austin, November 1987.
4. Won, M. C., B. F. McCullough, and W. R. Hudson, "Evaluation of Proposed Texas SDHPT Design Standards for CRCP," Research Report 472-1, Center for Transportation Research, The University of Texas at Austin, April 1988.
5. McCullough, B. F., J. C. M. Ma, and C. S. Noble, "Limiting Criteria for the Design of CRCP," Research Report 177-17, Center for Transportation Research, The University of Texas at Austin, August 1979.
6. Zollinger, D. G., "Investigation of Punchout Distress of Continuously Reinforced Concrete Pavement," Ph.D. diss., University of Illinois at Urbana-Champaign, 1989.
7. Suh, Y. C., B. F. McCullough, and K. Hankins, "Development of Randomness Index and Application," Transportation Research Board, January 1991 (to be published).
8. Mindess, S., and F. Young, *Concrete*, Englewood Cliffs, NJ: Prentice-Hall, 1981.
9. Mehta, P. K., *Concrete Structure, Properties, and Materials*, Englewood Cliffs, NJ: Prentice-Hall, 1986.
10. Samarai, M., S. Popovics, and V. M. Malhotra, "Effect of High Temperatures on the Properties of Fresh Concrete," Transportation Research Record No. 924, 1983, pp 42-50.
11. Kosmatka, S. H., and W. C. Panarese, *Design and Control of Concrete Mixtures*, 13th ed., PCA, 1988.
12. Samarai, M., S. Popovics, and V. M. Malhotra, "Effect of High Temperatures on the Properties of Hardened Concrete," Transportation Research Record, 924, pp 50-56.
13. "Recommended Practice for Hot Weather Concreting," Proposed by ACI Committee 305, *ACI Journal*, July 1971.
14. Mironov, S. A., "Some Generalizations in Theory and Technology of Acceleration of Concrete Hardening," Symposium on Structure of Portland Cement Paste and Concrete, Special Report 90, Highway Research Board, 1966.

15. *Concrete Manual: A Manual for the Control of Concrete Construction*, 8th ed. (revised), U.S. Department of the Interior, Bureau of Reclamation, 1979.
16. Carino, N. J., and H. S. Lew, "Temperature Effects on Strength/Maturity Relations of Mortar," *ACI Journal*, No. 80-17, May-June 1983.
17. "Strength Gain and Temperature Effects," *New Zealand Concrete Construction*, pp 3-7, July 1983.
18. Neville, A. M., *Properties of Concrete*, 3rd ed., NY: John Wiley & Sons, Inc., 1981.
19. Klieger, P., "Effect of Mixing and Curing Temperature on Concrete Strength," *ACI Journal*, No. 54, pp 1063-1081, June 1958.
20. Davis, R. E., H. E. Davis, and E. H. Brown, "Plastic Flow and Volume Changes of Concrete." (n.d.)
21. Emborg, M., and S. Bernander, "Temperature Stresses in Early-age Concrete Due to Hydration," *Nordic Concrete Research*, No. 3, pp 28-48, December 1984.
22. Kasai, Y., K. Yokoyama, and I. Matsui, "Tensile Properties of Early-Age Concrete," *Mechanical Behavior of Materials, Proceedings of the International Conference on Mechanical Behavior of Materials, Vol 4*, The Society on Material Science, Japan, pp 288-299, 1971.
23. Kasai, Y., K. Yokoyama, I. Matsui, and K. Tobinai, "Tensile Properties of Early-age Concrete," Vol II, *Proceedings of the 1974 Symposium on Mechanical Behavior of Materials*, The Society of Materials Science, Japan, pp 433-441, August 1974.
24. Fouad, F. H., and H. L. Furr, "Behavior of Portland Cement Mortar in Flexure at Early Ages," *ACI Symposium of Early-age Concrete*, Chicago, 1985.
25. Shaffer, R. K., and C. D. Jensen, "Continuously Reinforced Concrete Pavements in Pennsylvania: A Six-Year Progress Report," *HRB proceedings*, No. 5, pp 83-98, 1963.
26. Witkoski, F. C., and R. K. Shaffer, "Continuously Reinforced Concrete Pavement in Pennsylvania," *HRB Bulletin 214*, 1959, pp 80-97.
27. Won, M. C., "A Mechanistic Analysis of Continuously Reinforced Concrete Pavement Considering Material Characteristics, Variability, and Fatigue," Ph.D. diss., The University of Texas at Austin, December 1988.
28. McCullough, B. F., and T. P. Chesney, "Sixteenth Year Progress Report on Experimental Continuously Reinforced Concrete Pavement in Walker County," *Research Report 177-6*, Center for Transportation Research, The University of Texas at Austin, April 1976.
29. Witkoski, F. C., and R. K. Shaffer, "Continuously Reinforced Concrete Pavements in Pennsylvania," *HRB Bulletin 238*, 1960, pp 1-19.
30. Mailvaganam, N. P., R. S. Bhagrath, and K. L. Shaw, "Effect of Admixtures on Portland Cement Concretes Incorporating Blast Furnace Slag and Fly Ash," *Fly Ash, Silica Fume, Slag and Other Mineral By-products in Concrete*, Vol I, Publication SP-79, ACI, 1983, pp 519-537.
31. Barrow, R. S., and R. L. Carrasquillo, "The Effect of Fly Ash on the Temperature Rise in Concrete," *Research Report 481-2*, Center for Transportation Research, The University of Texas at Austin, February 1988.
32. Carrette, G., and V. M. Malhotra, "Early-age Strength Development of Concrete Incorporating Fly Ash and Condensed Silica Fume," *Fly Ash, Silica Fume, Slag and Other Mineral By-products in Concrete*, Vol II, Publication SP-79, ACI, 1983, pp 765-773.

33. Lessard, S., P. C. Aitcin, and M. Regourd, "Development of a Low Heat of Hydration Blended Cement," *Fly Ash, Silica Fume, Slag and Other Mineral By-products in Concrete*, Vol II, Publication SP-79, 1983.
34. Tamas, F. D., "Acceleration and Retardation of Portland Cement Hydration by Additives," Symposium on Structure of Portland Cement Paste and Concrete, SP-90, HRB, 1966.
35. Fulton, F., *Concrete Technology*, Johannesburg, South Africa: Portland Cement Institute, 1964, p 208.
36. Tynes, W. O., "Temperature Rise of Mass Concrete Mixtures with Water-reducing and Retarding Admixtures," *Temperature and Concrete*, ACI Publication, SP-25, 1971, pp 291-300.
37. Burke, J. E., and J. S. Dhamrait, "A Twenty-Year Report on the Illinois Continuously Reinforced Pavement," Highway Research Record, No. 239, HRB, 1968.
38. *AASHTO Guide for Design of Pavement Structures*, American Association of State Highway and Transportation Officials, 1986.
39. Hughes, B. P., and T. Mahmood, "An Investigation of Early Thermal Cracking in Concrete and the Recommendations in BS 8007," *The Structural Engineer*, Vol 66, No. 4/16, February 1988.
40. Russell, H. W., and J. D. Lindsay, "Three-Year Performance Report on Experimental Continuously Reinforced Concrete Pavement in Illinois," Highway Research Board Proceedings, 1950.
41. "Continuously Reinforced Concrete Pavement," National Cooperative Highway Research Program Synthesis 16, 1973.
42. Lindsay, J. D., "A Ten-Year Report on the Illinois Continuously Reinforced Pavement," Highway Research Board, Bulletin 214, 1959.
43. Anderson, V. L., and R. A. McLean, *Design of Experiments: A Realistic Approach*, NY: Marcel Dekker, Inc., 1974.
44. Hansen, T. C., and A. H. Mattock, "Influence of Size and Shape of Member on the Shrinkage and Creep of Concrete," *ACI Journal*, Proceedings, Vol 63, No. 2, pp 267-289, February 1966.
45. Tremper, B., and D. L. Spellman, "Shrinkage of Concrete: Comparison of Laboratory and Field Performance," National Academy of Sciences, Highway Research Record, No. 3, 1963.
46. Al-Sugair, F. H., and J. A. Almudaiheem, "Further Modification of the Ross Equation to Predict the Ultimate Drying Shrinkage of Concrete," *ACI Materials Journal*, pp 237-240, May-June 1990.
47. Yoder, E. J., and M. W. Witczak, *Principles of Pavement Design*, 2nd ed., NY: John Wiley & Sons, Inc., 1975.
48. Gutierrez, M., and B. F. McCullough, "Summary Report for 1978 CRCP Condition Survey in Texas," Research Report 177-20, Center for Transportation Research, The University of Texas at Austin, January 1981.
49. "Failure and Repair of Continuously Reinforced Concrete Pavement," National Cooperative Highway Research Program Synthesis 60, July 1979.
50. Taute, A., and B. F. McCullough, "Manual for Condition Survey of Continuously Reinforced Concrete Pavements," Research Report 177-19, Center for Transportation Research, The University of Texas at Austin, February 1981.

51. Gutierrez de Velasco, M., and B. F. McCullough, "Rigid Pavement Network Rehabilitation Scheduling Using Distress Quantities," Research Report 249-5, Center for Transportation Research, The University of Texas at Austin, August 1983.
52. Torres-Verdin, V., C. L. Saraf, and B. F. McCullough, "Evaluation of the Effect of Survey Speed on Network-level Collection of Rigid Pavement Distress Data," Research Report 388-2, Center for Transportation Research, The University of Texas at Austin, December 1984.
53. Saraf, C. L., V. Torres-Verdin, and B. F. McCullough, "Manual for Condition Survey of Continuously Reinforced Concrete Pavements," Research Report 388-3, Center for Transportation Research, The University of Texas at Austin, May 1985.
54. Saraf, C. L., B. F. McCullough, and W. R. Hudson, "Condition Survey and Pavement Evaluation of Existing and Overlaid Rigid Pavements," Research Report 388-5F, Center for Transportation Research, The University of Texas at Austin, November 1985.
55. McCullough, B. F., A. Abou-Ayyash, W. R. Hudson, and J. P. Randall, "Design of Continuously Reinforced Concrete Pavements for Highways," Research Report NCHRP 1-15, Center for Transportation Research, The University of Texas at Austin, August 1974.

APPENDIX A
NEW DESIGN STANDARD, CRCP(B)-89B

APPENDIX B
CYLINDER TEST RESULTS

Table B.1 Cylinder test results (SH6-summer)

PROPERTY	CAT	LAB/FIELD	3DAY	7DAY	28DAY
SPLIT TENS. (psi)	SRG	LAB	464.7 (66)*	518.2 (21)	558.7 (60)
		FIELD		539.8 (32)	600.1 (48)
	LS	LAB	423.4 (40)	505.2 (40)	515.7 (70)
		FIELD		488.8 (34)	496.5 (27)
E (Million psi)	SRG	LAB	5.25 (0.85)	5.25 (1.15)	4.77 (0.94)
		FIELD		5.16 (0.73)	5.4 (0.99)
	LS	LAB	4.94 (0.63)	3.91 (0.74)	5.24 (0.46)
		FIELD		3.98 (0.91)	5.53 (0.66)
COMP. STR. (PSI)	SRG	LAB	5120 (201)	5801 (354)	6497 (387)
		FIELD		5677 (395)	6252 (350)
	LS	LAB	5282 (1022)	6261 (956)	6108 (1253)
		FIELD		5807 (1163)	7372 (859)

* Number within parenthesis represents standard deviation of 6 cylinders (2 trucks X 3).

			14DAY	17DAY	24DAY	25DAY	27DAY	28DAY	31DAY	32DAY
SHRINKAGE (Microstrain)	SRG	LAB	128.8	132.9	164.7	161.9	174.4	204.8	189.6	201.3
		FIELD			177.4	189.8	191.9	208.5	214	220.2
			11DAY	14DAY	21DAY	22DAY	24DAY	25DAY	28DAY	29DAY
	LS	LAB	103.8	98.97	161.8	163.9	183.9	197	196.3	201.9
		FIELD	103.8		128.7	143.8	154.9	159.7	170.8	173.5

THERM. COEFF. (Microstrain)	SRG	LAB=4.8
		FIELD=5.5
	LS	LAB=2.9
		FIELD=3.1

Table B.2 Cylinder test results (BW8-winter)

PROPERTY	CAT	LAB/FIELD	3DAY	7DAY	28DAY
SPLIT TENS. (psi)	SRG	LAB	398.7 (21)*	492.1 (30)	535.8 (28)
		FIELD		471.8 (16)	558.1 (19)
	LS	LAB	435.2 (42)	479.7 (13)	454.3 (51)
		FIELD		453.4 (28)	477.6 (54)
E (Million psi)	SRG	LAB	4.79 (0.90)	5.37 (0.53)	4.78 (0.18)
		FIELD		5.36 (0.45)	4.68 (0.69)
	LS	LAB	4.28 (0.39)	4.90 (0.63)	4.19 (0.48)
		FIELD		4.79 (0.09)	4.14 (0.05)
COMP. STR. (PSI)	SRG	LAB	3480 (229)	4907 (531)	6083 (308)
		FIELD		4597 (207)	5567 (227)
	LS	LAB	4246 (224)	5063 (316)	6122 (522)
		FIELD		4913 (561)	5886 (641)

* Number within parenthesis represents standard deviation of 6 cylinders (2 trucks X 3).

		3DAY	5DAY	6DAY	14DAY	21DAY	26DAY	77DAY	96DAY	
SHRINKAGE (Microstrain)	SRG	LAB						255	280	
		FIELD	43	38	110	163	168	243	293	295
			3DAY	5DAY	6DAY	13DAY	20DAY	25DAY	76DAY	95DAY
	LS	LAB							270	275
FIELD		10	30	60	55	75	105	210	225	

THERM. COEFF. (Microstrain)	SRG	LAB=8.1
		FIELD=8.4
	LS	LAB=5.0
		FIELD=5.5

Table B.3 Cylinder test results (SH6-winter)

PROPERTY	CAT	LAB/FIELD	3DAY	7DAY	28DAY
SPLIT TENS. (psi)	SRG	LAB	314.0 (29)*	393.7 (27)	579.9 (48)
		FIELD		355.3 (22)	553.8 (72)
	LS	LAB	318.9 (32)	381.3 (25)	538.6 (54)
		FIELD		350.5 (36)	555.6 (25)
E (Million psi)	SRG	LAB	4.90 (0.82)	5.22 (0.58)	5.48 (0.55)
		FIELD		4.56 (0.48)	5.49 (0.61)
	LS	LAB	4.07 (0.56)	5.02 (0.61)	5.04 (0.28)
		FIELD		4.84 (0.54)	5.39 (0.40)
COMP. STR. (PSI)	SRG	LAB	3724 (628)	4901 (504)	5881 (517)
		FIELD		5202 (520)	5535 (900)
	LS	LAB	3728 (638)	5780 (378)	6818 (109)
		FIELD		5724 (208)	6747 (259)

* Number within parenthesis represents standard deviation of 6 cylinders (2 trucks X 3).

		3DAY	5DAY	6DAY	30DAY	49DAY			
SHRINKAGE (Microstrain)	SRG	LAB			90	170			
		FIELD	90	80	90	115	155		
			2DAY	28DAY	47DAY				
	LS	LAB		165	205				
FIELD		15	165	205					

THERM. COEFF. (Microstrain)	SRG	
		FIELD=6.6
	LS	
		FIELD=-3.8

Table B.4 Cylinder test results (IH45-winter)

PROPERTY	CAT	LAB/FIELD	3DAY	7DAY	28DAY
SPLIT TENS. (psi)	SRG	LAB	278.1 (14)*	429.2 (64)	531.1 (58)
		FIELD		431.0 (54)	464.6 (35)
	LS	LAB	441.9 (21)	489.2 (50)	543.3 (21)
		FIELD		487.9 (37)	571.5 (31)
E (Million psi)	SRG	LAB	3.51 (0.43)	4.70 (0.41)	5.07 (0.34)
		FIELD		5.36 (0.41)	5.50 (0.68)
	LS	LAB	4.12 (0.25)	4.59 (0.52)	4.88 (0.41)
		FIELD		4.58 (0.50)	5.01 (0.29)
COMP. STR. (PSI)	SRG	LAB	3660 (368)	4282 (583)	5273 (728)
		FIELD		4217 (359)	5273 (640)
	LS	LAB	3869 (237)	6122 (273)	7496 (319)
		FIELD		6054 (191)	7095 (214)

* Number within parenthesis represents standard deviation of 6 cylinders (2 trucks X 3).

		3DAY	6DAY	7DAY	9DAY	11DAY	26DAY	45DAY
SHRINKAGE (Microstrain)	SRG	LAB					445**	495**
		FIELD	45	75	85	105	135	220
			3DAY	5DAY	12DAY	16DAY	25DAY	38DAY
	LS	LAB			150	165		215
FIELD		40	80			150	210	

** Mold of the cylinder had been removed during the curing.

THERM. COEFF. (Microstrain)	SRG	
		FIELD=6.6
	LS	
		FIELD=4.1

APPENDIX C

TIME PLOT OF THE SLAB AND AIR TEMPERATURE FOR 3 DAYS AFTER CONSTRUCTION

(Note: Fresh concrete temperature and the time of concrete placement at each location of the thermocouples are given in Table 2.2)

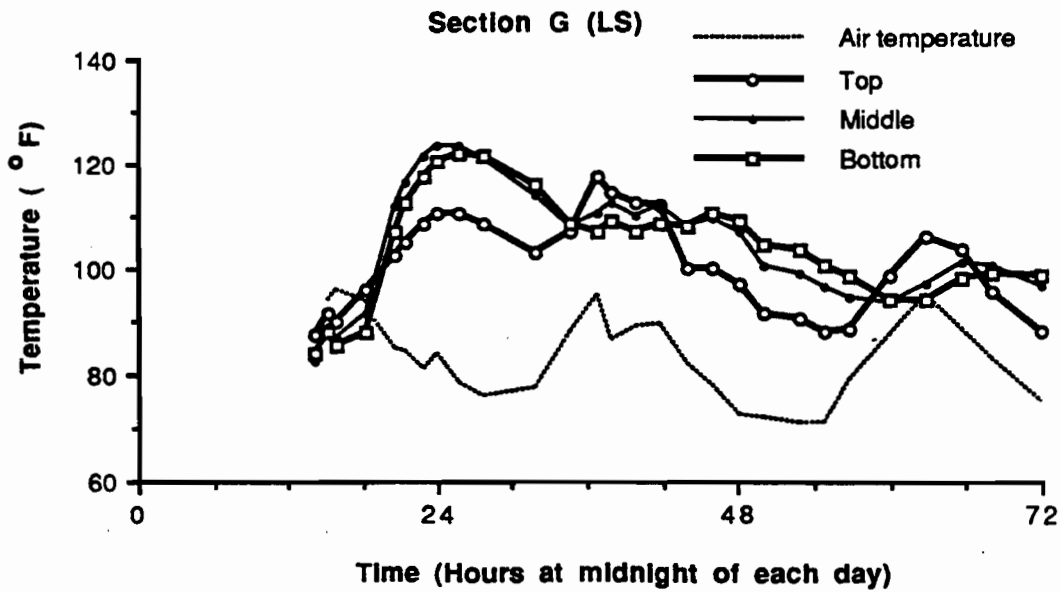
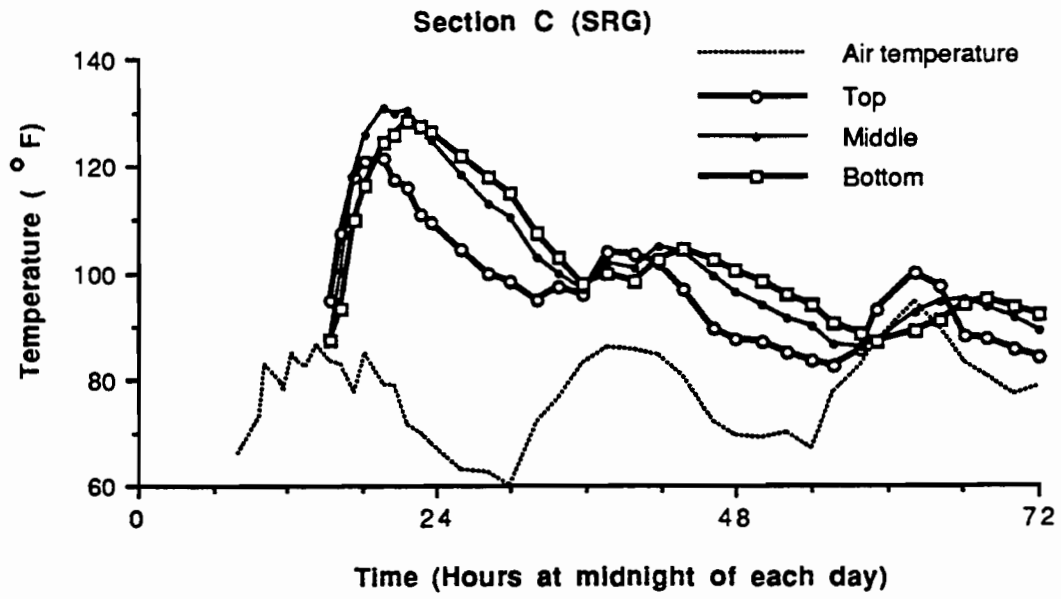
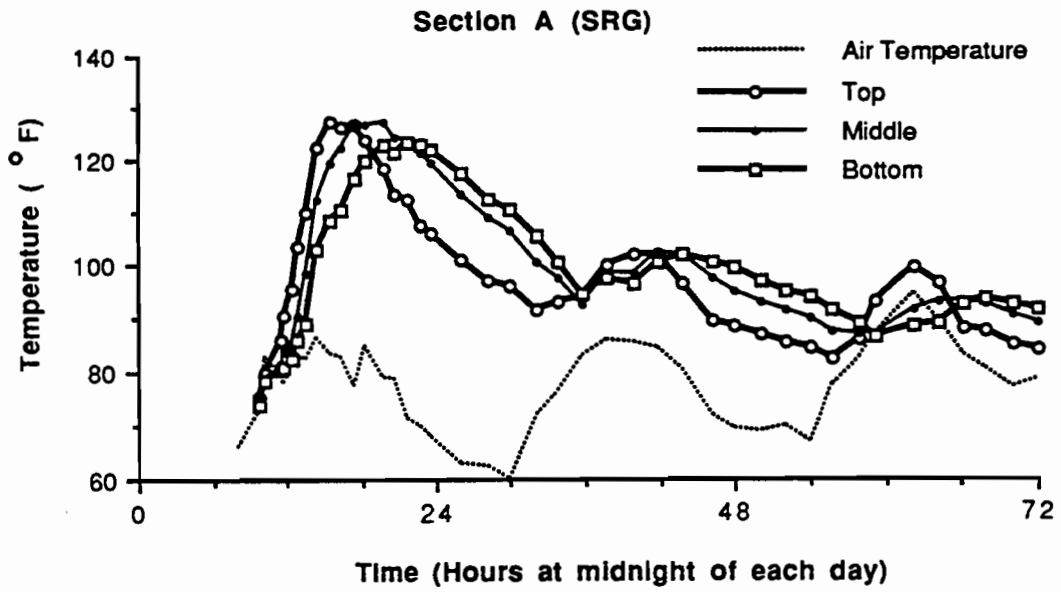


Figure C.1 Time plot of the slab and air temperature for three days after construction (SH6-summer)

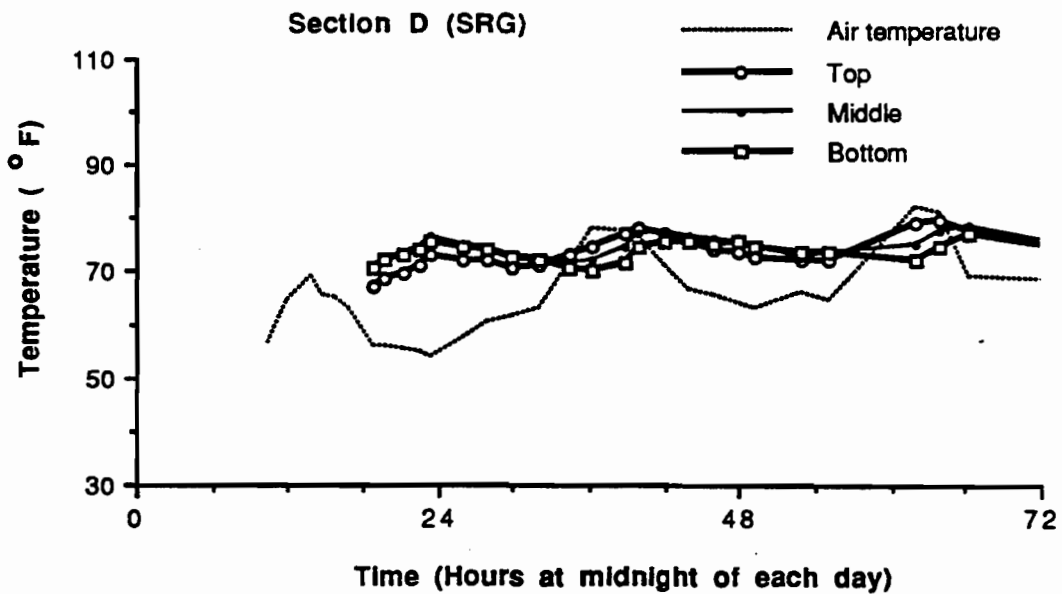
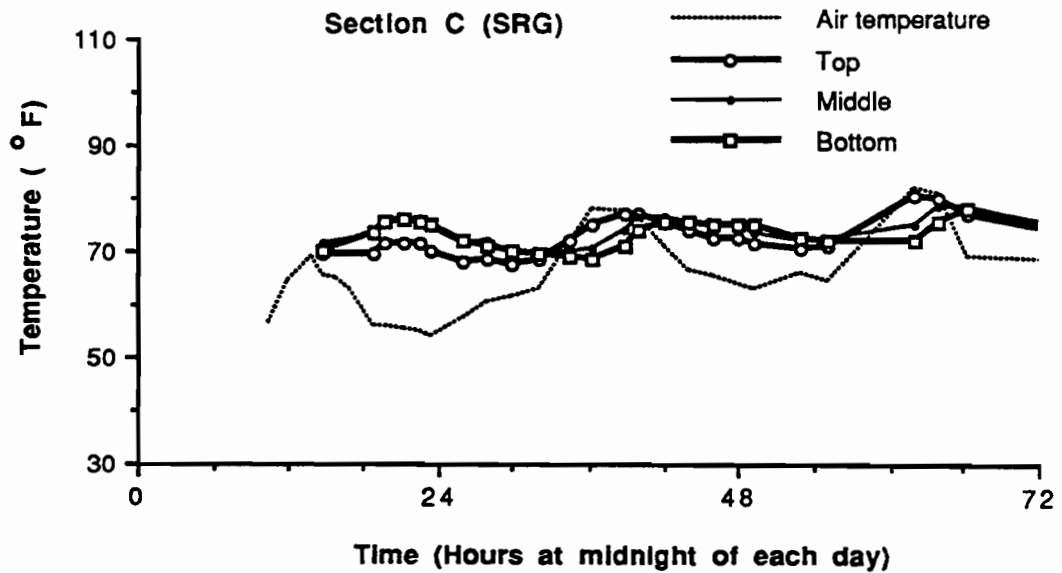
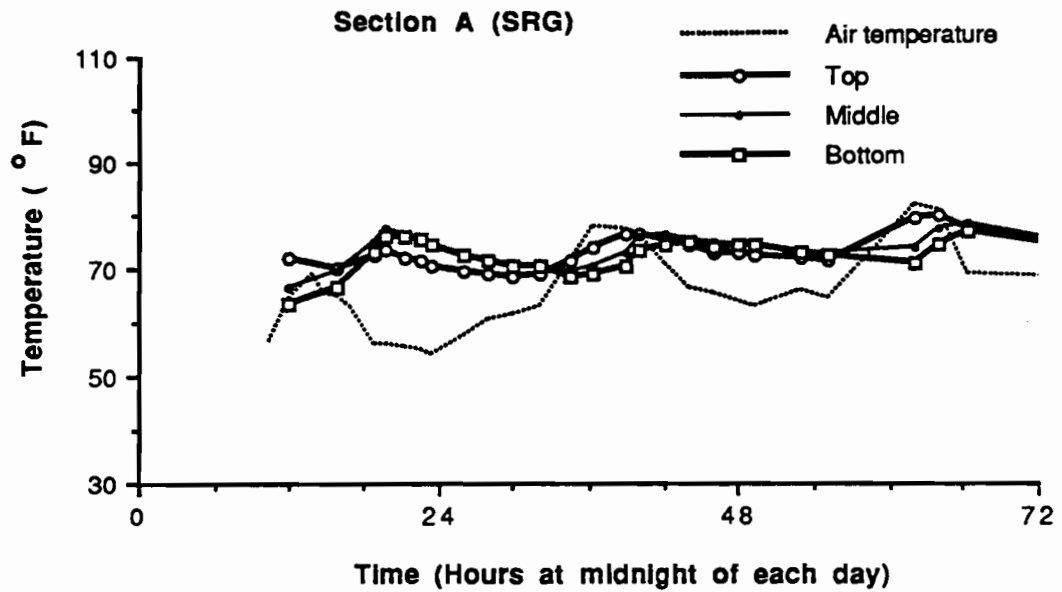


Figure C.2 Time plot of the slab and air temperature for three days after construction (BW8-winter)

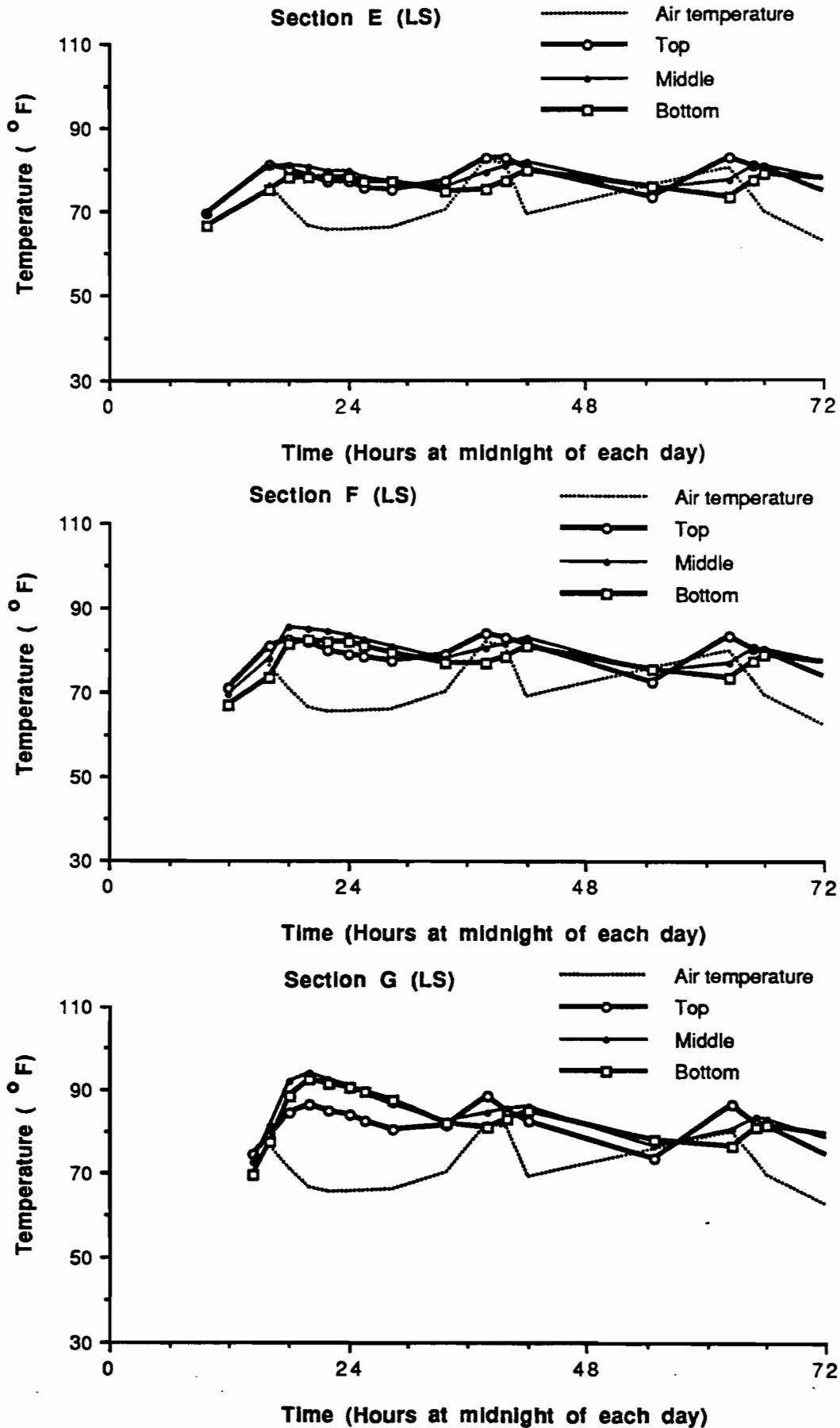


Figure C.2 Time plot of the slab and air temperature for three days after construction (BW8-winter)-continued

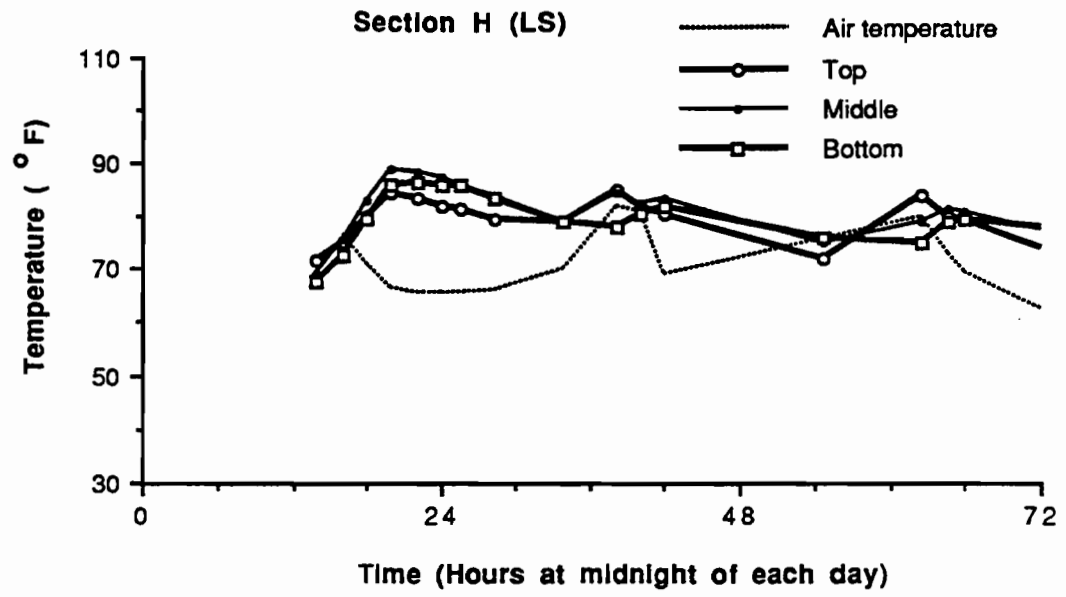


Figure C.2 Time plot of the slab and air temperature for three days after construction (BW8-winter)-continued

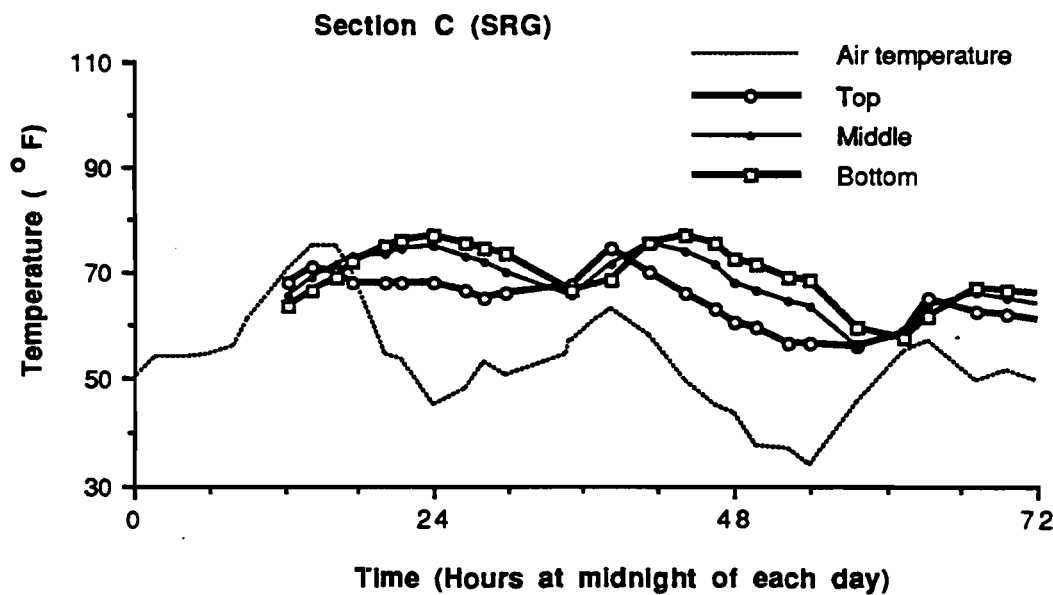
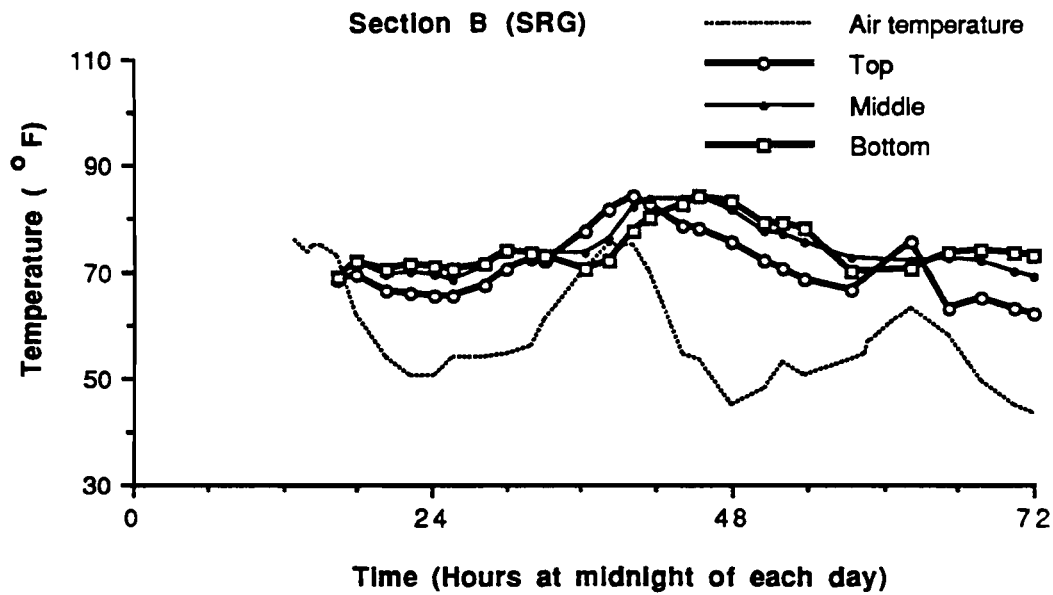
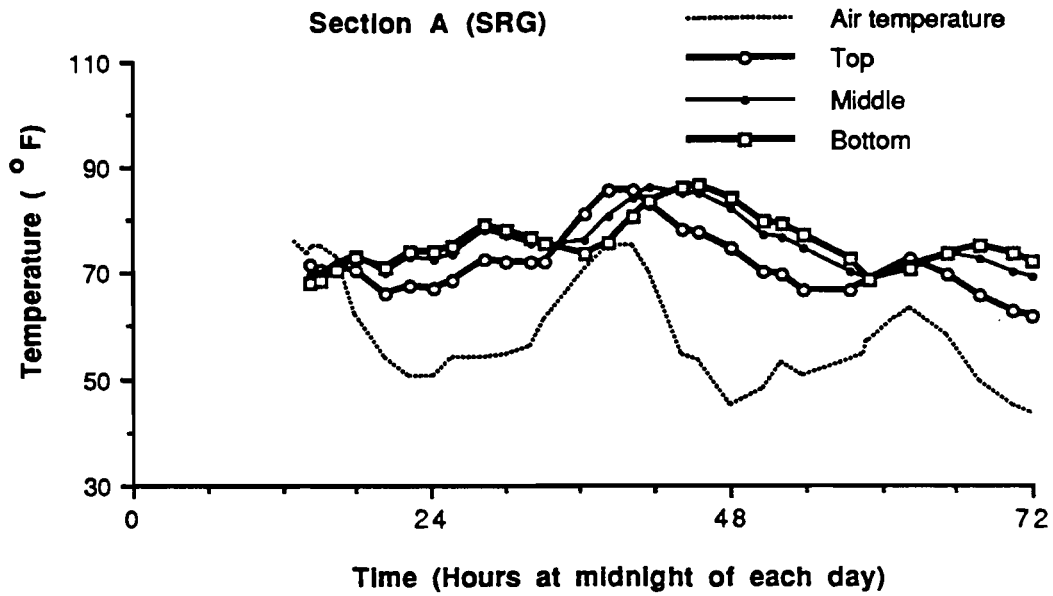


Figure C.3 Time plot of the slab and air temperature for three days after construction (SH6-winter)

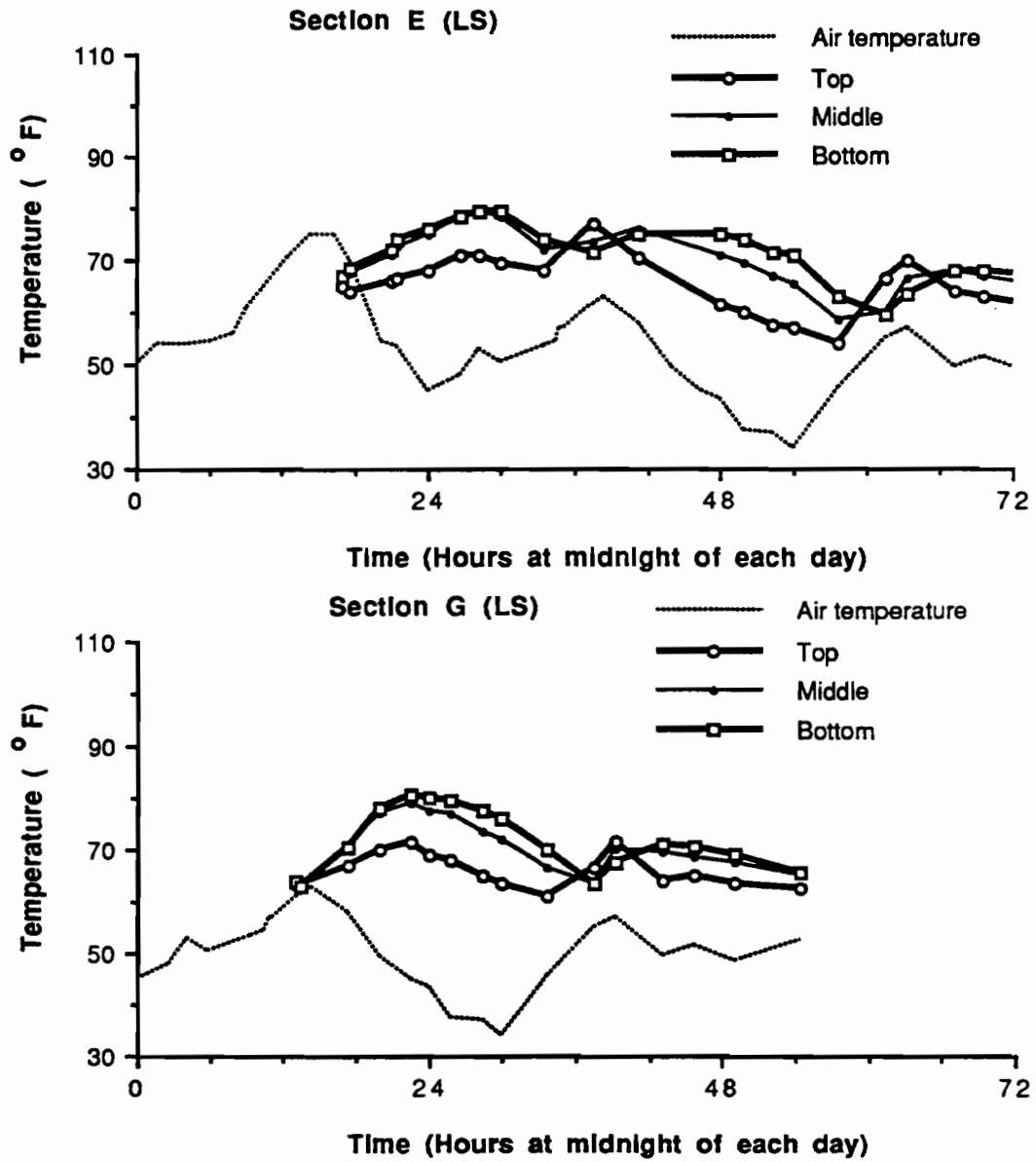


Figure C.3 Time plot of the slab and air temperature for three days after construction (SH6-winter)-continued

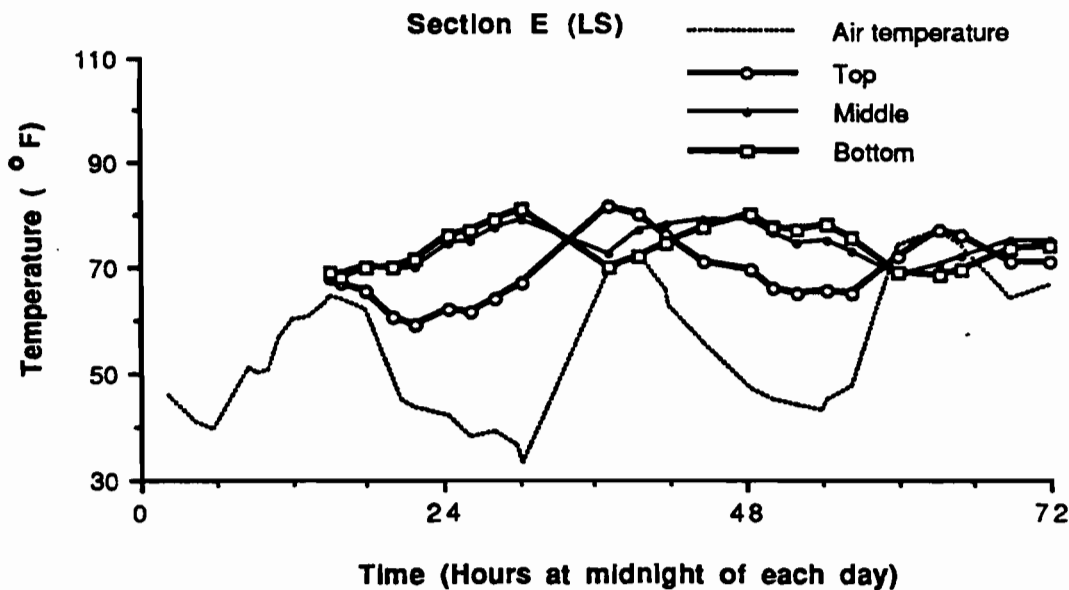
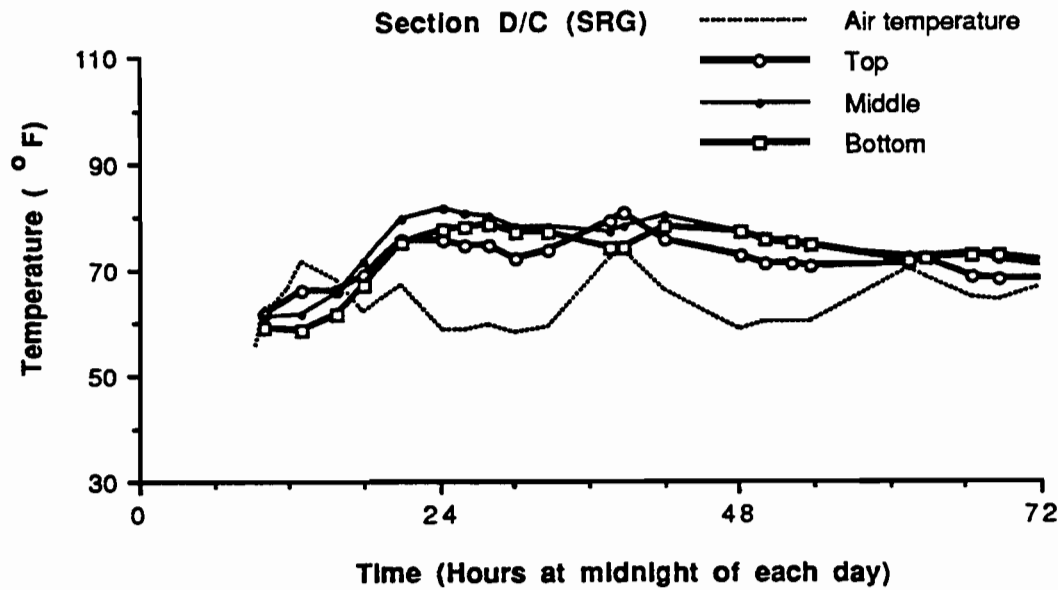
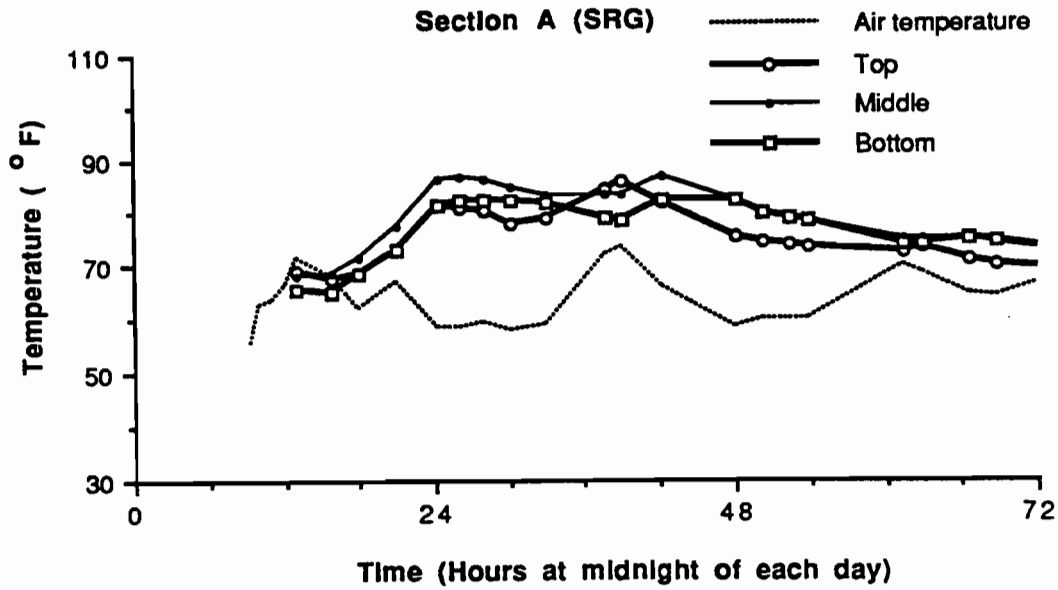


Figure C.4 Time plot of the slab and air temperature for three days after construction (IH45-winter)

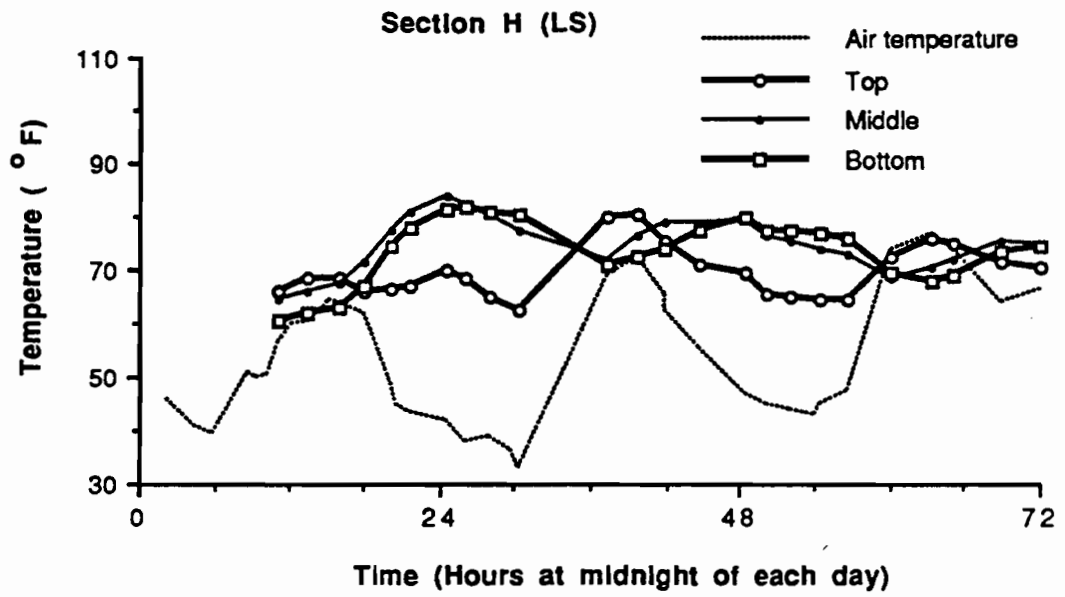


Figure C.4 Time plot of the slab and air temperature for three days after construction (IH45-winter)-continued

APPENDIX D

**WEATHER INFORMATION DURING THE
SHORT-TERM MONITORING**

Table D.1 Weather information (SH6-summer)

DATE	TIME	WEATHER	SOLAR RAD.	AIR TEMP
	(Decimal)		(Btuh/sq. ft)	(°F)
6/16/90	8.00	CLEAR	.	66.0
	9.83	CLEAR	.	73.0
	10.08	CLEAR	.	83.0
	11.50	CLEAR	285	79.6
	11.75	CLEAR	285	78.0
	12.33	CLEAR	285	85.2
	12.75	CLEAR	290	83.4
	13.42	CLEAR	280	82.6
	14.33	CLEAR	280	86.4
	15.42	CLEAR	290	83.4
	16.33	CLEAR	290	83.0
	17.25	CLEAR	275	77.4
	18.33	CLEAR	240	85.2
	19.75	CLEAR	135	79.2
	20.67	CLEAR	.	79.2
21.67	CLEAR	.	71.6	
22.67	CLEAR	.	69.8	
23.67	CLEAR	.	68.0	
6/17/90	2.00	CLEAR	.	63.0
	4.33	CLEAR	.	62.4
	5.92	CLEAR	.	60.2
	8.00	CLEAR	260	71.8
	9.75	CLEAR	275	76.6
	11.75	CLEAR	280	82.8
	13.75	CLEAR	280	85.8
	15.75	CLEAR	295	85.6
	17.75	CLEAR	260	84.4
	19.75	CLEAR	120	80.6
	22.25	CLEAR	.	71.8
	24.00	CLEAR	.	69.6
6/18/90	2.00	CLEAR	.	69.0
	4.00	CLEAR	.	70.0
	6.00	CLEAR	.	67.0
	7.75	CLEAR	150	77.4
	9.75	CLOUDY	60	82.6
	11.33	CLEAR	320	87.0
	14.17	CLEAR	320	94.6
	16.08	RAIN	120	89.4
	18.17	CLDY/RAIN	40	83.2
	19.75	CLOUDY	10	80.4
	22.00	CLOUDY	.	76.8
	24.00	CLOUDY	.	78.4

Table D.1 Weather information (SH6-summer) - continued

DATE	TIME (Decimal)	WEATHER	SOLAR RAD. (Btuh/sq. ft)	AIR TEMP (°F)
6/19/90	2.17	CLOUDY	.	75.0
	4.17	CLOUDY	.	76.0
	6.42	CLOUDY	.	74.8
	8.42	CLOUDY	30	79.4
	9.83	CLOUDY	80	83.4
	13.58	CLEAR	290	92.0
	15.75	CLEAR	280	96.2
	18.67	CLEAR	210	90.8
	20.17	CLEAR	.	86.8
	21.00	CLEAR	.	84.6
	22.50	CLEAR	.	80.8
	23.50	CLEAR	.	79.2
6/20/90	2.00	CLEAR	.	76.8
	4.58	CLEAR	.	74.2
	8.08	CLEAR	40	76.6
	12.42	CLEAR	280	93.6
	15.83	CLEAR	280	89.0
	17.92	CLEAR	2	89.6
	22.05	CLEAR	.	76.6
	23.50	CLEAR	.	75.0
6/21/90	4.42	CLEAR	.	71.2
	9.03	CLEAR	120	81.2
	11.75	CLOUDY	150	85.4
	15.00	CLEAR	300	95.0
6/22/90	6.00	CLOUDY	.	71.4
	9.83	CLOUDY	60	86.0
	14.00	CLOUDY	70	88.0
6/24/90	9.00	CLOUDY	50	74.4
	14.00	CLOUDY	70	78.2
6/28/90	6.00	CLOUDY	.	70.2
	14.00	CLOUDY	140	86.4
6/29/90	6.00	CLOUDY	.	71.4
	14.00	CLOUDY	50	80.0
7/6/90	6.00	CLOUDY	.	73.8
	13.75	RAIN	50	81.0
7/11/90	8.00	CLOUDY	50	80.0
	14.17	CLOUDY	60	86.0

Table D.2 Weather Information (BWB-winter)

DATE	TIME	WEATHER	SOLAR RAD.	AIR TEMP
	(Decimal)		(Btuh/sq. ft)	(°F)
11/24/89	10.33	CLEAR/COOL	.	56.4
	12.00	CLEAR/COOL	.	64.4
	13.83	CLEAR/COOL	.	68.8
	14.83	CLEAR/COOL	.	65.4
	15.92	CLEAR/COOL	.	64.8
	16.83	CLEAR/COOL	.	63.0
	18.92	CLEAR/COOL	.	55.8
	19.83	CLEAR/COOL	.	55.8
	21.33	CLEAR/COOL	.	55.4
	22.50	CLEAR/COOL	.	54.8
	23.50	CLEAR/COOL	.	53.8
11/25/89	2.00	CLEAR/COOL	.	57.4
	4.00	PARTLY CLDY	.	60.6
	6.00	PARTLY CLDY	.	61.4
	8.00	PARTLY CLDY	20	62.8
	10.50	CLOUDY	60	71.6
	12.25	PARTLY CLDY	73	77.8
	14.83	PARTLY CLDY	75	77.6
	16.00	CLEAR	.	76.6
	18.00	CLEAR	.	70.8
	20.00	CLEAR	.	66.4
	22.00	CLEAR	.	65.6
11/26/89	1.25	CLEAR	.	63.2
	5.00	CLEAR/FOGGY	.	66.2
	7.00	FOGGY	.	64.6
	14.00	CLEAR	270	82.0
	16.00	CLEAR	180	81.0
	18.33	CLEAR	.	69.0
11/27/89	6.75	CLEAR	.	67.4
	14.25	PARTLY CLDY	130	80.4
	16.50	PARTLY CLDY	20	75.4
	18.10	PARTLY CLDY	.	69.6
11/28/89	4.50	PARTLY CLDY	.	60.8
	5.83	PARTLY CLDY	.	55.8
	14.33	PARTLY CLDY	130	62.0
	16.00	PARTLY CLDY	50	60.8
	18.00	CLOUDY	.	57.4
11/29/89	3.33	RAIN	.	48.6
	6.17	CLOUDY	.	44.0
	14.00	PARTLY CLDY	100	54.2

Table D.2 Weather information (BW8-winter) - continued

DATE	TIME (Decimal)	WEATHER	SOLAR RAD. (Btuh/sq. ft)	AIR TEMP (°F)
11/30/89	6.00	MISTY RAIN	.	41.4
	8.07	CLOUDY	.	44.0
	14.07	CLDY/RAIN	.	46.2
	15.66	CLOUDY	.	47.8
12/1/89	6.25	CLOUDY	.	43.4
12/5/89	6.00	CLEAR	.	39.0
	14.00	PART CLDY	50	68.8
12/8/89	6.00	CLEAR	.	37.2
	14.50	OVERCAST	.	41.0
12/15/89	6.00	FOGGY	.	50.4
	12.00	CLEAR	270	62.0
	15.75	COOL/CLEAR	210	49.6
12/20/89	14.75	CLEAR	140	46.6
12/21/89	6.42	OVERCAST	.	29.6

Table D.3 Weather information (SH6-winter)

DATE	TIME	WEATHER	SOLAR RAD.	AIR TEMP
	(Decimal)		(Btuh/sq. ft)	(°F)
1/10/90	13.00	CLEAR	.	76.0
	14.08	CLEAR	.	73.6
	14.35	CLEAR	.	74.4
	14.50	CLEAR	.	74.8
	15.20	CLEAR	.	74.8
	16.42	CLEAR	.	73.2
	18.00	CLEAR	.	62.2
	20.33	CLEAR	.	53.8
	22.17	CLEAR	.	50.4
	1/11/90	0.17	FOGGY	.
1.67		FOGGY	.	54.0
4.25		FOGGY	.	54.0
6.00		FOGGY	.	54.6
8.00		CLOUD	7	56.2
9.00		CLOUD	25	61.0
12.33		CLEAR	160	70.4
14.25		CLEAR	160	75.0
15.08		CLEAR	.	
16.17		CLEAR	70	75.0
17.00		CLEAR	.	
17.50		CLEAR	8	69.8
20.10		CLEAR	.	54.4
21.10		CLEAR	.	
21.50		CLEAR	.	53.4
24.00		FOGGY	.	44.8
1/12/90	2.67	FOGGY	.	48.0
	4.17	FOGGY	.	53.0
	5.92	CLEAR/COOL	.	50.4
	9.42	CLEAR/COOL	80	53.6
	10.50	CLEAR/COOL	.	54.4
	10.75	CLEAR/COOL	.	57.2
	11.08	CLEAR	.	57.0
	13.00	CLEAR	.	61.2
	13.50	CLEAR	.	61.4
	14.33	CLEAR	160	62.8
	17.25	CLEAR	10	57.8
	20.00	CLEAR/COOL	.	49.6
	22.50	CLEAR/COOL	.	44.8
	24.00	CLEAR/COOL	.	43.6

Table D.3 Weather Information (SH6-winter) - continued

DATE	TIME	WEATHER	SOLAR RAD.	AIR TEMP
	(Decimal)		(Btuh/sq. ft)	(°F)
1/13/90	1.83	CLEAR/COOL	.	37.6
	4.33	CLEAR/COOL	.	36.8
	6.00	CLEAR/COOL	.	34.2
	9.67	CLEAR/COOL	120	45.6
	13.50	CLEAR/COOL	170	55.0
	15.25	CLEAR/COOL	130	57.0
	19.17	CLEAR/COOL	.	49.6
	21.67	CLOUDY	.	51.4
1/14/90	1.12	CLOUDY	.	48.4
	6.50	CLOUDY	.	52.4
1/15/90	10.67	CLOUDY	65	68.2
1/16/90	9.17	CLOUDY	.	63.6
	9.75	CLOUDY	.	69.8
1/18/90	10.50	CLDY/RAIN	.	71.6
	11.25	CLOUDY	.	70.4
1/19/90	11.25	CLDY/RAIN	50	72.2
	11.75	CLDY/RAIN	40	71.4
1/20/90	8.83	CLDY/COOL	15	49.6
	9.58	PART/CLDY	130	51.8
1/25/90	12.33	CLEAR/COOL	200	54.8
	13.17	CLEAR/COOL	200	55.2
2/1/90	7.08	CLDY/RAIN	.	65.6
2/14/90	8.58	CLOUDY	30	66.8

Table D.4 Weather information (IH45-winter)

DATE	TIME (Decimal)	WEATHER	SOLAR RAD. (Btuh/sq. ft)	AIR TEMP (°F)
1/14/90	9.33	CLOUDY	27	55.6
	10.00	CLOUDY	.	62.6
	10.92	CLOUDY	.	63.6
	12.00	PART CLDY	75	66.6
	13.00	PART CLDY	120	71.4
	15.83	CLOUDY	.	68.0
	17.98	CLOUDY	.	62.0
	21.00	PART CLDY	.	67.2
1/15/90	0.25	CLOUDY	.	58.4
	1.95	CLOUDY	.	58.4
	3.92	CLEAR	.	59.4
	6.08	CLEAR	.	58.2
	8.83	CLOUDY	20	59.2
	13.67	CLOUDY	50	71.8
	14.92	CLOUDY	150	73.6
	18.13	CLEAR	.	65.8
1/16/90	0.08	CLOUDY	.	58.6
	2.13	CLOUDY	.	59.8
	4.25	CLOUDY	.	59.8
	5.83	CLOUDY	.	60.2
	13.50	RAIN	35	69.8
	15.00	RAIN/CLDY	16	68.6
	18.60	RAIN/CLDY	.	64.4
	20.75	CLOUDY	.	64.0
1/17/90	0.83	RAIN/CLDY	.	67.0
	2.00	CLOUDY	.	66.2
	4.25	CLOUDY	.	65.8
	5.58	CLOUDY	.	66.2
	9.50	CLOUDY	13	67.4
	12.13	CLOUDY	30	72.2
	15.50	CLOUDY	40-100	71.4
	17.93	CLOUDY	.	69.8
20.42	CLOUDY	.	67.0	
1/18/90	0.25	CLOUDY	.	67.6
	2.00	RAIN	.	69.6
	4.25	RAIN/CLDY	.	66.6
	6.25	CLOUDY	.	67.2
	13.23	RAIN/CLDY	.	70.2
	17.35	CLOUDY	.	66.8
	23.25	WIND/CLDY	.	65.6

Table D.4 Weather Information (IH45-winter) - continued

DATE	TIME (Decimal)	WEATHER	SOLAR RAD. (Btuh/sq. ft)	AIR TEMP (°F)
1/19/90	6.25	RAIN/CLDY	.	65.6
	15.17	CLDY/RAIN	.	70.4
1/20/90	4.08	CLDY/COOL	.	50.2
	5.97	CLDY/COOL	.	49.8
	11.08	CLDY/COOL	70	54.8
	14.33	CLDY/COOL	50	55.2
	18.33	PART CLDY	.	50.6
1/21/90	2.17	CLEAR	.	45.8
	4.33	CLEAR	.	41.2
	5.90	CLEAR	.	39.6
	8.58	CLEAR	50	51.2
	9.25	CLEAR	80	50.0
	10.25	CLEAR	135	50.4
	11.08	CLEAR	170	56.4
	12.08	CLEAR	187	60.0
	13.50	CLEAR	165	60.4
	14.67	CLEAR	122	63.0
	15.17	CLEAR	.	64.4
	16.08	CLEAR	78	64.0
	18.00	CLEAR	.	62.2
	20.20	CLEAR	.	49.2
	20.67	CLEAR	.	44.8
21.75	CLEAR	.	43.4	
1/22/90	0.42	CLEAR	.	42.0
	2.08	CLEAR	.	38.0
	4.08	CLEAR	.	39.2
	5.75	CLEAR	.	36.4
	6.36	CLEAR	.	32.8
	13.25	CLEAR	190	69.0
	15.67	CLEAR	95	72.6
	17.83	CLEAR	.	65.4
	17.93	CLEAR	.	62.6
20.75	CLEAR	.	55.4	

Table D.4 Weather information (IH45-winter) - continued

DATE	TIME (Decimal)	WEATHER	SOLAR RAD. (Btuh/sq. ft)	AIR TEMP (°F)
1/23/90	0.33	CLEAR	.	47.0
	2.08	CLEAR	.	45.0
	4.12	CLEAR	.	44.2
	6.00	CLEAR	.	43.2
	6.42	CLEAR	.	45.0
	8.50	CLOUDY	15	47.6
	12.17	CLEAR	145	74.2
	15.25	PART CLDY	45	77.2
	17.00	PART CLDY	12	74.0
	21.00	PART CLDY	.	64.2
1/24/90	0.08	RAIN	.	66.6
	1.75	RAIN/CLDY	.	64.0
	4.11	RAIN/CLDY	.	62.8
	5.83	CLDY/RAIN	.	59.6
	6.55	RAIN/CLDY	.	58.8
	9.08	RAIN	10	58.6
	13.75	CLDY/RAIN	10	59.8
	22.25	CLOUDY	.	54.4
	1/25/90	4.17	CLEAR/COOL	.
5.00		CLEAR/COOL	.	43.4
5.83		CLEAR/COOL	.	41.4
9.33		CLEAR/COOL	120	46.2
16.17		CLEAR/COOL	100	60.2
22.00		CLEAR/COOL	.	35.0
1/26/90	4.12	CLEAR/COOL	.	30.2
	5.00	CLEAR/COOL	.	29.6
	6.12	CLEAR/COOL	.	30.0
	9.53	CLEAR/COOL	110	51.4
1/31/90	7.00	CLDY/COOL	.	47.8
2/15/90	9.45	CLOUDY	.	

APPENDIX E

GRAPHIC PLOTS OF TRANSVERSE CRACK PATTERNS

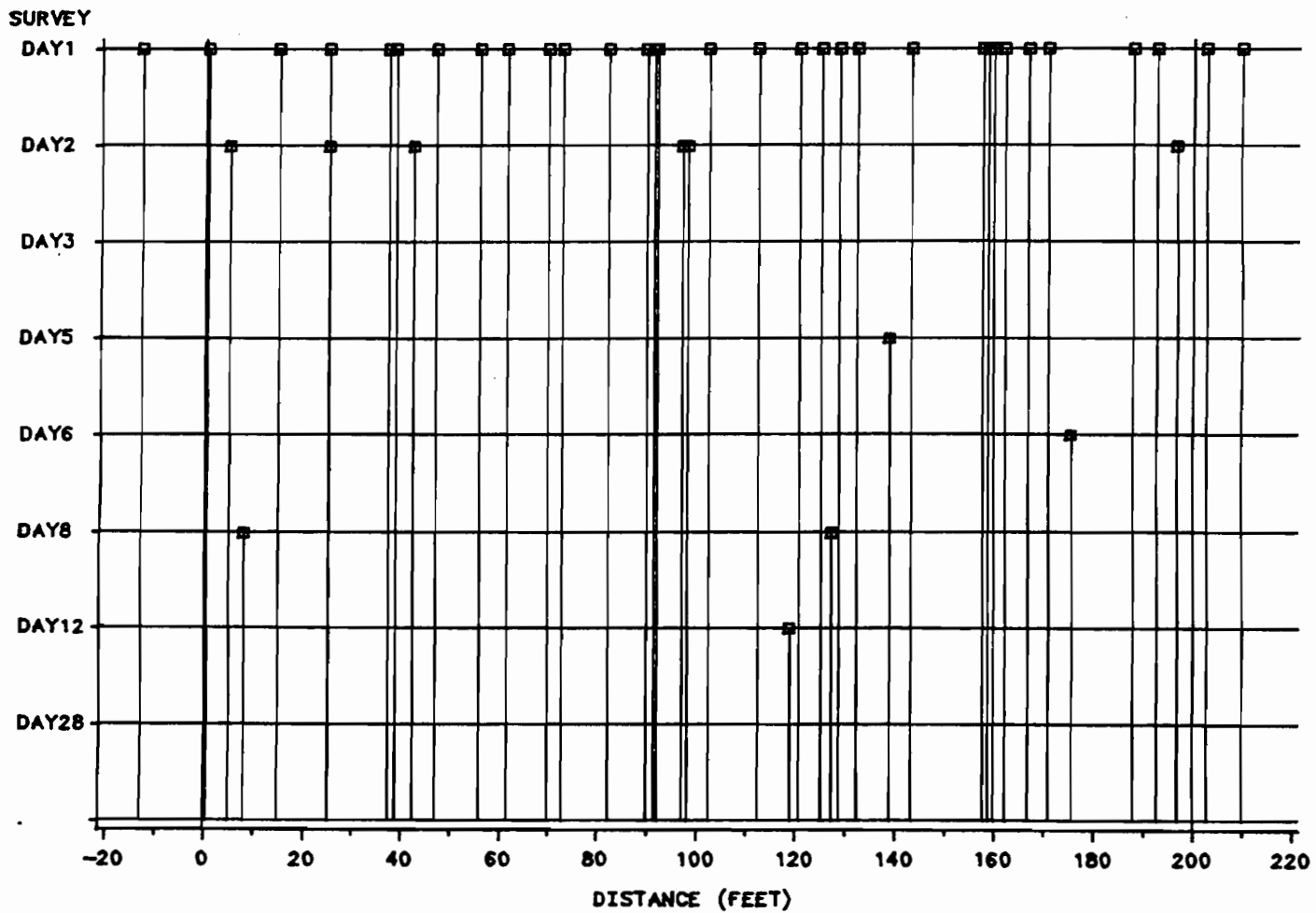


Figure E.1 Graphic plot of transverse crack pattern (SH6-summer, SRG, high steel)

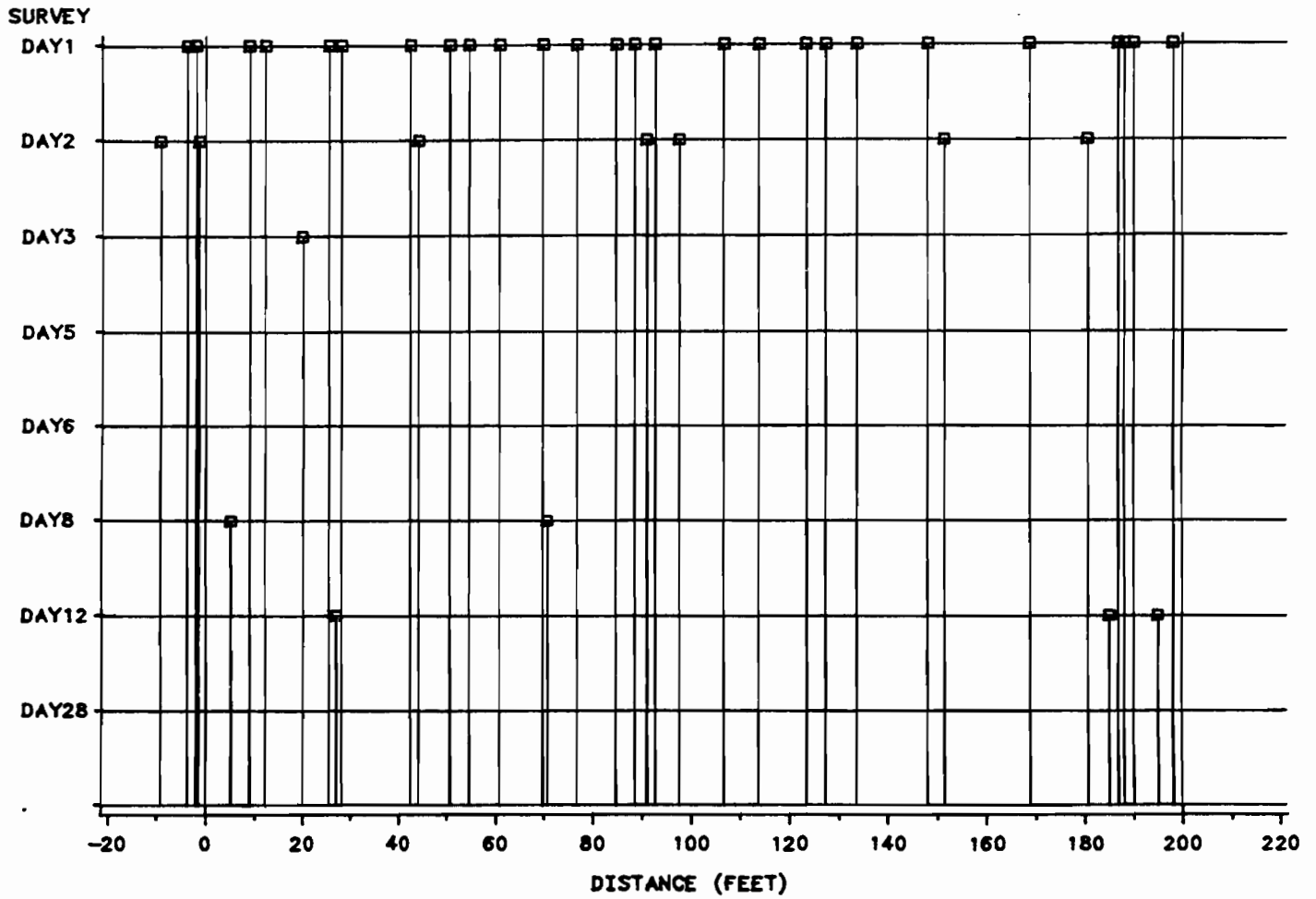


Figure E.2 Graphic plot of transverse crack pattern (SH6-summer, SRG, low steel)

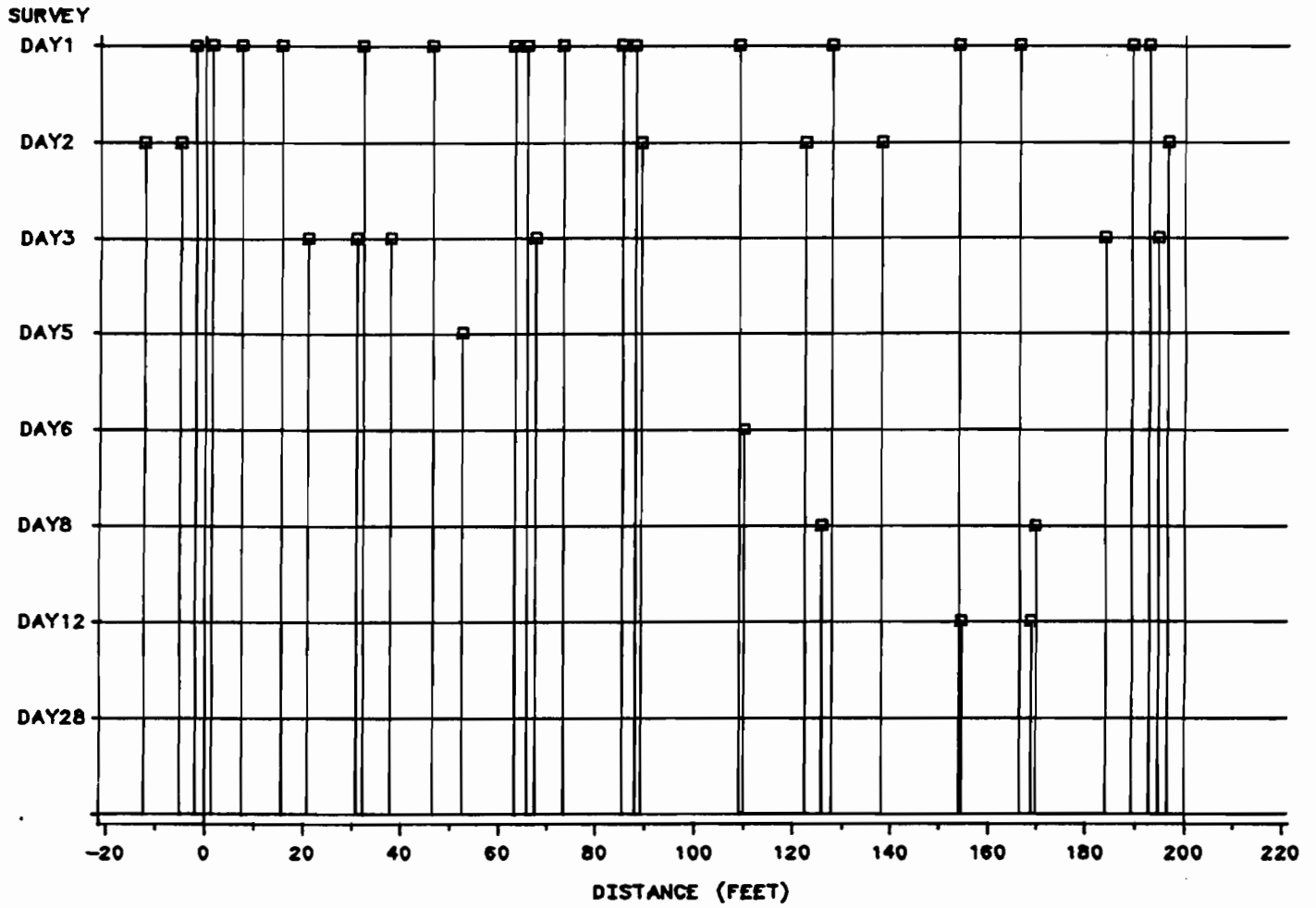


Figure E.3 Graphic plot of transverse crack pattern (SH6-summer, SRG, no. 7 bar-medium steel)

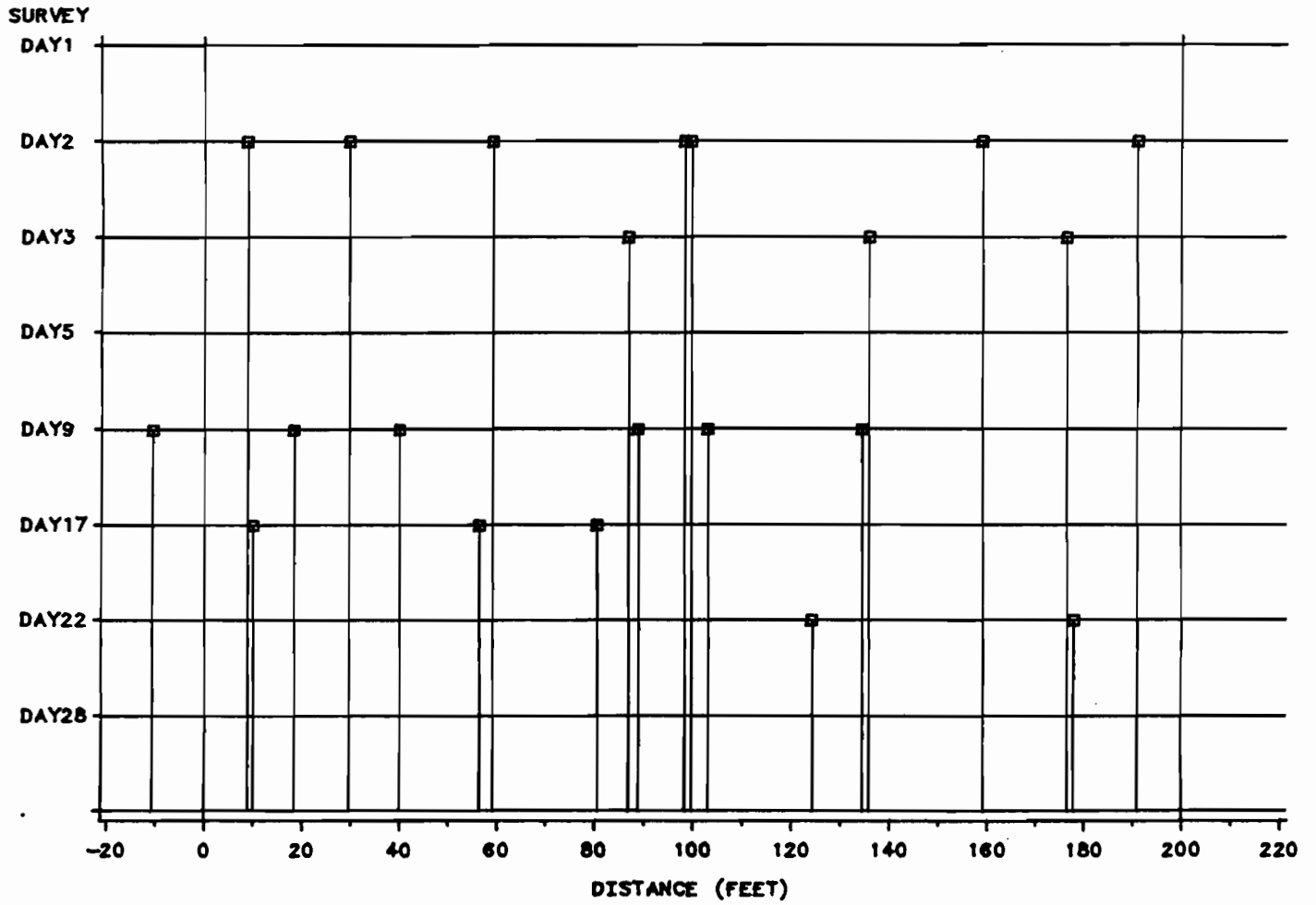


Figure E.4 Graphic plot of transverse crack pattern (SH6-summer, LS, high steel)

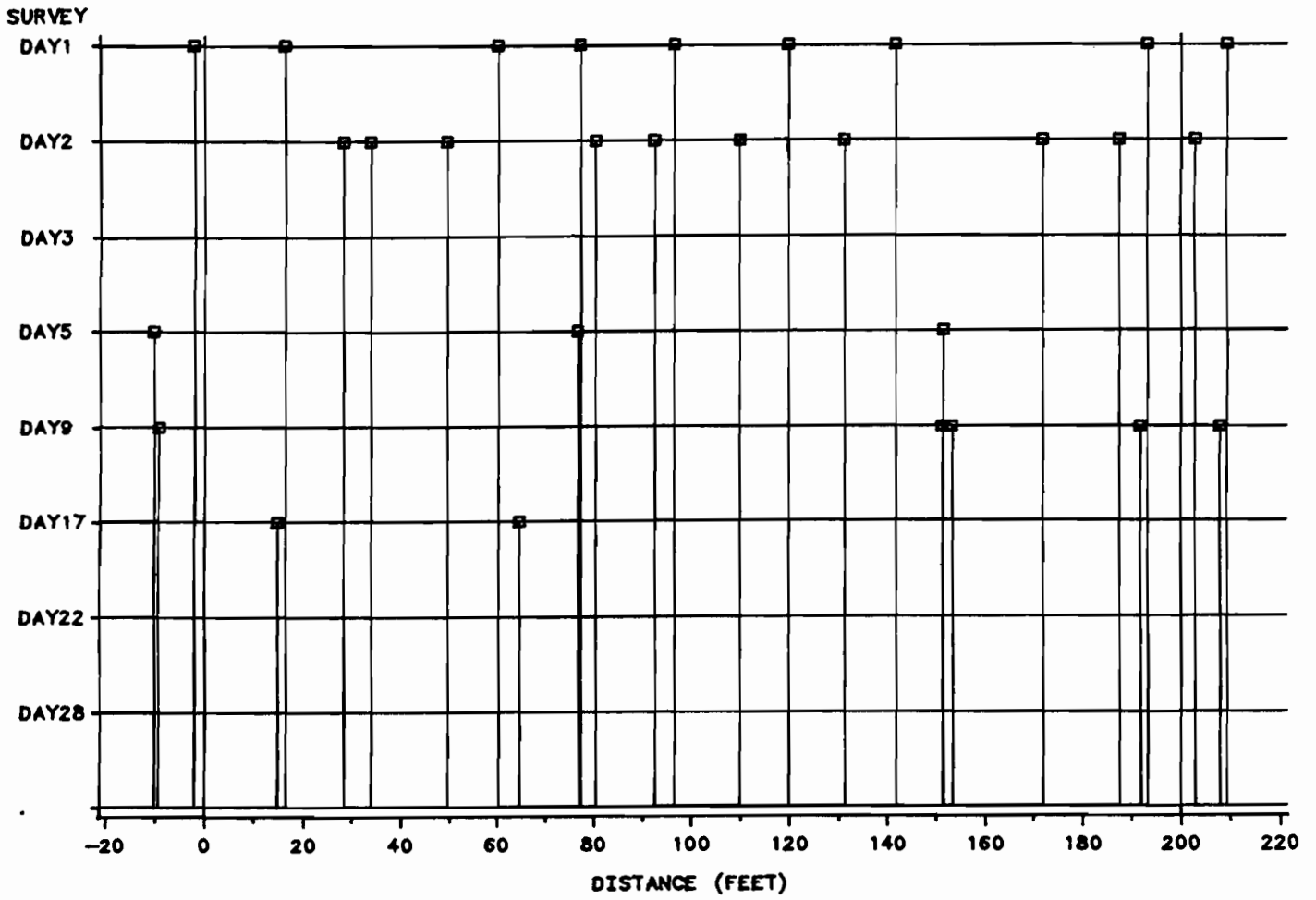


Figure E.5 Graphic plot of transverse crack pattern (SH6-summer, LS, low steel)

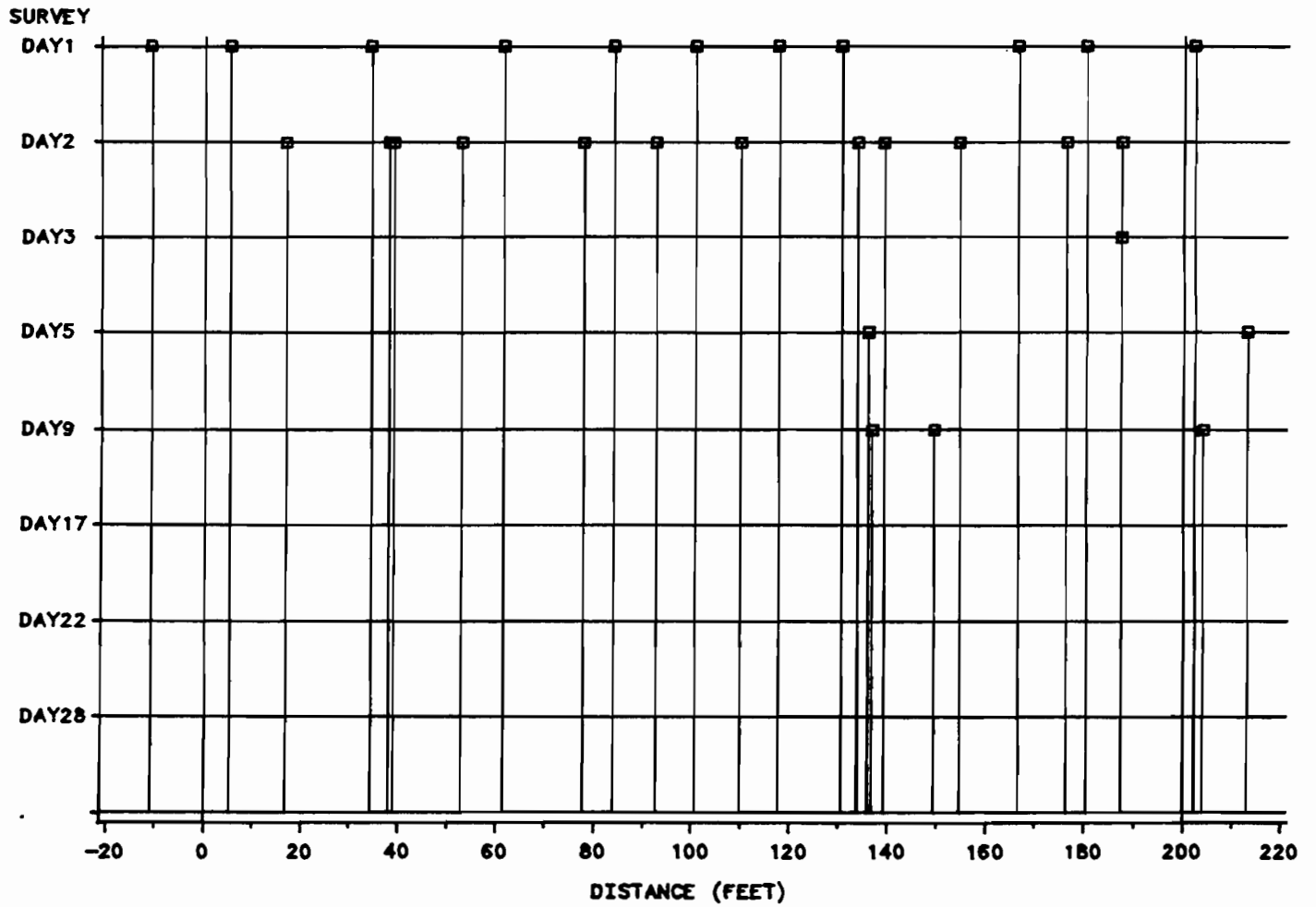


Figure E.6 Graphic plot of transverse crack pattern (SH6-summer, LS, no. 7 bar-medium steel)

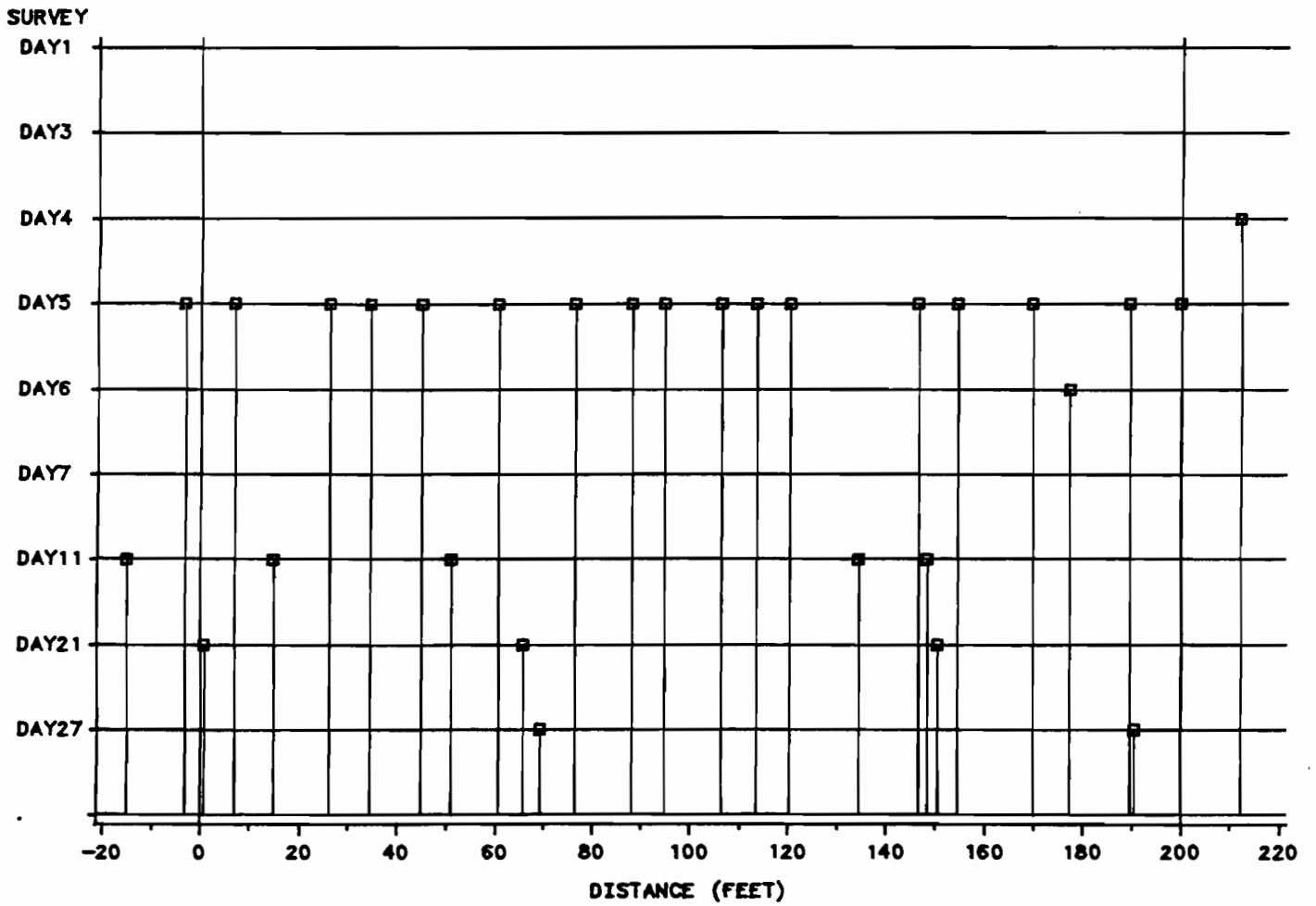


Figure E.7 Graphic plot of transverse crack pattern (BW8-winter, SRG, high steel)

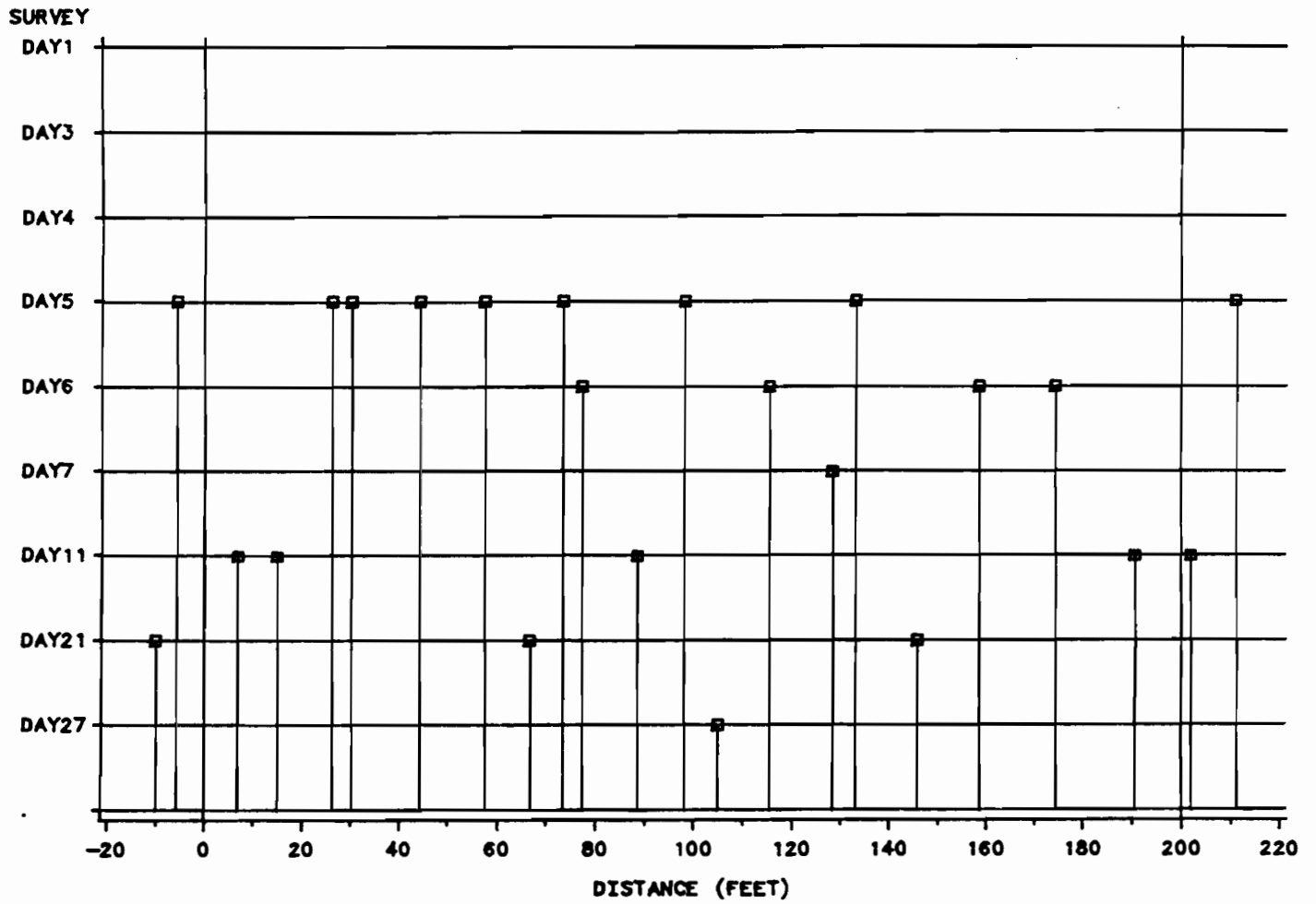


Figure E.8 Graphic plot of transverse crack pattern (BW8-winter, SRG, medium steel)

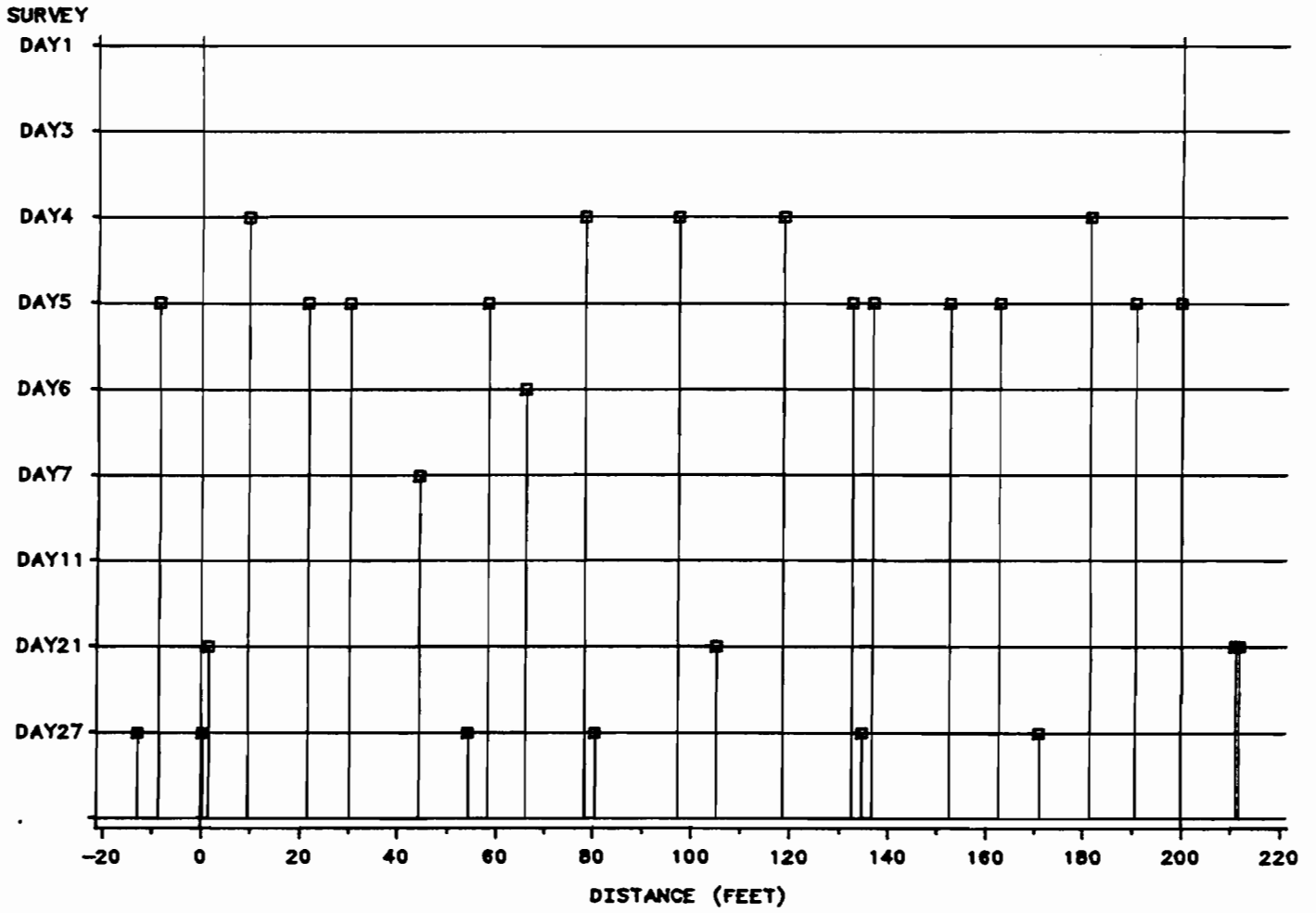


Figure E.9 Graphic plot of transverse crack pattern (BW8-winter, SRG, low steel)

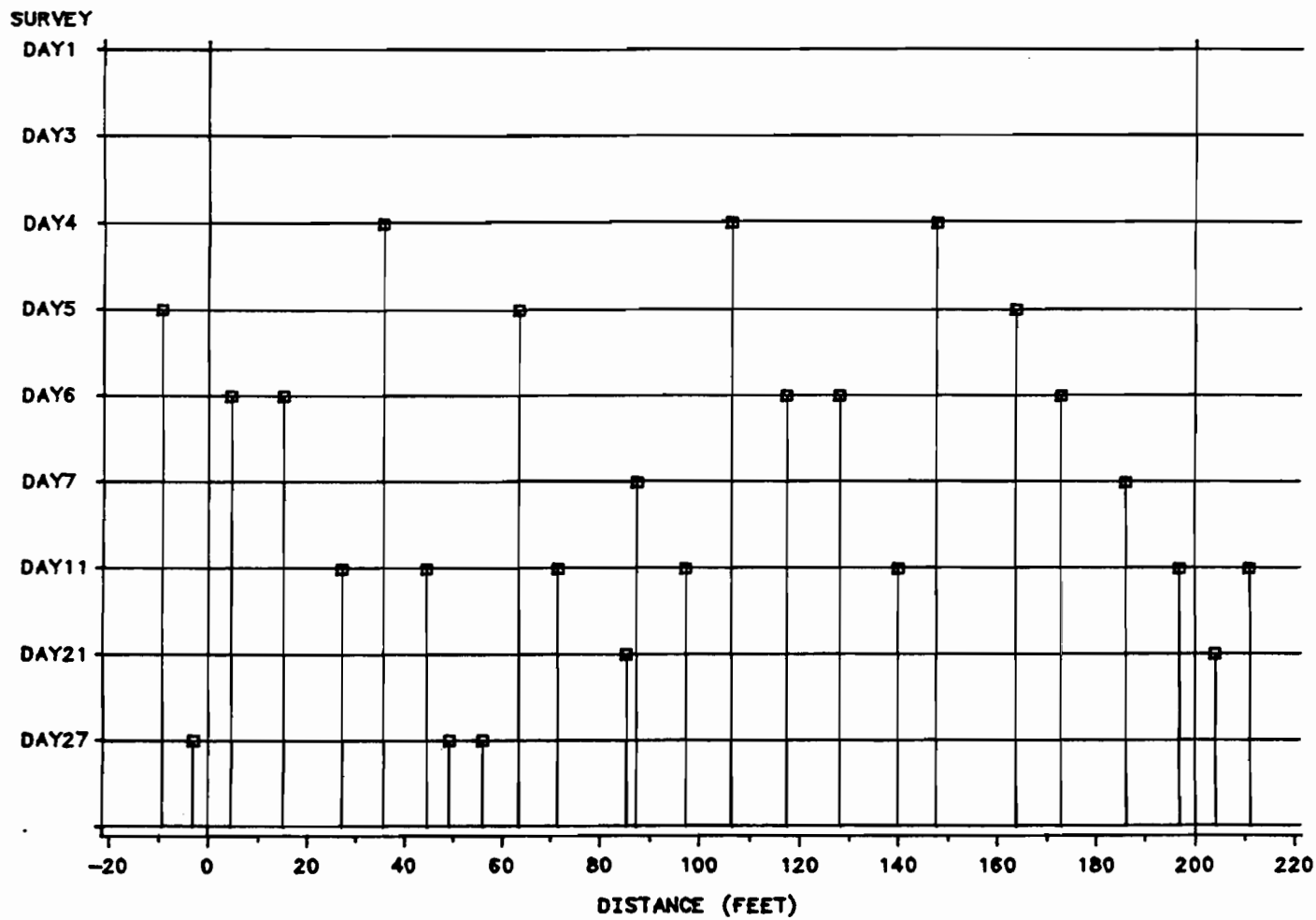


Figure E.10 Graphic plot of transverse crack pattern (BW8-winter, SRC, no. 7 bar-medium steel)

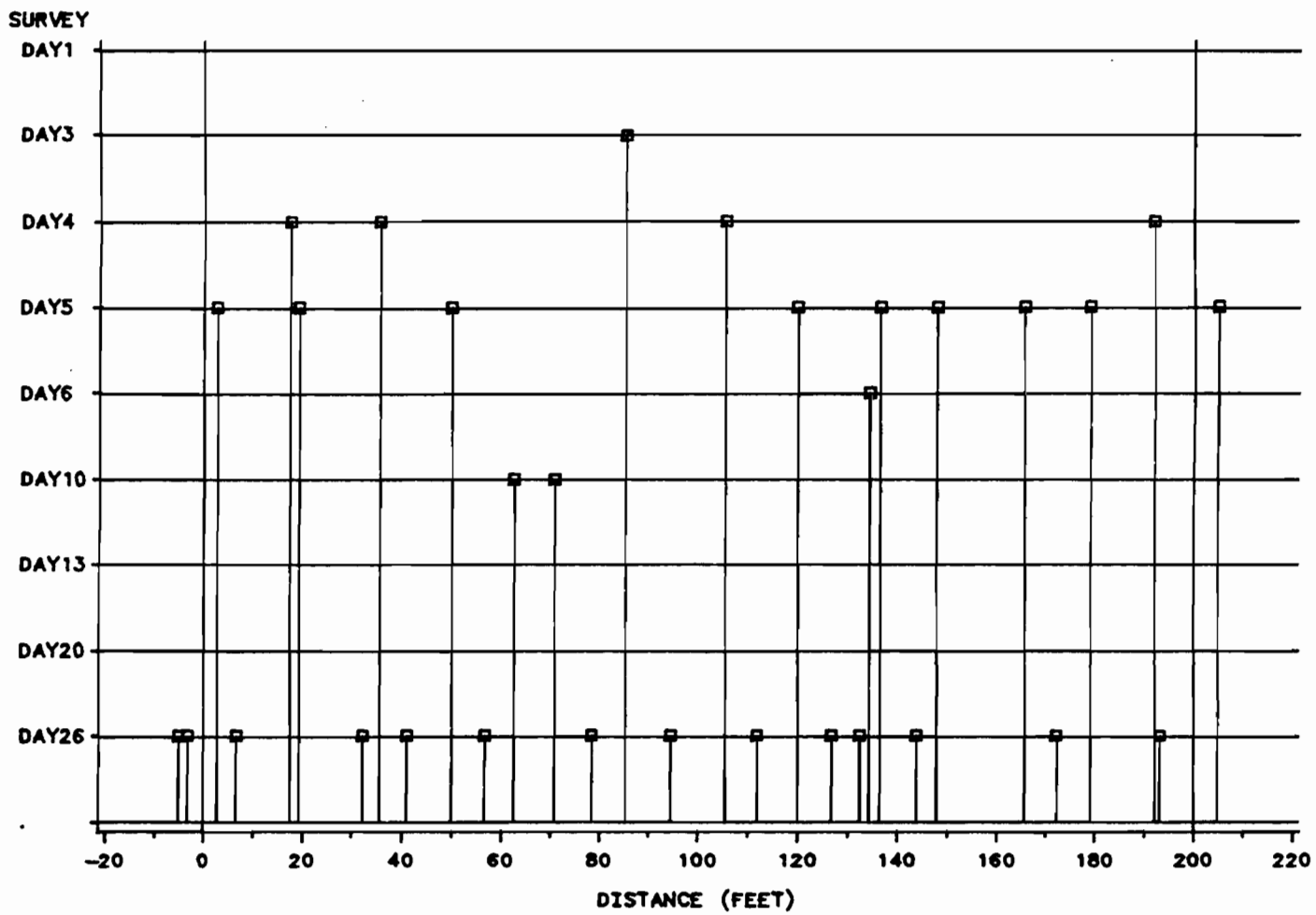


Figure E.11 Graphic plot of transverse crack pattern (BW8-winter, LS, high steel)

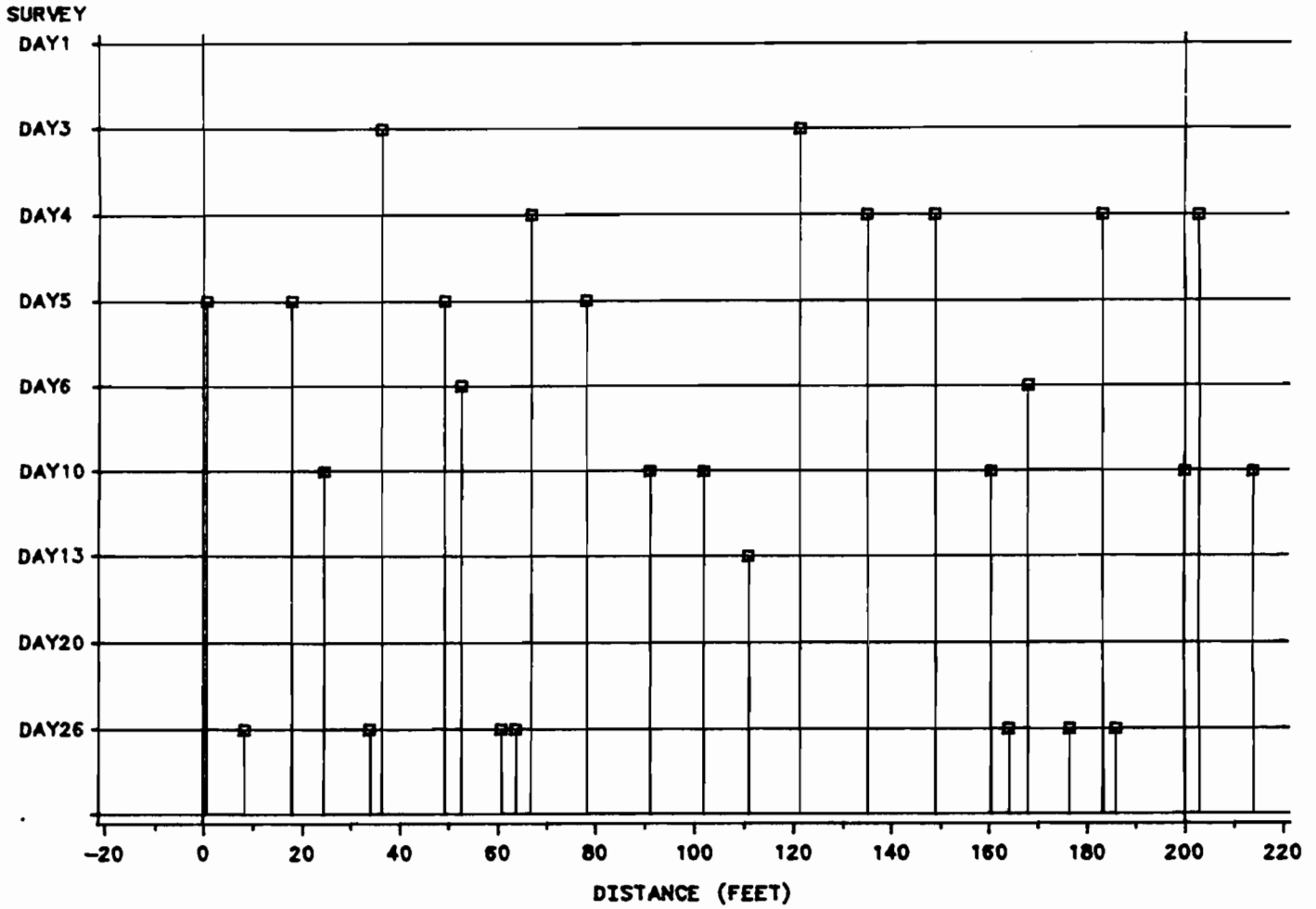


Figure E.12 Graphic plot of transverse crack pattern (BW8-winter, LS, medium steel)

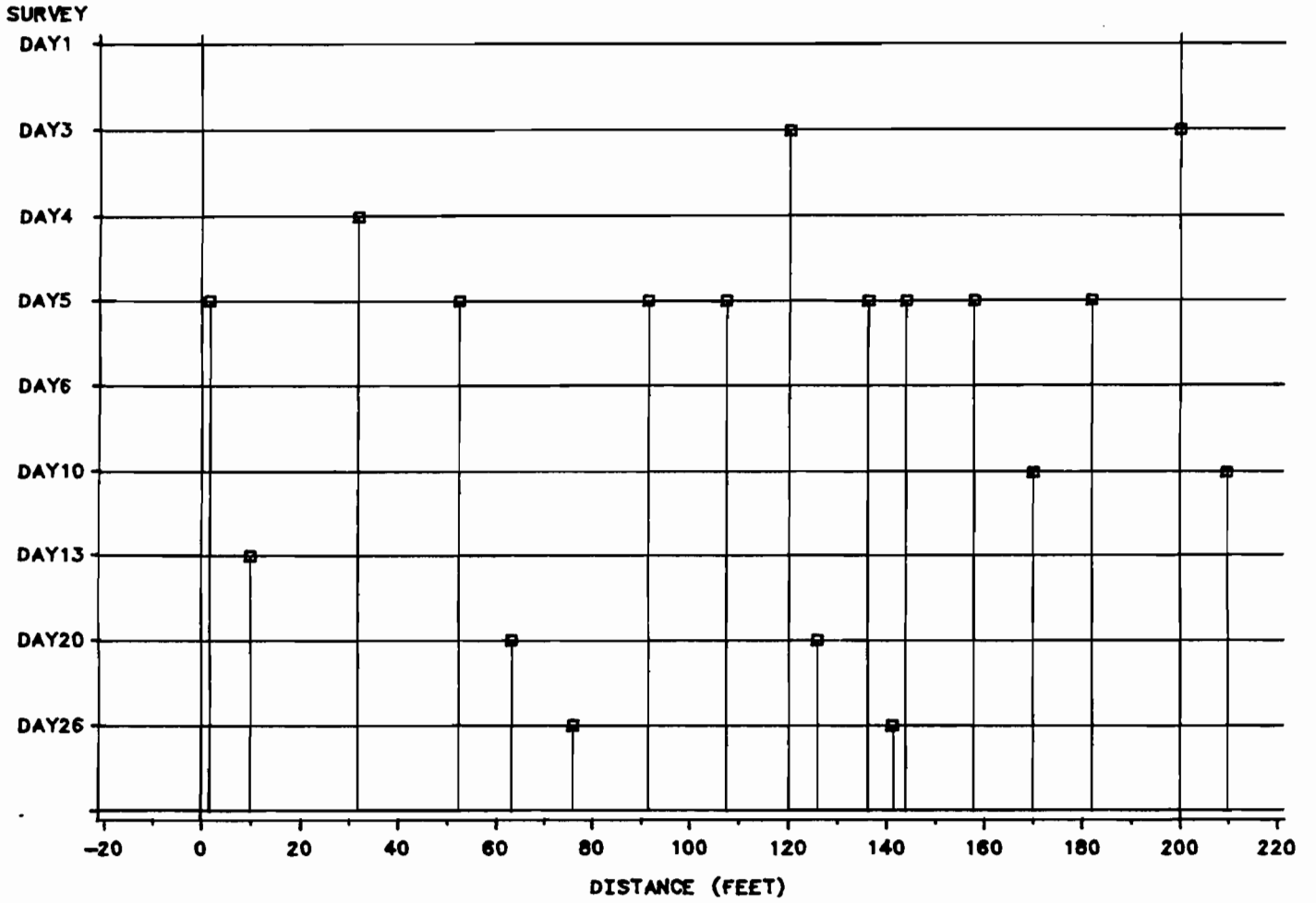


Figure E.13 Graphic plot of transverse crack pattern (BW8-winter, LS, low steel)

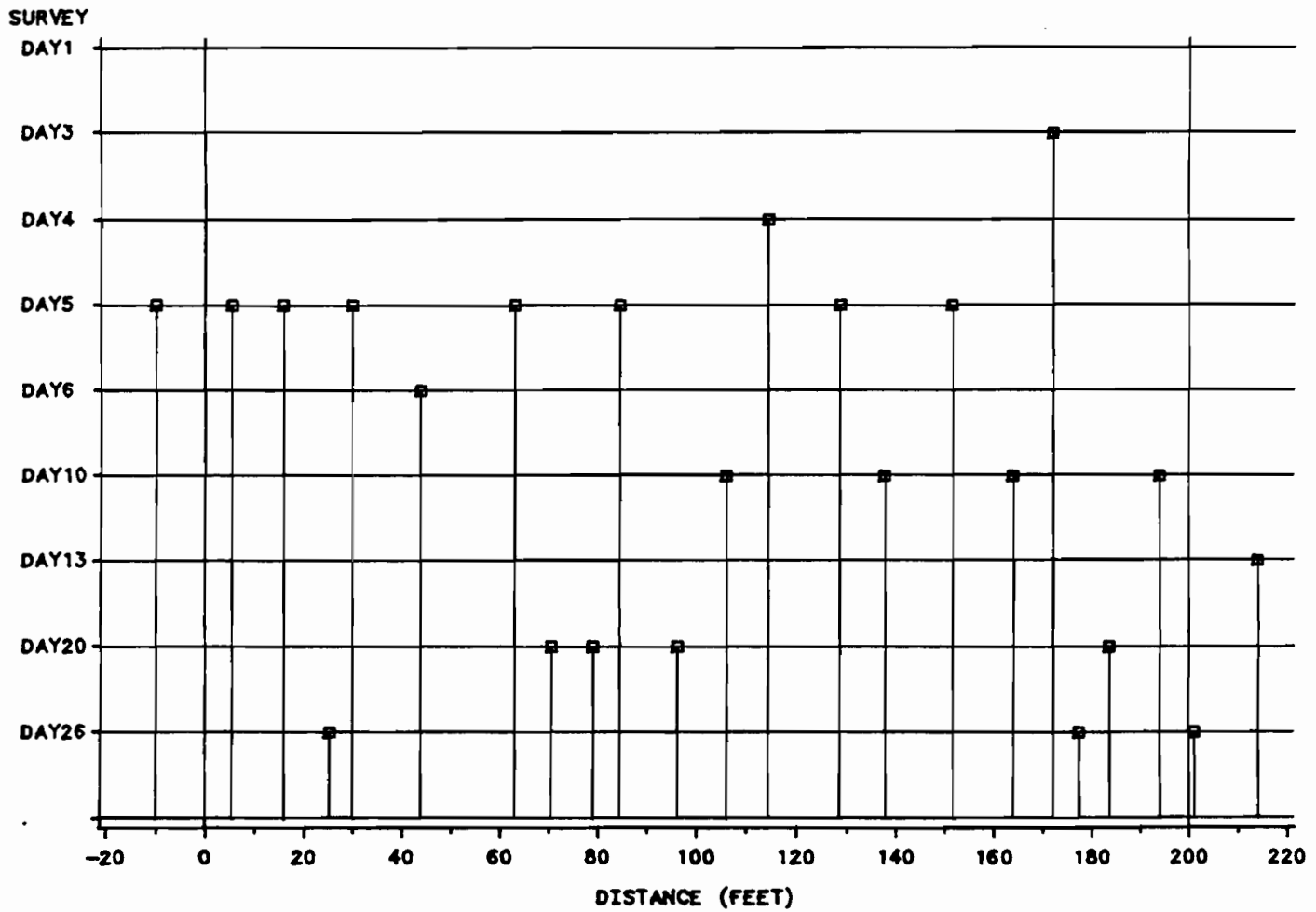


Figure E.14 Graphic plot of transverse crack pattern (BW8-winter, LS, no. 7 bar-medium steel)

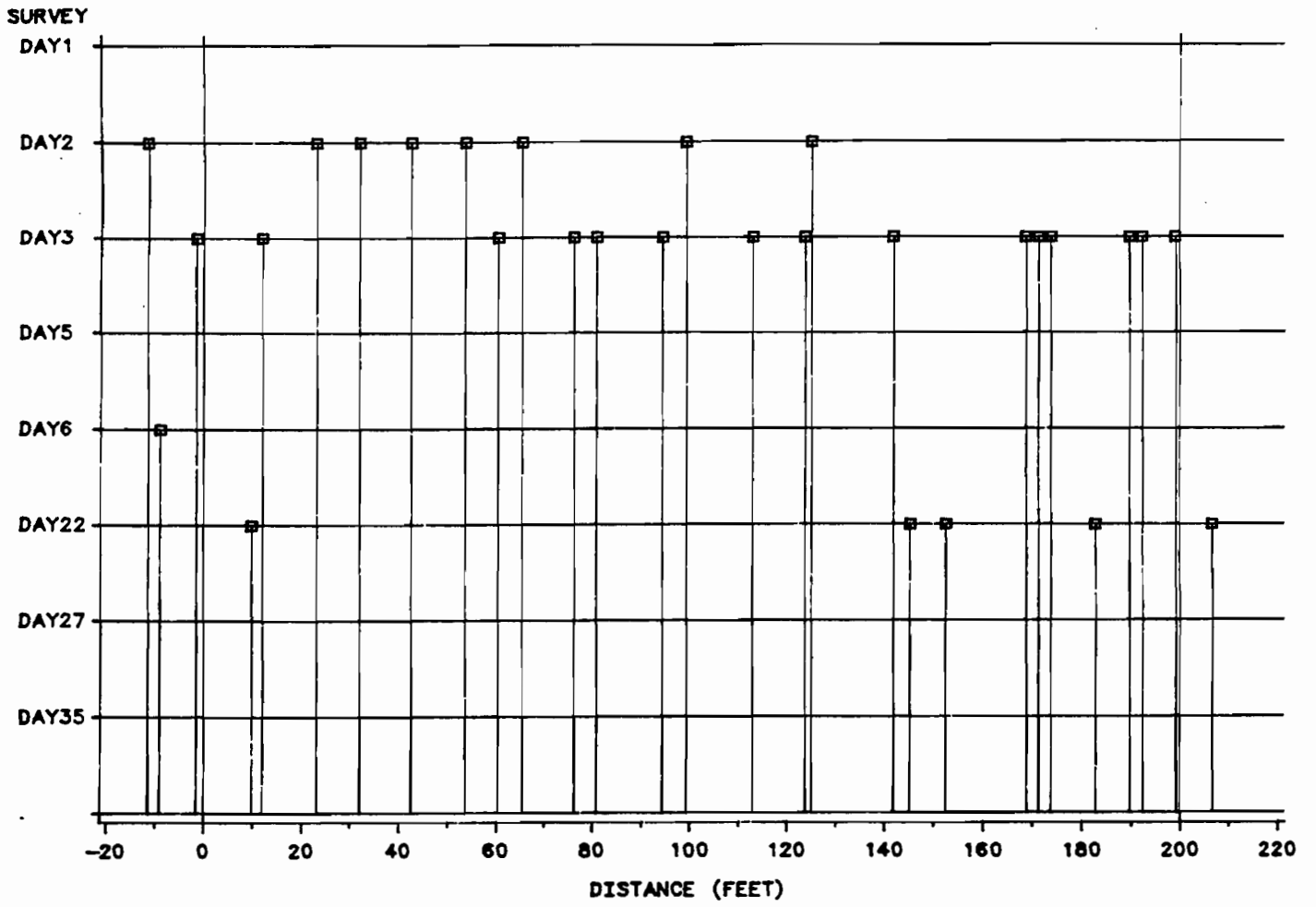


Figure E.15 Graphic plot of transverse crack pattern (SH6-winter, SRG, high steel)

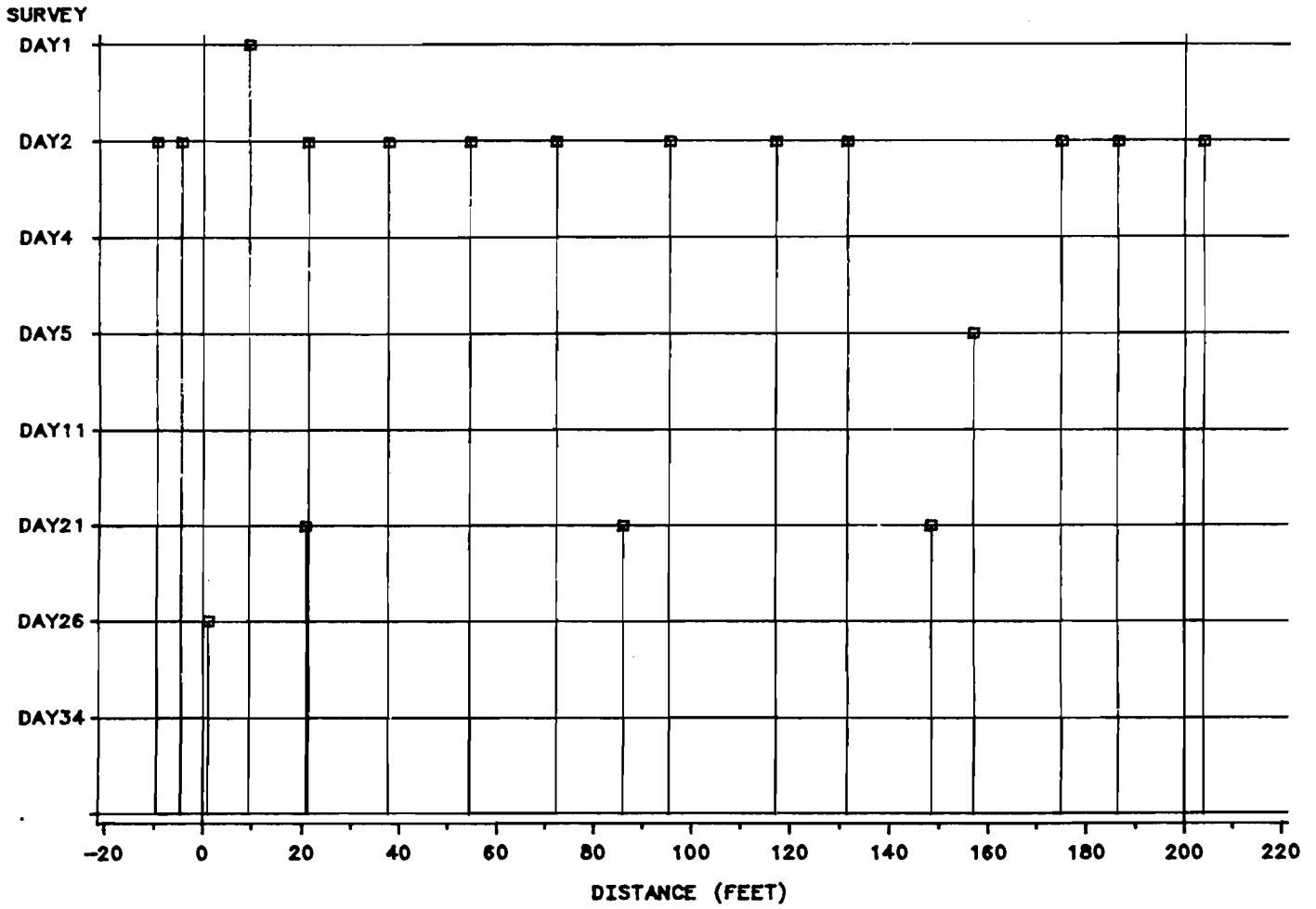


Figure E.16 Graphic plot of transverse crack pattern (SH6-winter, SRG, low steel)

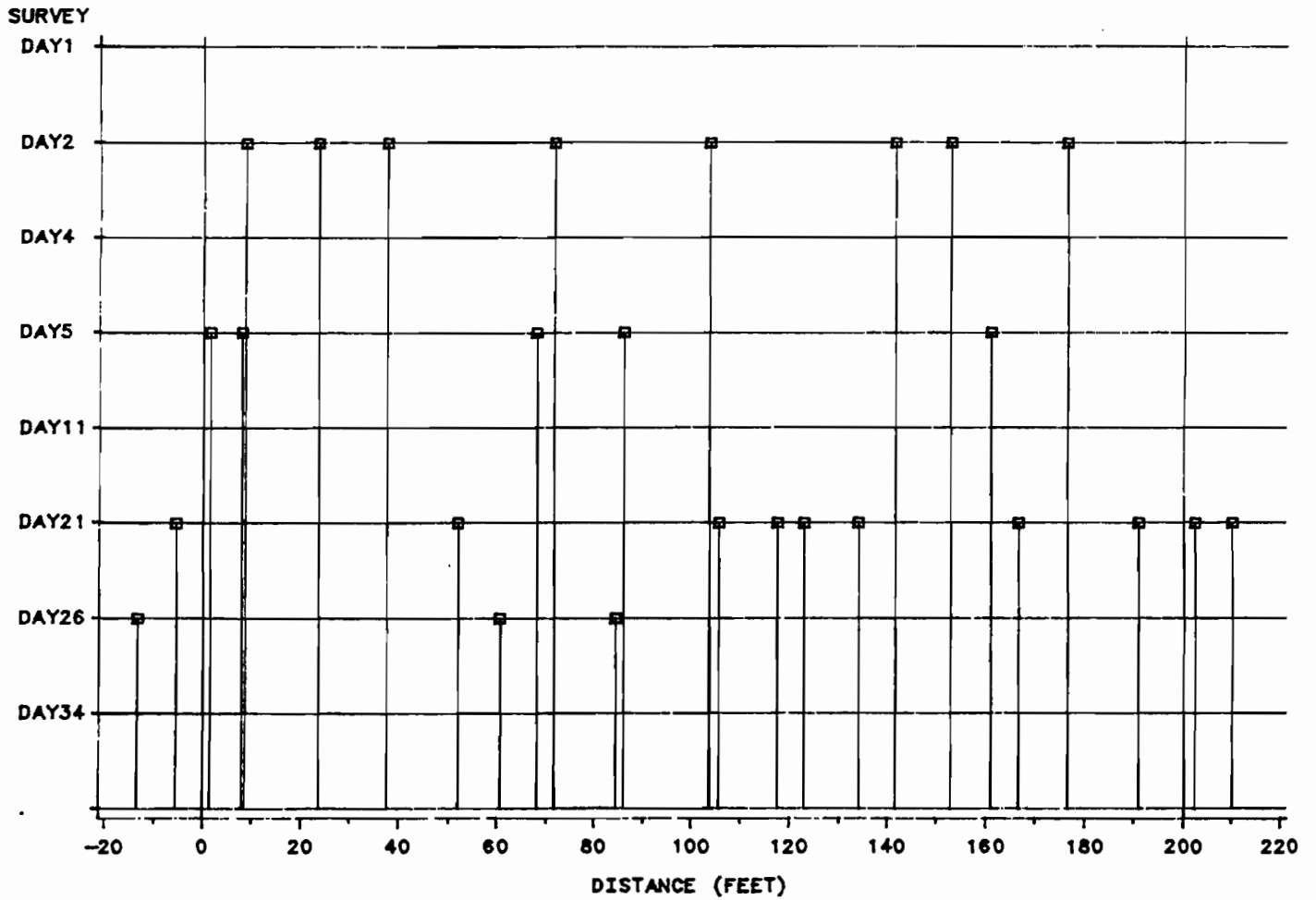


Figure E.17 Graphic plot of transverse crack pattern (SH6-winter, SRG, no. 7 bar-medium steel)

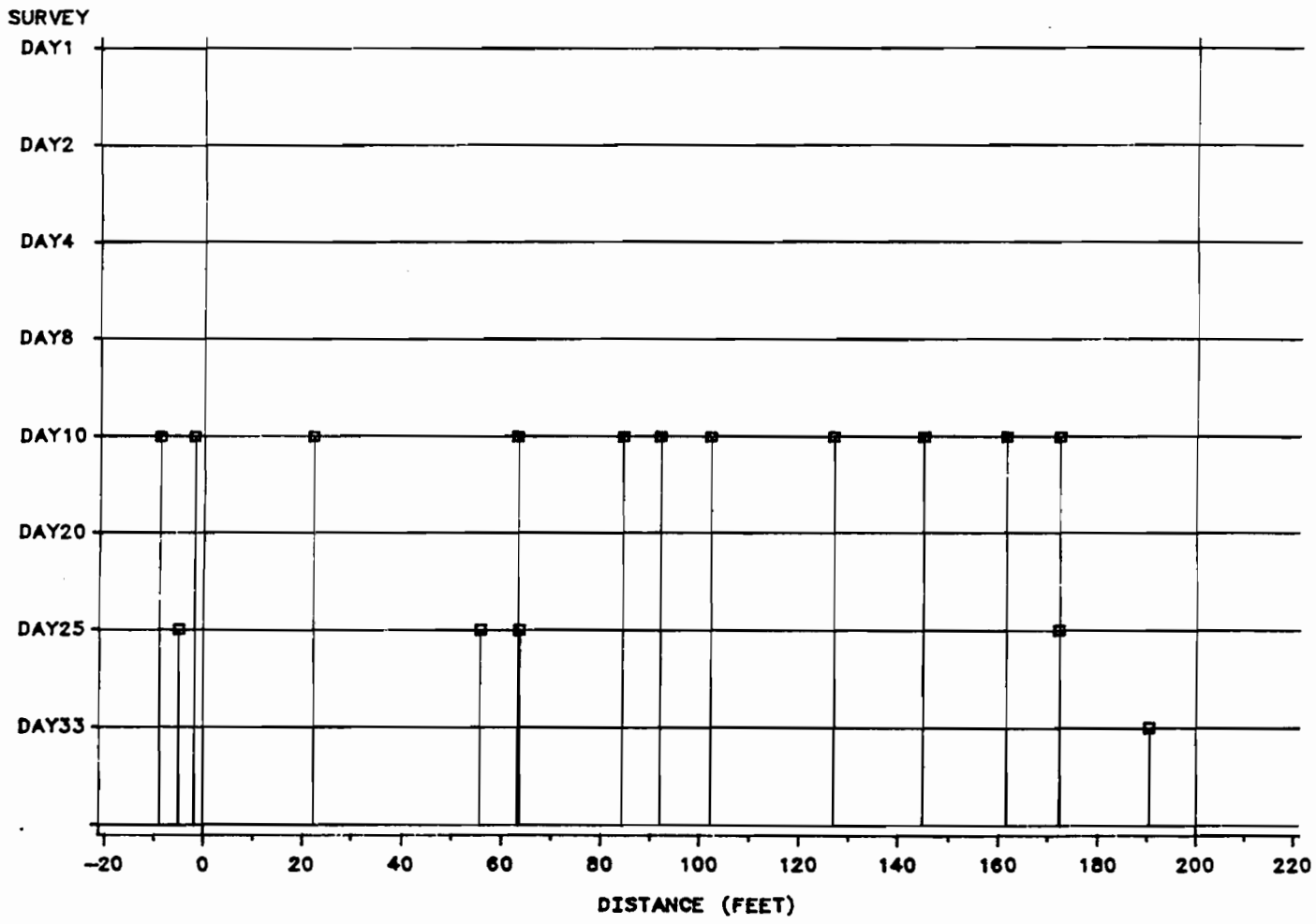


Figure E.18 Graphic plot of transverse crack pattern (SH6-winter, LS, high steel)

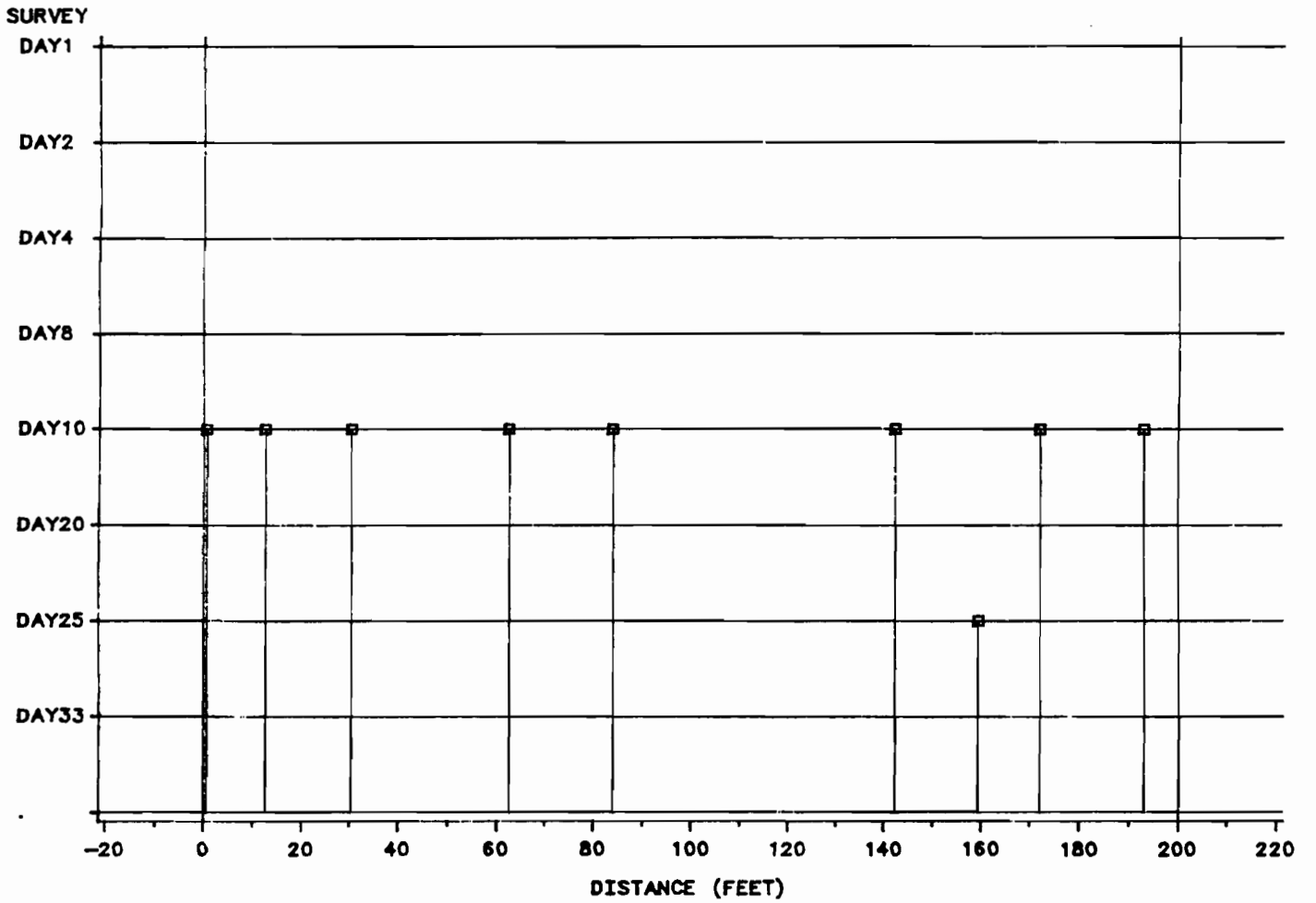


Figure E.19 Graphic plot of transverse crack pattern (SH6-winter, LS, low steel)

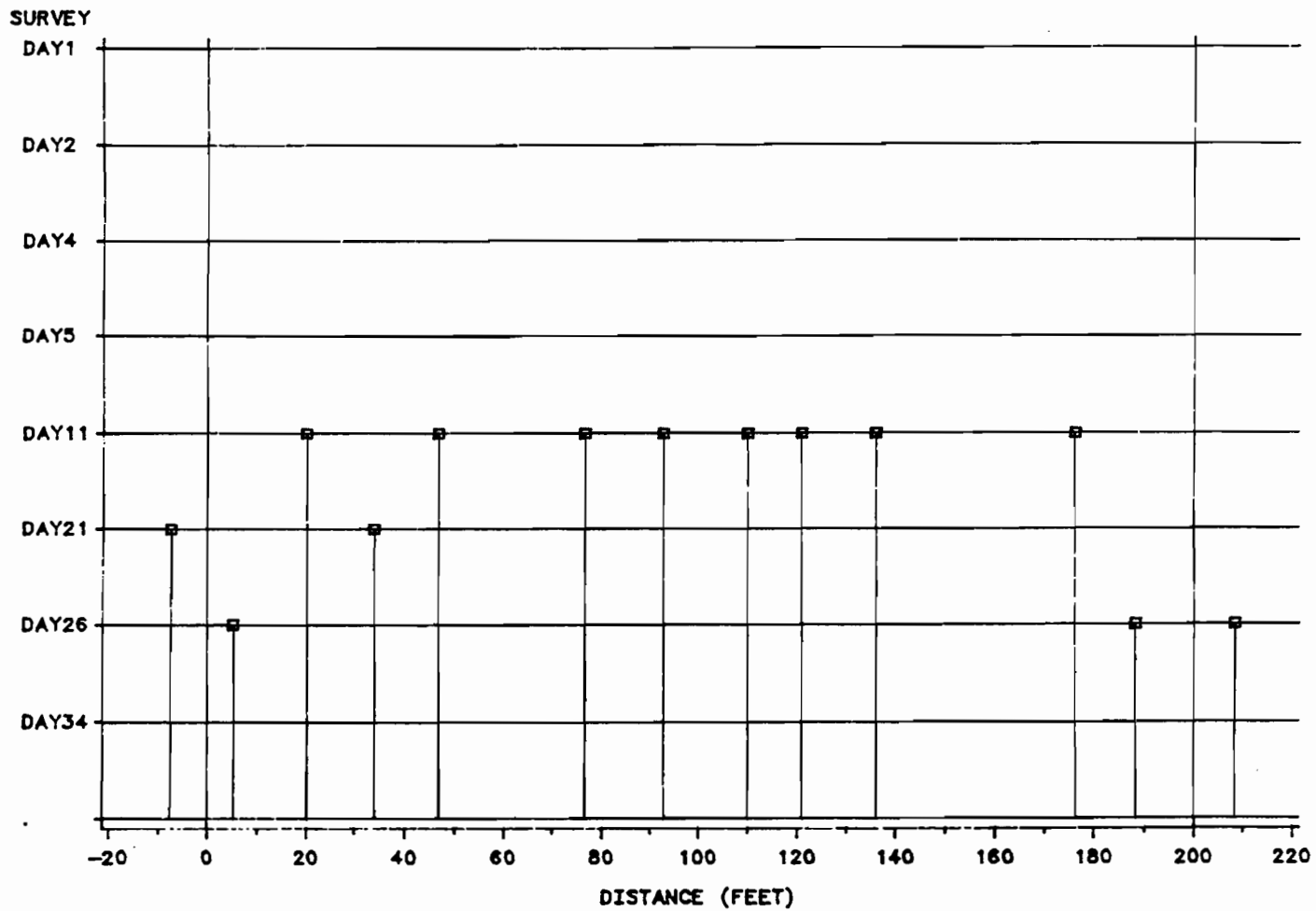


Figure E.20 *Graphic plot of transverse crack pattern (SH6-winter, LS, no. 7 bar-medium steel)*

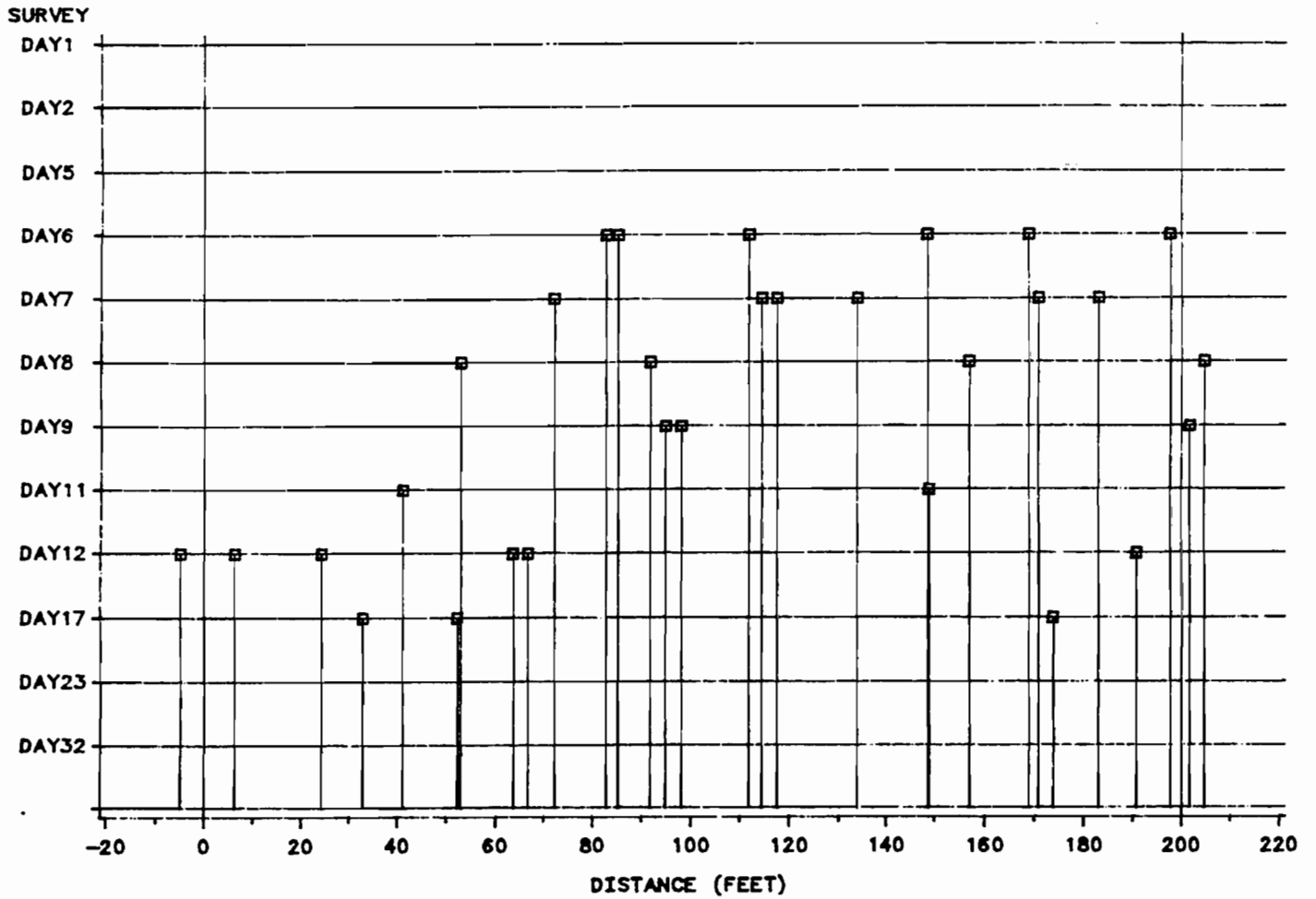


Figure E.21 Graphic plot of transverse crack pattern (IH45-winter, SRG, high steel)

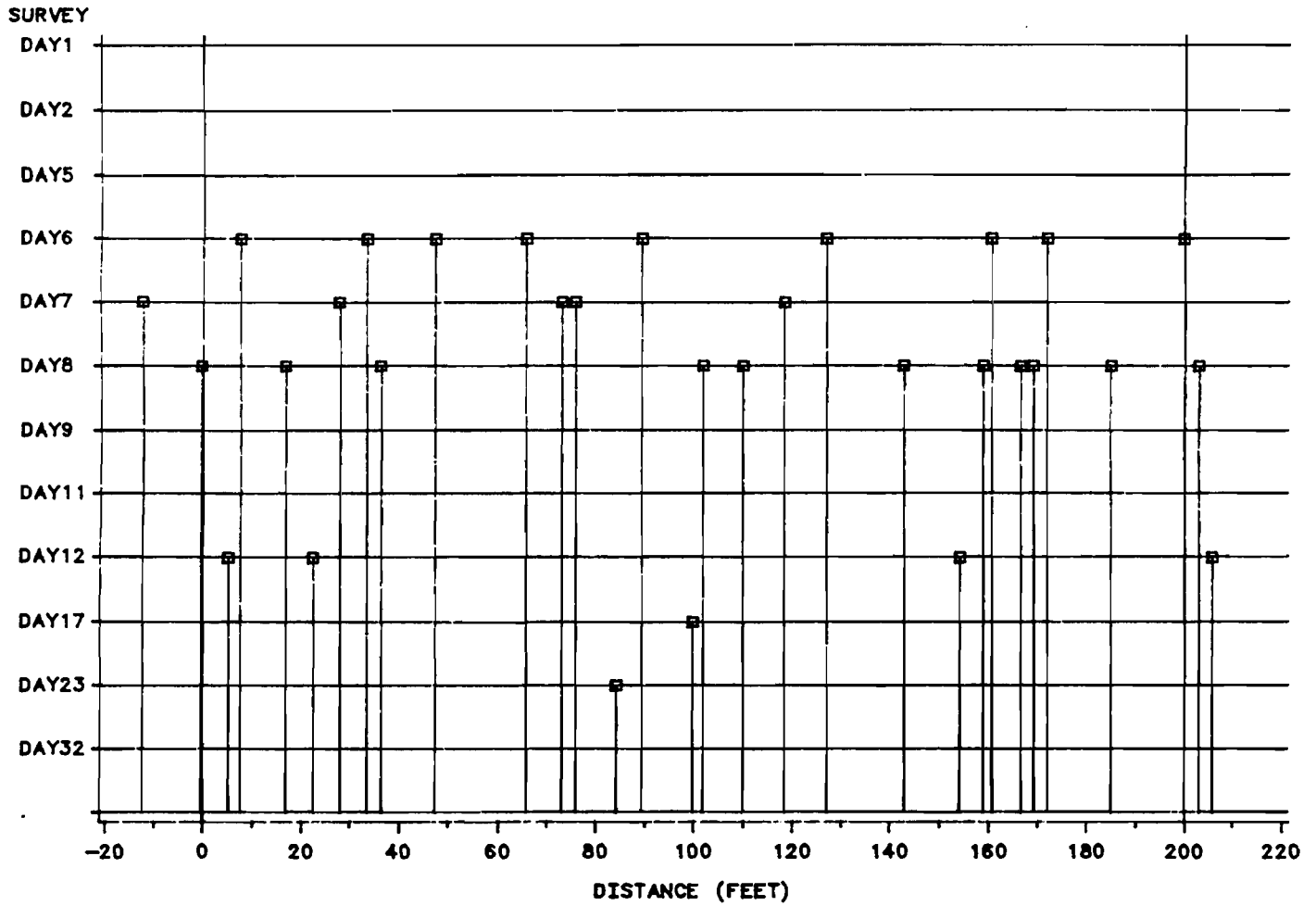


Figure E.22 Graphic plot of transverse crack pattern (IH45-winter, SRG, medium steel)

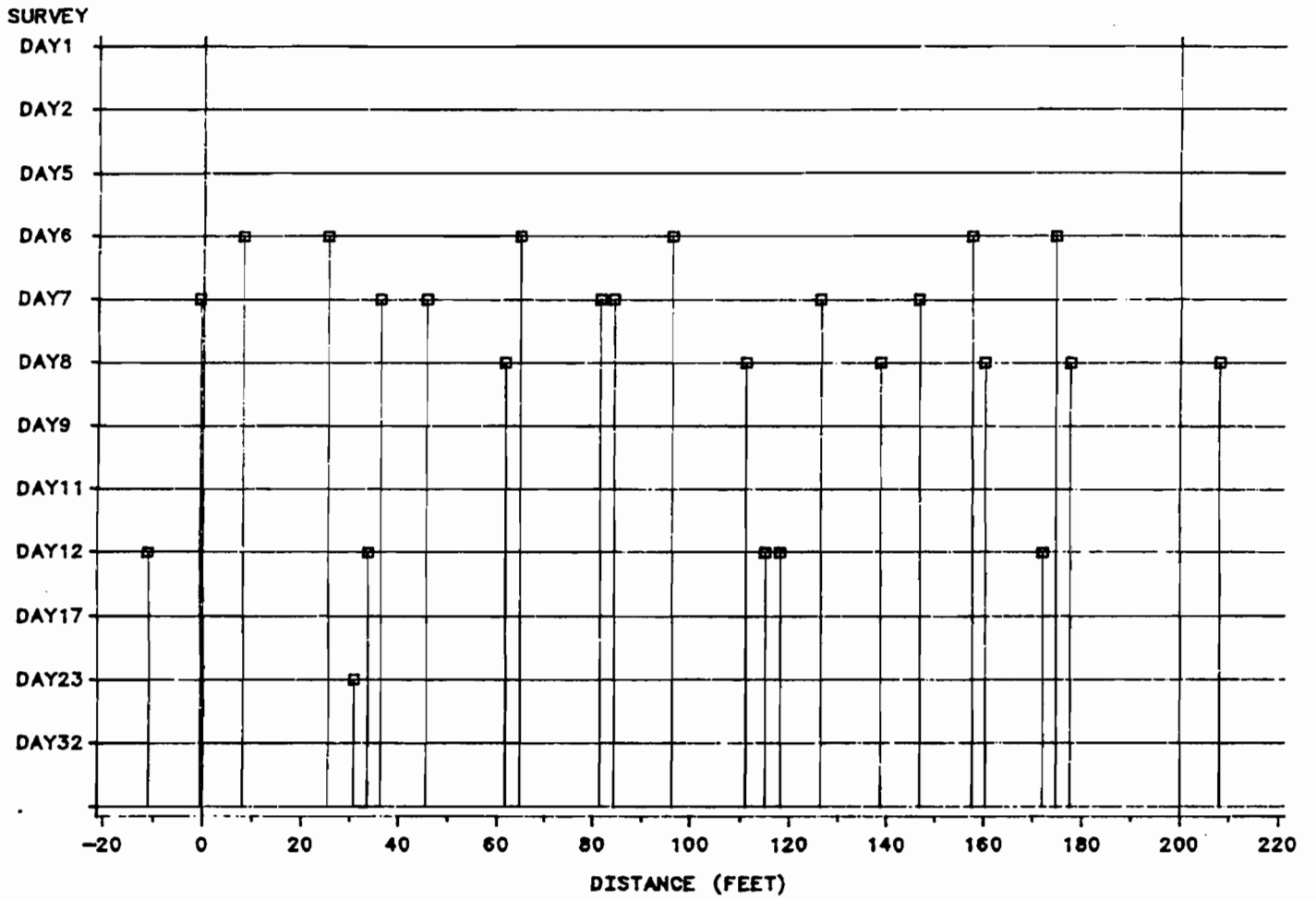


Figure E.23 Graphic plot of transverse crack pattern (IH45-winter, SRG, low steel)

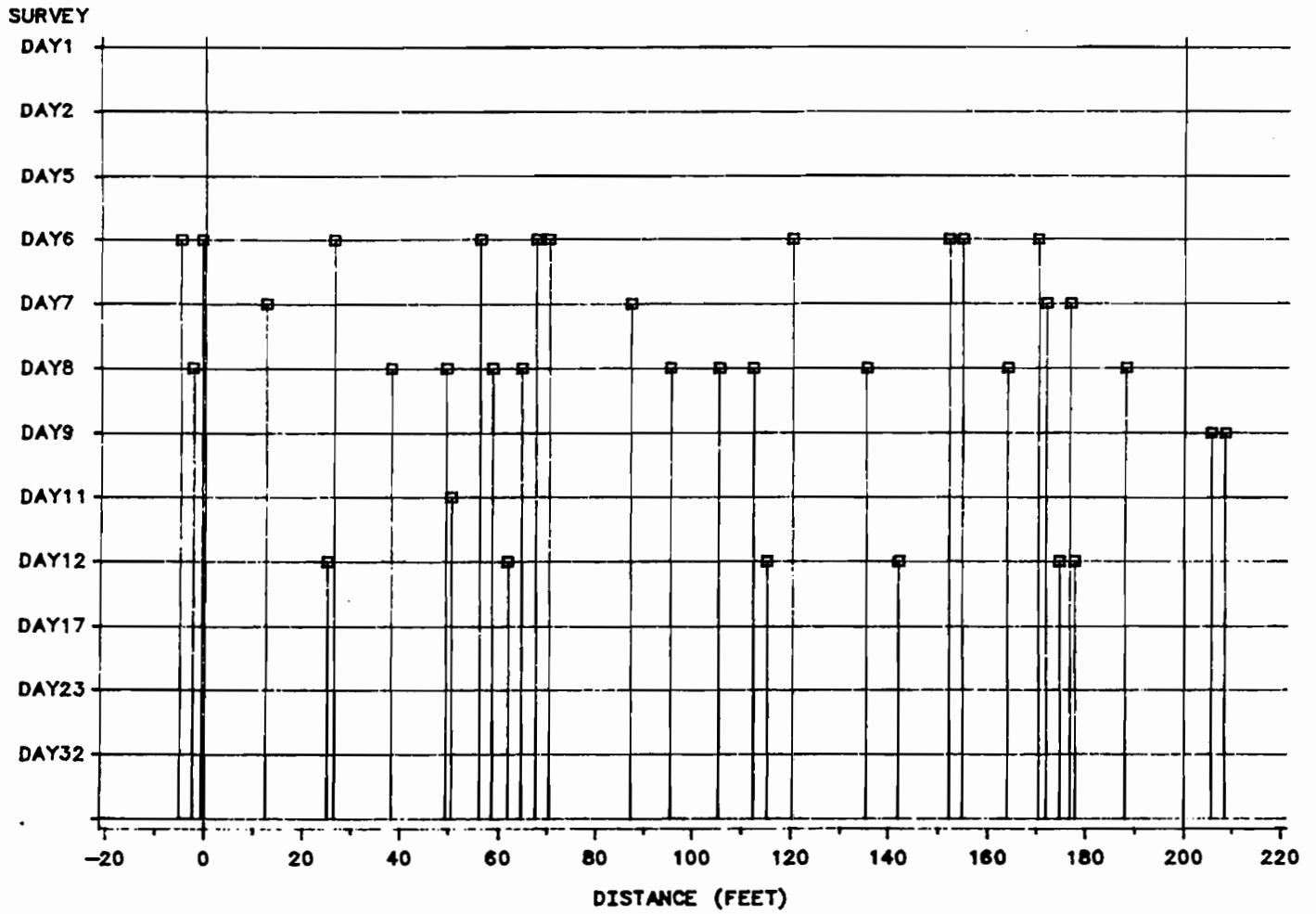


Figure E.24 Graphic plot of transverse crack pattern (IH45-winter, SRG, no. 7 bar-medium steel)

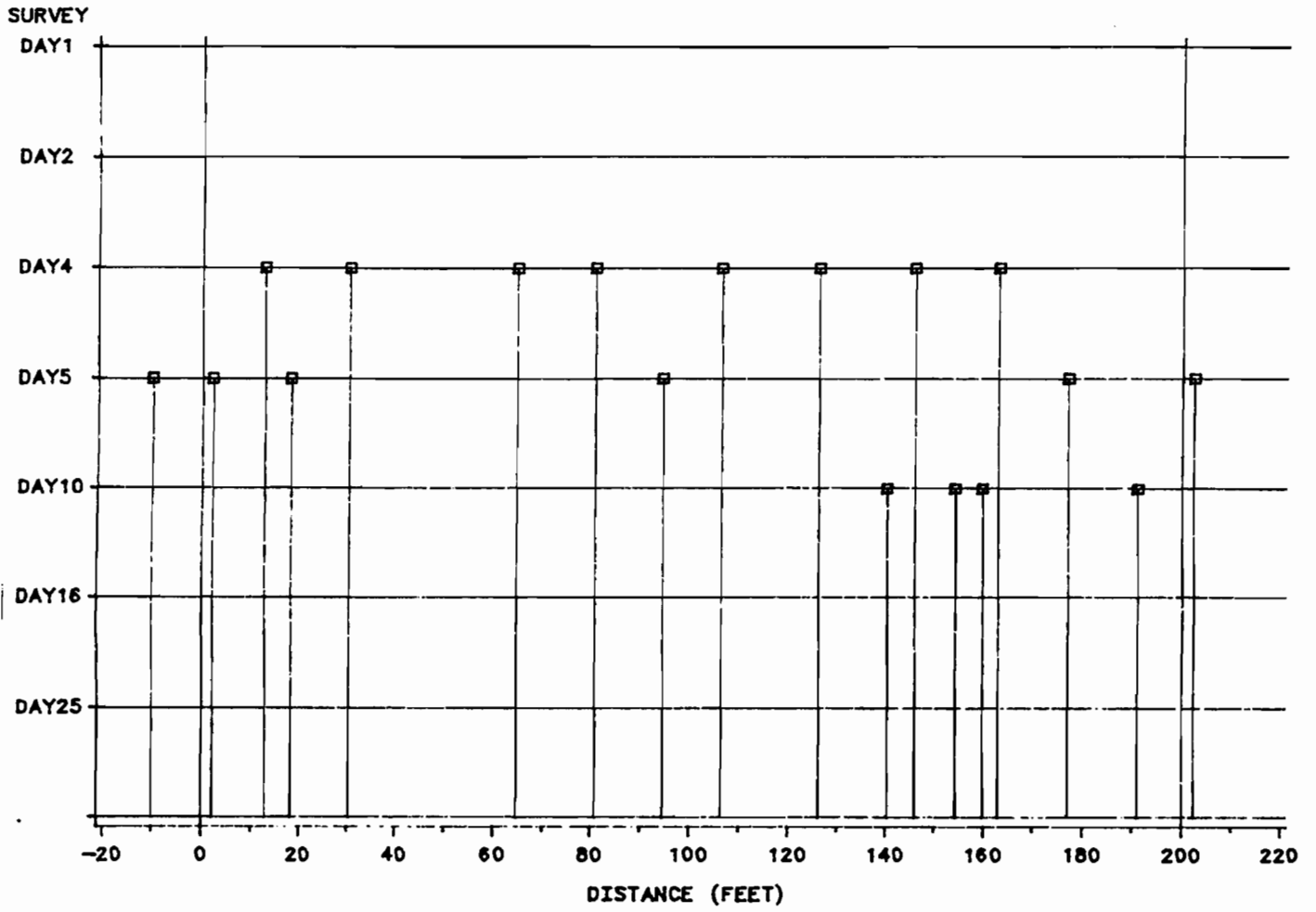


Figure E.25 Graphic plot of transverse crack pattern (IH45-winter, LS, high steel)

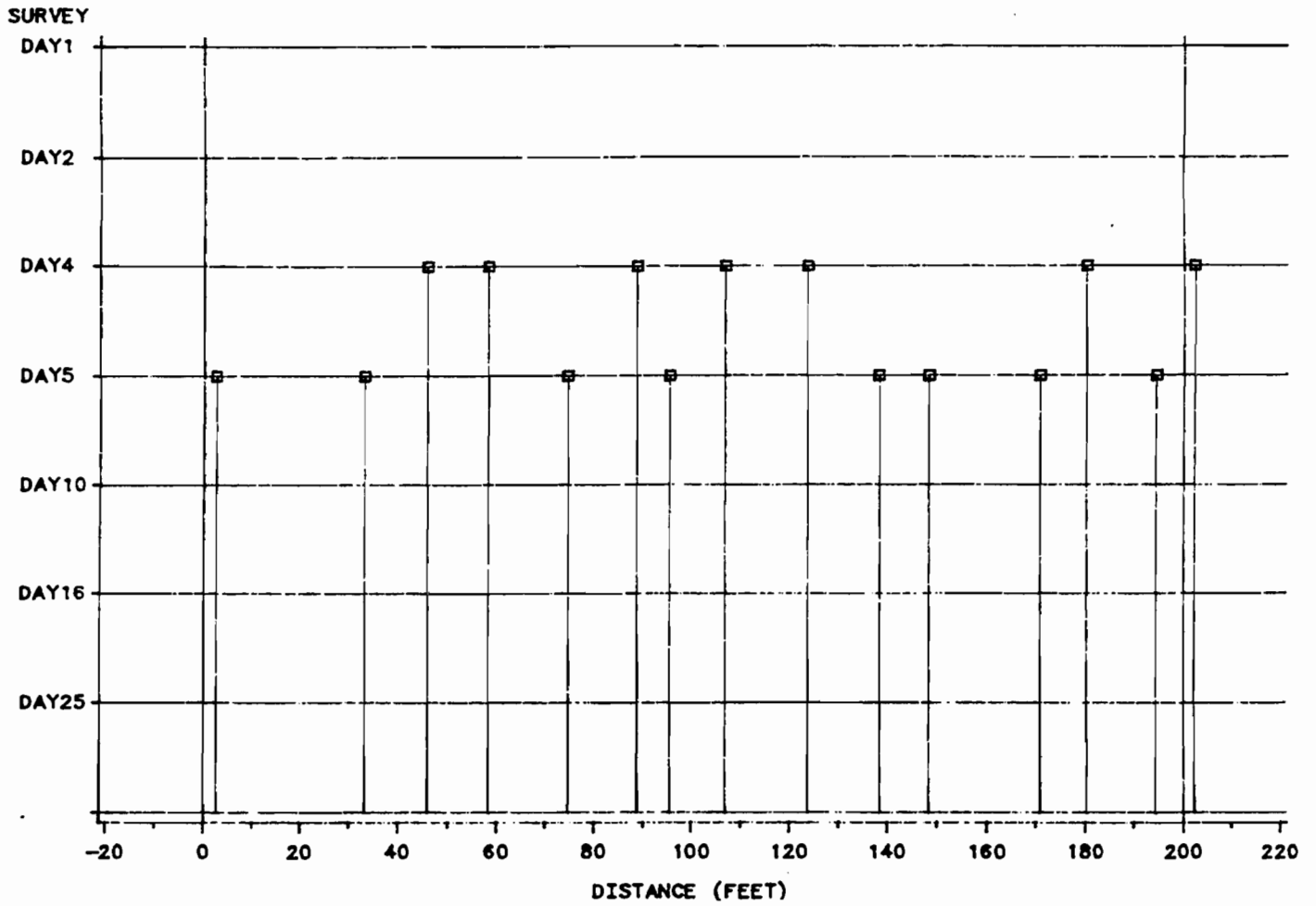


Figure E.26 *Graphic plot of transverse crack pattern (IH45-winter, LS, medium steel)*

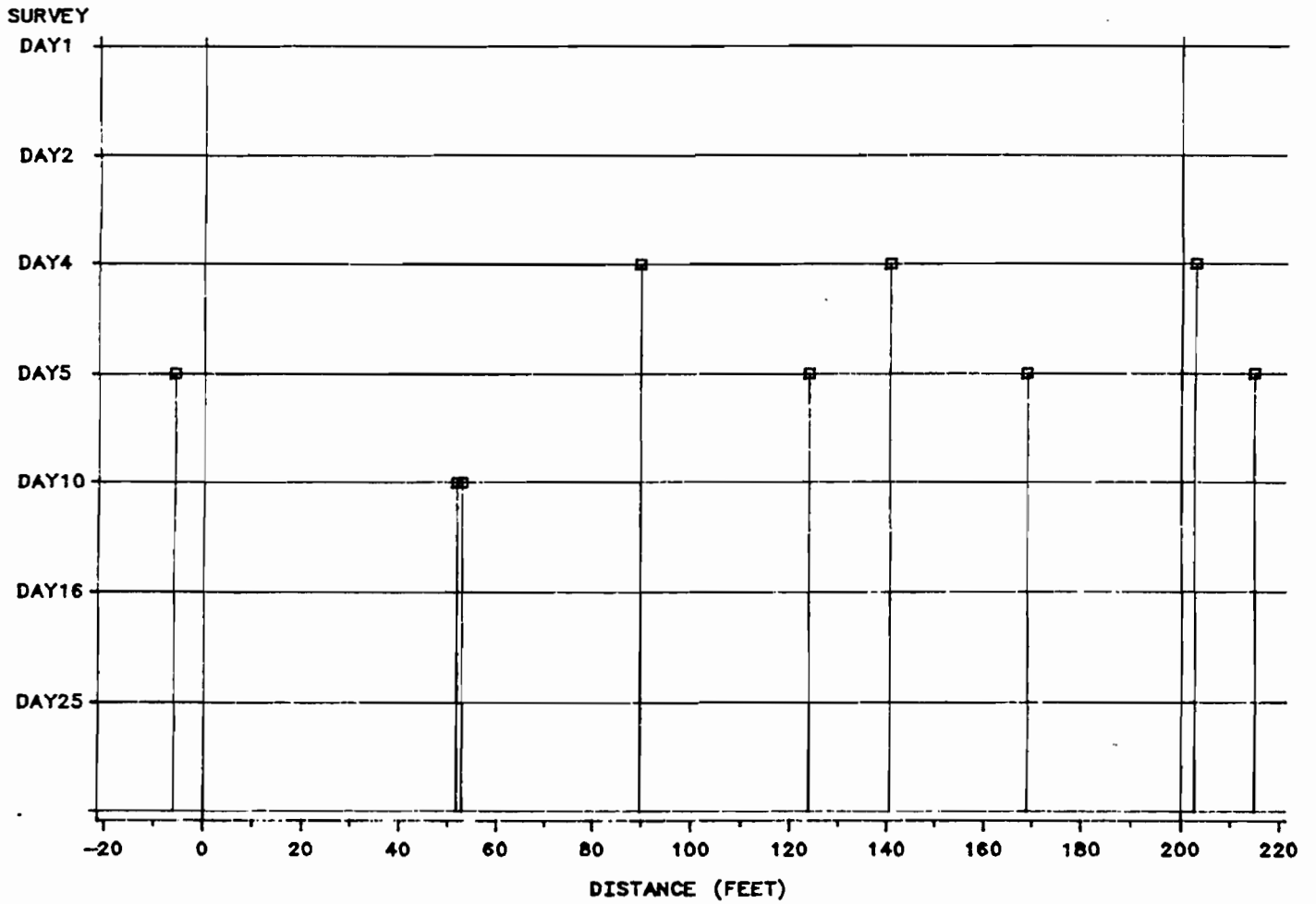


Figure E.27 Graphic plot of transverse crack pattern (IH45-winter, LS, low steel)

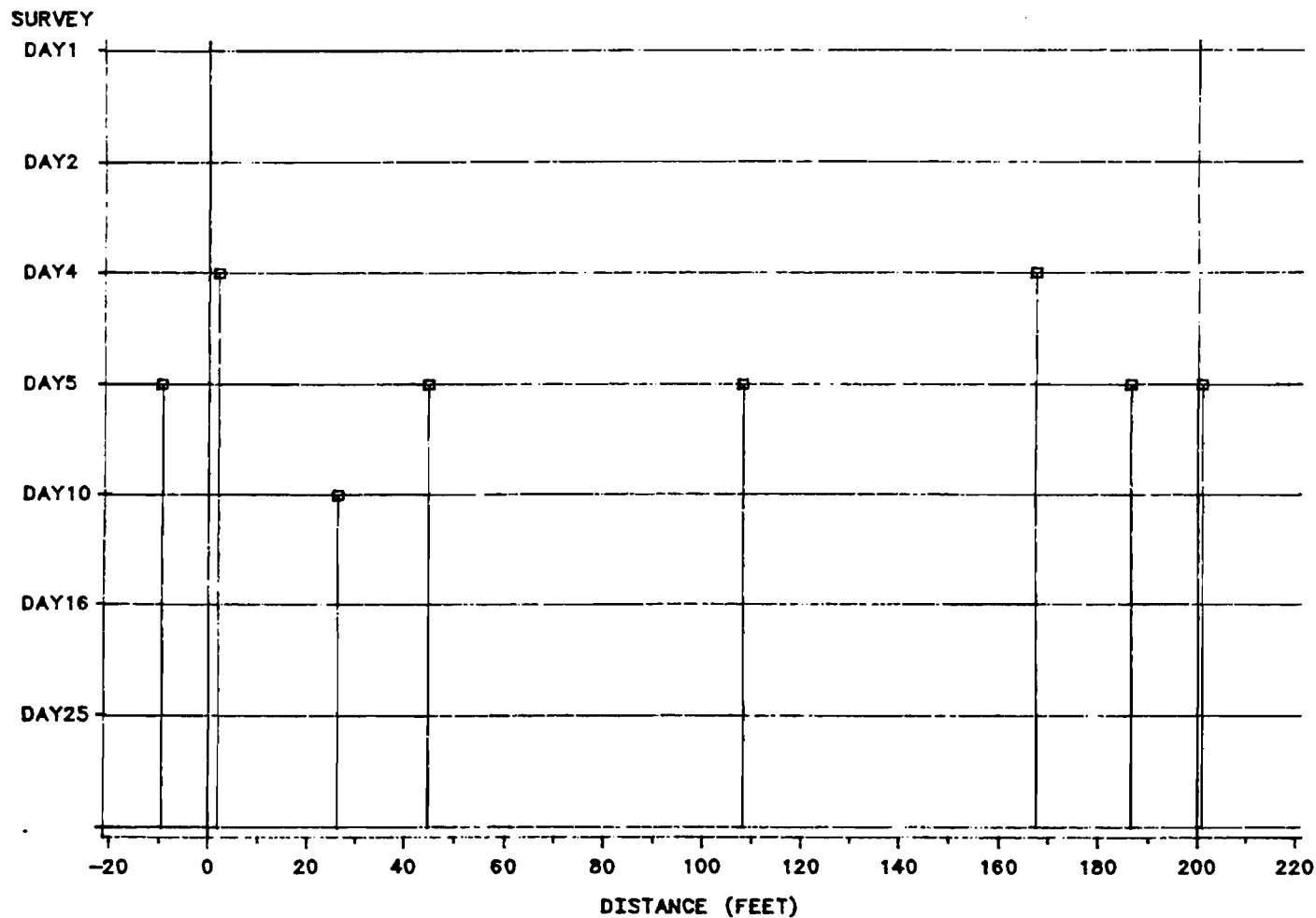


Figure E.28 Graphic plot of transverse crack pattern (IH45-winter, LS, no. 7 bar-medium steel)

APPENDIX F

DISTRIBUTION OF CRACK SPACINGS AT THE END OF SHORT-TERM MONITORING

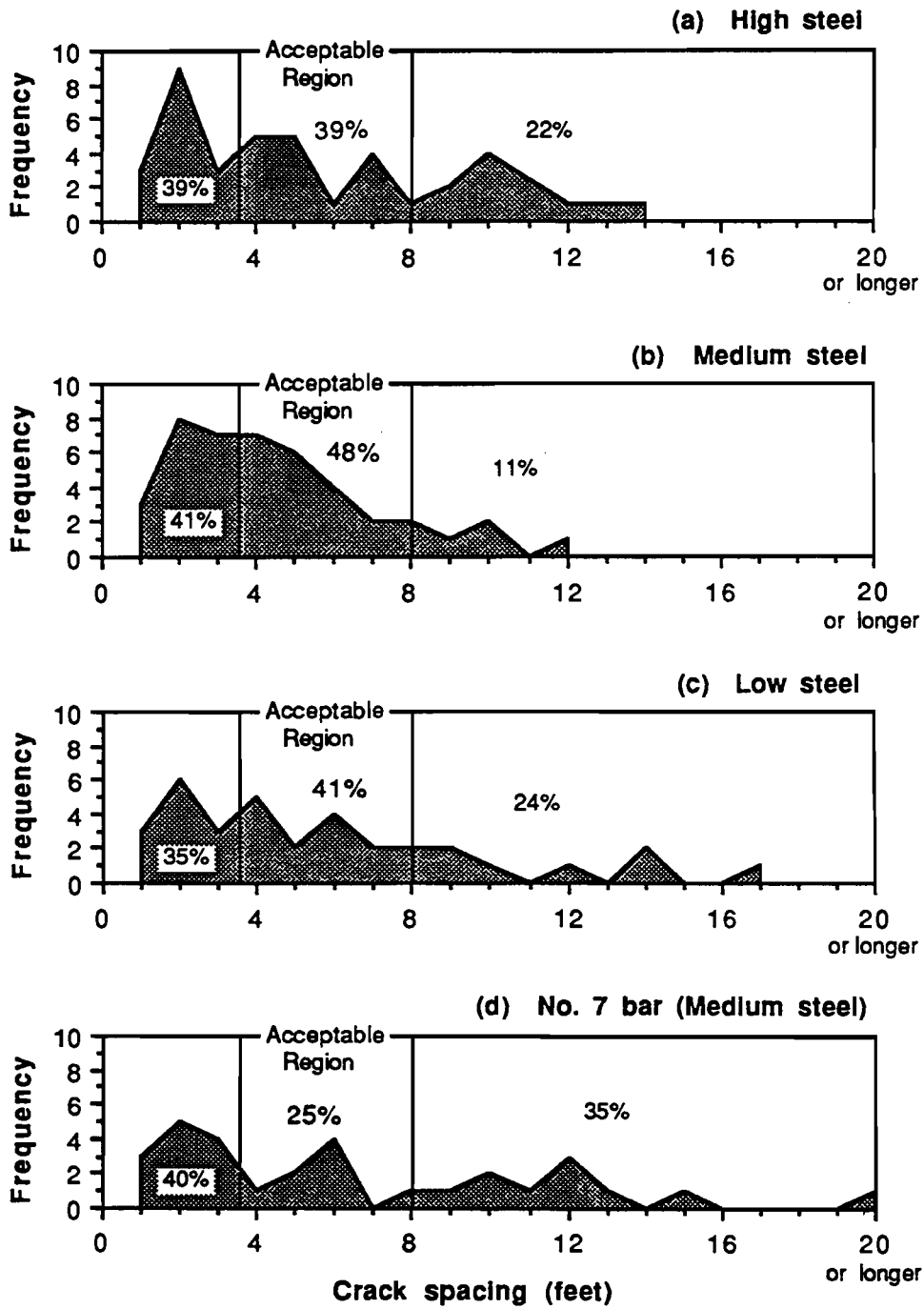


Figure F.1 Distribution of crack spacings at the end of short-term monitoring (SH6-summer, SRG)

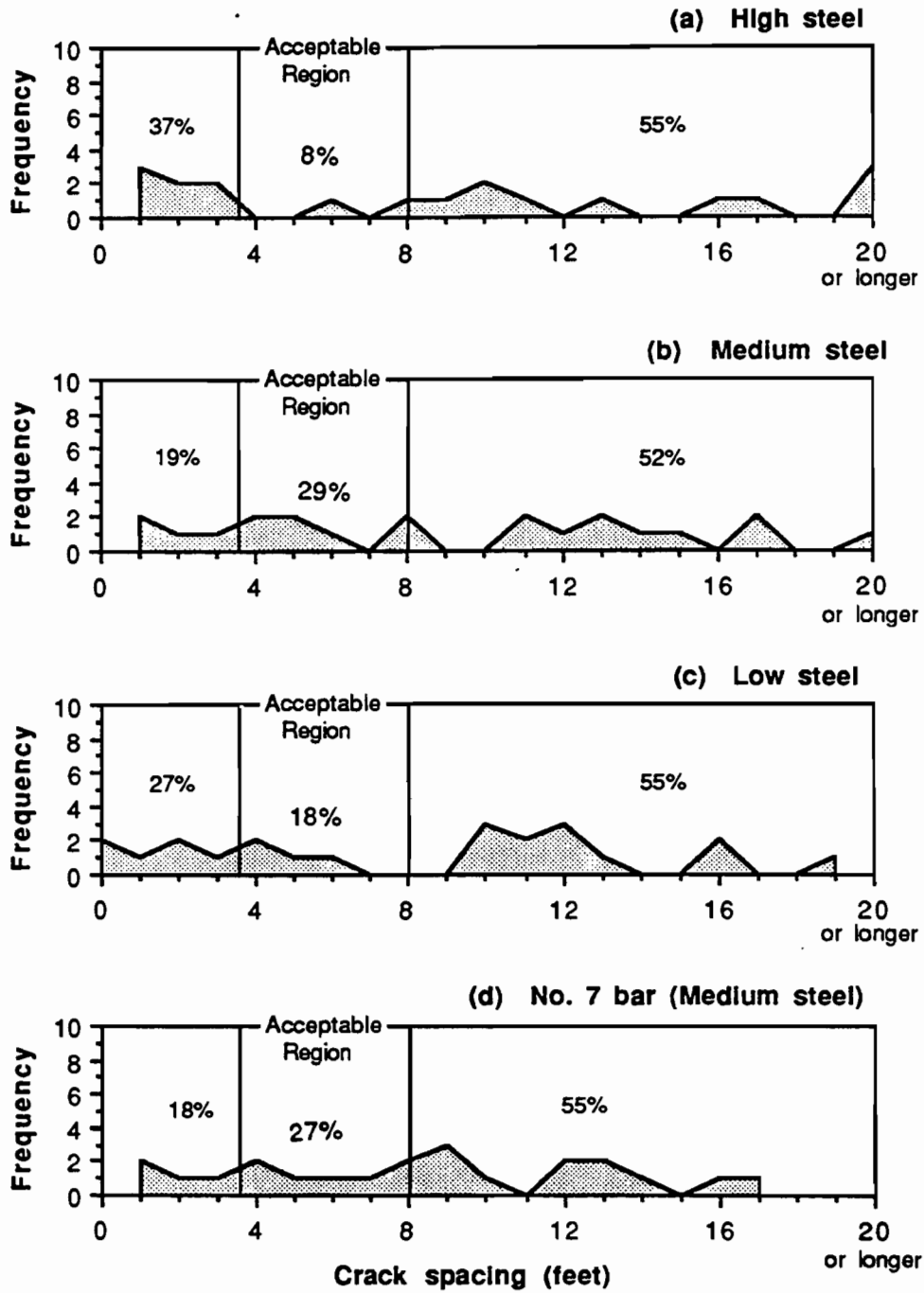


Figure F.2 Distribution of crack spacings at the end of short-term monitoring (SH6-summer, LS)

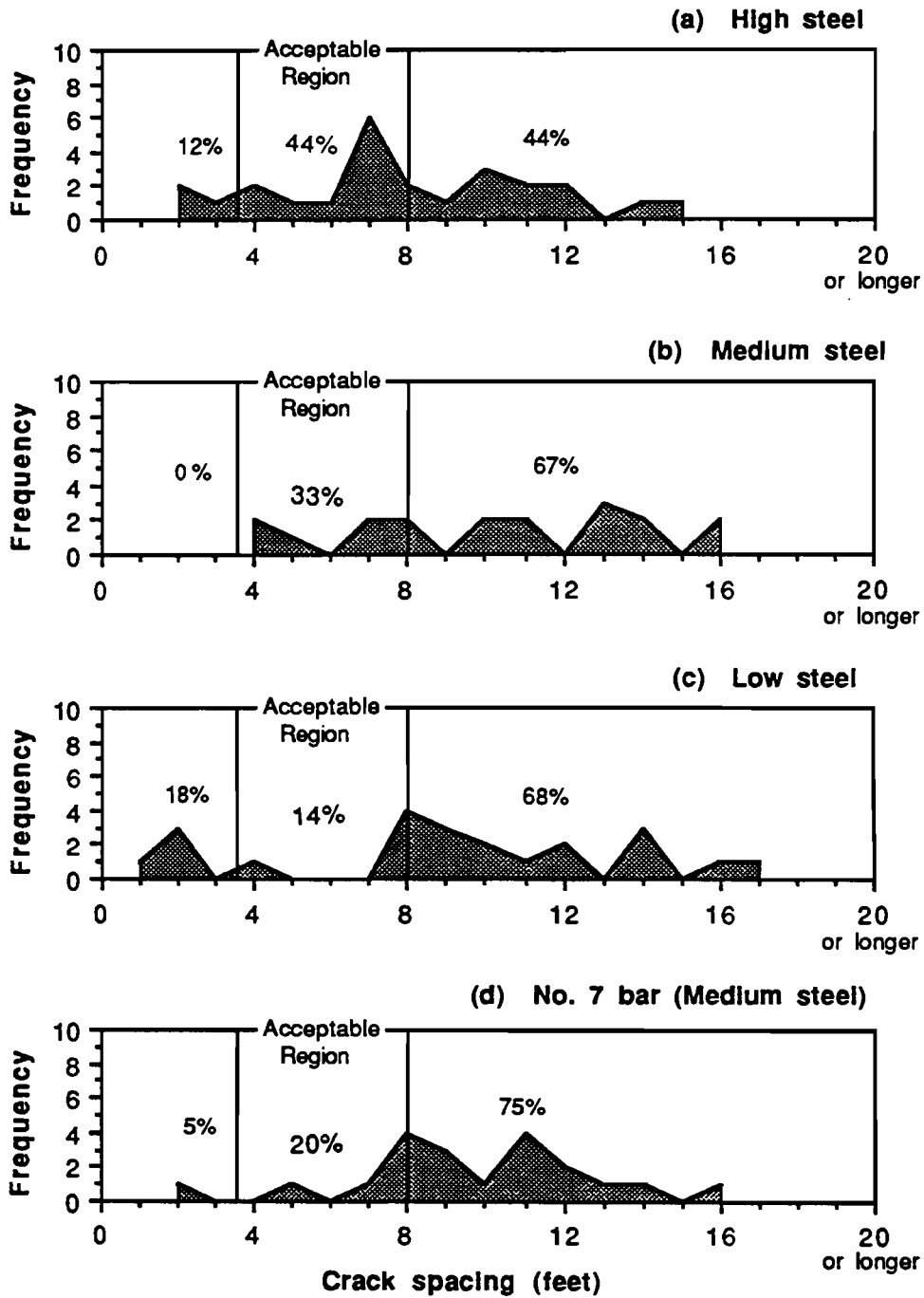


Figure F.3 Distribution of crack spacings at the end of short-term monitoring (BWB-winter, SRG)

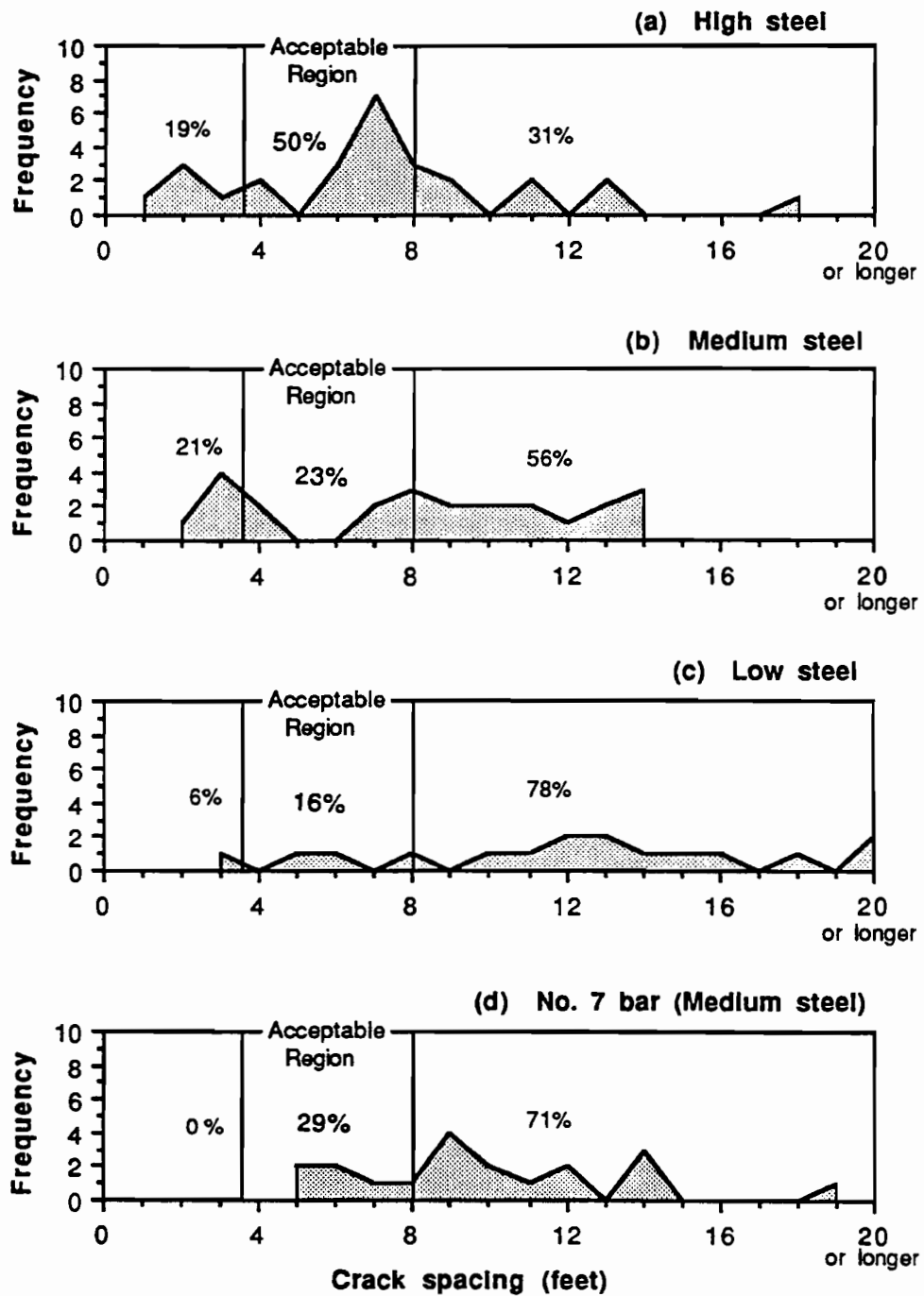


Figure F.4 Distribution of crack spacings at the end of short-term monitoring (BW8-winter, LS)

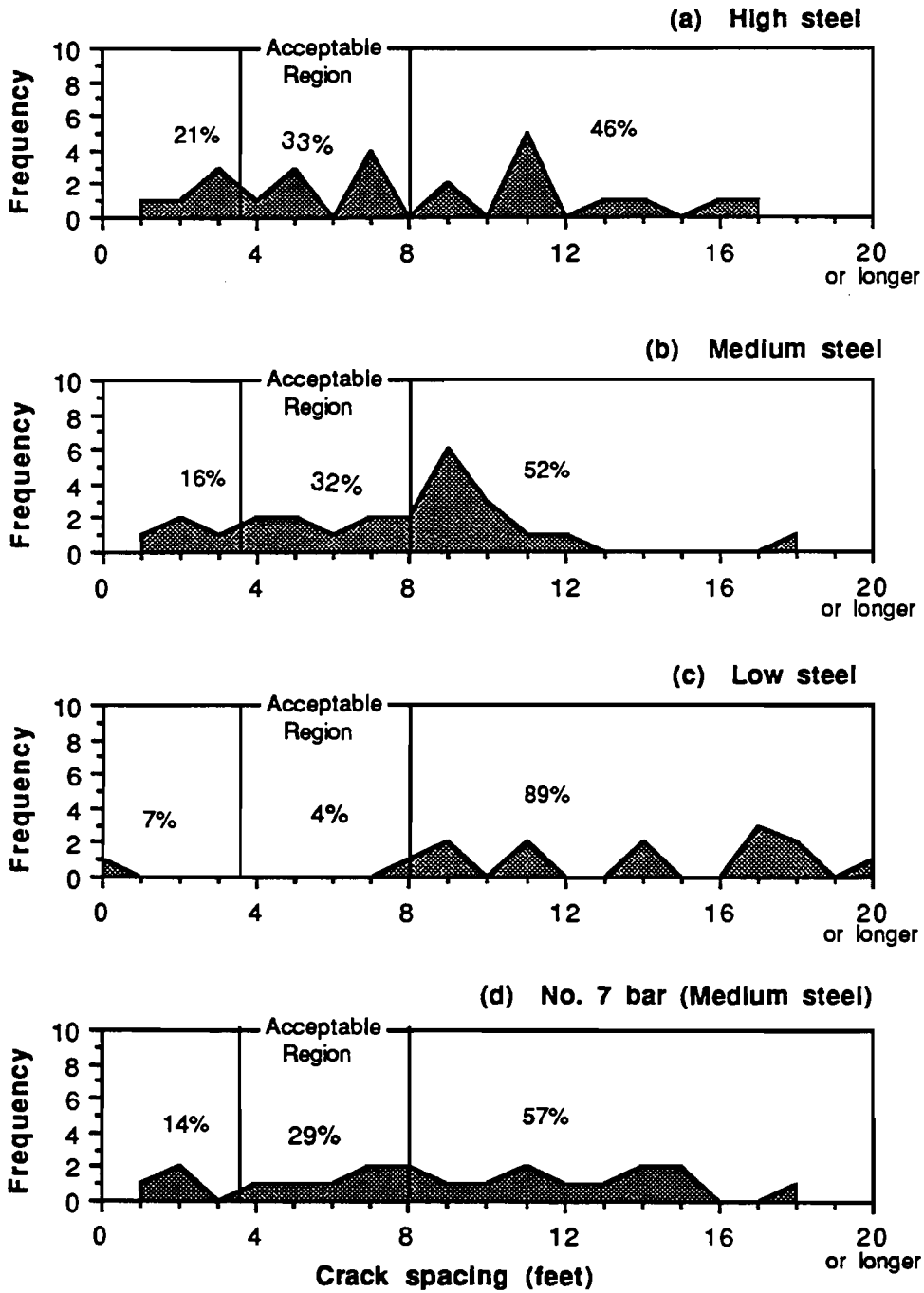


Figure F.5 Distribution of crack spacings at the end of short-term monitoring (SH6-winter, SRG)

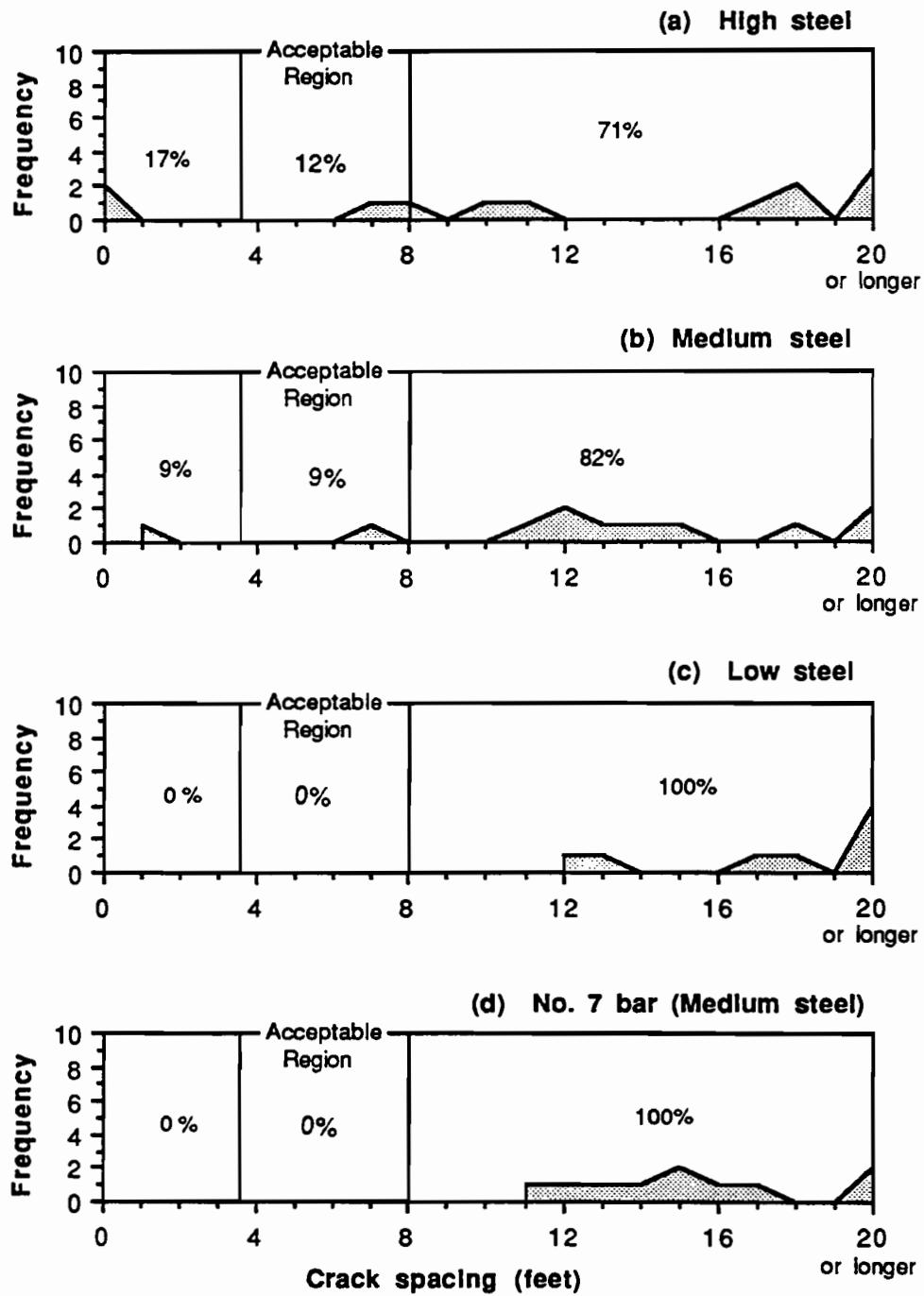


Figure F.6 Distribution of crack spacings at the end of short-term monitoring (SH6-winter, LS)

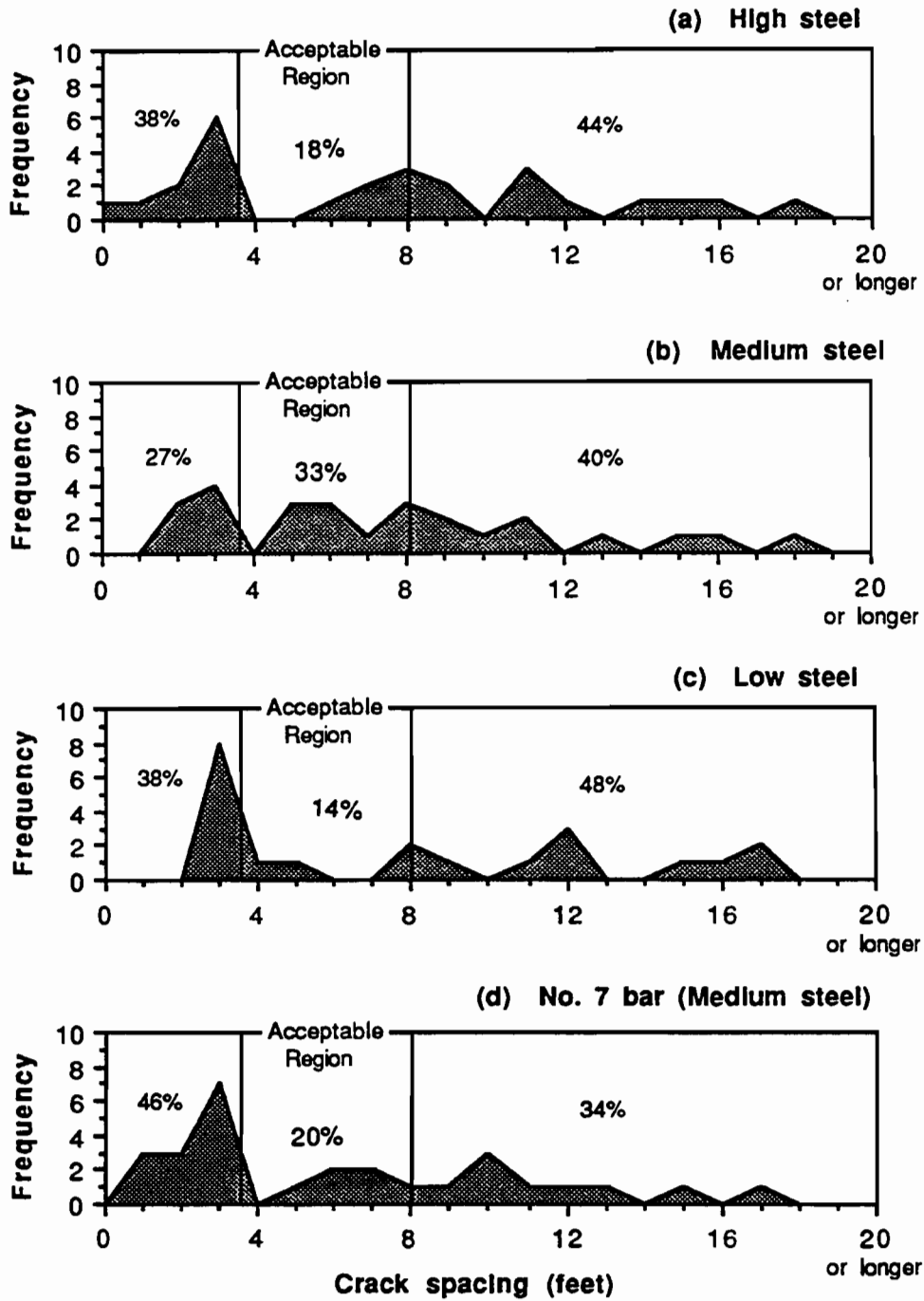


Figure F.7 Distribution of crack spacings at the end of short-term monitoring (IH45-winter, SRG)

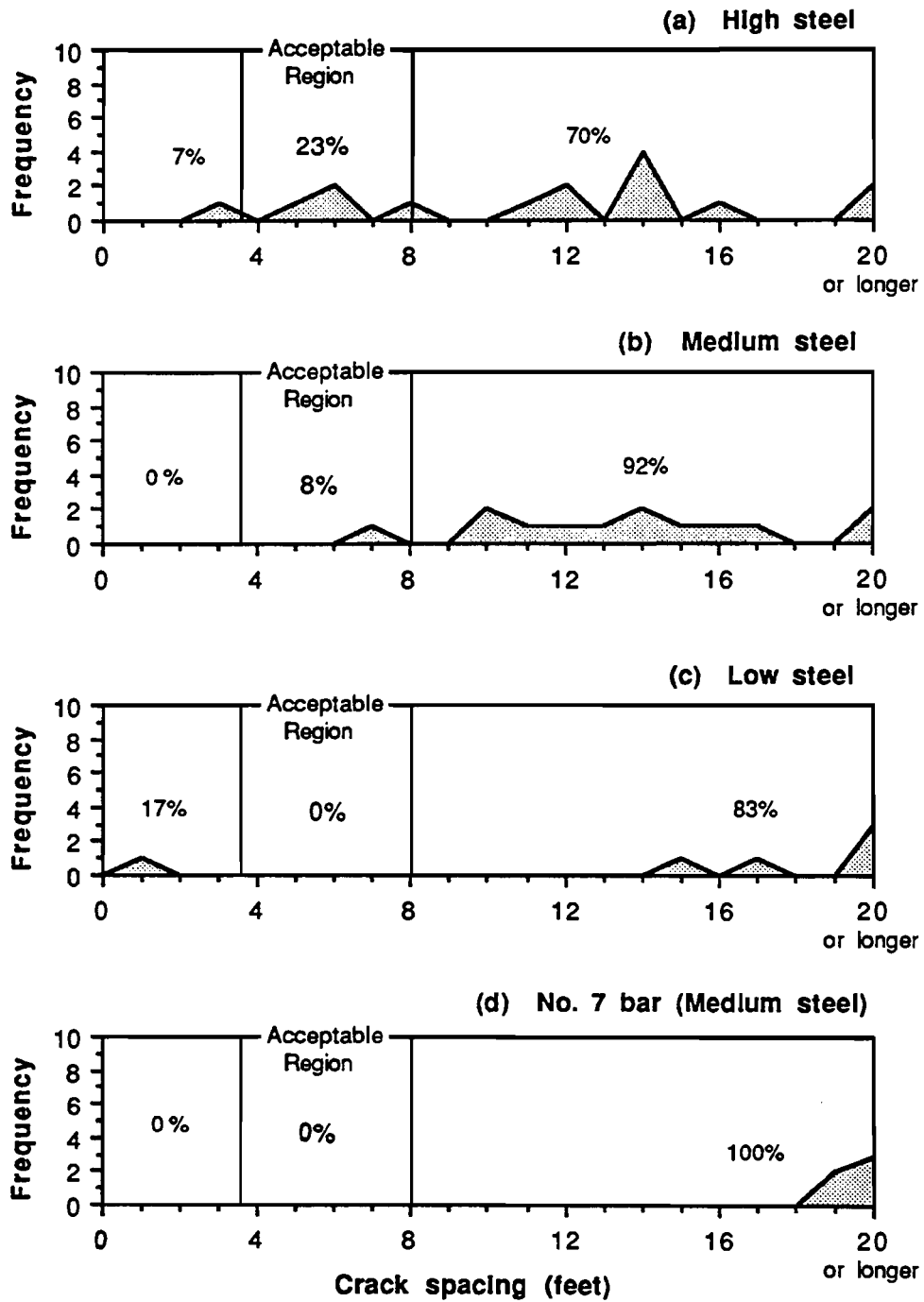


Figure F.8 Distribution of crack spacings at the end of short-term monitoring (IH4S-winter, LS)

APPENDIX G

**COMPARISON OF PREDICTED WITH
OBSERVED CRACK SPACINGS**

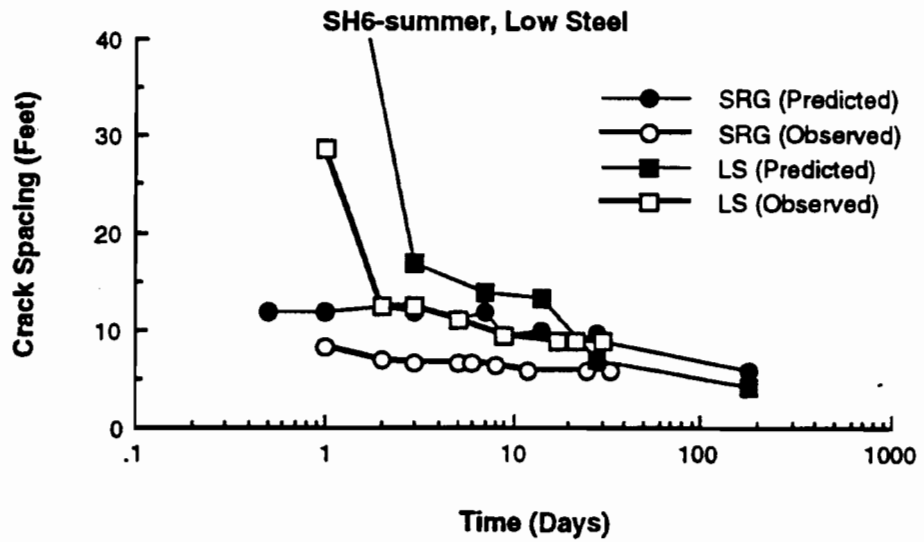
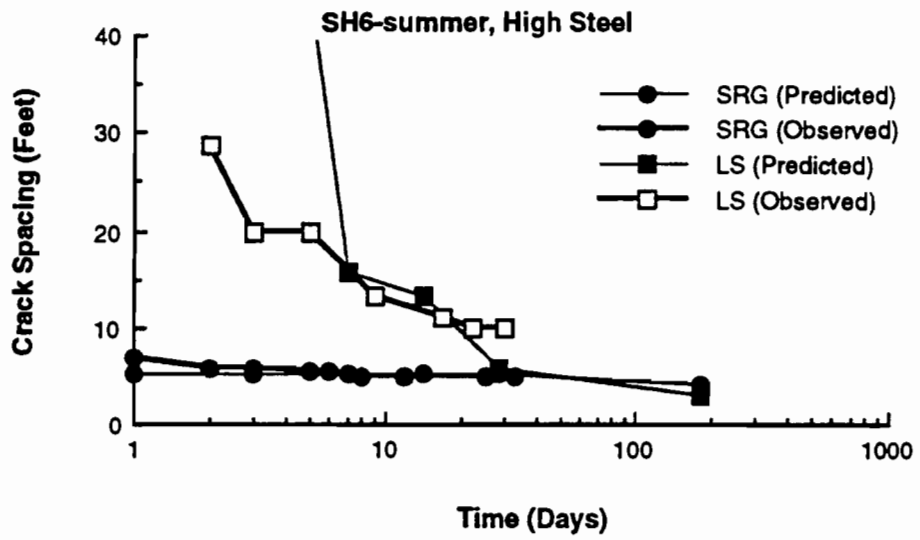
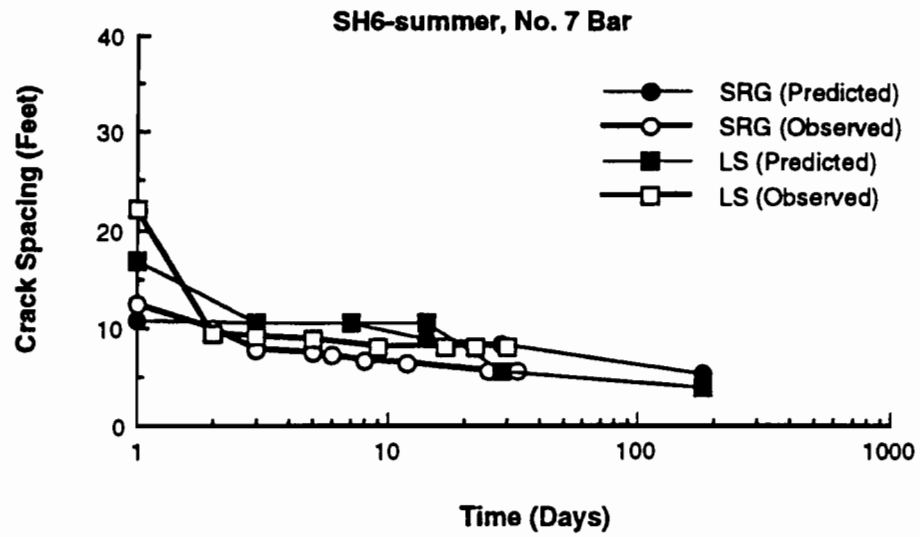


Figure G.1 Comparison of predicted crack spacings with observed crack spacings (SH6-summer)

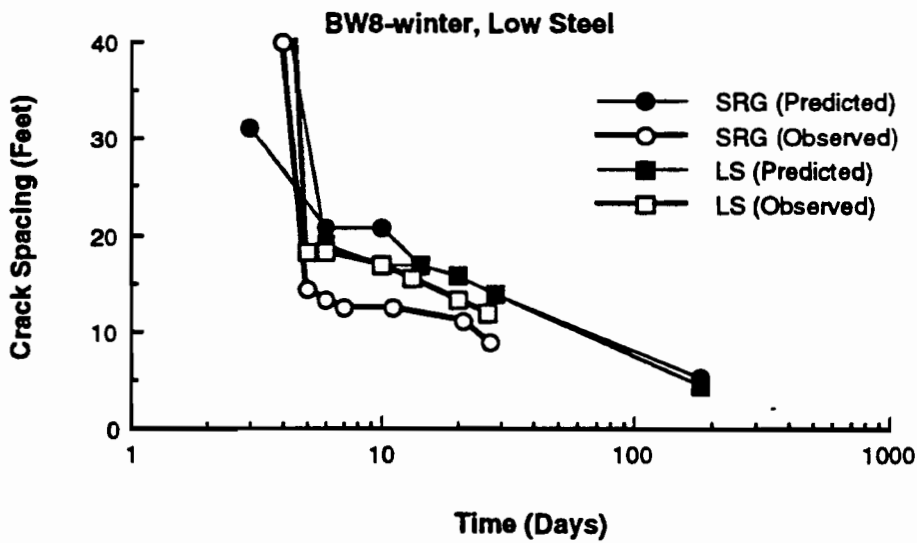
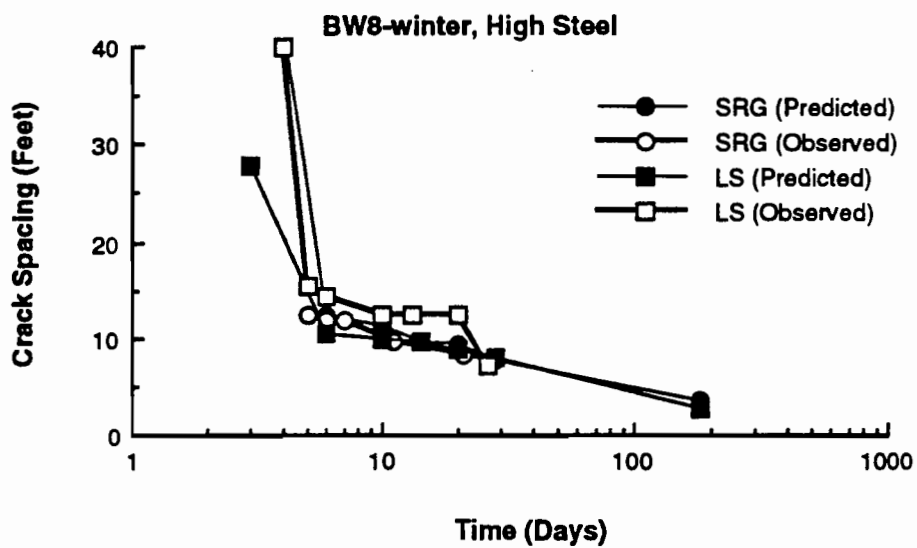
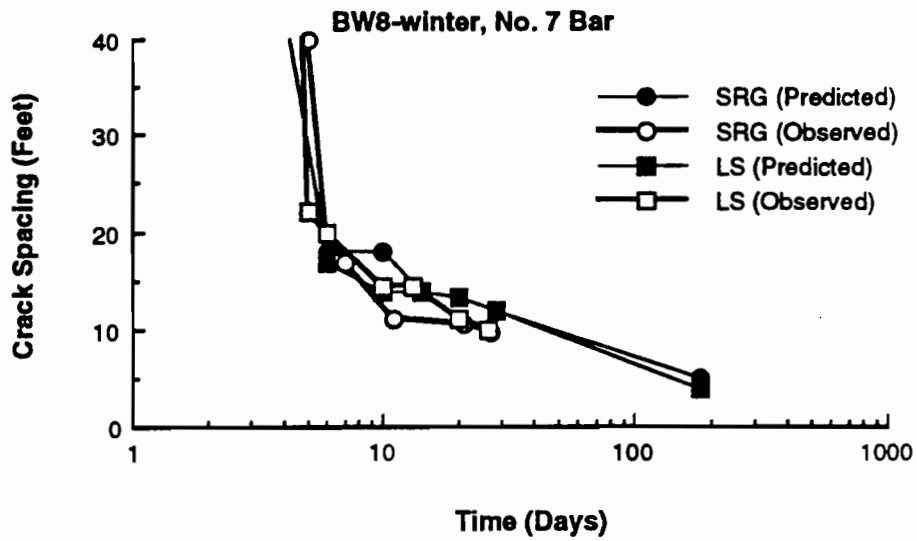


Figure G.2 Comparison of predicted crack spacings with observed crack spacings (BW8-winter)

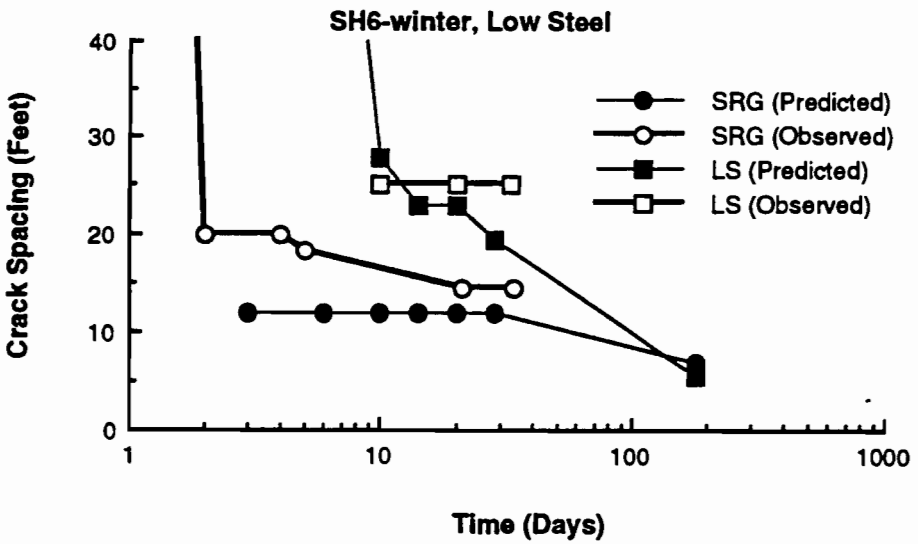
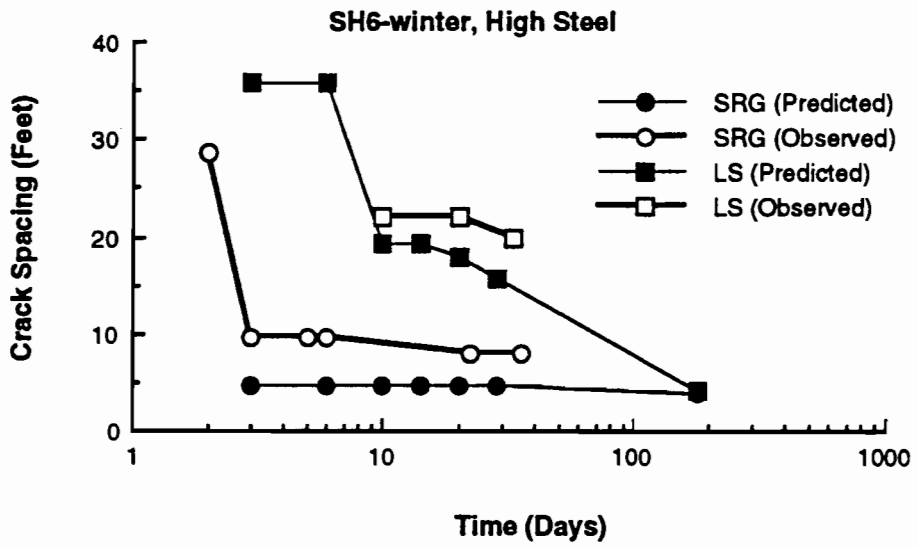
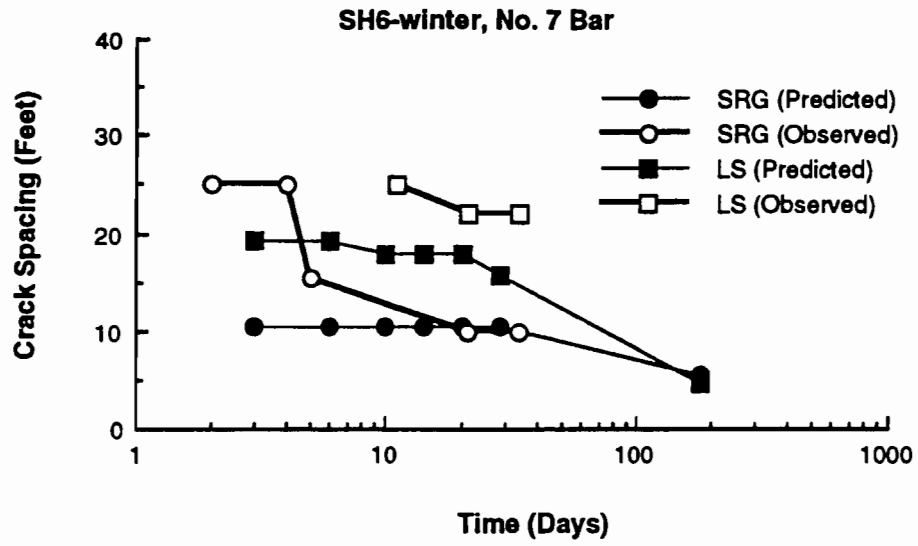


Figure G.3 Comparison of predicted crack spacings with observed crack spacings (SH6-winter)

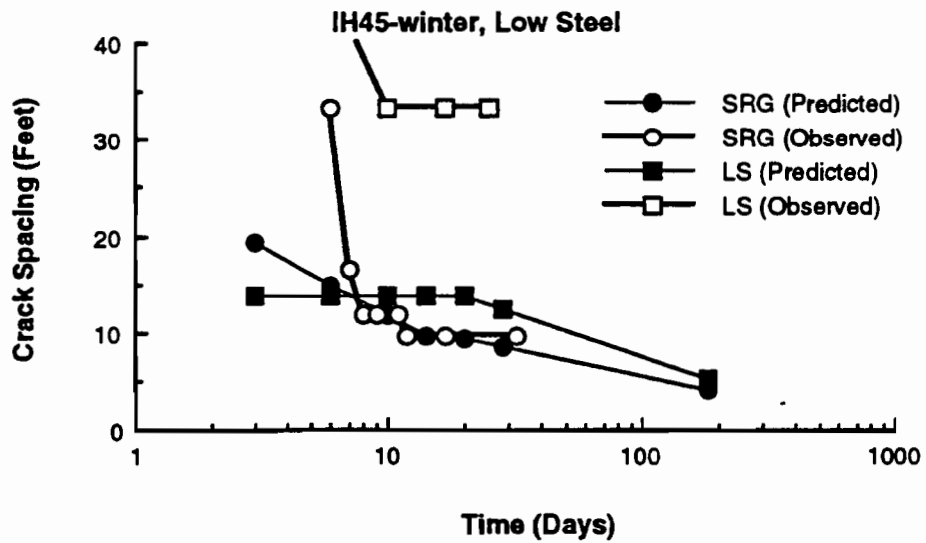
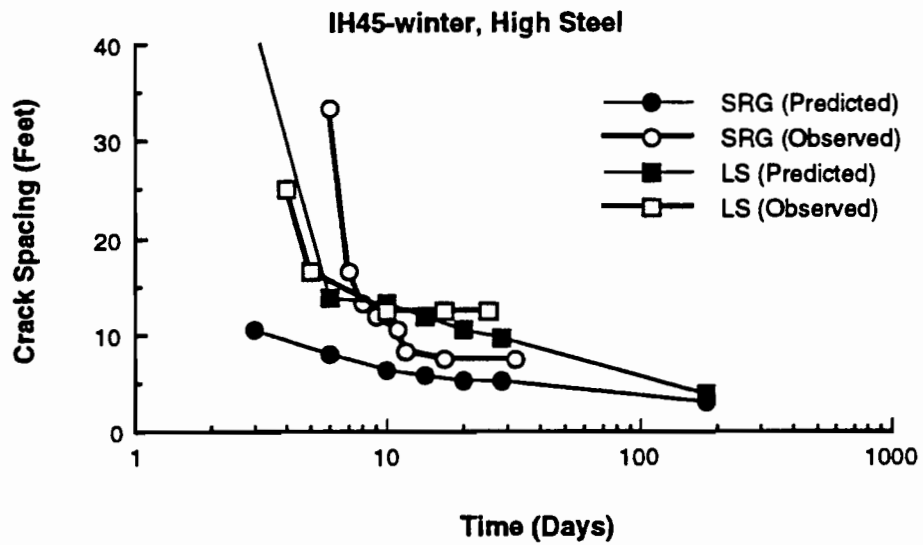
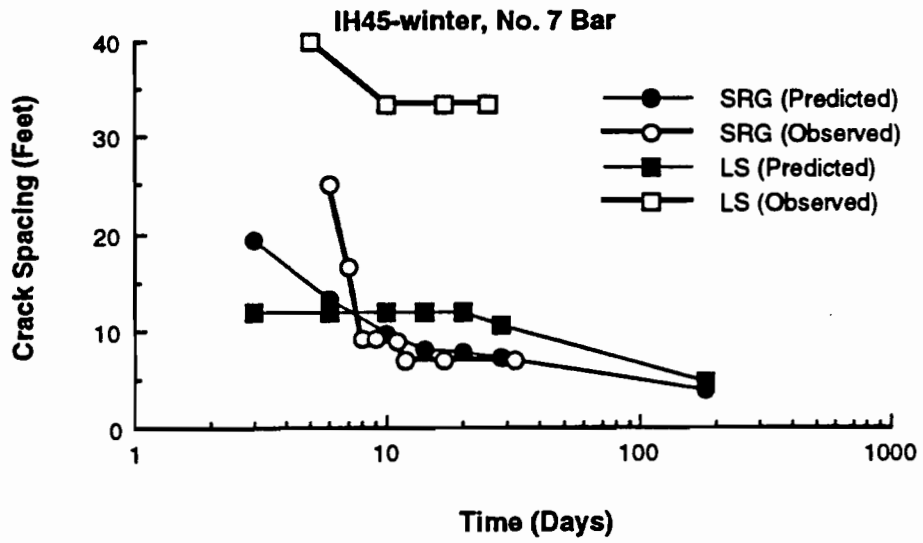


Figure G.4 Comparison of predicted crack spacings with observed crack spacings (IH45-winter)

APPENDIX H

COMPARISON OF PREDICTED WITH OBSERVED CRACK WIDTHS

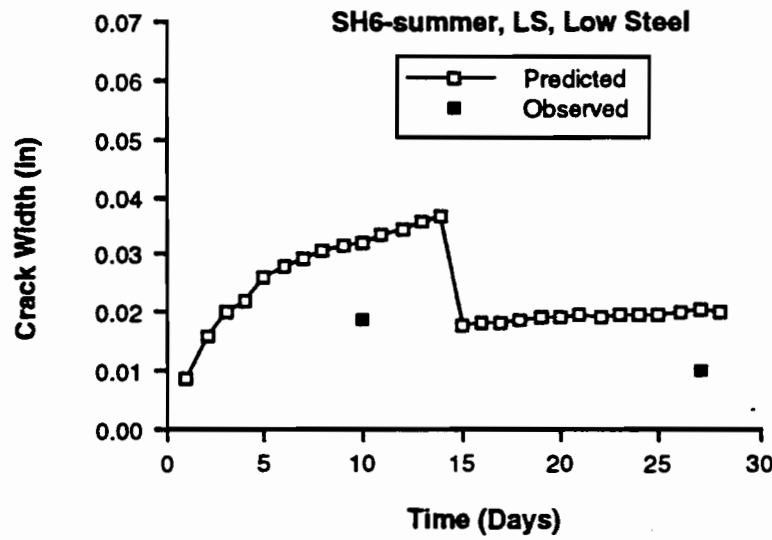
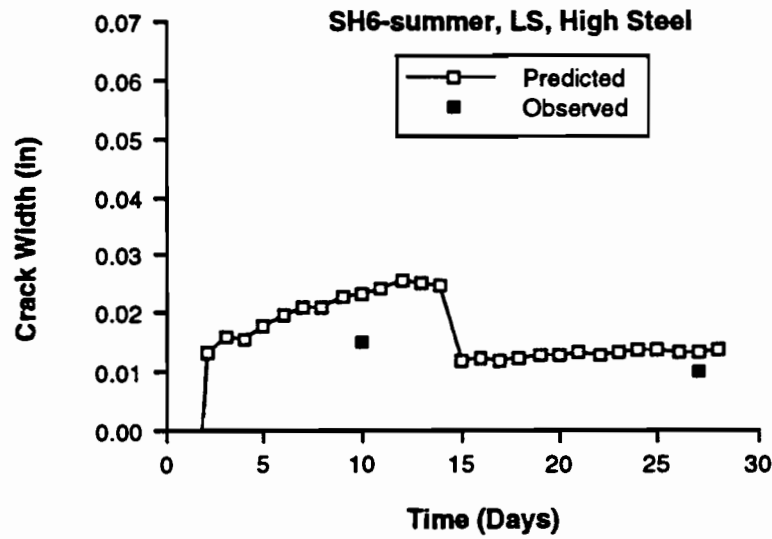
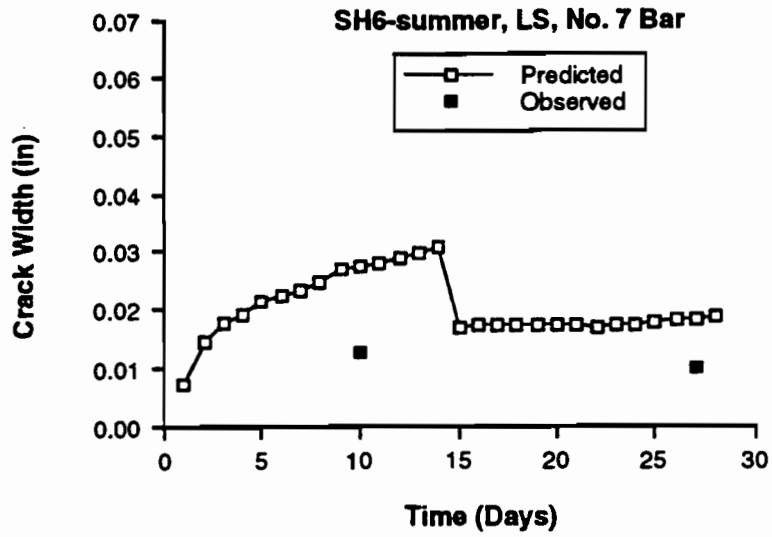


Figure H.1 Comparison of predicted crack widths with observed crack widths (SH6-summer)

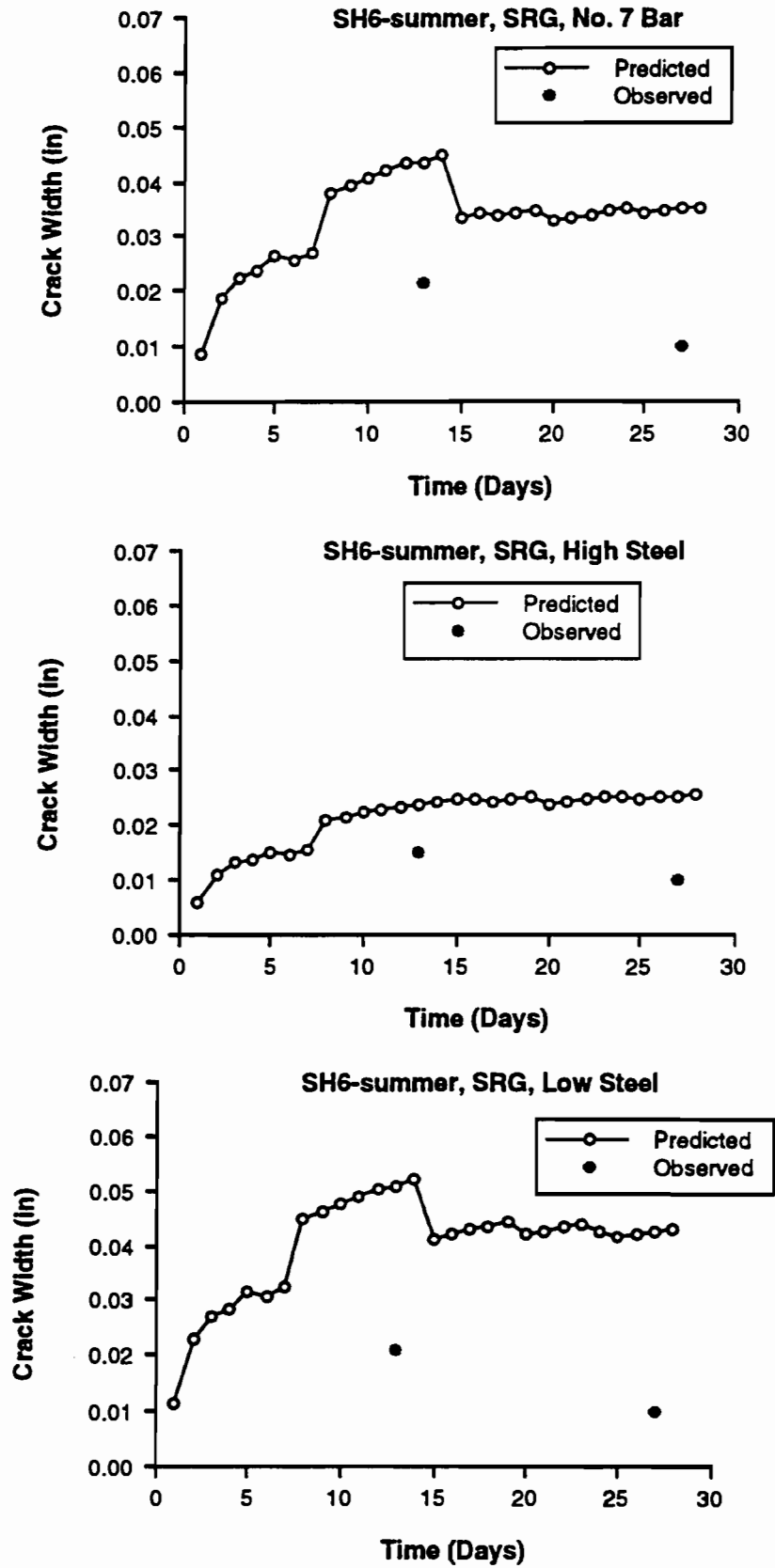


Figure H.1 Comparison of predicted crack widths with observed crack widths (SH6-summer) - continued

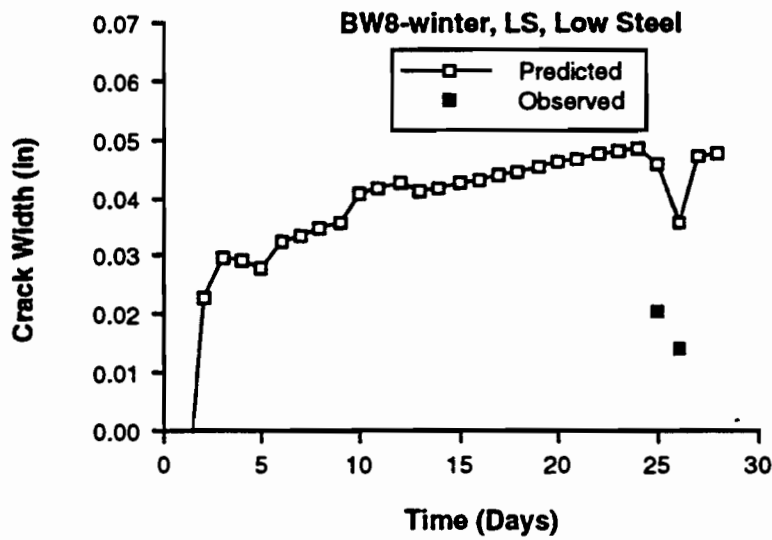
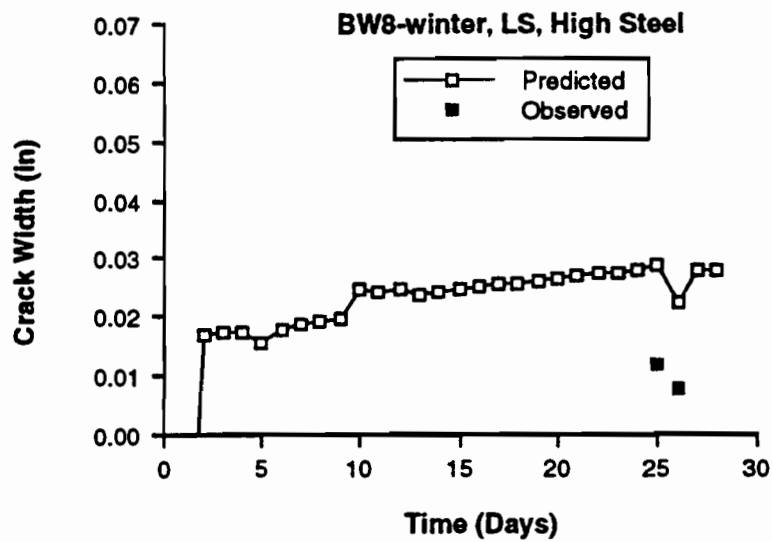
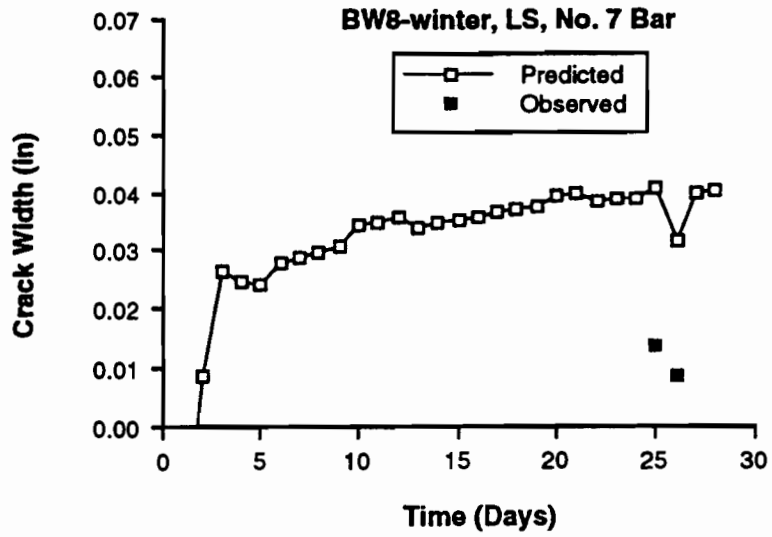


Figure H.2 Comparison of predicted crack widths with observed crack widths (BW8-winter)

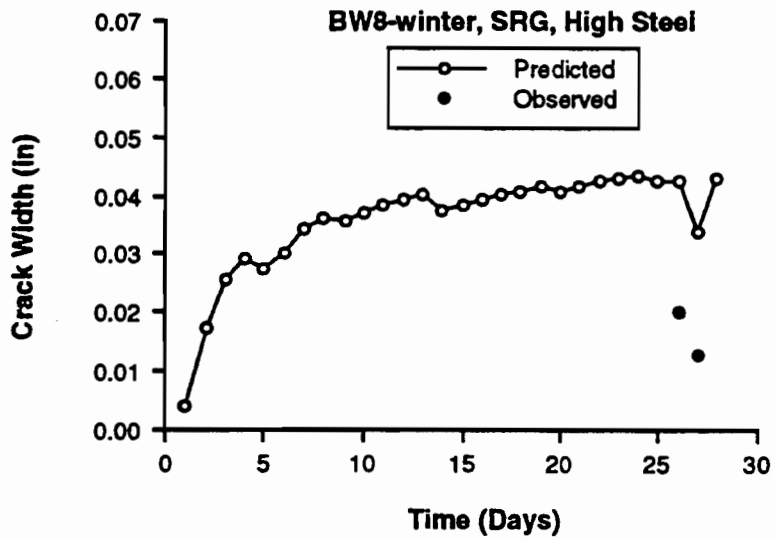
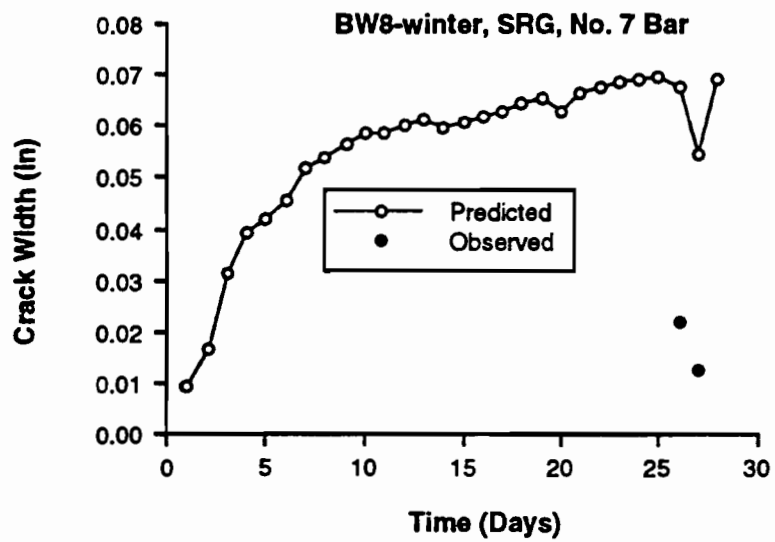
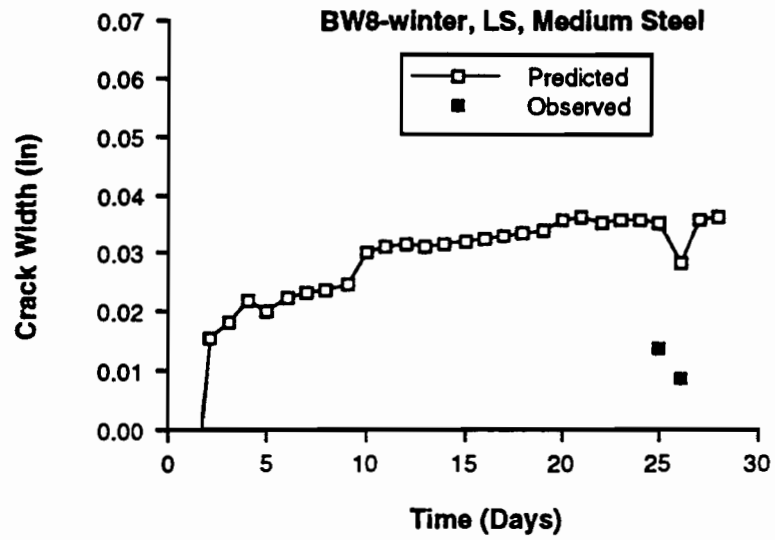


Figure H.2 Comparison of predicted crack widths with observed crack widths (BW8-winter) - continued

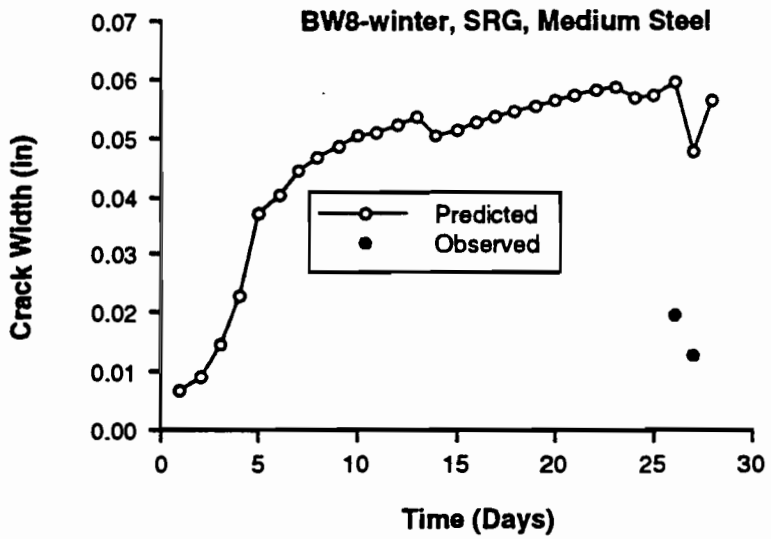
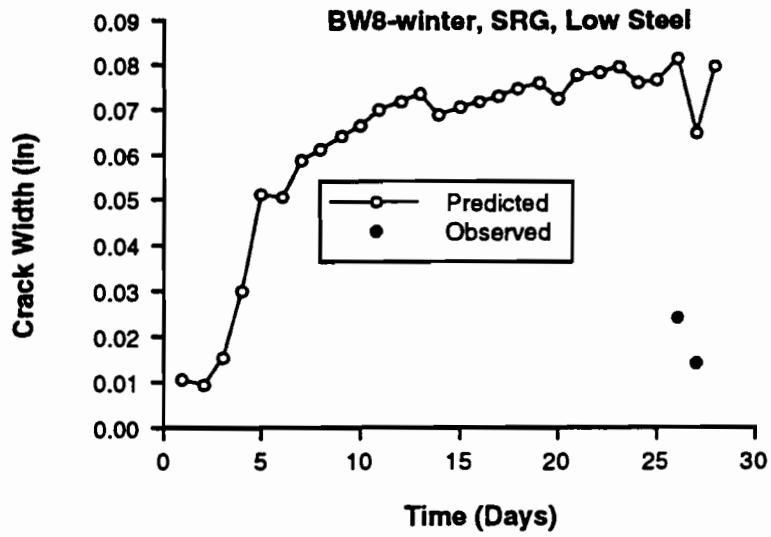


Figure H.2 Comparison of predicted crack widths with observed crack widths (BW8-winter) (continued)

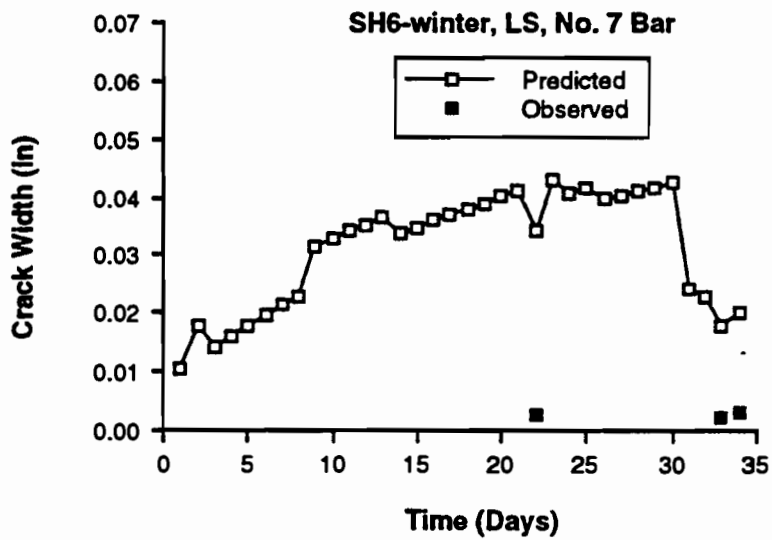


Figure H.3 Comparison of predicted crack widths with observed crack widths (SH6-winter)

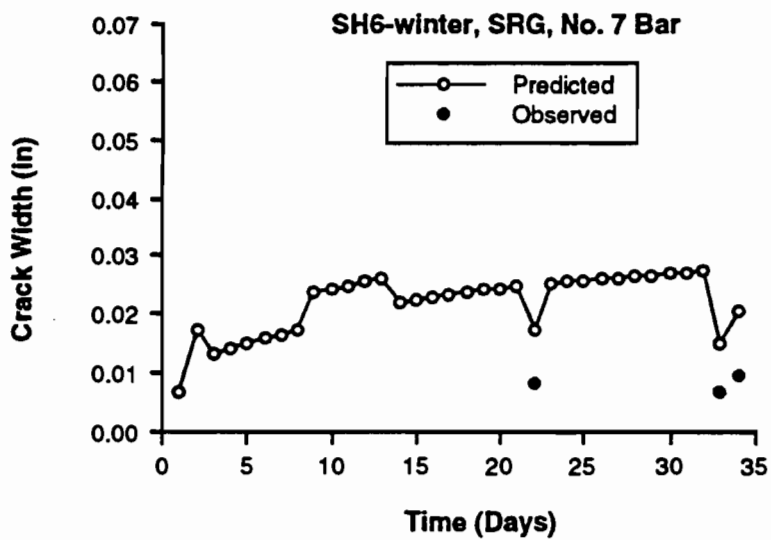
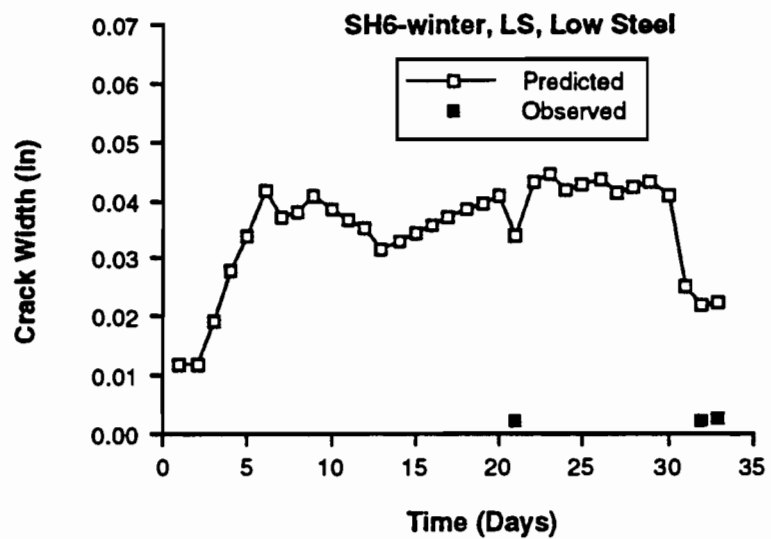
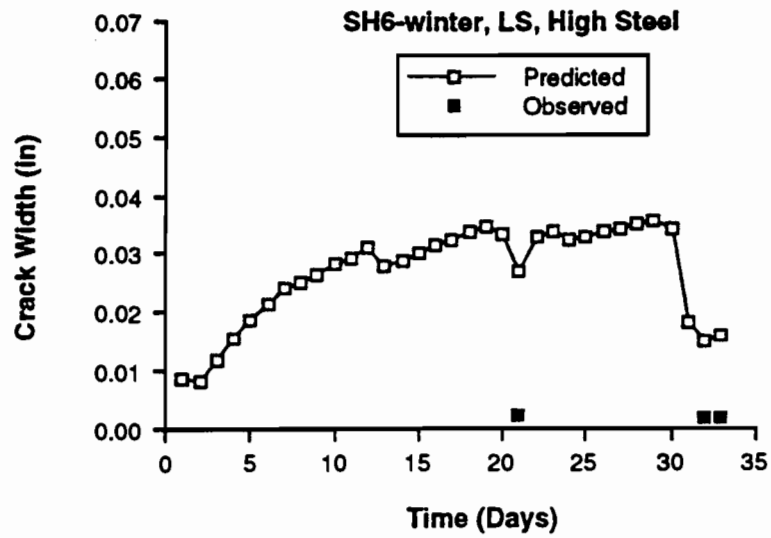


Figure H.3 Comparison of predicted crack widths with observed crack widths (SH6-winter) - continued

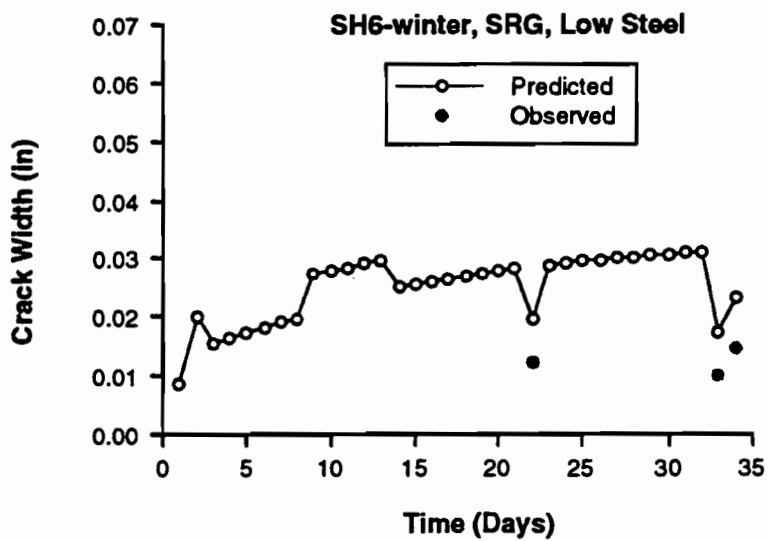
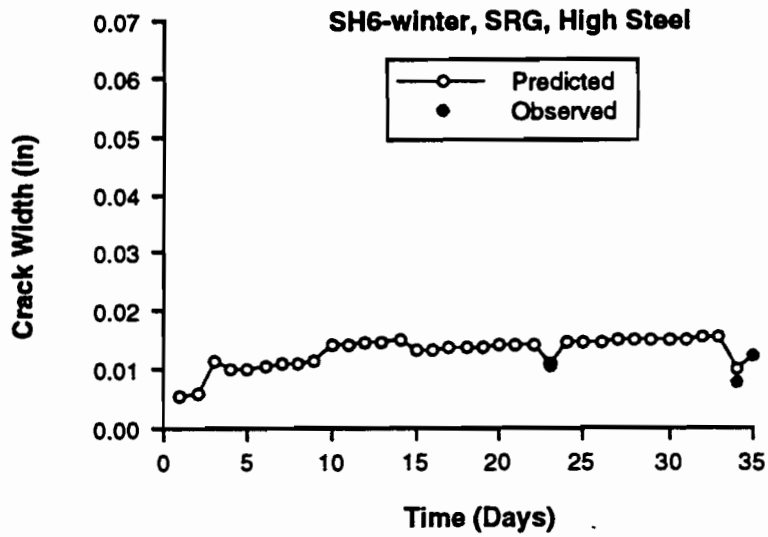


Figure H.3 Comparison of predicted crack widths with observed crack widths (SH6-winter) (continued)

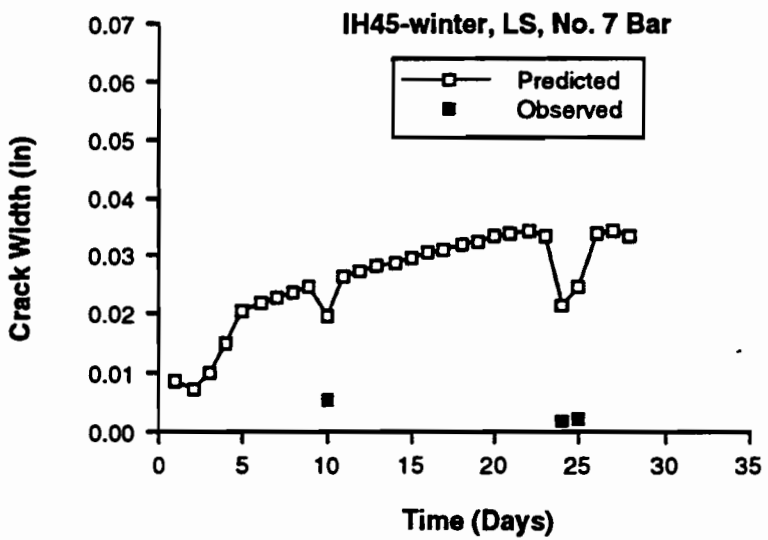


Figure H.4 Comparison of predicted crack widths with observed crack widths (IH45-winter)

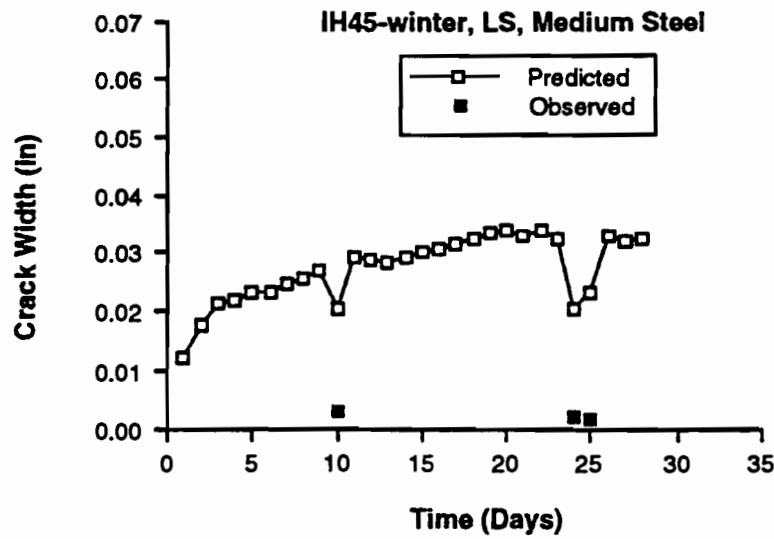
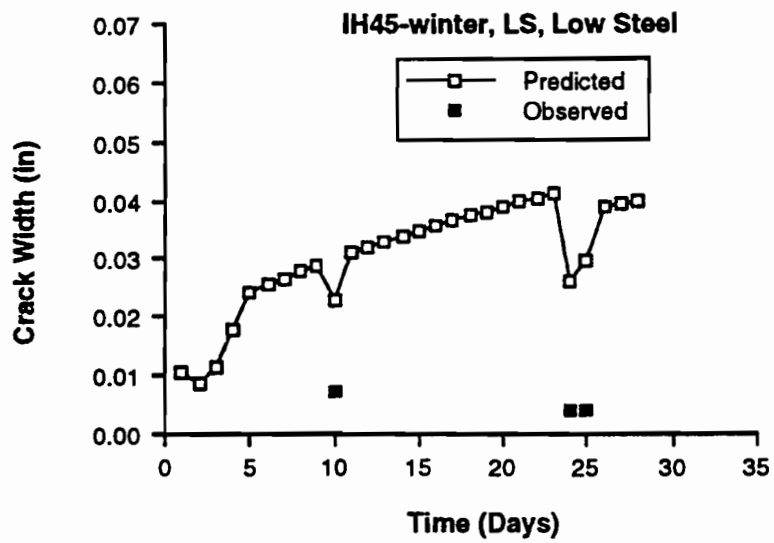
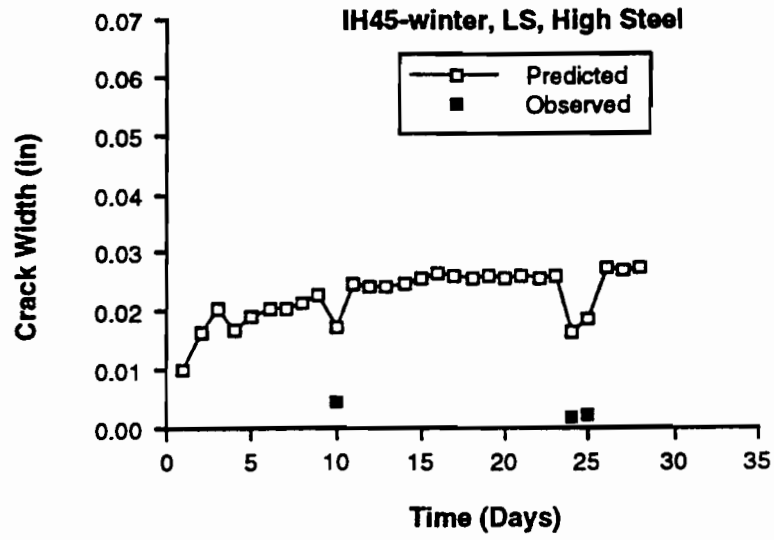


Figure H.4 Comparison of predicted crack widths with observed crack widths (IH45-winter) - continued

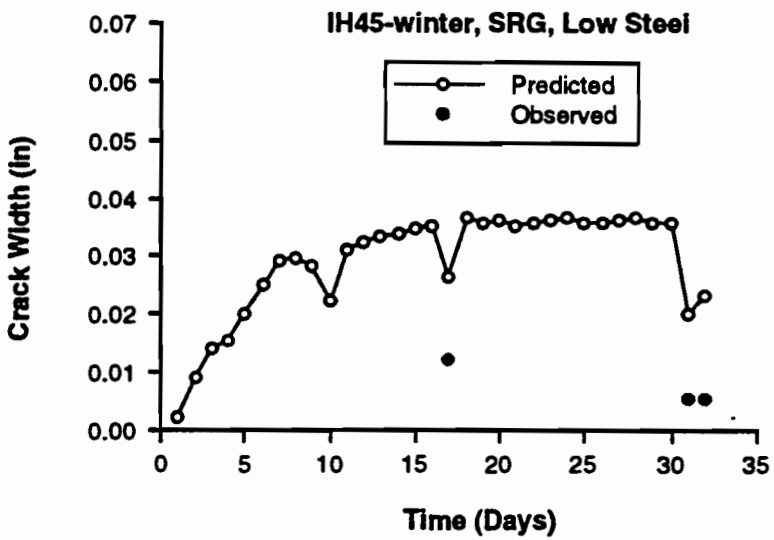
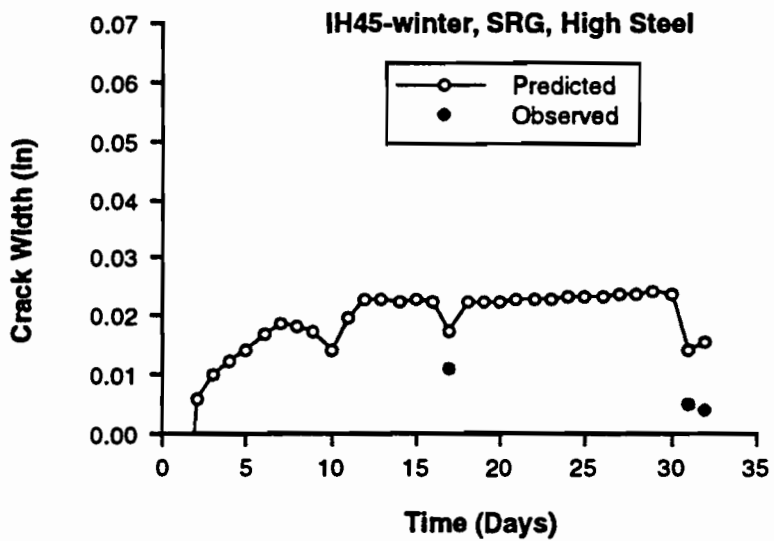
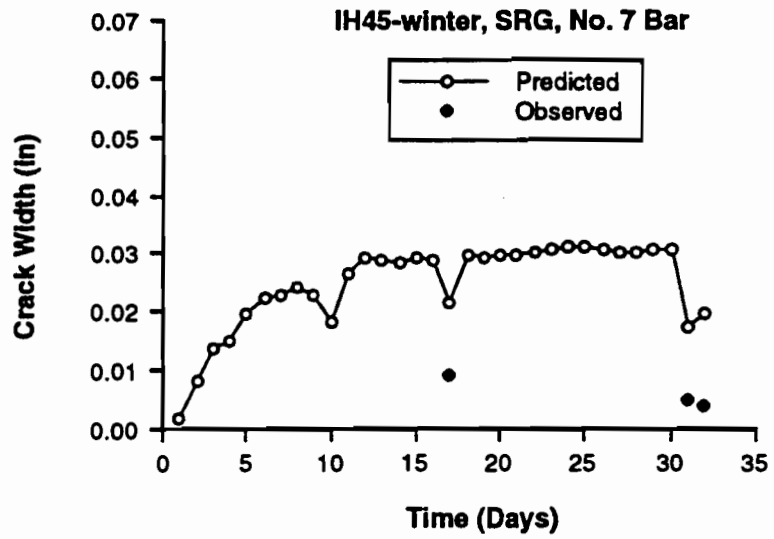


Figure H.4 Comparison of predicted crack widths with observed crack widths (IH45-winter) - continued

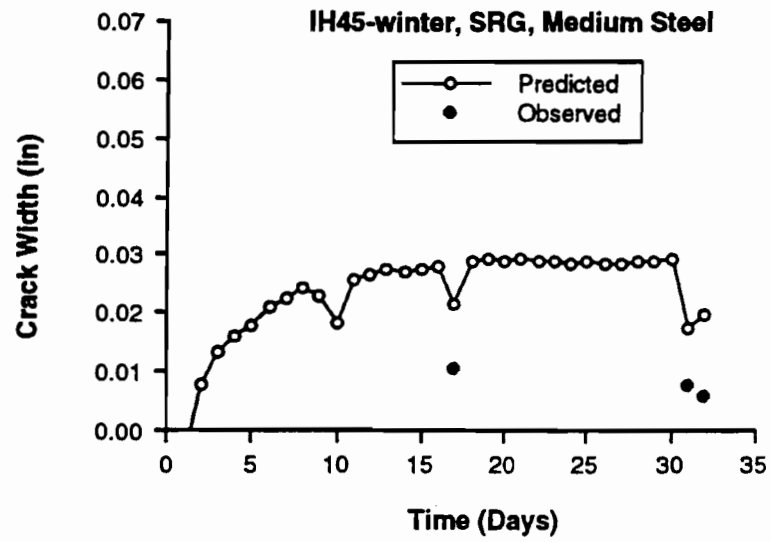


Figure H.4 Comparison of predicted crack widths with observed crack widths (IH45-winter) - continued